INVERSE ESTIMATION OF MATERIAL PARAMETERS, CONVECTIVE HEAT TRANSFER COEFFICIENTS AND FRICTION IN WARM FLAT ROLLING

A Thesis Submitted in Partial Fulfillment of the Requirements for the Degree of

DOCTOR OF PHILOSOPHY

by

Vinod Yadav

(Roll No. 11610339)

Department of Mechanical Engineering

Indian Institute of Technology Guwahati

Guwahati–781039

INDIA

April 2016

Department of Mechanical Engineering,
Indian Institute of Technology Guwahati,
Guwahati-781039,
INDIA

CERTIFICATE

It is certified that the work contained in the thesis entitled "**Inverse Estimation of Material Parameters, Convective Heat Transfer Coefficients and Friction in Warm Flat Rolling**" submitted by **Mr. Vinod Yadav** to the Indian Institute of Technology Guwahati for the award of the degree of Doctor of Philosophy has been carried out under our supervision in the Department of Mechanical Engineering, Indian Institute of Technology Guwahati. This work has not been submitted elsewhere for the award of any other degree or diploma.

12-04-2016

(Dr. U. S. Dixit)
Professor
Department of Mechanical Engineering,
Indian Institute of Technology Guwahati,
Guwahati-781039,
INDIA

(Dr. A. K. Singh)
Professor
Department of Civil Engineering,
Indian Institute of Technology Guwahati,
Guwahati-781039,
INDIA

Dedicated

To

My Teachers

Acknowledgements

I would like to express my sincere gratitude towards many people who have helped me during the tenure of my Ph.D. work at IIT Guwahati. I take this opportunity to express my deep gratitude to all of them for their support and help during various phases of my doctoral research work.

I would like to take this opportunity to express my sincere gratitude to my supervisors Prof. U.S. Dixit and Prof. A.K. Singh for their constant guidance and encouragement during the research work. I am especially grateful to my supervisors as without their support and advice, it would have not been possible for me to continue my doctoral research work. They helped me at various difficult phases of my work with their valuable guidance and moral support.

I am deeply indebted to my supervisor Prof. U.S. Dixit for his help throughout my Ph.D. thesis work. He has devoted more time for my guidance and I have no words to thank him. His guidance and motivation have been instrumental in completion of my research work. I shall always be grateful to him.

I would like to thank my doctoral committee members, Prof. Manmohan Pandey, Dr. R. Ganesh Narayanan and Prof. S. Talukdar for their valuable suggestions and encouragement during the period of my research work. I am also grateful to the former and present heads of the Department of Mechanical Engineering, Prof. P. Mahanta and Prof. A.K. Dass for extending various facilities during the tenure of my doctoral program. The financial assistance offered by the Department of Science and Technology (India) through grant DST/RC-UK/14-AM/2012 and Engineering and Physical Sciences Research Council (UK) through grant EP/K028316/1, sponsored project entitled 'MAST: Modeling of Advanced Materials for Simulation of Transformative Manufacturing Processes' is acknowledged.

I wish to express my sincere thanks to Mr. Rituraj Saikia, Mr. Sanjib Sarma, Mr. Pranjol Paul, Mr. Nabajyoti Dutta, Mr. Jiten Basumatary, Mr. Amal Kalita, Mr. Nip Borah, Mr. Raju Talukdar and Mr. S. Ahmed for their assistance during the experimental work. I sincerely thank Mr. N.K. Das, Mr. D. Chetri, Mr. N. Saikia, Mr. M. Sarma, Mr. B. Chandan, Mr. U. Gohain and Mr. M.C. Medhi for their help in conducting the experiments.

I express my sincere thanks to my friends Mr. Mustafa, Dr. M. Chandrasekaran, Mr. Rajkumar Shufen and Mr. Purnendu Mandal. Thanks are also addressed to Mr. Ravikant, Mrs. Hema Gurung, Mr. Saurabh Garg, Mr. Saptarshi Karmakar, Mr. Chandrahas Patel, Mr. Jyoti Doley, Mr. Polash Dutta, Mr. Rosang Pongen, Mr. Aghyad Eideh, Mr. Kalidasan, Mr. Besufekad, Mr. Woldetinsay, Mr. Vikash Vanik, Mr. Sujoy Tikader and Mr. Pramod Sahu for their help and support.

I acknowledge the moral support of Dr. Manjuri Hazarika, Dr. Sachindra Mahto, Dr. Ratnakar Das, Mr. Tomi Ado, Mr. Anil Mishra, Mr. Pradeep Biswal, Mr. Kaustubh Acharyya, Mr. Moasunep Jamir, Mr. Kamal Kumar Agarwal and Mr. Pawan Singotia during my research work. I shall always be grateful to my IITG and childhood friends for their great encouragement and wishes.

Finally, I bow my head to the God Almighty in deepest gratitude and seek blessings.

12th April 2016

Vinod Yadav
IIT Guwahati

Abstract

Flat rolling process is one of the most widely used metal forming processes in industries. In this process, the thickness of a sheet is reduced by passing it between two counter-rotating rolls. The rolling process can be classified into three categories *viz*., cold, warm and hot rolling based on the working temperature of the process. The warm rolling has some edge over the hot and cold rolling, for example, the lower load and energy requirement compared to cold rolling as well as the better surface finish and dimensional accuracy compared to hot rolling. The modelling of the rolling process is important for design, proper control and optimization of the process. Modelling of the process requires input data about material properties and friction. In batch production mode of rolling with newer materials, separate experiments need to be conducted for each material to determine the input parameters. Conducting separate experiments is tedious and time consuming as the work material gets changed frequently in batch production. In view of it, in the present thesis, an inverse methodology is proposed to estimate the material and process parameters in warm flat rolling by the measurement of exit temperature and slip. For this purpose, first steady-state thermo-mechanical modelling of warm flat rolling is carried out for the inverse estimation of mechanical properties and friction. Subsequently, a transient thermal analysis of the roll and strip together is carried out for the inverse estimation of thermal parameters.

A two-dimensional steady-state thermo-mechanical analysis of the flat rolling comprises two modules— deformation module and thermal module. Deformation module uses finite element method (FEM) based on Eulerian flow formulation. Thermal module uses analytical methods. The determination of temperature distribution in roll as well as strip through analytical methods has the advantage in terms of computational time. The proposed thermo-mechanical steady-state model for warm flat rolling is validated with the experimental results available in the literature. In the present work, a fast FEM analysis has also been proposed for the estimation of the steady-state temperature distribution in rolling process. The FEM results ensure the accuracy of the proposed model using analytical methods to find

out the temperature distribution in the roll and the strip. The results obtained by the analytical methods and the FEM model differ by less than about 8%.

For validating the transient analysis of warm flat rolling, in-house warm rolling experiments were conducted. The rolling experiments were carried out in a laboratory rolling mill. The experimental results were used to validate the proposed model by measuring the exit strip temperature at the surface as well as at the centerline. The coefficient of friction is estimated by inverse method based on the exit strip temperature measurement with the known material properties.

An efficient inverse methodology to determine the mechanical properties by the measurement of exit temperature and slip is proposed and validated experimentally. A heuristic method is used for the minimization of the error between the experimentally measured and the estimated temperature of exit strip. The inversely estimated flow stresses are compared with the experimentally measured flow stresses. The experimental flow stresses are obtained by conducting tensile tests at different temperatures. A good agreement between the inversely estimated and experimental flow stresses is observed with a variation of less than about 10%.

A transient thermal analysis is carried out for estimating the average thermal properties of the roll and the strip as well as friction by inverse modelling. The inverse modelling requires the transient temperature distribution at the exit strip at two locations. The coefficient of friction is estimated based on the slip measurement. For a fixed value of the coefficient of friction, the slip is unaffected by the thermal parameters. Based on the sensitivity study, a procedure to identify the parameters by inverse analysis is illustrated. It is seen that there are sufficient number of signals to predict the thermal parameters uniquely. The uniqueness of the solution has been studied heuristically and numerically. It is observed that the deviation of estimated and actual parameters is less than $\pm$ 7%.

The inverse methodology proposed in this thesis may be implemented in the shop floor for the online determination of material and process parameters in rolling process. The methodology can be extended to other metal forming process. Also, a methodology can be developed to estimate all material properties and friction parameter together.

Contents

List of Figures

List of Tables

Nomenclature

Roman letters

a,b	inner and outer roll radii of roll
b,n	material hardening parameters (used in Chapter 3)
A,B,C	constants of J-C material model
D'	deformed roll diameter
E_r	Young's modulus of the roll material
f	friction factor
F_r	roll force per unit width
h	roll gap (used in Chapter 5)
h_a	convective heat transfer coefficient at the surface of strip
h_c	heat transfer coefficient between the roll and the strip
h_e, h_i	convective heat transfer coefficient at the outer and inner periphery of roll, respectively
h_1, h_2	inlet and exit thickness of strip, respectively
k_a	thermal conductivity of air
k_r, k_s	thermal conductivity of roll and strip, respectively
K	constant of Hollomon's law
c_{pr}	specific heat of roll
c_{ps}	specific heat of strip
J_n, Y_n	Bessel function of first and second kind, respectively
l_d	contact length of roll and strip at the interface
L	length of bite zone
L_e	effective length of the arc of contact
m	positive integer (used in Chapters 3 and 4)
n	positive integer or zero (used in Chapters 3 and 4)

n	constant material parameters (used in Chapters 5 and 6)
m_1, n_1	constants of J-C material model
m_2	constant of specific material (used in Chapter 3)
n_2,n_3	constants of J-C modified model (used in Chapters 3)
n_4,n_5	temperature dependent parameters (used in Chapters 4)
$\bar{\mathrm{N}}_{ux}$	Nusselt number
p	hydrostatic pressure
Pe	Peclet number
P_f	power due to friction
P_p	power due to plastic deformation
Pr	Prandtl number
$\dot{q}$	heat flux input into the roll
$\dot{q}_f$	heat flux due to friction
$\dot{q}_s$	heat flux entering into the strip
Q_{av}	average heat flux applied at outer roll periphery
Q_T	total heat
$\dot{Q}$	rate of heat generation per unit volume
r-θ	polar coordinates
r_d	percentage reduction
R	undeformed roll radius
R'	deformed roll radius
Re_x	Reynolds number
S_{ij}	deviatoric part of the stress tensor
S_1,S_2	location of temperatures sensor 1 and sensor 2, respectively
t	time
t_i	component of traction vector
t_a	time spent by strip at roll bite
t_n, t_s	interfacial normal and shear stress components
T	temperature

T_{amb}	ambient temperature
T_e, T_i	medium temperature at outer and inner periphery of roll, respectively
T_m	melting temperature
$T_{\max}$	maximum temperature of the roll
T_R	roll torque per unit width
T_r	temperature of the roll
T_s	temperature of the strip
$T_o(\tau)$	imposed temperature field on roll, used in Eq. (3.23)
T_0	initial temperature of the roll and the strip
$T_0(y)$	initial temperature of the strip, used in Eqs. (3.39) and (3.41)
u	velocity of air
v_n	normal component of velocity
V	average speed of the strip
V_R	roll velocity
v_1, v_2	components of velocity vector
V_1, V_2	inlet and exit velocities of the strip, respectively
w	width of the strip
x-y	Cartesian coordinates of strip in Figure 3.6
x_1, x_2	Cartesian coordinates of strip in Figure 3.2

Greek letters

α	bite angle after roll deformation
α_r, α_s	thermal diffusivity of roll and strip, respectively
β	half arc of the heat source on the roll periphery
β_m	roots of the characteristics (used in Chapter 3 and 4)
β_1	constant material parameters of power law
ε_{eq}	equivalent (plastic) strain
$\dot{\varepsilon}_{eq}$	equivalent strain-rate
$\dot{\varepsilon}_0$	reference strain-rate

$\dot{\varepsilon}_{ij}$	strain rate tensor
ϕ	location of the heat source
γ	constant material parameters of power law
η	fraction of the plastic deformation work dissipating as heat
η_1	proportionality factor in Levy-Mises flow rule
σ_0	constant material parameters of power law
λ	heat partition factor
λ_n	roots of the characteristics equation (used in Chapter 3)
μ	equivalent Coulomb coefficient of friction
μ_l, μ_u	lower and upper limit equivalent Coulomb coefficient of friction (used in Chapter 5)
μ_a	dynamic viscosity of air
ν	kinematic viscosity of air
θ	angular displacement of roll
ρ_r, ρ_s	density of the roll and the strip, respectively
σ_y	flow stress of strip
ω	angular velocity of roll
ξ, ζ	Non- dimensional coordinates

Chapter 1

Introduction

1.1 Flat Rolling

Rolling is one of the oldest and most important metal forming processes. It plays an important role in industries due to its versatility and high production rate. It is an economical method for the manufacturing of metal strips or sheets. The development of rolling process dates back to the 15th century and it accounts for about 90 percent of all metal working processes (Kalpakjian, 2008). Most of the steels produced are rolled into strips, sheets, bars and other shapes such as I-beams and L cross-section. In a rolling process, the raw material (*i.e.*, ingot, billet, slab or sheet) is passed between a set of cylindrical rolls that are usually supported by back up rolls. The cylindrical rolls are rotated in opposite directions. During rolling, the roll gap being less than the thickness of the entering material, the rolls grip the material, reduce its thickness and force it through to the exit.

The final shape of the product requires the different types of rolling processes. In industry, various shapes of the rolled product obtained by different types of rolling processes *viz.*, flat rolling, ring rolling, profile rolling, thread rolling, tube rolling, and powder rolling. A variety of roll arrangements is found in the rolling mills such as two-high, four-high and planetary mills. Among all these processes, the most basic and widely used process is the flat rolling, where the rolled products are flat strips or sheets. In the process, the thickness of a sheet is reduced by passing it between two counter-rotating rolls. Figure 1.1 shows a three-dimensional

schematic diagram of a flat rolling process. The figure shows counter rotating rigid rolls, metal strip being rolled and the rolling direction.

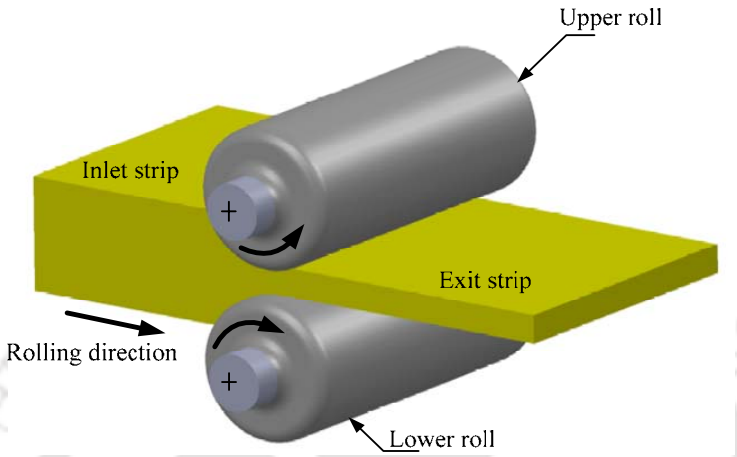

Fig. 1.1. Schematic diagram of flat rolling

Rolling process can be classified into three categories *viz*., cold, warm and hot rolling. It has been suggested (Hirschvogel, 1979; Hawkins, 1981; Hawkins, 1985; Pietrzyk and Lenard, 1990) that for hot rolling, the lower limit of the temperature range should be taken as $0.6T_m$, where T_m is the melting point of the metal in K. In hot rolling, the effect of strain hardening is removed by the relevant active dynamic and/or static softening mechanisms. In cold rolling, the upper limit of working temperature is $0.3T_m$ and strain hardening is not relieved. If the working temperature for the metal is 0.3–0.6 T_m during rolling, then it is defined as warm rolling process. In this range of temperature, the degree of strain hardening that occurs is less as compared to cold rolling.

Warm rolling combines the merits of hot and cold rolling, for example, lower load and energy requirement compared to cold rolling, better surface finish and dimensional precision than the hot rolling (Subramanian and Bourell, 1984). In addition, the mechanical properties may also be improved by warm deformation processing at certain intermediate temperature (Hawkins and Tsinopoulos, 1978). Also, the warm rolling is a cost saving process over the cold and hot rolling processes. This underscores its increased use as a manufacturing process in

industries. Table 1.1 summarized the merits and demerits of warm rolling over the hot and cold rolling.

Table 1.1. Merits and demerits of warm rolling compared to cold and hot rolling

	Warm rolling compared to cold rolling	Warm rolling compared to hot rolling
Merits	• Lower forces are required for deformation. • Less residual stresses get produced in the product. • Ductility of the material is increased. • Complex shape can be obtained by applying less energy. • It produces less anisotropy in the product.	• The product with improved strength properties may be obtained. • Less strain hardening occurs during the process. • Better precision of component is obtained. • Better surface finish and superior dimensional control of the product is obtained. • There is lesser thermal shock on the rolls. This causes lesser thermal fatigue on rolls and provides greater life.
Demerits	• Arrangement has to be made for the heating of the material. • Rolled product has poorer surface finish. • Arrangement for cooling of the rolls is needed for achieving long life of the rolls.	• Higher forces are required for deformation. • Rolled product has lesser ductility. • New grains cannot be formed in the product after rolling.

The modelling of warm rolling process drew the attention of a number of researchers in view of its significant contribution to the overall cost of the product (Subramanian and Bourell, 1984; Hawkins, 1985; Koohbor, 2015). The modelling is essential for the proper control and optimization of the process. This requires the input data about material properties as well as process parameters. In batch production mode of rolling with newer materials, it may be difficult to determine the input parameters offline. In view of it, in this thesis, a methodology to estimate these parameters by the measurement of exit temperature and slip is developed. The main focus of this thesis is the inverse estimation of material parameters, convective heat

transfer coefficient and friction in warm flat rolling. The practical importance of inverse estimation of material and process parameters in rolling process is briefly described in the next section.

1.2 Importance of Inverse Estimation in Flat Rolling Process

The mathematical modelling of rolling process has drawn the attention of a number of researchers. Different analytical and finite element method (FEM) based models have been developed to find out the roll-force, roll-torque, slip, temperature of the roll and temperature of the strip. However, the difficulty in using these models is that many times the input data about material properties and the process parameters are not known. These material properties and the process parameters can be determined by experiments. Conducting separate experiments for the determination of material properties are tedious and time consuming. Moreover, in a dynamic environment, the work material is changed frequently. The inverse method is of great importance for finding out the material properties and the coefficient of friction in rolling (Lenard and Zhang, 1997; Byon *et al*., 2008). The inverse method utilizes the output response of the process to estimate the input parameters. This needs an optimization technique to minimize the error between the computed and the measured data. The inverse method allows reducing the experimentation for estimating the material properties and the coefficient of friction. The method may be implemented in the shop floor for the online determination of material and process parameters in rolling process.

Figure1.2 shows a schematic diagram of continuous casting where molten metal is directly coming into the mold through tundish. In continuous casting, the slab is made directly from the molten metal, whose material properties are not known. The slab is subsequently rolled into strip in a continuous manner. The inverse methodology can be used for estimating the material properties of the slab, which will be useful for the control of the subsequent rolling process. Moreover, it may be possible to predict the product quality with proper mathematical modelling.

A direct mathematical model is essential for carrying out the inverse estimation. In the present thesis, an inverse methodology is proposed to estimate the mechanical properties, thermal parameters and the coefficient of friction based on the exit temperature of the rolled strip measurement.

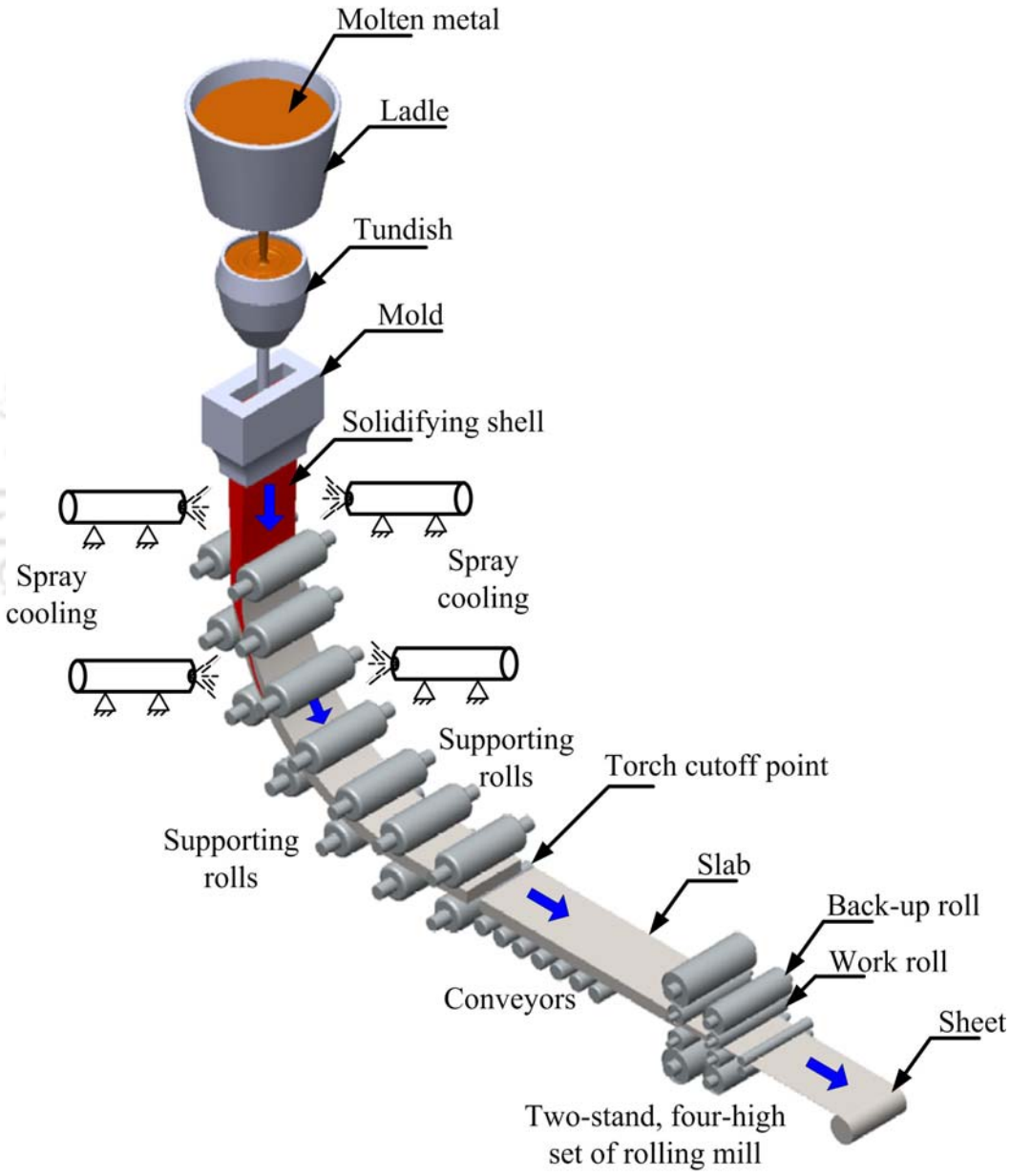

Fig. 1.2. Schematic diagram of continuous casting with subsequent rolling

1.3 Scope and Objectives of the Present Thesis

In the existing literature, most of the studies deal with the determination of roll-force, roll-torque, slip, stresses, strain-rate, strain in the deformation zone, and temperature of the roll as well as strip with the given input parameters. The determination of the input parameters is very crucial due to certain difficulties involved in the experimentation. For example, the flow stress is a function of strain, strain-rate and temperature; however, often this can be determined only as a function of strain and temperature due to the unavailability of high strain-rate material testing facility. This may result in inaccuracy in the analysis. In actual practice, the strain rate significantly affects the flow stress. In the present work, an inverse methodology is proposed, which is capable of estimating the flow stress as a function of strain, strain-rate and temperature by performing a few experiments on the rolling mill itself. The inverse estimation of the thermal properties of materials and the convective heat transfer coefficient in rolling has not been studied by any researcher. The proposed methodology can also be used to obtain the thermal properties of the materials and the convective heat transfer coefficients.

1.4 Organization of the Thesis

The thesis consists of eight chapters, which are organized as follows:

- The current chapter provides the introduction along with the primary objectives and organization of the thesis.
- Chapter 2 presents a review of literature of the deformation as well as thermal modelling of rolling, inverse estimation of material parameters and the coefficient of friction. Inferences from the literature review and detailed objectives of the present thesis have been outlined.
- Chapter 3 presents the steady-state thermo-mechanical model of warm flat rolling. The three different methods to obtain the temperature distribution in the roll are described along with the comparative study. The parametric study is also carried out.

- In Chapter 4, transient thermal analysis of warm flat rolling is presented along with the experimental validation. In-house warm rolling experiments were conducted at different inlet strip temperatures and thickness reductions of strip. The methodology for carrying out the transient analysis of the roll and strip together is presented.
- Chapter 5 deals with the estimation of coefficient of friction in flat rolling by different methods. The coefficient of friction is estimated based on temperature measurement of exit strip by inverse method.
- In Chapter 6, an inverse method to obtain the mechanical parameters and the coefficient of friction in flat rolling based on exit strip steady-state temperature distribution and slip is presented.
- In Chapter 7, inverse estimation of thermal parameters and the coefficient of friction in flat rolling based on transient temperature distribution of exit strip and slip is carried out.
- Conclusion and scope for future work are presented in Chapter 8 followed by references and appendices.

Chapter 2

Literature Survey

2.1 Introduction

Rolling is one of the most popular metal forming processes to reduce the thickness of the sheet. In rolling process, the sheet is passed between two counter-rotating rolls to achieve the desired reduction in the thickness. The process is classified into three categories based on working temperature *viz*., hot, warm and cold rolling. The proper estimation of temperature is important for all kinds of rolling processes, because it greatly influences the lubricant behavior, roll wear and the properties of the rolled product (Louaisil *et al*., 2009).

Warm rolling combines the advantages of hot and cold rolling, for example, lower load and energy requirement compared to cold rolling, better surface finish and dimensional precision than the hot rolling (Subramanian and Bourell, 1984). In addition, the mechanical properties may also be improved by warm deformation processing at certain intermediate temperature. The thermo-mechanical modelling of rolling is essential to analyze the roll force, roll torque, stresses, strain-rates, strains, forward slip, temperature of strip and temperature of roll.

In this chapter, a review of the available literature on the thermo-mechanical modelling of rolling processes is presented. Section 2.2 presents the various approaches of investigations for the mathematical modelling of the deformation analysis of the strip in rolling. The thermal analyses of the strip and the roll carried out by several researchers are presented in Section 2.3. Section 2.4 presents the review of the studies on friction at the roll-strip interface. Section 2.5 discusses the

various techniques for the inverse modelling in the rolling processes. The inference from the literature of the flat rolling process is discussed in Section 2.6. Detailed objectives of the present thesis are presented in Section 2.7.

2.2 Deformation Analysis

A number of theoretical models have been developed during the past decades by making several simplified assumptions to simplify the complex behaviour of the rolling process. The suitability of the developed models depends on the assumptions used. The validity of the assumptions depends on the desired outputs of the model. This section presents a review of the literature from the simplified models to the present day computational methods on the deformation analysis of the rolling. The methods of deformation analysis are slab method, slip-line field method, upper-bound method and finite element method.

2.2.1 One-dimensional Models

The one-dimensional model is mostly based on the slab method to obtain the roll-pressure distribution at the roll-strip interface. The slab method assumes that the metal deforms uniformly in the deformation zone. The metal being deformed is decomposed into slabs. For each slab, simplifying assumptions are made mainly with respect to the stress distributions. Force balance for the slab results in differential equations which are solved either by the closed form analytical methods or numerical methods. The constants of integration are evaluated using appropriate boundary conditions.

The pioneering work carried out by Karman (1925) was the beginning of the mathematical modelling of the rolling process. The author suggested the theory of homogenous deformation based on the equilibrium of forces at an infinitesimal small slab element in the deformation zone of the strip. The slab method is used for analyzing the rolling process to obtain the roll-pressure distribution at the roll-strip interface. Figure 2.1 shows the equilibrium forces acting on an infinitesimal small slab element specified by the angular coordinate ϕ in the roll bite of strip. In the figure, p is the roll pressure, μ is the coefficient of friction, σ_x is the mean

horizontal stress in the slab and R' is the deformed roll radius. Orowan (1943) used a graphical-numerical method of computaional in order to determine the roll pressure distribution, roll torque and the power consumption considering the non-homogeneous deformation. He considered the Coulomb friction model with material incompressibility. Roll flattening is taken into account using Hitchcock (1935)'s formula.

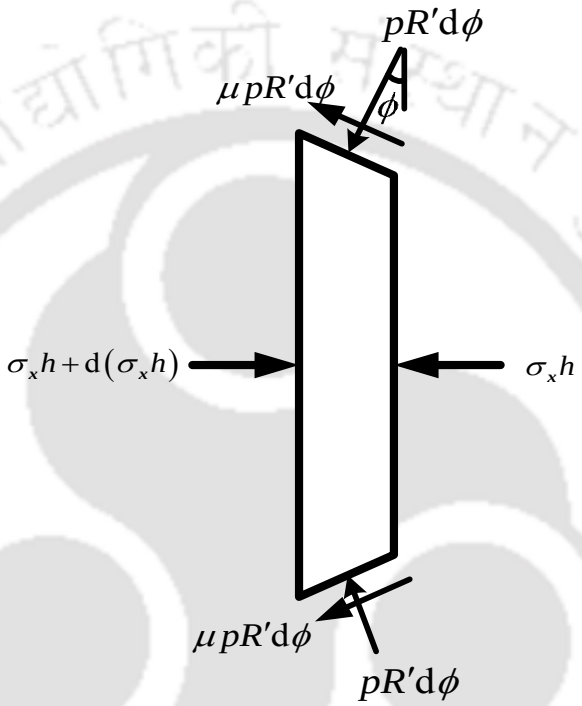

Fig. 2.1. The force acting on the slab at the exit of the roll bite

As pointed out by Hartley *et al.* (1989), the von Karman equation is clearly based on the assumptions and approximations that might cause serious inconsistencies under certain conditions. For example, in cold rolling, at the lower coefficient of friction, the deformation of the material is nearly homogeneous, but the validity of the homogeneous deformation theories becomes weaker by increasing the coefficient of friction. The surface layer is likely to be deformed more than the central region in the deformation zone.

The advantages of Orowan (1943) model over the Karman (1925) model are as follows: (a) the assumption of plane sections remains plane after deformation reduces the problem to one-dimensional, (b) both slipping and sticking friction is

included and (c) the work-hardening of the material is taken into account. Bland and Ford (1948) simplified Orowan's equations by making an assumption of the small contact angle involved. The authors derived equations for obtaining the roll force and the roll torque with and without the front and back tensions. Bland and Sims (1953) developed an approximate analysis for the rolling considering the effects of elastic deformation at the entry and exit of the deformation zone.

Alexander (1972) used the Orowan's model for computing the roll-force and the roll-torque considering inhomogeneous deformation. Roychoudhury and Lenard (1984) modified the model of Orowan (1943). They obtained the elastic deformation of the roll by incorporating a two-dimensional theory of elasticity instead of Hitchcock (1935)'s formula. The Hitchcock's formula is given as

$$R' = R\left(1+\frac{16\left(1-\nu_r^2\right)}{\pi E_r}\frac{F_r}{\delta}\right), \tag{2.1}$$

where F_r is the roll force per unit width of the strip, ν_r is the Poisson's ratio of the roll material, E_r is the Young's modulus of the roll material and δ is the draft. However, the formula is not suitable for foil rolling. The Hitchcock's formula of roll deformation has been used by many researchers. The elastic loading and unloading regions in the rolled strip at the entry and exit are analyzed using the one-dimensional theory of elasticity. The locations of the elastic and/or plastic interfaces are determined during the solution procedure by using the Huber-von Mises criterion of plastic flow.

In earlier studies, the roll force is obtained by integrating the roll pressure distribution along the arc of contact. For avoiding the integration and also convenient form for the calculation of the roll force, Eklund (1933) had proposed the following equation based on the study of metal flow during plastic deformation:

$$F_r = \bar{\sigma}\sqrt{\frac{D'\delta}{2}}\left(1+\frac{1.6f\sqrt{\frac{D'\delta}{2}}-1.2\delta}{h_1+h_2}\right), \tag{2.2}$$

where F_r is the roll force, $\bar{\sigma}$ is the mean plane yield strength, D' is the deformed roll diameter, $\delta = (h_1 - h_2)$ is the draft, f is the Coulomb's coefficient of friction, and h_1 and h_2 are the inlet and exit thickness of the strip respectively. The formula provided by Eklund's was very popular in the past due to its simplicity. Later on Roberts (1965) proposed a simplified model assuming uniformity of pressure along the arc of contact. As the variation of pressure in the bite zone is not taken into account, this model may be called a zero-dimensional model. The relation to obtain the roll force can be written as

$$F_r = \sigma_c \left(l_p + l_E + L_F \right) = \sigma_c L_e, \tag{2.3}$$

where σ_c ,l_p, l_E, l_F and L_e are the average compressive yield strength, the lengths associated with the actual plastic reduction of the strip, the flattening of the work rolls by the normal roll force and the flattening due to frictional effects, effective length of the arc of contact (not equal to the actual), respectively. The calculation of the effective length is provided in the book by Roberts (1978) in detail. The work roll flattening is calculated based on Hitchcock (1935)'s formula.

Of late, the slab method has been replaced by more sophisticated methods. However, a few researchers have used the slab method with modified analysis of roll deformation for thin strips or temper rolling analysis. Fleck and Johnson (1987) studied the foil rolling by assuming that the rolls remain circular. The extension of Fleck and Johnson (1987) model was carried out by Fleck *et al*. (1992) to develop a theory for cold rolling of foil. They considered Coulomb friction model and deformation of the rolls is modeled by treating them as elastic half-spaces. However, they did not take into account the effect of frictional traction on roll deformation and strain hardening. In their model, the roll–strip interface is split into 5 zones *viz*., elastic zone at entry, plastic reduction at entry, no-slip neutral zone, plastic reduction at exit and elastic zone at exit (Fig. 2.2). The inlet and outlet thicknesses of the strip are denoted by h_1 and h_2, respectively. In zone II, thickness is reduced from h_1 to h. The strip thickness is approximately constant at h in zone III. The strip thickness reduces from h to h_2 in zone IV. Zone I and zone V are often negligible barring the case rolling of very thin foil. The equilibrium of the strip is used to find the variation of pressure with rolling direction in the slipping zones. For the no-slip

neutral zone, a matrix equation is assembled for relating the roll deformation to the normal pressure that is inverted to find the pressure distribution in this region. To satisfy the continuity conditions at the boundaries between each of the zones, the positions of these boundaries are obtained using Newton–Raphson scheme.

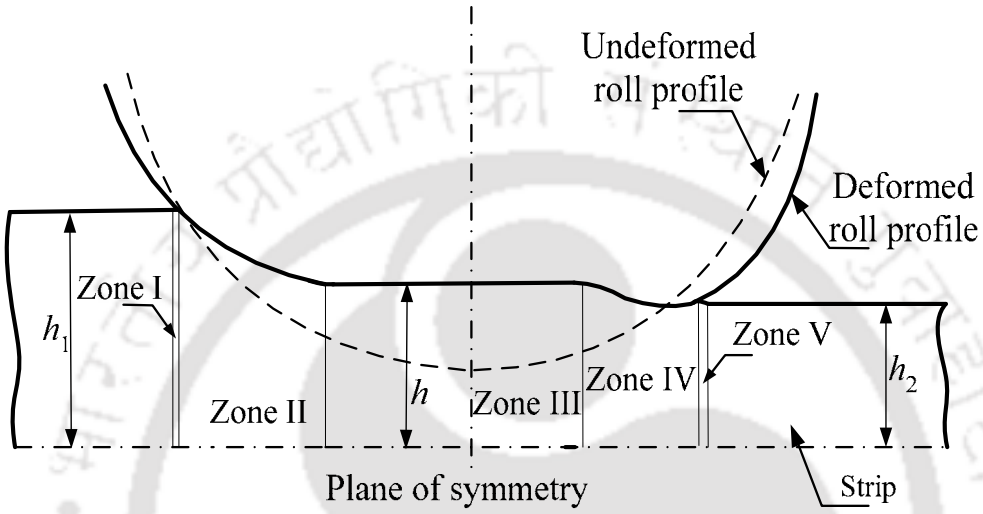

Fig. 2.2. A schematic diagram of thin foil rolling showing 5 zones as per the model of Fleck *et al*. (1992) (1-D representation)

Yuen *et al*. (1996) extended the work of Fleck *et al*. (1992) to incorporate strain hardening and the variation of yield stress in the roll bite. They also conducted the experiments to validate the results obtained from the theoretical model. Le and Sutcliffe (2001) developed an analytical model for the analysis of cold rolling of thin strip and foil. They followed the model proposed by Fleck *et al*. (1992), but relaxed their assumption of flat central neutral zone. Instead they used Hook's law for plane strain condition to calculate the pressure profile in the central region. Shi *et al*. (2001) observed significant difference between the roll torque computed by the energy balance method and by balancing the moments of forces exerted on the roll by the strip. As the center of the roll may not be at the point at which the moment is taken, the energy method is more reliable compared to the method of taking moments. Kumar and Dixit (2006) studied the foil rolling by incorporating the effect of the strain hardening and friction. In their slab method model, the roll torque is calculated by balancing the energy.

Recently, Chen *et al*. (2014) improved Karman (1925) differential equation to adapt it for hot rolling and obtained the roll-pressure distribution in the roll bite. In their model, the roll bite is divided into slipping and sticking friction zones. The authors assumed that the slipping friction occurred if the frictional stress was less than the shearing yield limit of the rolled metal. If the frictional stress was equal to the shearing yield limit, then the sticking friction occurred. For different zones, the corresponding friction laws are applied to derive the differential equation.

The slab method is suitable for plane strain conditions and is based on several assumptions. The limitation of the slab method is its inability to incorporate non-homogenous deformation. In the following subsections, the slip-line field, upper bound and finite element models are presented, which provide greater insight into the deformation in rolling.

2.2.2 Slip-line Field Models

A slip-line is a shear line which is tangent to the surface of the maximum or minimum shear stress at every point. During rolling process, the material slips (deforms) along the slip lines. The slip lines also satisfy the yield condition and represent a possible flow field everywhere in the deformation zone of the metal. The boundaries between the roll and the metal (strip) outside the plastic zone are treated as rigid zones. The slip-line method is based on several assumptions. The slip-line field approach is limited to the plane-strain problems. However, the slip-line method has been applied to many practical problems giving good agreement with the experimental observations. The slip-line field method has also been used for analyzing the rolling process.

The slip-line method is a mathematically well defined method to obtain the stress field in a plane strain metal forming problem. However, it becomes very difficult to find a slip-line field which satisfies all the imposed boundary conditions for complicated tool geometry and the computational time increases tremendously with increasing geometrical complexity.

Hartley *et al*. (1989) presented a detailed review on the applicability of slip-line field method to analyze the rolling processes. Alexander (1955) presented a slip line field solution for hot rolling of wide sheets. The slip-line field solutions for cold rolling were proposed by Firbank and Lancaster (1965, 1966 and 1967). They

calculated the velocity distribution, local stresses and pressure distribution. Firbank and Lancaster (1965) proposed a slip line field solution, which predicts a pressure drop in the middle of the arc, an unrealistic observation. The solution based on the slip-line field considering lubricated cold rolling problem is reported by Firbank and Lancaster (1966 and 1967).

Collins (1968) presented a matrix algebraic representation of slip-line geometries. He developed the computational procedure by approximating the linear operators using finite-dimensional matrices. Further, he presented a slip line field solution that showed the presence of small rigid regions in the arc of contact. However, work hardening of the material was not considered. Dewhurst *et al.* (1973) presented a series of slip-line field solutions for hot rolling of wide strip. These solutions are obtained numerically by solving the governing differential equations. Nepershin (1999) analyzed a symmetrical steady-state plane strain hot rolling problem by the slip-line method considering a rigid-plastic material model.

Recently, Oluwole and Olaogun (2011) presented a detailed review on the different methods to analyze the rolling processes. The authors analyzed cold rolling sheet mill by slip-line field method for the first and second passes in a lubricated 4-high reversing mill. The results obtained from their model are validated experimentally. The authors concluded that each rolling pass needs construction of separate slip-line fields.

The slip-line field method is suitable for plane strain conditions and is based on several assumptions. The main drawback of the slip-line method is its inability to incorporate strain hardening effect easily. Solving the complex problems associated with metal forming is difficult task by slip-line field method. Hence, other methods have been tried by many researchers. The methods like upper bound method and finite element analysis were used to analyze the rolling process.

2.2.3 Upper Bound Models

The upper bound method is a technique based on the assumed kinematically admissible velocity field, which satisfies the continuity equation and all the velocity boundary conditions. The total power obtained based on the assumed velocity

provides an upper bound on the actual power. This method does not impose any requirement of stress equilibrium and stress boundary conditions. This method is used for estimating the power in rolling. Johnson and Kudo (1960) used upper bound solution to estimate the temperature distribution using the concept of stream line for a material which is deformed plastically at faster rate. The work of plastic deformation was calculated using upper bound method. The authors neglected the loss due to conduction and radiations while assuming the temperature of rolled metal same as the surrounding temperature. The material has been assumed to be rigid-perfectly plastic. Green and Wallace (1962) developed an upper bound approach assuming that the material in the roll gap is rigid-perfectly plastic and the shear stress along the arc of contact attains the value of the shear yield stress in plane strain. It was extended by Green *et al*. (1964) to include the cases of slipping and combined slipping and sticking.

Avitzur (1964) applied the upper bound method for the analysis of rolling process by assuming a continuous velocity field. It provides an expression for the roll torque and the neutral point location for non-hardening material. However, the important design parameters such as roll-force and pressure distribution were not determined. Zhu and Avitzur (1988) analyzed the central burst and split end defects in plane strain rolling by applying the upper bound method coupled with the principle of minimum energy. They applied the concept that the defects occur if the power required for defect-free rolling is more than the power required in the presence of defects.

Lahoti *et al*. (1980) studied the effects of the roll-force and the roll-torque at different reductions theoretically as well as experimentally. In their model, they used Hill's (1963) kinematically-admissible velocity field to derive the expressions for the strain-rate components and equivalent strain-rate. They also used upper bound method for estimating the lateral spread, elongation, boundaries of deformation zone and the location of neutral point.

In general, the upper bound method provides the velocity, strain rate and strain fields but it is unable to determine the accurate stress distribution in the deforming material. In view of this, Marques and Martins (1990) analyzed the plane strain rolling process by dividing the deformation zone into several sub-domains.

The study is based on a general kinematically admissible velocity field using the method of weighted residuals to determine the stress field. Doğruoğlu (2001) introduced a method to construct the kinematically admissible velocity field in the deformation zone. The author introduced elliptical flow lines to represent the flow material in the deformation zone. Sezek *et al*. (2008) developed a three-dimensional model of the plate rolling process using the upper bound method. They used dual stream functions for deriving a kinematically admissible velocity field considering spread.

Limitations of using the upper bound method when there is Coulomb's friction at the interface have been pointed by Drucker (1954). Collins (1969) observed that the usual definition of a kinematically admissible velocity field is unnecessarily restrictive when the upper bound theorem is applied. The author also developed a generalized upper bound theorem which can be used to solve many problems of practical interest in the presence of Coulomb's friction. The FEM model of Dixit and Dixit (1996) incorporated this generalized upper bound theorem for the accurate estimation of neutral point. Sheikh (2009) used the upper bound method to estimate the power in the rolling of strip. The temperature distribution in the strip is also determined.

2.2.4 Models based on Finite Element Methods

Traditional methods used to analyze the rolling processes *viz*., slab method, slip-line field method and upper bound method are based on several assumptions and provide limited information about the deformation. The finite element method coupled with analytical approaches is capable for the fast and complete information of the field variables. The fully analytical models are inadequate for the modelling of forming processes with high complexity. Conceivably the most versatile of the computer-based analysis method is the finite element method. In this method the material to be processed is mathematically divided into many elements or domains each of which is assumed to deform in very simple manner but collectively deform in a very complex manner.

Finite element method (FEM) originated in the field of structural analysis. It has been rapidly expanding to a wider range of non-structural problems for which exact solutions cannot be found with the traditional techniques. As the finite element method together with high-speed computers is capable of predicting the detailed distribution of field variables. The models are considered to be two-dimensional (plane strain) or three-dimensional. Predominantly, finite element analysis of metal forming problems involves large strain and inclusion of material as well as geometric nonlinearities. The finite element method is expected to be used for simulating metal forming processes, because realistic boundary conditions and material properties can be taken into account. In most of the rolling analyses, the roll is modeled as a rigid or an elastic body. For material behaviour, viscoplastic, rigid-plastic, elasto-visco-plastic or elastic-plastic model is used. Finite element method is preferred to other methods, as it is able to relax many of the simplifying assumptions; it can easily incorporate non-homogeneity of deformation, temperature dependent material properties and different friction models.

A number of researchers have employed finite element method for analyzing the rolling problem. Domanti and McElwain (1998) reviewed works of many researchers that are based on the finite element modelling as well as other traditional methods in the flat rolling of the metal strip or sheet. Finite element analysis for rolling process has primarily followed two parallel approaches namely Eulerian flow formulation and updated Langragian formulation. Literature also contains another hybrid model, which is termed as mixed or combined Eulerian-updated Langragian formulation (Abo-Elkhier, 1997).

In the updated Lagrangian formulation, the mesh moves and deforms in space, in accordance with the deformation history of the material (Shangwu *et al*. 2003). In an early attempt, Tamano (1973) formulated an elastic-plastic material model which is suitable for small reduction skin-pass rolling. Liu *et al*. (1985) incorporated an elastic-plastic finite element model to solve a plane-strain rolling problem. The yielding is based on von-Mises criterion and plastic flow on the Prandtl-Reuss relationship. The effect of unloading is also included. Shivpuri and Chou (1989) included dynamic effect in the elastic-plastic finite element analysis of strip rolling. They observed that the elastic response of the roll has a major influence

on roll force and roll torque results at high R/h_1 ratios (roll radius to strip thickness ratio). Lindgren and Edberg (1990) used explicit as well as implicit finite element formulation in the simulation of rolling. They reported that the roll force prediction using both the formulations is in better agreement with the experimental results. Further, they discussed some of the advantages of explicit formulation over implicit formulation. Lee (1998) carried out a three-dimensional elastic-plastic finite element analysis of strip rolling. The material to be rolled is assumed to be an elastic-plastic solid which undergoes large elastic and plastic strains during the rolling process. Most of the researchers have used Eulerian flow formulation for analyzing the rolling process because in the updated Lagrangian formulation finite element mesh may be completely distorted after a number of increments in the case of large deformation. Remeshing becomes inevitable, which is inefficient and computationally expensive (Gelton and Koter, 1982). Abo-Elkhier (1997) also illustrated the advantages of Eulerian flow formulation over the updated Lagrangian formulation while modelling of strip cold rolling using Eulerian fixed mesh technique.

In the past, researchers have assumed no slipping between the strip and the roll surfaces to provide a simple velocity boundary condition in plane-strain rolling. Employing this assumption, Tamano and Yangimoto (1975) determined the stress and strain distributions in skin-pass rolling by the elastic-plastic finite element method. In their approach, the error in the stress due to the numerical integration accumulates significantly when a large deformation is simulated. Rao and Kumar (1979) analyzed a plane strain rolling problem using the finite element method. The incremental displacement method was used for the non linear analysis of the problem. They studied the convergence of the method, the flow of the material under the rolls and the pressure distribution on the rolls.

In Eulerian or flow formulation, the material to be rolled is considered as a rigid-plastic material behaving like non-Newtonian fluid and a spatial description is used, whose independent variables are the present position occupied by the particle and present time. As this method fixes the attention on a given region of space, it is suitable for the steady-state problems. The application of the rigid-plastic

formulation for simulating metal forming processes started about in 1970s and with pioneering works of Lee and Kobayashi (1973) and Zienkiewicz and Godbole (1974) who considered the metal forming process (like extrusion and punching) as a flow of plastic solid and developed a rigid-plastic finite element technique. Zienkiewicz *et al*. (1978) considered the rolled material to be rigid-visco-plastic and incompressible. They simulated the friction at the roll-strip interface by introducing a thin layer whose yield strength is assumed to be function of the friction and mean stress of the material. However, neutral point was not estimated in their formulation.

Atreya and Lenard (1979) developed a model that is a combination of a finite element method and slab method. The model describes the roll deformation with an elastic finite element model while the strip deformation is described with a slab model. The roll torque obtained from the model is in better agreement with the experimental results in comparison to Orowan (1943) model. However, the roll-force predicted by Orowan (1943) model is more accurate. Mori *et al*. (1982) minimized a functional with respect to the position of neutral point in their formulation, thus making the analysis more realistic. They have used Coulomb's friction model in their formulation. Velocity-dependent friction frictional stress for the treatment of the neutral point problem was developed by Li and Kobayashi (1982). Assuming the existence of rigid-plastic material and rigid roll, Li and Kobayashi (1982) have compared their predictions with the previously reported experimental results in the literature and observed that there is a good agreement between the FE based results and experimental results.

Park and Kobayashi (1984) used the rigid-visco-plastic FE method for three-dimensional analyses. They found that the interface friction did not remain constant during deformation. Kim *et al*. (1991) studied the three dimensional shape rolling by extending the two dimensional rigid-plastic FEM model with the slab method. Gratacos *et al*. (1992) considered the elastic deformation of the rolls in their finite element analysis for thin strip rolling. Hwang and Joun (1992) developed an approach based on the rigid-viscoplastic finite element method and employed a penalty algorithm to relax the contact boundary condition for the determination of the stress distributions at the roll-strip interface. Prakash *et al*. (1995) presented a FEM formulation in which the neutral point is found iteratively from the condition

that the interfacial shear stress changes its sign at the neutral point. Dixit and Dixit (1996) proposed a model for steady-state plane strain cold rolling of a strain hardening material using the mixed pressure velocity formulation to measure the deformation and torque of the material. The model is able to predict important design parameters without any need of a highly refined mesh in the plastic zone. The authors also carried out the analysis with the help of fuzzy set theory in which the material properties and the coefficient of friction are taken as fuzzy input parameters. Dixit and Dixit (1997a) extended their FEM model to present the results of modelling of anisotropy for cold flat rolling using an appropriate yield anisotropy criterion. Dixit and Dixit (1997b) further attempted the different approaches for determining the residual stress and discussed the difficulties associated with the methods. The authors reported a simplified approach to find the longitudinal residual stress (stress in the direction of rolling) using the flow formulation. A detailed parametric study was carried out to show the influence of process parameter on the residual stress distribution pattern. Thomson (1982) and Malinowski and Lenard (1992) used updated Lagrangian formulation and mixed Eulerian-updated Lagrangian, respectively. However, these approaches are computationally expensive. Chandra and Dixit (2004) studied the temper rolling process using a rigid-plastic FEM model. They analyzed the roll deformation by assuming the roll to be an elastic half-space.

Artificial neural network models have been used for faster prediction of the roll force and roll torque. Some researchers attempted to assist the FEM model by a neural network modelling for enhancing the computational efficiency. For example, Gudur and Dixit (2008a) presented a methodology for assisting a FEM model by neural network modelling. The authors employed a neural network model for the prediction of velocity field and location of neutral point. The neural network is trained by using the data obtained from a FEM model. The well trained neural network provides a highly accurate guess of a complete velocity field and the location of neutral point, which is employed for finding out the refined velocity field and pressure field using an FEM model. The refined velocity and pressure field is post processed for computing the roll force, roll torque, stress, strain-rate and strain

fields. It is observed that the neural network assisted FEM modelling has a potential of providing a highly accurate results with less computational time.

A few researchers employed neural networks modelling for the prediction of roll force and roll torque (Larkiola *et al*., 1998; Gunasekera *et al*., 1998; Chun *et al*., 1999; Dixit and Chandra 2003; Yang *et al*., 2004). In most of these works, neural networks are trained using the data obtained from either FEM model or experimental results. Theses trained networks have the capability to predict roll force and roll torque. However, these models did not predict stress, strain-rate and strain fields. Gudur and Dixit (2008b) used the finite difference method (FDM) to obtain the pressure field. The authors used a mixed pressure-velocity FEM formulation to obtain the velocity field during the rolling process. In their work, the values of Levy-Mises coefficient and strain-rate components are predicted by neural network modelling. These values were required for the FDM model for solving the momentum equation. It was found that the proposed method provides a good agreement with experimental results.

Zhang *et al*. (2010) developed a fast rigid-plastic FEM model for the online estimation of the roll force. The authors employed five-step procedure to obtain the roll force in plane strain rolling. First a refined neural network was established to generate the initial guess. The initial guess is treated as an input for the Newton-Raphson iteration. Secondly, the Hessian matrix is divided into sub-domains for performing the parallel computation. Thirdly, a method is employed to speed up the line search for the relaxation factor. Fourthly, the energy functional is partitioned according to the numbering of elements for parallel computing. Finally, an energy method with high numerical stability is proposed for predicting the rolling force. The fast rigid-plastic FEM is able to enhance the computational speed along with the required accuracy.

The finite element method (FEM) is widely used for analyzing complex rolling process. This method is capable of predicting quite accurate deformation behaviour such as stress distribution, roll force, roll torque, forward slip and temperature of the roll and strip. The analyses using FEM techniques can be computationally expensive and the time required for a fully converged solution.

Figure 2.3 shows some of the major contributions in the modelling of deformation in the rolling process.

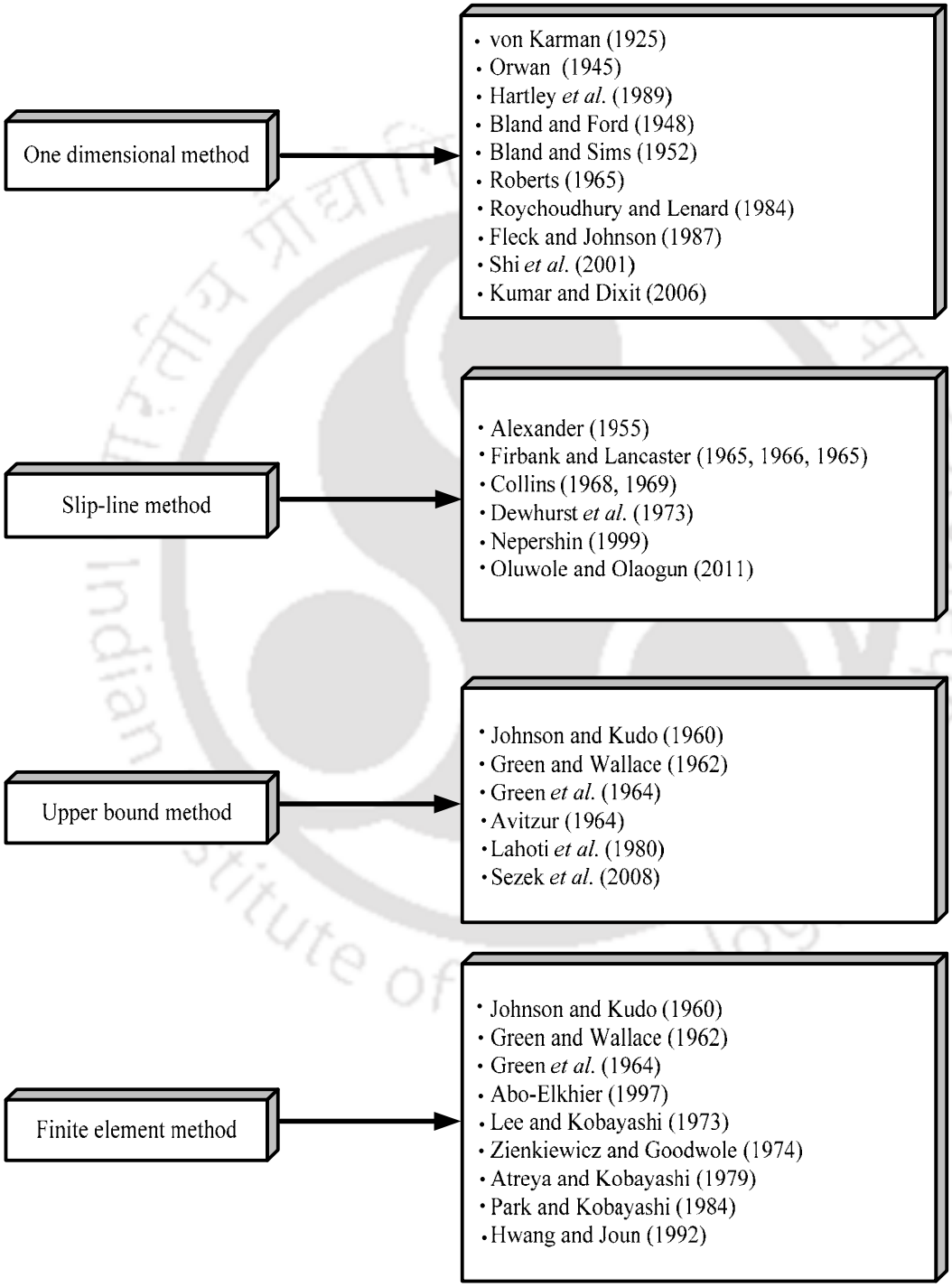

Fig. 2.3. Representative papers in the deformation modelling of rolling process

2.3 Thermal Analysis

In the literature, various methods have been employed to solve the governing heat transfer differential equation. The analytical and numerical methods are used to obtain the temperature field in the roll and the strip. The analytical methods are usually based on the separation of variables or integral transform techniques and the numerical methods include the finite difference method (FDM) and finite element method (FEM). Several researchers carried out both the steady-state as well as the transient temperature distribution in the rolls and the strip, whilst many concentrated on the steady-state solutions (Hwang *et al*., 1993; Tseng, 1993; Galntuchi and Tricarico, 1999; Shahini, 2009; Khalili *et al*., 2012; Koohbor *et al*., 2015). In the following subsections, the different methods used to compute the temperature distribution in the rolls and the strip are summarized.

2.3.1 Method of Separation of Variables

In the method of separation of variables, the underlying assumption is that the solution function can be broken down to as a product of two or more functions, which contains the lesser number of the variables than the original solution function. Patula (1981) used a classical approach of separation of variables with complex functions to obtain the steady-state temperature distribution in the roll. An Eulerian reference frame has been used. The axial heat conduction in the roll is neglected considering the length of the roll to be large. The thermal properties considered are independent of temperature. However, only the roll was analyzed; the analysis of the strip has not been carried out.

Tseng *et al.* (1990) developed an analytical model to determine the temperature distribution of the rolls and strip using an Eulerian approach. The strip temperature is obtained by solving the governing heat transfer equation using the method of separation of variables. The roll temperature is estimated using the Fourier integral technique. At the roll-strip interface, the average temperatures of the roll and the strip are matched. Thus, a perfect contact between the roll and the strip is assumed. Yuan (1985) has considered a scale layer between the roll and the strip. The heat generation due to the plastic deformation and friction is calculated

numerically by Maslen and Tseng (1981) model, which is essentially a slab method model.

Arif *et al*. (2004) studied the temperature distribution in the rolls and the strip based on the work of Patula (1981) and Tseng *et al*. (1990). However, the difference is that they considered a non-uniform heat input into the roll from the strip in the analysis. They carried out the deformation as well as steady-state thermal analysis of the strip. The flow stress model in the strip takes into account the effect of the strain, strain-rates and the temperature. However, the roll deformation is not considered. The maximum 5% deviation is observed by employing the assumption of uniform heat input to the roll.

2.3.2 Integral Transform Technique

The integral transform of a function $f(t)$ is defined by the following definite integral:

$$F(\beta) = \int_a^b K(\beta, t) f(t) \mathrm{d}t . \tag{2.4}$$

This function $F(\beta)$ is called the integral transform and $K(\beta, t)$ is called the integral kernel of the transform. The integral transform method solves the partial differential equations along with initial and boundary conditions. Laplace transform is a type of integral transform.

Fischer *et al*. (2001) used a Laplace transform technique to find the temperature distribution in the roll. They neglected the heat conduction in the circumferential direction considering high rotational speed. Fischer *et al*. (2004) proposed an approximate solution for plane strain hot rolling using Laplace transform technique and compared it with the FEM results of Sun *et al*. (1998) and Hwang *et al*. (2002). The maximum deviation is lesser than 10%.

A transient analysis is carried out by DesRuisseaux and Zerkle (1970) using the Laplace transform technique. They presented an analytical approach to compute transient temperature distributions and circumferential stresses in a work-roll surface. The analytically obtained temperature distribution of the work-roll surface is compared with experimental results of Stevans *et al*. (1971). Guo (1998) proposed a Laplace transform method to obtain transient solution for a particular boundary condition. The Duhamel's theorem was used to obtain the complete solution for

various boundary conditions. However, the thermal analysis of the strip was not carried out.

2.3.3 Finite Difference Method

The finite difference method (FDM) is a numerical method for solving differential equations by approximating them with difference equations, in which finite differences approximate the derivatives. The domain is partitioned in space as well as in time and solution is calculated at the discrete points in the space and time. In essence, the differential equation gets converted into a system of simultaneous equations. To obtain the temperature between two adjacent points of the finite difference grid, the interpolation can be carried out.

Lahoti *et al*. (1978) presented a finite difference method (FDM) model to find the temperature distribution in the roll and the strip. The upper bound method is used to estimate the roll force and roll torque under hot rolling conditions. Tseng (1984) developed an FDM model to estimate the temperature distribution in the roll and the strip. The input data for the heat generation was taken by the direct measurement of power. Further, the 6.5% of the 90% total power was assumed to dissipate as friction heat. An Eulerian formulation is employed. Considering high speed rolling, an upwind differencing scheme is chosen to overcome the numerical instability. Assuming the surface temperatures of the roll and the strip becomes equal by neglecting the thermal resistance of the film at the interface (Tseng, 1984):

$$\left(T_r\right)_b = \left(T_s\right)_b, \tag{2.5}$$

where subscript *b* represents boundary, respectively. The heat flux into the roll and the strip at the interface must equal the heat generated by friction, *i.e*.,

$$k_r\left(\frac{\partial T}{\partial r}\right)_{br} + k_s\left(\frac{\partial T}{\partial n}\right)_{bs} = q_f, \tag{2.6}$$

where $\partial/\partial n$ represents differentiation along the normal to the strip boundary (positive outward), k_r and k_s are the thermal conductivity of the roll and the strip, respectively, q_f is the heat generated due to friction at the roll-strip interface. The boundary condition for the remaining region of the roll circumference is

$$k_r\frac{\partial T\left(R,\theta\right)}{\partial r} = h\left(\theta\right)\left\{T_\infty - T\left(R,\theta\right)\right\}, \tag{2.7}$$

where T_∞ is the ambient or coolant temperature. However, the methods require too much computational time. Wilson *et al*. (1989) estimated temperature distributions at the roll-strip interface in cold rolling using an FDM model. Only advection parallel to the roll-strip interface and conduction along the thickness direction is considered. The heat distribution between the roll and the strip is obtained by matching the surface temperatures of the roll and the strip.

Chang (1999) used an FDM model assuming a steady state rolling condition and a non-uniform heat flux in the deformation zone to predict the work-roll temperature field and the resulting stresses. Luo and Keife (1998) used an FDM model to investigate the temperatures distribution in the roll and the foil considering the affect of lubricant. Khan *et al*. (2004) studied the temperatures distribution in the roll and the strip using FDM. FDM is a well-established technique for determining the temperature distribution in the roll and the strip. However, it requires a lot of computational time.

2.3.4 Finite Element Method

The finite element method (FEM) has attracted a number of researchers as it helps to find different process parameters and develop the model in rolling process. It gives detailed information about the required force, stress, strain, strain-rate and the roll and strip temperatures distribution of the process. The models can be two dimensional (plane strain) or three dimensional. FEM has been widely used for the modelling of deformation in the rolling. However, like FDM, FEM also requires too much computational time. Shifting of the preference of the researchers from FDM to FEM can also be attributed to the availability of a number of commercial FEM packages. A brief literature review on the estimation of temperature in rolling are presented.

Hwang *et al*. (1993) carried out both deformation and thermal analyses using rigid-viscoplastic FEM model. An iterative scheme is adopted for metal flows and temperature in hot strip rolling. It is assumed that the friction heat is equally divided into the roll and the strip. Sheikh (2009) presented an FEM model coupled with an upper bound method to predict the temperatures distribution during hot strip rolling.

Khalili *et al*. (2012) used combined FEM and slab method to predict the thermo-mechanical behaviour of the roll and the strip during warm strip rolling.

A number of mathematical models are developed to estimate the transient temperature distribution in rolling. Lee *et al*. (2000) presented an FEM based three-dimensional thermal analysis of the roll. The deformation analysis was not carried out; instead a constant value of heat flux input into the roll was assumed. The computational time issue was not discussed. The predicted results match well with the model of Guo (1998) for two dimensional case.

Pietrzyk and Lenard (1990) studied the effect of the temperature rise of the roll during flat rolling by FEM and experiments. They conducted the rolling experiments at different working temperatures and validated their FEM model. Galantucci and Tricarico (1999) carried out the thermo-mechanical simulation of rolling process. However, detailed description of the FEM formulation has not been provided. The sensitivity study of rolling parameters, *viz*., rolling speed, roll radius and reductions in strip was carried out by calculating the temperature. The temperature was calculated at the surface of the plate as well as the roll periphery.

Using FEM, Serajzadeh *et al.* (2002) obtained the transient temperature distribution in the roll and the strip in a multi-stand mill. They also conducted the experiments to validate the FEM model. The hybrid model to analyze the hot rolling was proposed by Serajzadeh (2006). The thermal and deformation analyses were carried out by FEM. During analysis, the flow stress data as a function of strain, strain-rate and temperature was supplied with the help of an artificial neural network (ANN). The model was examined on a low carbon steel strip and a reasonable agreement is shown with experimental data.

Kiuchi *et al*. (2000) developed a three-dimensional FEM model to investigate the temperature distribution in the roll and the strip. The heat generations due to friction and plastic deformation were estimated by FEM. Tudball and Brown (2006) developed a transient 3D FEM model to estimate the temperature distribution in hot rolling of steel. The model was validated with plant recorded data. Yu *et al*. (2012) studied the temperature distribution in the rolling of cold magnesium alloy strips with heated roll.

FEM and FDM based models provide a reasonably accurate temperature distribution in the roll and the strip, but these methods require a lot of computational time. The analytical solutions are usually in the form of summation of some infinite series, in which a judicious decision is required regarding the finite number of terms needed for convergence. Figure 2.4 mentions the representative papers of thermal modelling.

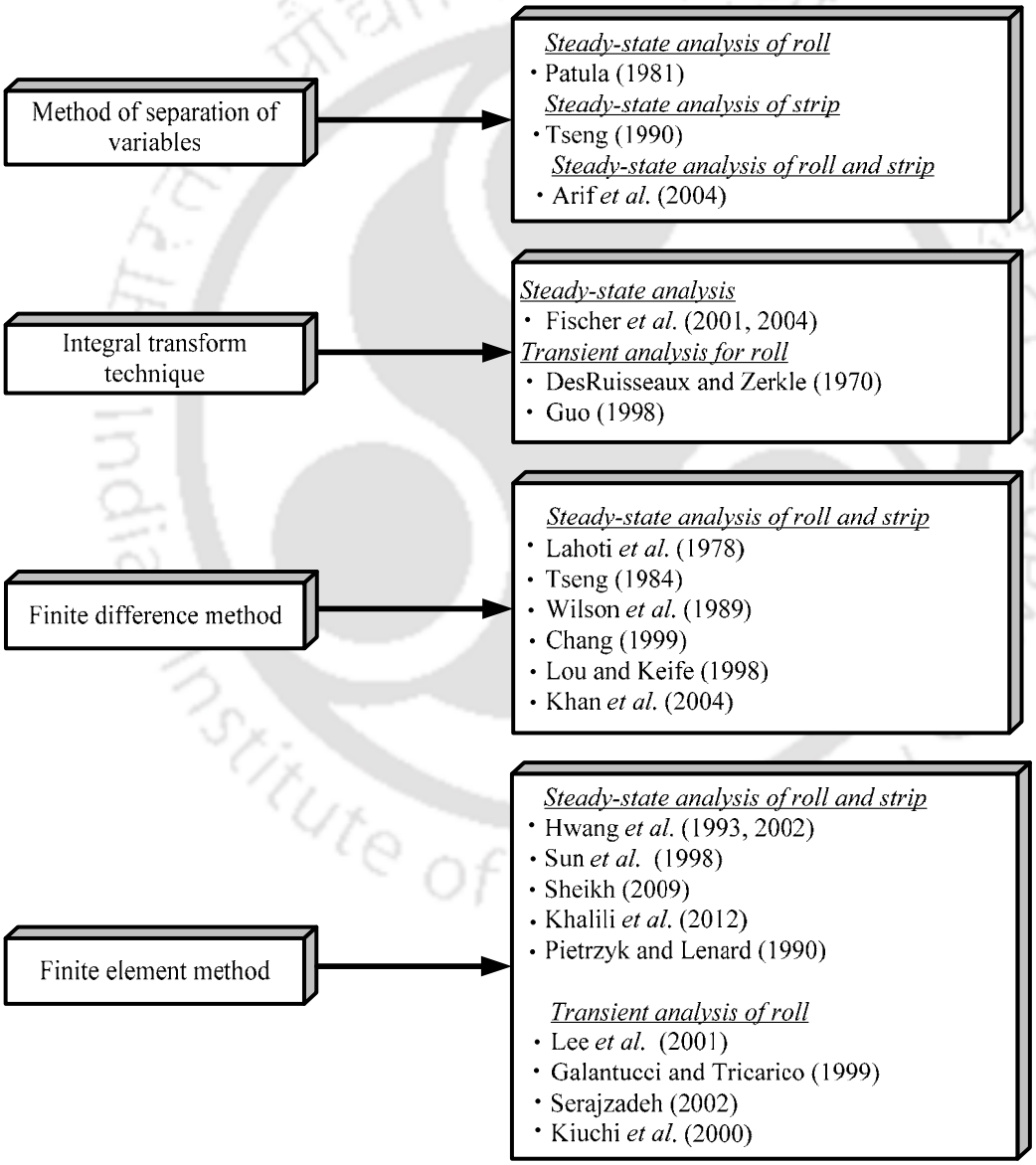

Fig. 2.4. Representative papers in the thermal modelling of rolling process

2.4 Friction at the Roll-Strip Interface

The study of friction remains fundamental to the development of all rolling models. In fact, the process of rolling actually takes due to friction. At the roll-strip interface, both normal and shear stresses exists but moves along with the strip as it passes between the rolls. In addition, the frictional force changes direction within a small contact region. A number of experimental investigates have been carried out to indicate that the ratio of frictional force to normal force is not constant but varies along the contact length.

2.4.1 Experimental Investigation on Friction

In the beginning, experimental investigations of friction at the roll-strip interface and roll pressure distribution in the roll gap were carried out by Seibel and Lueg (1933). The author conducted several experiments to obtain the friction at the roll-strip interface for considering the strip made of copper, iron and aluminum strip. The material of roll was an annealed aluminum for conducting all the experiments. The authors used piezoelectric technique where pressure was transmitted through the transducers that were embedded in the roll. Rooyen and Backofen (1957) mounted two pressure-sensitive pins into the surface of the rolls. One pin was mounted radial to the roll and one at an oblique angle. This concept enabled separation of the normal and frictional stresses. Al-Salehi *et al*. (1973) estimated the friction using smaller pin transducers to measure stresses along the arc of contact and mill mounted load and torque cells to measure roll loads and torque during cold rolling. Lenard (1991 and 1992) estimated the average coefficient of friction in dry rolling and it was observed that material yield strength, hardness and strain hardening exponent influenced the friction. Jeswiet and Cao (1994) performed experiments to measure normal and friction forces at the roll-strip interface in dry cold rolling of aluminum. The authors discussed the effect of the degree of aspect ratio (width/thickness) upon friction and normal forces.

Stephson (1983) pointed out the reliability and practical significance of measurements using embedded pins. Later on, an improved pin technique was developed by Tuncer and Dean (1987). The authors used a conical pin fitting into a conical bore in the roll. The aim was to prevent the material from penetrating the roll

at high pressure. Lenard and Kalpakjian (1991) conducted the experiments to measure the coefficient of friction at the roll-strip interface as a function of speed and temperature of the strip.

Tieu and Liu (2004) measured friction variation along the roll-strip interface by using a sensors-roll, where four pin-transducers are embedded in the sensor roll. The authors observed that the coefficient of friction was not constant along the contact length of the roll-strip interface and there was an error in matching the peak pressure with the location of the neutral point. Jeswiet *et al*. (2006) studied the various methods for measuring the friction in rolling that have been used in the past. The authors concluded that some of the recent sensor–designs may be useful to measure the accurate friction.

Instead of assuming a constant coefficient of friction along the roll-strip interface, Rao and Lee (1989) used experimentally measured velocity profile (the ratio of the interface velocity at any location to the exit strip velocity) along the contact length as an input to FEM model for analyzing strip rolling. The authors obtained the variation of the coefficient of friction in the contact region by taking the ratio of shear stress to normal pressure. They found the coefficient of friction does not remain constant in the roll gap. Other researchers also observed the variation of friction at the roll-strip interface (Rooyen and Backofen, 1957; Al-Salehi *et al*., 1973).

2.4.2 Theoretical Investigation on Friction

In a simplified mathematical modelling of rolling process, Roberts (1976) described a method of finding the coefficient of friction from the roll and strip material data. In most of the early mathematical modelling of rolling processes, either Coulomb's friction model or constant friction model is employed. Wanheim and Bay (1978) suggested an improved model for the frictional shear stress, assuming it to be a certain function of the roll pressure p and friction factor m. The authors observed that at low normal pressure $\left(p/\sigma_Y < 1.5\right)$, the friction stress is proportional to the normal stress whereas at high normal pressure $\left(p/\sigma_Y > 3\right)$, the friction is almost constant. The two ranges are combined via an intermediate transition region.

The appropriateness of Wanheim and Bay's friction model was shown by Christensen *et al*. (1986) and Zhang and Bay (1997) for analyzing the plate and cross shear plate rolling, respectively. Cross shear rolling is a process in which each work roll rotates with different peripheral speed. Richelson (1991) incorporated Coulomb's as well as Wanheim and Bay's friction model in their finite element formulation for simulating the plane-strain rolling. Later on, Richelson (1994) analyzed the combined contact and friction problem using an interface element, using a realistic friction model with a non-linear dependence of the friction stress on the normal pressure.

Lenard (2000) presented a review of various techniques to obtain the friction in metal rolling. Kumar and Dixit (2006) used Wanheim and Bay's model for the analysis of foil rolling process. They observed that friction model has great influence on qualitative and quantitative prediction of foil rolling process. Frictional shear stress predicted by Wanheim and Bay's model is considerably lower than these predicted by Coloumb's model at high pressure is also observed. Li *et al*. (2003) applied the digital image correlation technique to measure the velocity distribution in roll gap during cold rolling. The digital image correlation technique allowed capturing the various rolling parameters, *viz*., the neutral point location, neutral angle, forward slip, backward slip, length of arc of contact. The authors estimated that the coefficient of friction based on the forward slip measurement. Jiang *et al*. (2008) observed the variation of friction in both longitudinal and transverse directions at the roll-strip interface.

2.5 Research on Inverse Techniques

The mathematical modelling of rolling has drawn attention of a number of researchers. Various analytical and numerical models are developed to find the roll force, roll torque, slip and temperature of the roll and strip. However, the difficulty in using these models is that often some thermal and material parameters of the strip and the roll as well as the coefficient of friction are unknown. In batch production mode of rolling with newer materials, separate experiments need to be conducted for each material to determine the input parameters. Conducting separate experiments is

tedious and time consuming as the work material gets changed frequently in batch production. An inverse modelling that reduces the experimental efforts provides an alternative possible way to find out the material and process parameters. The inverse methodology proposed in this thesis can be implemented in the shop floor for the online determination of material and process parameters in rolling process. In the present era, use of inverse modelling is important for accurate and efficient modelling of rolling. In inverse modelling, a suitable optimization technique is used to identify the unknown parameters when the measured results are closer to those calculated by the direct models. The direct model relies on the analytical and/or numerical models. The results obtained from analytical and/or numerical model are compared with the experimental results. The values of unknown parameters are obtained by minimizing the error between the measured and the calculated dependent parameter.

Several authors have been attempted to find the coefficient of friction, heat flux input into the roll and the material properties of the strip by using inverse analysis. Lenard and Zhang (1997) estimated the friction through an inverse technique by matching the measured and computed roll force, roll torque and forward slip. Lenard and Nad (2002) estimated the coefficient of friction in rolling as a function of process and material parameters by an inverse analysis. The basis was matching of the measured and calculated roll force and roll torque.

Kusiak *et al*. (1996) proposed a methodology for the evaluation of material parameters in hot forming of metals by an inverse analysis. The methodology was tested for hot compression of medium carbon tool steel. Cho and Ngaile (2003) proposed an inverse method to determine the flow stresses and the coefficient of friction. The inverse method was based on the minimization of the difference between the experimental loads and the corresponding FEM predictions. In their work, the rigid visco-plastic finite element formulation was used to obtain the flow stress while optimization algorithm adjusted the parameters used in the simulation until the calculated response matched the experimental measurements within a specified tolerance. Han (2005) applied a modified two-specimen method (MTSM) for the online determination of flow stresses and the coefficient of friction in rolling.

In their method, the strip is rolled twice with two different sets of roll radii. Instead of real experiments, ABAQUS FEM simulations were used for validating the methodology.

Cho and Altan (2005) proposed an inverse method to determine flow stress and friction factor of the bulk and sheet materials under isothermal condition. First, the material parameters are determined by minimizing the difference between the experimental and calculated loads. Afterwards, the shape of the deformed specimen was compared with the computed shape. If they did not match, the friction factor was adjusted in order to reduce the difference in the next iteration. The methodology was applied to the ring compression and the modified limiting dome height test. Byon *et al*. (2008) proposed inverse method for the prediction of flow stress-strain curve and coefficient of friction using actual mill data. The roll force and forward slip is taken as the basis for inverse estimation. In their work, forward slip decides the coefficient of friction and the material parameters are subsequently obtained based on roll force matching.

Huang *et al*. (1995) applied the conjugate gradient method to estimate the heat flux and the temperature distribution in the roll. The method requires the measurement of surface temperature of the roll. Yoneyama *et al*. (1999) conducted the experiments to measure the temperature of roll surface at the contact zone during the hot rolling of aluminum sheet. A number of temperature sensors were embedded on the roll surface to analyze the influence of different rolling process parameters. Further, a one-dimensional FDM model was used to predict the heat transfer coefficient (HTC) at the interface between roll and the sheet. HTC is calculated in an inverse way by comparing the measured and calculated temperatures.

Hsu *et al*. (2000) predicted the thermal behaviour of work-roll in rolling by three-dimensional inverse model. The temperature measurements are carried out at several locations inside the roll. Chen and Yang (2010) proposed an inverse analysis to estimate the heat flux at the roll-strip interface by measuring the temperature distribution of roll. In their analysis, the strip was not included. It was assumed that the heat flux entering into the roll is constant. For validation of the proposed method, the simulated temperatures were used instead of the real experiments.

Weisz-Patrault *et al.* (2011) proposed an inverse method to determine the temperature field at the surface of the roll by measuring the temperature using thermocouple at only one point of the roll. Further, they extended their work (Weisz-Patrault *et al.*, 2012; Weisz-Patrault *et al.*, 2013) to predict the contact stress in the roll gap by measuring the stress tensor with fiber optics at only one point of the roll. Weisz-Patrault *et al*. (2012) proposed an inverse method to determine the temperature field at the surface of the roll by measuring the temperature using thermocouple at only one point of the roll. The inverse method was applied on the basis of the thermal analysis of the roll. In their recent paper (Weisz-Patrault *et al.* 2014), they presented a fully three-dimensional inverse analytical method to determine the temperature field and the heat fluxes (input into the roll) by measuring temperatures at several locations in the rolls.

Yadav *et al*. (2011a) proposed an inverse method for estimating the coefficient of friction based on the exit strip temperature measurement. A methodology to predict the coefficient of friction and flow stress of the strip material by inverse method based on the measurement of the forward slip and exit strip temperature was presented for cold rolling in Yadav *et al*. (2011b). Figure 2.5 shows the some of the representative work in the inverse estimation of rolling process parameters.

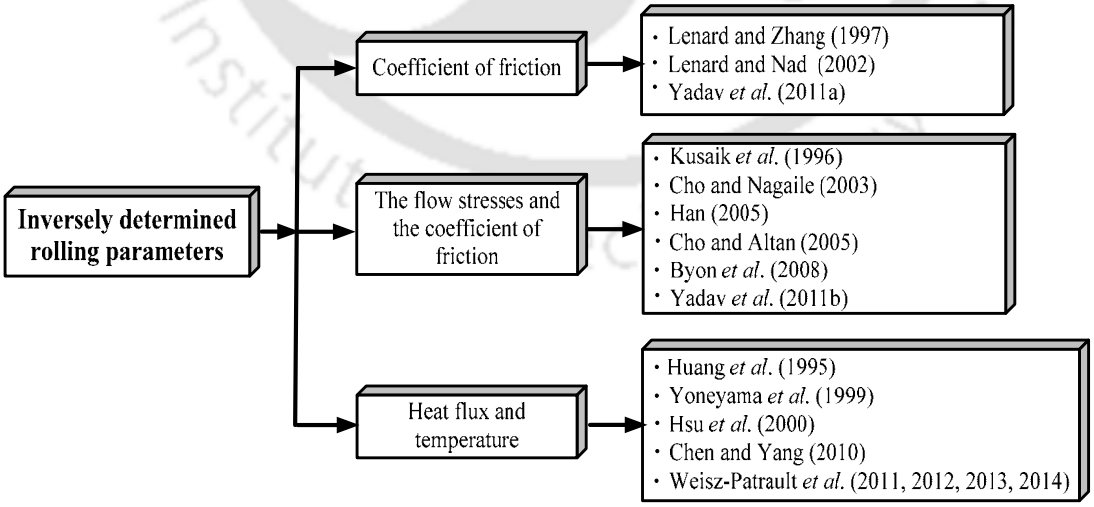

Fig. 2.5. Representative papers in the inverse modelling of rolling process

In the rolling industry, the feed forward and feed backward models have been implemented to stabilize the process. The purpose of feed forward and feed backward models is used to control the rolling process parameters *viz*., thickness of the rolled strip, temperature of the strip and the roll, *etc*. The applications of advanced control techniques and an efficient mathematical model are essential to get the better rolled product quality and fast production rate. The inverse models described in the present thesis can be used in feed forward or feed backward models to control the temperature, roll force, roll-torque and slip for enhancing the product quality. For example, Rigler *et al*. (1996) proposed the strategy to control the thickness of rolled strip and temperature distributions in the strip during multi-stand hot rolling. They implemented Kalman filter algorithms in the mathematical modelling to identify the local changes in the rolling process parameters *viz*., thickness and temperature of the strip. The feed forward control system was used to get exact accuracy in the strip thickness at the finishing stage in multi-stand rolling mill. Heeg *et al*. (2007) developed the strategy to feed forward control of the plate thickness in reversing the plate mills. They suggested that the direct measurement of the plate thickness is the difficult task during rolling. Therefore, the thickness is controlled indirectly by means of calculating the quasi-static stretch of the mill as a function of measured roll-forces.

2.6 Inference from the Literature

In the field of metal forming, the flat rolling process drew the significant attention of the researchers. The literature survey reveals that most of the works have been reported on the cold and hot rolling processes. The warm flat rolling is less investigated compared to the cold and hot flat rolling. Commonly, industries find easier to carry out either cold or hot rolling. Warm rolling is an intermediate stage and it is important to decide proper temperature range for it. Recently, warm rolling process has been considered as an efficient means to produce flat steel products due to its considerable cost saving as well as desired product properties (Koobhor, 2015). Yanushkevich *et al*. (2016) analyzed the warm rolling process for enhancing the mechanical properties of the rolled strip at elevated temperatures. The influence of temperature on mechanical properties considering warm and hot rolling is studied by Belyakov *et al*. (2016). The

authors found that rolling under warm working conditions can be considered as the promising thermo-mechanical treatment for production of advanced high-Mn TWIP/TRIP steels with desirable mechanical properties. The warm flat rolling process provides the following advantages:

- It requires lower loads and energies compared to cold rolling.
- It achieves better surface finish and dimensional accuracy compared to hot rolling.
- It is an efficient process to produce flat steel products due to its ability to obtain the desired rolled sheet properties at reduced cost.

Due to the above advantages, the present thesis work focuses on the warm flat rolling process. The warm flat rolling process is carried out by a few researchers considering steady-state temperature distribution. Recently, Koohbor (2015) mentioned that warm rolling is becoming an efficient means to produce flat steel at low cost. For maintaining the proper productivity and quality of the product, mathematical modelling of the warm rolling process is an essential requirement. There are major uncertainties associated with the modelling of any sort of rolling process (Domanti and McElwain, 1998). The first of these concerns is the nature of the contact between the roll and the strip and to find out the friction. The direct measurement of friction by experiment is difficult. The second major uncertainty lies in the description of the material properties. In view of these, the present thesis is proposing a methodology to find out the material parameters as well as the coefficient of friction dependant on the process parameters.

A few researchers have attempted to find out the material parameters and the coefficient of friction of the rolled sheet in warm rolling. There are only a few publications that try to present in depth information. Some challenging issues are as follows:

- In the literature, most of the researchers analyzed the rolling process considering the steady-state temperature distribution in the roll and strip. A few researchers have attempted to study the transient behaviour of either the roll or the strip (Lee *et al*., 2000; Guo, 2000; Serajzadeh *et al*. 2002). However, none of the researchers have carried out the coupled transient

thermo-mechanical analysis taking into account the roll and the strip together. Therefore, there is a need to develop an integrated thermo-mechanical model for complete understanding the transient behaviour of the flat rolling process.

- Most of the models are based on FEM and/or FDM to obtain the temperature distribution in rolling but they are computationally expensive. In the present era, FEM based packages are easily available to analyze the thermo-mechanical behaviour of the rolling process. Some of the authors have carried out (Galantucci and Tricarico, 1999; Shahani *et al*., 2009; Koohbor, 2015) thermo-mechanical analysis using FEM based packages. But their analysis requires too much computational time. Hence, there is a need to develop an efficient methodology for enhancing the computational efficiency to obtain the temperature distribution in rolling.
- The warm flat rolling is performed at elevated temperatures, but below the recrystallization temperature. Therefore, the flow stresses of the rolled sheet is reduced and also some amount of strain hardening is achieved (Hirschvogel, 1979). Hawkins (1985) reported that the component produced by warm working is usually heat treated for improving the microstructure developed during warm working process. A proper mathematical model for warm rolling with ability for inverse estimation is of paramount importance.
- A few researchers have proposed the inverse methodology to obtain the flow stresses and the coefficient of friction in rolling based on roll-force and roll-torque measurement (Lenard and Nad, 2002; Cho and Ngaile, 2003; Byon *et al*., 2008). It is not convenient to measure the roll-torque and roll-force during rolling in practice. However, the temperature at the exit of the roll bite can be easily measured using non-contact type temperature sensor in the shop floor. This provides a scope in determining the material parameters and coefficient of friction on the basis of temperature measurement using an inverse methodology.

2.7 Objectives of the Present Thesis

Based on the literature survey and major challenges identified, it is decided to investigate the following aspects of the warm flat rolling process in this thesis:

1. **Modelling of warm flat rolling:** A thermo-mechanical modelling of the roll and the strip in the warm flat rolling process will be carried out. The modelling will include the deformation analysis of strip using FEM and the thermal analysis of roll and the strip by an analytical method. The thermal analysis will be simulated in ABAQUS for validating the analytical model. The thermo-mechanical model (described in the following chapter) will be capable of determining the steady-state as well as the transient temperature distribution in the warm flat rolling. The experimental verification of the thermo-mechanical model will also be carried out. The coefficient of friction between the roll and the strip will be determined experimentally.
2. **Inverse analysis based on temperature measurement in warm flat rolling:** Mathematical model of flat rolling process requires the knowledge of material parameters and the friction between the strip and the roll. Material parameters are obtained by carrying out compression and/or tensile tests. Conducting separate experiments for the determination of material parameters and friction is tedious and time consuming. Moreover, in a dynamic environment, the work material is changed frequently. In view of this, the present thesis proposes an inverse methodology to obtain the material parameters, convective heat transfer coefficients and the coefficient of friction. In inverse analysis following sub-objectives are covered:
    - Estimating the coefficient of friction by measuring the temperature at the exit assuming that the material properties are known.
    - The determination of the mechanical properties and the coefficient of friction based on the measurement of temperature at the exit (at one point) and slip.

- The determination of the thermal parameters and coefficient of friction based on the measurement of temperature at the exit (at two points) and slip.

The research plan is shown in Fig. 2.6.

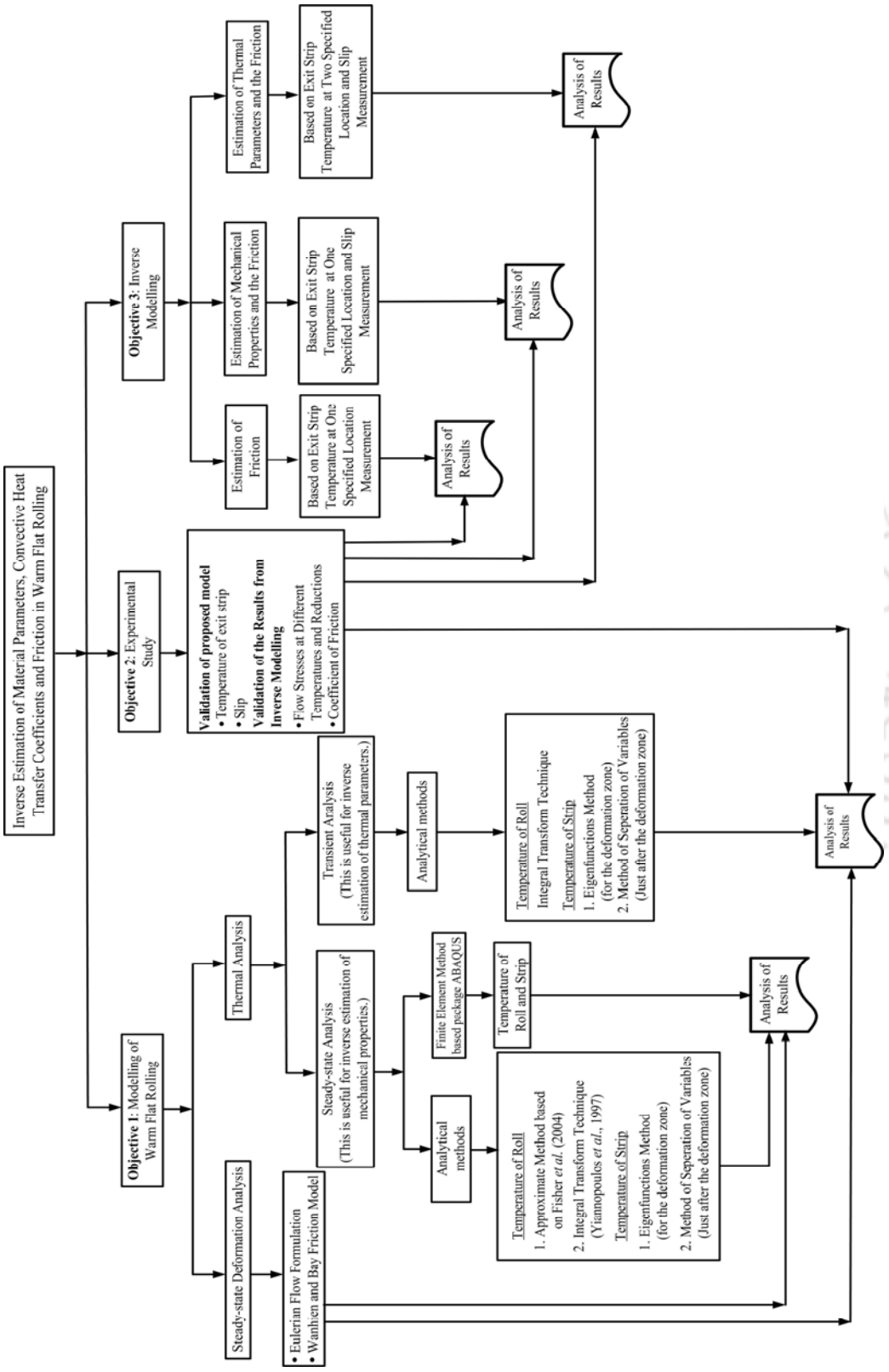

Fig. 2.6. Research plan in the form of flow chart

Chapter 3

A Steady-State Thermo-Mechanical Model of Warm Flat Rolling Process

3.1 Introduction

Flat rolling is an important industrial bulk metal forming process. In this process, the thickness of a sheet is reduced by passing it between two counter-rotating rolls. The warm flat rolling is an efficient process to produce flat steel products due to its ability to obtain the desired rolled sheet properties at reduced cost (Hawkins, 1985). It is important to improve the process productivity and the quality of the rolled sheet. For maintaining the proper productivity and quality of the sheet, mathematical modelling of the warm rolling process is an essential requirement. During warm flat rolling, strip is rolled at an intermediate temperature such that the flow stress of the rolled sheet reduces without alteration in the microstructure. Here, a steady-state thermo-mechanical modelling of warm flat rolling process is developed. The particular emphasis is on predicting the temperature of the exited strip, which can be helpful in an inverse analysis. The measurement of the temperature is relatively easier in comparison to roll force and roll torque measurement and it can help in the inverse estimation of material parameters as well as the coefficient of friction.

In this chapter, a two-dimensional thermo-mechanical modelling of warm flat rolling is described. The deformation analysis is carried out by the finite element method (FEM) model based on Eulerian flow formulation of Dixit and Dixit (1996). Subsequently, thermal analysis of the roll and the strip is carried out by two analytical methods and an FEM model. The methods of thermal analyses are compared. The organization of the chapter is as follows. Section 3.2 presents an

overview of the developed thermo-mechanical model for warm flat rolling. The deformation analysis of strip by FEM is described in Section 3.3. Section 3.4 presents the approximate method for computing the temperature distribution in the roll. Section 3.5 presents the integral transform technique to find out the temperature distribution in the roll. The analytical model for the estimation of temperature distribution in strip is presented in Section 3.6. The finite element analysis for finding out the temperature distribution in the roll and the strip is described in Section 3.7. Section 3.8 presents a comparative study of the proposed thermo-mechanical model of warm flat rolling using analytical methods and an FEM model. Section 3.9 discusses the validity of the assumption that average temperatures of roll and strip at the roll-strip interface are equal. The influence of different process parameter on the average temperature distribution of the roll and the strip is illustrated in Section 3.10. Section 3.11 concludes the chapter.

3.2 An Overview of a Thermo-Mechanical Model of Warm Flat Rolling

In this section, an overview of thermo-mechanical model for plane strain warm flat rolling is described. The analysis comprises two modules– deformation module and thermal module. Deformation module is based on the Eulerian flow formulation of finite element method (FEM). In this work, two analytical methods and one FEM model have been considered for thermal module. Initially, the deformation module takes the mechanical properties of the strip corresponding to the entry temperature. The deformation and friction powers provided by the deformation module are used as input in thermal module. From the output of the thermal module, the temperature in the deformation zone can be obtained. Now, deformation module is activated again to carry out the analysis with mechanical properties corresponding to the temperature of the deformation zone. Figure 3.1 shows the overall view for the development of an integrated model for warm flat rolling. It consists of two modules— (1) deformation analysis of strip considering constitutive relation and friction model and (2) thermal analysis of the roll and the strip.

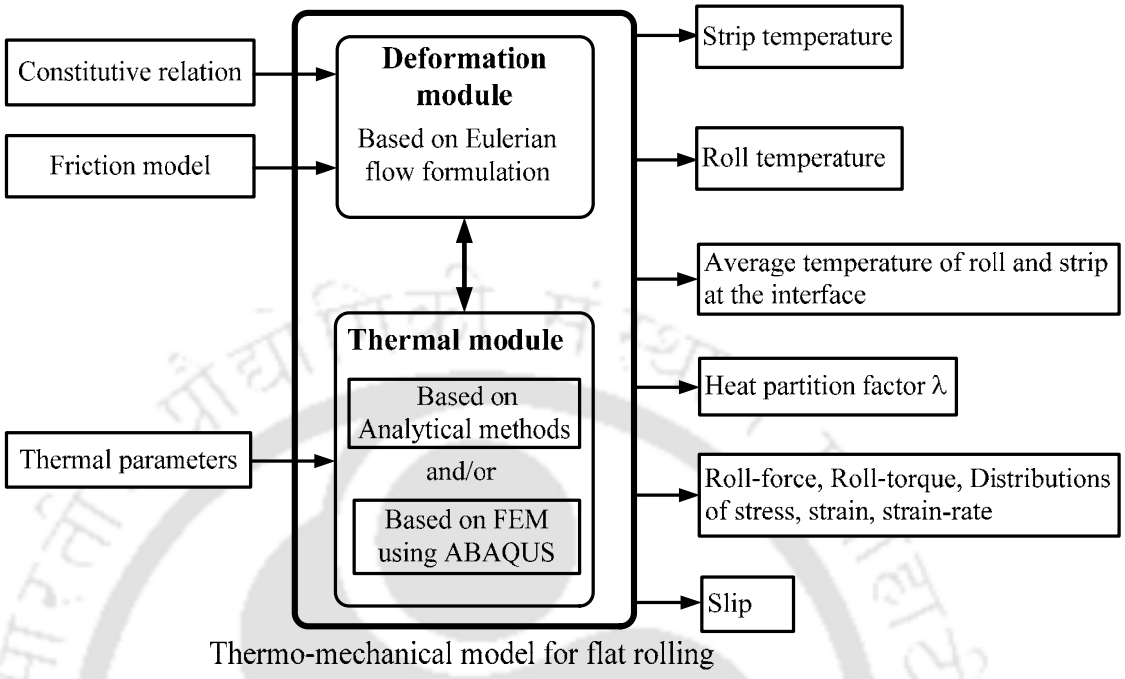

Fig. 3.1. An overview of thermo-mechanical model of plane strain rolling

For the thermal analysis, two sub-modules are developed for obtaining the temperature distribution. One sub-module finds the temperature distribution in the strip. The other sub-module estimates the temperature distribution in rolls, when the heat transfer through the roll-strip interface is known. Actual heat transfer through the roll-strip interface is not known. Here, it is obtained by an inverse procedure such that both the modules predict the same average temperature at the interface of roll and strip. If Q_T is the total heat generated due to friction and plastic deformation, the quantity λQ_T is assumed to pass to the rolls and $(1-\lambda)Q_T$ remains in strip. The value of partition factor λ is obtained to match the temperatures at the roll-strip interface from both the sub-modules. These sub-modules are described in Sections 3.3–3.7. The equality of average temperatures of the roll and strip at the interface implies zero contact resistance. Justification for this assumption is provided in Section 3.9. This assumption has been employed by Komanduri and Hou (2001) in analyzing the temperature distribution in the sliding systems and by Wilson *et al*. (1989) for analyzing the temperature distribution in dry rolling. It is not difficult to relax this assumption. The heat flow can be taken directly

proportional to temperature difference between the roll and the strip and inversely proportional to thermal resistance between the roll and the strip. However, it has not been considered in the present work.

The algorithm of the whole procedure for the determination of heat partition factor λ is as follows:

Step 1: Carry out the deformation analysis using FEM module based on Eulerian flow formulation.

Step 2: Assume that all the frictional heat goes into the roll and 90% of plastic deformation power goes as heat into the strip. A part of frictional heat may go into the strip as well depending on the relative temperature difference between roll and strip, but it is better to begin the analysis by assuming that the roll is colder than strip due to forced or natural cooling, causing entire frictional heat to flow into the roll. Assumption of 90% of energy of plastic deformation dissipating as heat and remaining as increase in the internal energy of metal is commonly made in metal forming (Jiang *et al*., 2004 and Khalili *et al*., 2012).

Step 3: Carry out thermal analysis of roll and strip. Use modules for the estimation of roll and strip temperatures.

Step 4: If average temperature of the strip and roll are equal at the interface go to Step 7.

If the average temperature of the strip at the interface is less than average temperature of roll then go to Step 5.

If the average temperature of the strip at the interface is greater than average temperature of roll then go to Step 6.

Step 5: Transfer the appropriate amount of heat from roll to strip for making the roll and strip average temperatures at the interface equal. This can be done using bisection method (Gerald and Wheatley, 1997). Go to Step 7.

Step 6: Transfer the appropriate amount of heat from strip to roll for making the roll and strip average temperatures at the interface equal. This can be done using bisection method. Go to Step 7.

Step 7: Record the temperatures distribution of roll and strip. At the obtained temperature of strip, find out the material properties. If the material properties are

significantly different, go to Step 1 and carry out the next iteration with new material properties. Else stop.

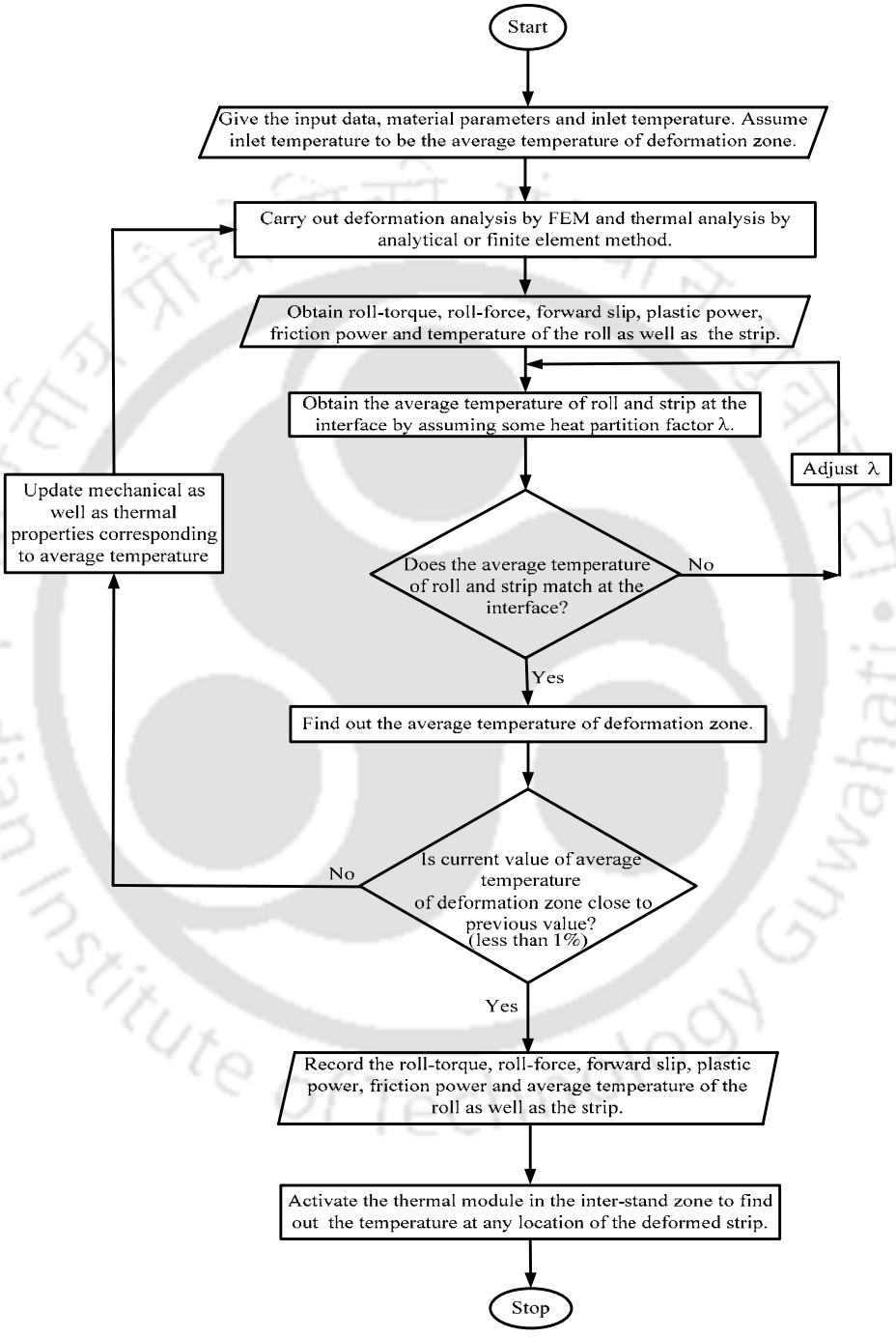

Fig. 3.2. A flow chart illustrating the methodology of thermo-mechanical modelling of flat rolling

The material properties (flow stresses) are updated after the each iteration with the corresponding average temperature of the deformation zone. It is to be noted that the flow stresses are updated till the average temperature of the deformation zone gets converged. The convergence is considered to be achieved if there is less than 1% change in temperature distribution in the deformation zone as illustrated in the flow chart (Fig. 3.2). With this much change in temperature distribution, material properties will not be significantly different. Figure 3.2 shows the flowchart of the procedure for determining the temperature in rolling. To start with initially, the deformation analysis is carried out using FEM with the mechanical properties at the initial strip temperature and then the thermal analysis is carried out. After the strip temperatures are obtained by thermal analysis, the deformation analysis is again carried out with the mechanical properties corresponding to previous thermal analysis temperature. This procedure is repeated till the convergence is obtained. The convergence of the iteration is said to be obtained if there is no substantial change in temperature distribution in the deformation zone. It is to be noted that temperature dependent mechanical properties are considered for the deformation analysis.

3.3 Deformation Analysis by Finite Element Method

Considering plane strain condition, an FEM based Eulerian flow formulation is employed to analyze stresses, roll torque, roll-force, strain, strain-rate and forward slip. The formulation of Dixit and Dixit (1996) has been used. It should be mentioned that this formulation is based on the steady-state deformation of the strip. Due to the symmetry, only upper half domain is considered in the analysis. The finite element mesh of the strip along with the boundary conditions is shown in Fig. 3.3. A fine mesh is used in the deformation zone and coarse meshes are used in the inlet and exit zones. The element height is gradually reduced from the center to the surface of the strip. This is because the stress gradient is expected to be higher in the vicinity of the roll-strip interface. The elastic deformation is small as compared to plastic deformation. As the goal is to find out the powers, the elasticity

is neglected and the plastic strain can be considered as the total strain. Roll deformation is taken into account using well-known Hitchcock's formula (Dixit and Dixit, 2008).

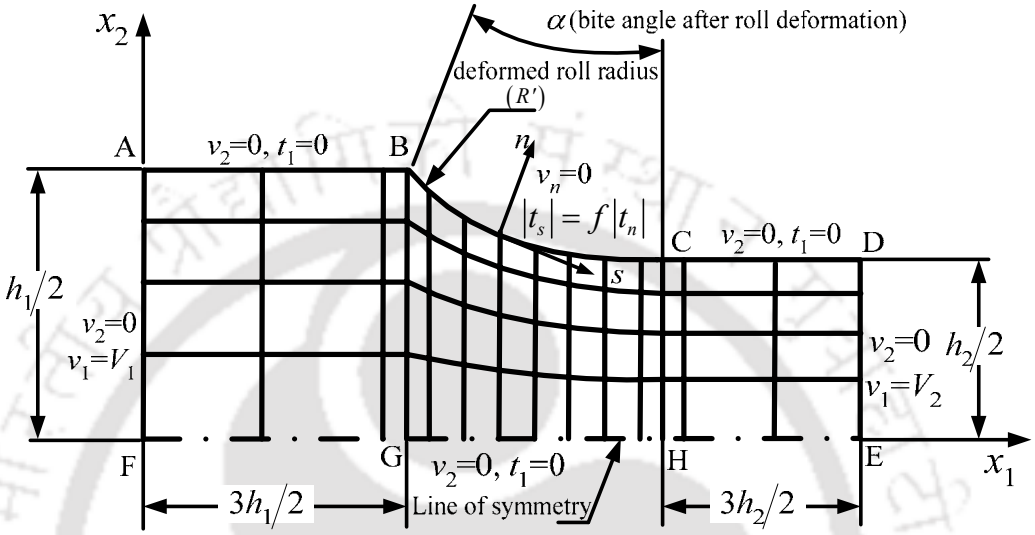

Fig. 3.3. A meshed domain of strip with boundary conditions

The rigid-plastic material behaviour is assumed. As per the Levy-Mises flow rule, the deviatoric part S_{ij} of the component of stress tensor σ_{ij} is related to the component of strain-rate $\dot{\varepsilon}_{ij}$ as

$$S_{ij} = 2\eta_1 \dot{\varepsilon}_{ij}\,, \tag{3.1}$$

where η_1 is the proportionality factor. It is to be noted that the plastic incompressibility condition is implicit in Eq. (3.1). The use of von-Mises yield criterion provides

$$\eta_1 = \frac{\sigma_y}{3\dot{\varepsilon}_{eq}}, \tag{3.2}$$

where $\dot{\varepsilon}_{eq}$ is the equivalent strain-rate defined by

$$\dot{\varepsilon}_{eq} = \sqrt{\frac{2}{3}\dot{\varepsilon}_{ij}\dot{\varepsilon}_{ij}}\,. \tag{3.3}$$

In the above expression, the Einstein summation convention is employed. Considering plane strain, the indices *i* and *j* vary from 1 to 2. In unabridged form,

$$\dot{\varepsilon}_{eq} = \sqrt{\frac{2}{3}\left(\dot{\varepsilon}_{xx}^2 + \dot{\varepsilon}_{yy}^2 + 2\dot{\varepsilon}_{xy}^2\right)}. \tag{3.4}$$

The flow stresses of the strip may be described by Johnson-Cook (J-C) model (Johnson and Cook, 1983):

$$\sigma_y = \left(A + B\varepsilon_{eq}^{n_1}\right)\left[1 + C\ln\frac{\dot{\varepsilon}_{eq}}{\dot{\varepsilon}_0}\right]\left[1 - \left(\frac{T - T_{amb}}{T_m - T_{amb}}\right)^{m_1}\right], \tag{3.5}$$

where A, B, C, m_1 and n_1 are the material constant, $\dot{\varepsilon}_0$ is the reference strain-rate, T_{amb} is the ambient temperature of the strip and T_m is the melting temperature of the strip. The J-C model has a fairly wide range of applicability.

Two-dimensional continuity and momentum equation for the steady state process are solved, which are given in index notation as

$$\frac{\partial v_i}{\partial x_i} = 0, \tag{3.6}$$

$$\frac{\partial \sigma_{ij}}{\partial x_j} \equiv -\frac{\partial p}{\partial x_i} + \frac{\partial S_{ij}}{\partial x_j} = 0, \tag{3.7}$$

where p is the hydrostatic pressure. These constitutive relations are implemented using Eulerian based finite element formulation (Dixit and Dixit, 1996). Roll-force, roll-torque, stresses, strain and slip are obtained. Wanheim and Bay (1978) friction model is used instead of Coulomb's model. At low normal pressure, the Wanheim and Bay (1978) model matches with the Coulomb's model and at high normal pressure, it approaches constant friction factor model. In between there is a smooth transition zone. In the notations of this chapter, f is the ratio of the magnitudes of normal and tangential tractions at the roll-work interface and μ is the equivalent Coulomb coefficient of friction. The Galerkin formulation given by Dixit (1997) is briefly described in Appendix A.

Following the standard Galerkin formulation, the global equations after application of all the boundary conditions are obtained in the following form:

$$[K]\{\Delta\} = \{F\}, \tag{3.8}$$

where $[K]$ is the global coefficient matrix, $\{\Delta\}$ is the global vector of nodal values of velocity and pressure and $\{F\}$ is the global right-hand side vector. The 9 nodes per element are chosen for velocity components and 4 nodes for pressure. Once the solution is obtained in the form of nodal velocities v_i and pressure, the secondary variables, *viz*., roll-force, roll-torque, stresses, strain, and slip are computed. The roll force per unit width (F_r) is given by

$$F_r = \int_0^{l_d} \left(t_n \cos\phi - t_s \sin\phi\right) \mathrm{d}s \,, \tag{3.9}$$

where l_d is the arc of contact, ϕ is the angular position of the point on the roll-strip interface, t_s and t_n are the tangential and normal components of interfacial stress vector $\boldsymbol{t}$. The roll torque per unit width (T_R) is computed by following relationship

$$T_R = \frac{PR}{V}, \tag{3.10}$$

where V is the surface velocity of the roll (equal to the velocity of strip at neutral point), R is the roll radius and P is the total power. The total power P consists of following two parts:

(i) Power required for plastic deformation given by

$$P_p = \int_A S_{ij}\dot{\varepsilon}_{ij}\mathrm{d}A. \tag{3.11}$$

(ii) Power required to overcome friction at the work-roll interface given by

$$P_f = \int_0^{l_d} |t_s||\Delta v_s|\mathrm{d}\Gamma \,, \tag{3.12}$$

where Δv_s is the relative velocity with respect to the neutral point velocity.

3.4 Approximate Temperature Distribution in Roll by Adapting the Method of Fischer *et al*. (2004)

The temperature distribution within the roll is obtained by solving two-dimensional heat transfer equation considering Eulerian reference frame. The following assumptions are made:

(i) The heat transfer along the axial direction to the roll is negligible. Thus, the problem is essentially two-dimensional.

(ii) Thermal properties of the roll material are independent of the temperature. These are taken as the properties at average temperature.

(iii) Heat flux input into the roll is uniform along the roll-strip interface.

(iv) The rotational speed of the roll is constant.

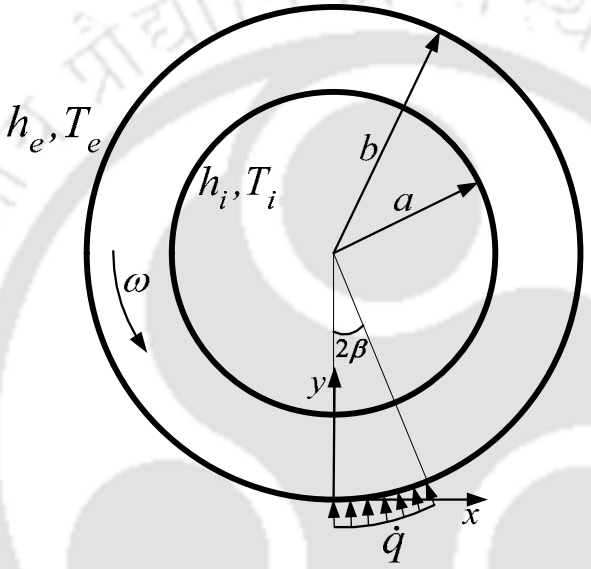

Fig. 3.4. A stationary heat source with rotating roll

Figure 3.4 shows a rotating roll with heat flux at a fixed location. Heat conduction is considered for a plane configuration by representing the roll as a circular disk (considering the case of plain-strain rolling). There are a number of methods for the estimation of temperature in rolling. The prominent among them are finite element method (FEM) and finite difference method (FDM). Some analytical solutions have also been proposed, which invariably are in the form of summation of infinite series containing Bessel functions (Patula, 1981; Yiannopoulos *et al*., 1997). These methods are useful for an accurate analysis, but often the designer or control engineer is interested in a fast estimation by sacrificing the accuracy to some extent. The present work proposes an approximate method for the estimation of temperature distribution in the roll. The proposed method is simpler and faster compared to available methods in literature such as solution

employing Bessel function and Fourier series expansion by Patula (1990) and Yiannopoulos *et al*. (1997).

Here, the temperature distribution in the roll is computed based on the superposition of steady-state temperature from the work of Fischer *et al*. (2004) and the average temperature of the roll at any radial location calculated from heat balance equation. Superposition provides the steady-state temperature distribution within the roll along the radial as well as circumferential directions. An Eulerian reference frame is applied with a horizontal x-direction on the surface of the halfplane and the y-direction pointing towards the inside of the roll as shown in Fig. 3.4. The roll is considered as a half plane. The heat source $\dot{q}$ acts in the interval [0, 2β] on the surface and is assumed to be spatially fixed, too. Hence, the roll material moves with respect to this coordinate system with the angular velocity ω. Introducing the material derivative, the governing heat conduction equation in the steady-state is

$$\frac{\partial^2 T}{\partial x^2}+\frac{\partial^2 T}{\partial y^2}=\frac{\omega R}{\alpha_r}\frac{\partial T}{\partial x}, \tag{3.13}$$

where ω is the angular velocity of roll, R is the radius of roll and α_r is the thermal diffusivity of roll. The Peclet number (P_e), the ratio of advective transport rate to diffusive transport rate, is given by

$$P_e=\frac{\omega R^2\beta}{2\alpha_r}\ . \tag{3.14}$$

For large Peclet number, the heat conduction in the direction y (or radial) only is relevant (Fischer *et al*., 2004). Thus, Eq. (3.13) becomes

$$\frac{\partial^2 T}{\partial y^2}=\frac{\omega R}{\alpha_r}\frac{\partial T}{\partial x}, \tag{3.15}$$

with initial condition

$$T=T_0 \quad \text{at} \quad t=0, \tag{3.16}$$

and boundary condition

$$k\frac{\partial T}{\partial y}=\begin{cases}-\dot{q}(x) & \text{for} \quad 0\le x\le 2b\beta,\ y=0\\ 0 & \text{for} \quad x>2b\beta,\ y=0\end{cases}. \tag{3.17}$$

Considering non-dimensional coordinates $x=2\beta b\xi$, $y=\delta\zeta$, where δ is heat penetration depth given by (Fischer *et al*., 2004)

$$\delta=\sqrt{\frac{2b\beta\alpha_r}{\omega R}}, \tag{3.18}$$

the temperature distribution for zero initial temperature in the roll is obtained as (Fischer *et al*., 2004)

$$T(\xi,\zeta)=T_{\max}\left\{\sqrt{\xi}\exp\left(-\frac{\zeta^2}{4\xi}\right)-\frac{\sqrt{\pi}}{2}\zeta\left(1-\operatorname{erf}\left(\frac{\zeta}{2\sqrt{\xi}}\right)\right)\right\} \quad \text{for } 0\le\xi\le 1, \tag{3.19}$$

$$T(\xi,\zeta)=T_{\max}\left\{\begin{aligned}&\sqrt{\xi}\exp\left(-\frac{\zeta^2}{4\xi}\right)-\frac{\sqrt{\pi}}{2}\zeta\left(1-\operatorname{erf}\left(\frac{\zeta}{2\sqrt{\xi}}\right)\right)\\&-\left(\sqrt{\xi-1}\exp\left(-\frac{\zeta^2}{4(\xi-1)}\right)-\frac{\sqrt{\pi}}{2}\zeta\left(1-\operatorname{erf}\left(\frac{\zeta}{2\sqrt{\xi-1}}\right)\right)\right)\end{aligned}\right\} \quad \text{for } \xi>1 \tag{3.20}$$

where $T_{\max}$ is given as

$$T_{\max}=\sqrt{\frac{8}{\pi}\frac{b\beta\alpha_r}{\omega R}}\frac{\dot{q}}{k_r}, \tag{3.21}$$

and $\dot{q}$ is the constant heat flux in the interval [0, 2β]. In Eqs. (3.19) and (3.20), erf is the error function. Here, the error function corresponds to the diffusion equation of heat transfer. The error function is defined as

$$\operatorname{erf}(x)=\frac{2}{\sqrt{\pi}}\int_0^x\exp\left(-\eta^2\right)\mathrm{d}\eta. \tag{3.22}$$

Equations (3.19) and (3.20) provide the temperature distribution for initial condition of zero temperature distribution in the roll. For the steady-state case, a

constant temperature $T_o(\tau)$ is imposed at radial location corresponding to τ such that

$$T_o(\tau)+\frac{\int_0^{(\pi/\beta)} T(\xi,\tau)\mathrm{d}\xi}{(\pi/\beta)}=T_{avg}(\tau), \tag{3.23}$$

where $T_{avg}(\tau)$ is the average temperature of the surface at the radial location corresponding τ, which is obtained as follows.

At steady state, the heat balance provides

$$2\pi a h_i(T_a-T_i)+(2\pi-2\beta)bh_e(T_b-T_e)=2\beta b\dot{q}, \tag{3.24}$$

where $\dot{q}, a, b, T_a, T_b, T_i, T_e, h_i$ and h_e are the heat flux, inner radius of roll, outer radius of roll, average temperature of inner radius, average temperature of outer radius, ambient temperature at inner roll periphery, ambient temperature at outer roll periphery, convective heat transfer coefficient at the inner radius and convective heat transfer coefficient at the outer radius of the roll, respectively. As there are two unknowns, *viz.*, T_a and T_b, one additional equation is needed which is provided by the boundary condition at inner periphery of the roll:

$$\left\{-k_r\frac{\partial T}{\partial r}+h_i(T_a-T_i)\right\}_{r=a}=0. \tag{3.25}$$

The finite difference form of the above equation is described in Appendix B. Substitution of $\frac{\partial T}{\partial r}$ from Appendix B in Eq. (3.25) provides

$$h_i(T_a-T_i)=2bk_r\frac{T_b-T_a}{b^2-a^2}. \tag{3.26}$$

Solving Eqs. (3.24) and (3.26), the average temperatures T_a and T_b along the roll periphery are obtained. It can be assumed that average temperatures are the linear function of radial distance and thus knowing the outer and inner average temperatures, the average temperature $T_{avg}(\tau)$ at any radial distance can be obtained. Equation (3.23) can now provide temperature $T_o(\tau)$ to be superimposed on the temperature distribution for different radial locations.

3.5 Computing Temperature Distribution in Roll using Integral Transform Technique of Yiannopoulos *et al.* (1997)

In this section, the solution of two-dimensional heat conduction equation with time-dependent, non-homogeneous boundary condition is presented using Lagrangian approach. Let the heat input be given at outer radius b in the zone 2β angular displacement as shown in Fig. 3.5. Remaining outer surface of the roll is subjected to convective heat loss. The inner surface at radius a is subjected to convective loss only. The work roll is assumed to be rigid, fixed in space and heat source rotates with constant angular velocity ω.

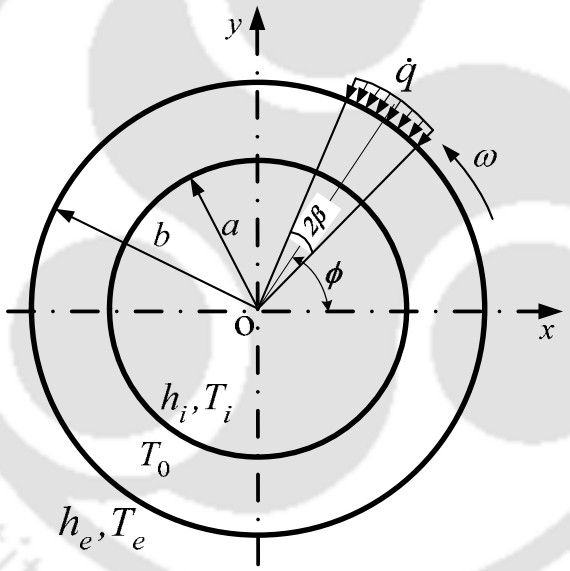

Fig. 3.5. A moving heat source with stationary roll

Consider the roll as a hollow cylinder, the governing differential equation in $r-\theta$ coordinate system for heat conduction is given for the domain $a < r < b$ as

$$\frac{\partial^2 T}{\partial r^2}+\frac{1}{r}\frac{\partial T}{\partial r}+\frac{1}{r^2}\frac{\partial^2 T}{\partial \theta^2}=\frac{1}{\alpha_r}\frac{\partial T}{\partial t} \tag{3.27}$$

where α_r is the thermal diffusivity of work-roll given by

$$\alpha_r=\frac{k_r}{\rho_r c_{pr}}. \tag{3.28}$$

In Eq. (3.28), k_r is the thermal conductivity of roll material, ρ_r is the mass density and c_{pr} is the specific heat. The boundary conditions are expressed as

$$k_r \frac{\partial T}{\partial r} + h_e \left(T - T_e\right) = \dot{q}\left(\theta\right) \qquad \text{at } r = b \tag{3.29}$$

$$-k_r \frac{\partial T}{\partial r} + h_i \left(T - T_i\right) = 0 \qquad \text{at } r = a \tag{3.30}$$

where $\dot{q}\left(\theta\right)$ is the heat flux at the outer surface, h_e is the convective heat transfer coefficient at the outer surface, h_i is the convective heat transfer coefficient at the inner surface, T_i is the ambient temperature at the inner roll periphery and T_e is the ambient temperature at the outer roll periphery. The heat flux at the outer surface at any time is expressed as

$$\dot{q}\left(\theta\right) = \begin{cases} \dot{q} & \text{for } \left(\phi - \beta\right) \le \theta \le \left(\phi + \beta\right) \\ 0 & \text{for } \left(\phi + \beta\right) \le \theta \le \left(2\pi + \phi - \beta\right) \end{cases}. \tag{3.31}$$

The initial condition is expressed as

$$T\left(r, \theta, t\right) = T_0 \quad \text{for } t = 0 \quad \text{in region } a < r < b, \tag{3.32}$$

where T_0 is an initial temperature of the roll.

Details of the derivation of solution are described in Appendices C and D. The heat conduction equation is solved using integral transform method. The temperature distribution from the solution is obtained as (Yiannopoulos *et al.*, 1997)

$$\begin{aligned} T\left(r, \theta, \phi, t\right) = {} & T_0 \sum_{m=1}^{\infty} \frac{R_0\left(\beta_m, r\right)}{F_0} G_0 \exp\left(-\alpha_r \beta_m^2 t\right) \\ & + \left(\pi H_e T_e + \frac{\dot{q}}{k_r}\beta\right) \sum_{m=1}^{\infty} \frac{R_0\left(\beta_m, r\right)}{F_0} \left(1 - \exp\left(-\alpha_r \beta_m^2 t\right)\right) \\ & + \frac{\pi^2}{2} H_i a T_i \sum_{m=1}^{\infty} \frac{R_0\left(\beta_m, r\right)}{F_0} R_0\left(\beta_m, a\right) \left(1 - \exp\left(-\alpha_r \beta_m^2 t\right)\right) \\ & + 2\frac{\dot{q}}{k_r} \sum_{n=1}^{\infty} \sum_{m=1}^{\infty} \frac{R_n\left(\beta_m, r\right)}{F_n} \frac{\sin n\beta}{n} \\ & \times \frac{\cos n\left(\theta - \phi\right) - \lambda_n \sin n\left(\theta - \phi\right) + \left(\lambda_n \sin n\theta - \cos n\theta\right) \exp\left(-\alpha_r \beta_m^2 t\right)}{1 + \lambda_n^2}, \end{aligned} \tag{3.33}$$

where $\lambda_n = \omega n/(\alpha_r \beta_m)$. The expressions for $R_0(\beta_m, r)$, $R_0(\beta_m, a)$, $R_n(\beta_m, r)$, F_0, F_n, G_0, H_i and H_e are provided in Appendices C and D. It is to be noted that Eq. (3.33) provides the transient as well as steady-state temperature distribution in the roll. The steady-state temperature distribution in the roll is obtained when $t \to \infty$. The time dependent terms appearing in exponential form vanish as the time variable becomes large enough. Thus, only the sinusoidal and constant terms remain in Eq. (3.33) yielding the following equation:

$$T(r,\theta,\phi) = \left(\pi H_e T_e + \frac{\dot{q}}{k_r}\beta\right)\sum_{m=1}^{\infty}\frac{R_0(\beta_m, r)}{F_0} + \frac{\pi^2}{2} H_i a T_i \sum_{m=1}^{\infty}\frac{R_0(\beta_m, r)}{F_0} R_0(\beta_m, a) + 2\frac{\dot{q}}{k_r}\sum_{n=1}^{\infty}\sum_{m=1}^{\infty}\frac{R_n(\beta_m, r)}{F_n}\frac{\sin n\beta}{n}\frac{\cos n(\theta-\phi) - \lambda_n \sin n(\theta-\phi)}{1+\lambda_n^2} \quad (3.34)$$

The temperature distribution in the roll as a function of radial and circumferential coordinates is obtained by rotating the heat source with a constant angular velocity (ω). The rotating heat source position, ϕ may be expressed as a linear function of ω such that $\phi = \omega t$, where t is the time parameter.

Using Eq. (3.34) the steady-state temperature distribution in the roll at any r-θ locations can be obtained for any angular velocity, ω of the rotating heat source. Here, θ represents the any circumferential location at which temperature is to be measured and ϕ represents the circumferential location of the rotating heat source at the outer roll periphery. For any fixed θ, the temperature distribution in the roll can be determined as a function of ϕ.

3.6 An Analytical Model for Temperature Distribution in Strip

The temperature distribution in the strip can be obtained by solving the heat conduction equation in the bite zone (BCHG) and the outer zone (CDEH) as shown in Fig. 3.6. It is assumed that the plastic deformation occurs in the strip in the domain BCHG, although the actual plastic deformation zone depends on the

process parameters. It is observed that about 90% of the work of plastic deformation gets converted into heat (Jiang *et al*., 2004 and Khalili *et al*., 2012). Assumption of 90% of plastic deformation going as heat and remaining to increase the internal energy of metal is commonly taken in metal forming (Serajzadeh and Mohammadzadeh, 2007).

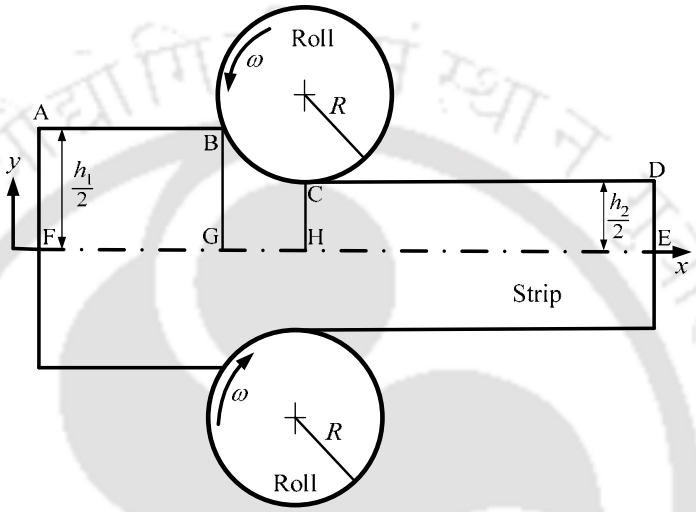

Fig. 3.6. A schematic diagram of flat rolling

The heat generated due to frictional work is distributed in the roll and strip (depending upon the difference of roll and strip temperature). Assume that the total heat Q_T comprises the total heat due to plastic deformation, frictional heat and heat due to movement of hot strip. A portion of this heat, λQ_T goes into the roll and $(1-\lambda)Q_T$ remains in the strip. The value of heat partition factor λ is obtained by matching the average surface temperature of the roll and the strip at roll-strip interface. The methodology for this has been already explained in Section 3.2.

The temperature distribution in the bite zone (BCHG) and after the roll bite of the strip is obtained following an approach similar to the work of Kim *et al*. (2009). The expression for rate of heat generation per unit volume $\dot{Q}$ and average heat flow rate at the roll-strip interface $\dot{q}_s$ in the present work differs from the expression taken by Kim *et al*. (2009). Kim *et al*. (2009) employed mathematical expression developed by Lee *et al*. (2004) on the basis of FEM. However, in the present work these powers are calculated by FEM model described in Section 3.3.

For the sake of completeness, the analytical solutions of Kim *et al*. (2009) and its modification have been described here.

Considering the heat transfer in the longitudinal direction of the strip to be insignificant, Kim *et al*. (2009) employed heat conduction equation given as

$$\frac{\partial}{\partial y}\left(k_s \frac{\partial T(y,t)}{\partial y}\right)+\dot{Q}(y)=\rho_s c_{ps}\frac{\partial T(y,t)}{\partial t}, \tag{3.35}$$

with the boundary conditions

$$\frac{\partial T(y,t)}{\partial y}=0 \quad \text{at} \quad y=0, \tag{3.36}$$

$$k_s \frac{\partial T(y,t)}{\partial y}=\dot{q}_s \quad \text{at} \quad y=h, \tag{3.37}$$

where ρ_s is the density, c_{ps} is the specific heat, k_s is the thermal conductivity and h is the average semi-thickness of the strip. The initial condition is

$$T(y,0)=T_0(y). \tag{3.38}$$

The above differential equation with boundary conditions is solved using eigenfunctions method. Details of the derivation is given in the Appendix E. Temperature distribution in the bite zone as per the coordinate system of Fig. 3.6 is given by

$$T_e(y,t)=\frac{1}{h}\int_0^h T_0(y)\,\mathrm{d}y+\frac{1}{h\rho_s c_{ps}}\left(\dot{q}_s+\int_0^h \dot{Q}\,\mathrm{d}y\right)t+\sum_{n=1}^{\infty}\left[\left\{\exp\left(-\lambda_n^2\frac{k_s}{\rho_s c_{pss}}t\right)\left\{a_n(0)+\frac{2(-1)^n}{h\rho_s c_{ps}}\int_0^t\left(\dot{q}_s\exp\left(\lambda_n^2\frac{k_s}{\rho_s c_{ps}}t\right)\right)\mathrm{d}t\right\}\right\}\right.$$
$$\left.+\frac{2}{\lambda_n^2 k_s h}\left(1-\exp\left(-\lambda_n^2\frac{k_s}{\rho_s c_{ps}}t\right)\right)\int_0^h \dot{Q}\cos(\lambda_n y)\mathrm{d}y\right]\cos(\lambda_n y), \tag{3.39}$$

where

$$\lambda_n=\frac{n\pi}{h} \tag{3.40}$$

and

$$a_n(0)=\frac{2}{h}\int_0^h T_0(y)\cos(\lambda_n y)\,\mathrm{d}y, \tag{3.41}$$

$T_0(y)$ is the initial strip temperature, h is the average thickness of strip at deformation zone, k_s is the thermal conductivity of strip, ρ_s is the density of strip,

c_{ps} is the specific heat of strip, $\dot{Q}$ is the heat generated per unit of volume, $\dot{q}_s$ is the average heat flow rate to the strip at the roll and strip interface. It can be noted that there is no variation of temperature along longitudinal direction in the deformation zone as observed by Kim *et al*. (2009). The same observation was found by FEM analysis of the roll and the strip. The approximate time t_a spent by the strip in the roll bite can be calculated by dividing L with the average velocity of the strip. The time t_a is substituted in Eq. (3.39) to obtain the temperature in the roll bite. The rate of heat generated per unit volume $\dot{Q}$ and the average heat flow rate to the strip at the roll-strip interface $\dot{q}_s$ are given by

$$\dot{Q} = \frac{0.9 P_P}{0.5\left(h_1 + h_2\right) L w}, \tag{3.42}$$

$$\dot{q}_f = \frac{P_f}{w l_d}, \tag{3.43}$$

where P_p, P_f, h_1, h_2, L, w and l_d are the plastic deformation power, friction power, sheet thickness at inlet, sheet thickness at outlet, length of plastic deformation zone (=GH in Fig. 3.6), width of the sheet and contact length of roll and strip respectively. The plastic deformation power P_P and friction power P_f are obtained from the deformation module. In the present work, P_P and P_f are estimated by an FEM based deformation module using Eqs. (3.11) and (3.12), respectively. It is assumed that there is no variation of temperature along longitudinal direction in the deformation zone. The approximate time t_a spent by the strip in the roll bite can be calculated by dividing L with the average velocity of the strip. This time t_a is put in Eq. (3.39) to obtain the temperature in the roll bite. Equation (3.39) provides approximate temperature in the bite zone, assuming that there is no significant change in the temperature in the longitudinal direction.

From the exit of roll bite to the temperature sensor (location where measurement of temperature is needed), the heat transfer is governed by

$$\frac{\partial}{\partial y}\left(k_s \frac{\partial T(y,t)}{\partial y}\right) = \rho_s c_{ps} \frac{\partial T(y,t)}{\partial t}, \tag{3.44}$$

with boundary conditions

$$\frac{\partial T(y,t)}{\partial y} = 0 \text{ at } y = 0, \tag{3.45}$$

$$-k \frac{\partial}{\partial y}\left(\frac{\partial T(y,t)}{\partial y}\right) = h_a \left\{T(y,t) - T_a\right\} \quad \text{at } y = \frac{h_2}{2}, \tag{3.46}$$

where h_a is the heat transfer coefficient and h_2 is the exit thickness of the strip. The initial condition is

$$T(y,0) = T_e(y,t_a). \tag{3.47}$$

The solution of the one dimensional heat conduction problem is obtained by the method of separation of variables.

Details of the derivation of solution are described in Appendix F. The temperature distribution of strip at the exit side is given as (Kim *et al*., 2009):

$$T(y,t) = T_a + \sum_{n=1}^{\infty} \exp\left(-\frac{k_s}{\rho_s c_{ps}} \lambda_n^2 t\right) \left\{ \frac{4\lambda_n \int_0^{\frac{h_2}{2}} T_e(y,0)\cos(\lambda_n y)\,dy - 4T_a \sin\left(\lambda_n \frac{h_2}{2}\right)}{\lambda_n h_2 + \sin(\lambda_n h_2)} \right\} \cos(\lambda_n y), \tag{3.48}$$

where $T_e(y,0)$ is the temperature at the exit of deformation zone that corresponds to time t=0, T_a is the temperature of the coolant, h_a is the convective heat transfer coefficient at the strip surface and λ_n is the positive roots of the transcendental equation obtained by solving the following equation:

$$k_s \lambda_n \sin\left(\lambda_n \frac{h_2}{2}\right) - h_a \cos\left(\lambda_n \frac{h_2}{2}\right) = 0. \tag{3.49}$$

3.7 Determination of Temperature Distribution in Roll and Strip by Finite Element Method

In this section, finite element method (FEM) based model is presented to estimate the temperature in the strip and the roll. A two-dimensional thermal problem is solved assuming constant heat flux input into the roll at the roll-strip interface. Figure 3.7(a) shows the thermal and geometric boundary conditions of the roll. The convective heat transfer loss in air at the outer and inner periphery of the roll is considered. For finding out the temperature distribution in the roll, the roll is assumed to be stationary and heat flux is moving around its outer periphery with constant angular velocity. Figure 3.7(b) shows the thermal boundary conditions of the strip. It is assumed that heat loss at the outer surface of strip is zero except at the roll-strip interface. Due to symmetry, the heat loss at the centerline of the strip is zero.

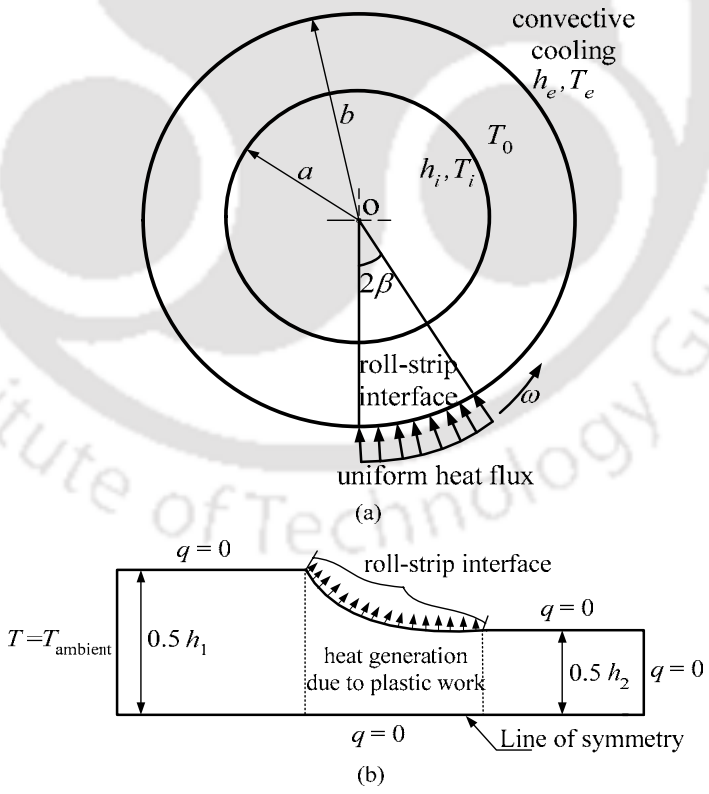

Fig. 3.7. Boundary conditions for the FE model: (a) thermal boundary conditions for the roll and (b) thermal boundary conditions for the strip

There are many commercial FEM based packages for modelling the manufacturing processes, like DEFORM that can solve the coupled thermo-mechanical rolling process. Often these packages are used as black box and the user does not have full control over the package. However, general purpose FEM packages like ANSYS and ABAQUS are easily available and affordable. The present work uses an FEM flow formulation (Dixit, 1997) for the deformation analysis. The heat flux due to plastic deformation and friction is calculated employing Eqs. (3.42) and (3.43). Here, a general purpose code ABAQUS 6.10 taking heat flux into account is used for carrying out the thermal analysis.

The average temperature of roll and strip is obtained at the roll-strip interface separately. The matching of the average temperature of roll and strip is carried out by adjusting the heat input rate into the roll from the strip at the roll-strip interface. It is assumed that the quantity λQ_T pass to the rolls and $(1-\lambda)Q_T$ remains in the strip, where Q_T is the rate of heat input. The value of heat partition factor λ is obtained to match the average temperature of the roll and strip at the interface. The methodology for finding out the value of λ has been presented in Section 3.2.

3.7.1 Temperature Distribution in Roll

The temperature distribution in the roll is obtained by providing a specified heat flux. Here, the problem is formulated in the ABAQUS considering the roll and strip separately. The steady-state temperature is obtained by carrying out a transient heat transfer till the steady-state is attained. It is observed that for attaining the steady-state, the analysis requires a screen time of about 2 hours. In the present work, an attempt has been made for reducing the computational time to find out the steady-state temperature distribution in the roll by FEM. For improving the computational efficiency, a methodology is developed to obtain the steady-state temperature distribution in the roll. A 4-noded linear quadrilateral element (DCC2D4) is chosen for heat transfer analysis of both roll and strip.

The methodology for determining the steady-state temperature distribution in roll is as follows:

Step 1: First obtain the circumferentially averaged temperature of roll by applying the uniform heat flux around its periphery. The average heat flux Q_{av} applied along the outer periphery is calculated by the formula $Q_{av} = \frac{2\beta}{360°} \times \lambda Q_T$, where 2β is the bite angle and λQ_T is the heat input rate at the roll gap. (As discussed in Section 3.2, λ is an adjustable parameter that is determined by matching the average temperature of roll and strip at the interface).

Step 2: The entire outer periphery is divided into *n* equal parts for applying heat source as shown in Fig. 3.8a. Each part is further subdivided into *m* user defined parts depending on the requirement of mesh refinement. Depending on the bite angle, the heat source may occupy *m* subdivisions at a time. A transient analysis is carried out in which at each time step, the heat sources moves counterclockwise by one subdivision. The initial temperature in the transient analysis is taken as circumferentially averaged temperature. The temperature at the end of each time increment is measured at the lowest point of the roll, *i.e.* at P. Thus, at each time increment, temperature at P indicates the temperature at different angular locations of heat flux. (Angular location of the heat flux is specified by the leftmost point of the heat flux). Once the temperature at the point P is obtained for various angular locations between 0° to 360°, the steady state temperature distribution can be plotted. One can note that the temperature due to moving heat source at a fixed point is same as the temperature at corresponding angular location due to rotating roll and fixed heat source.

Step 3: The procedure of Step 2 is repeated several times, till convergence is obtained. Convergence is assessed by comparing the maximum temperature with expected exact maximum temperature. The expected exact maximum temperature is obtained by convergence acceleration method of Aitken and Steffenson described in Zyczkowski (1981). As per this, let x_1, x_2 and x_3 denote the maximum temperature of three consecutive iterations. It is assumed that they approach their limit x as geometrical series *i.e.*,

$$\frac{x - x_1}{x - x_2} = \frac{x - x_2}{x - x_3}, \tag{3.50}$$

From the above equation, the expected exact temperature x can be calculated as

$$x = \frac{x_1 x_2 - x_2^2}{x_1 + x_3 - 2x_1 x_2} \quad . \tag{3.51}$$

The iterations are stopped when the error between the maximum temperature and expected exact maximum temperature is below a specified value. Figure 3.8a shows the location of the instantaneous moving heat source at the beginning over the outer periphery of the roll. The location of the moving heat source at any instant of time is shown in Fig. 3.8b. The temperature is recorded at location P as shown in Fig. 3.8 while heat source is rotating over the interface.

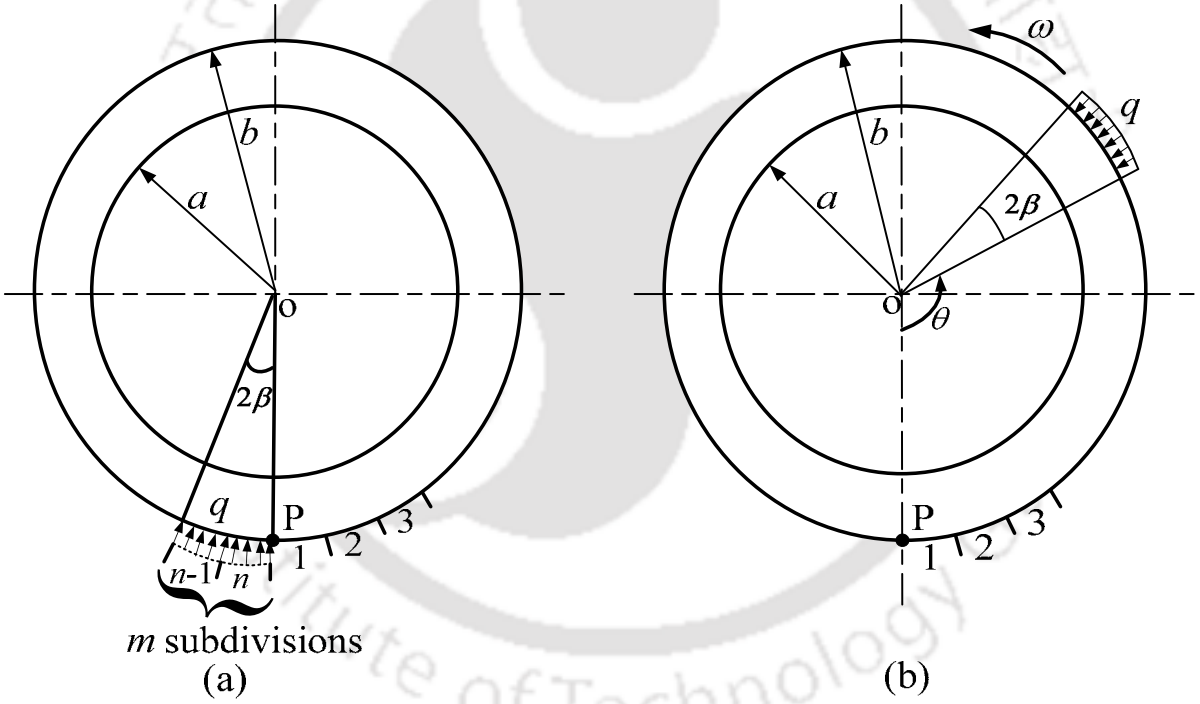

Fig. 3.8. Two dimensional configurations for temperature measurement in roll (a) position of heat source at the beginning and (b) instantaneous position of the heat source after rotating an angle θ

3.7.2 Temperature Distribution in Strip

The strip temperature is estimated by taking the boundary conditions shown in Fig. 3.7(b) and considering heat generation, a transient heat conduction analysis is carried out for a time interval of l_d/V , where l_d is the contact length and V is the average speed of the strip. The temperature obtained after this time interval is considered as steady-state temperature of the strip in the considered domain. The basis of this assumption is that on an average, any portion of the moving strip receives heat for a period of l_d/V . Moreover convective term in the heat conduction equation is small in comparison to heat generation due to plastic deformation and friction. The finite element based package, ABAQUS 6.10 version is used for heat transfer analysis of the strip and roll. The problem is solved using ABAQUS-Explicit code.

3.7.3 A Note on the Fast Estimation of Temperature Distribution by FEM

It is mentioned in Subsection 3.7.1 that to obtain the steady-state temperature in the roll by carrying out a transient heat transfer analysis in FEM takes about 2 hours of the screen time. However, employing the proposed methodology, the time required for the analysis is reduced to about less than 10 minutes. The computational time may be reduced further to less than 1 minute by solving it using DFLUX subroutine in ABAQUS. The DFLUX subroutine written in FORTRAN language is provided in Appendix G. The faster estimation of the temperature distribution in the roll may be attributed to the superimposition of the averaged steady-state temperature of roll with transient temperature. Initially, by applying the average heat flux around the outer roll periphery, the circumferentially averaged temperature of roll is obtained. Now, the circumferentially averaged temperature of the roll is treated as an initial temperature for the transient analysis. While employing the transient analysis, the maximum temperature of roll is calculated (at point P as shown in Fig. 3.8) after completing each revolution of the moving heat source. The convergence of the steady-state temperature is assessed by comparing the maximum temperature with expected exact maximum temperature. As the initial circumferential averaged temperature is superimposed to the transient temperature during the analysis

procedure, it reduces the number of iterations to reach the steady-state temperature. Due to this, the computational time for achieving the steady-state temperature in the roll is significantly reduced.

3.8 Comparison of Thermal Analysis by Analytical Methods and Finite Element Method

In this section, a comparative study of analytical methods and finite element method is presented. First the steady-state temperature is compared while considering a thermal analysis of roll only. Further, a thermo mechanical analysis of strip is carried out. Finally, the average temperature of the roll and strip at the roll-strip interface is calculated. For this an appropriate heat partition factor λ is determined by matching the average temperature of the roll and the strip at the interface.

3.8.1 Study on Mesh Sensitivity of FEM Model for Thermal Analysis

In order to select appropriate element size for the steady-state temperature distribution of the roll, a mesh sensitivity study is performed. The material of the roll and the strip is considered to be made of steel. The thermal material property and geometry of the roll is given in Table 3.1. The mesh sensitivity of the roll and the strip is done on the basis of maximum temperature measurement. Table 3.2 shows the maximum temperature of the roll after 20, 40 and 60 revolutions for different meshes, when the roll speed is 0.1 rad/s. The maximum temperature was recorded for different combination of mesh size for different number of revolutions. It is seen from Table 3.2 that although the maximum temperature keeps on increasing as the mesh is refined, the change is not much substantial. However, the computational time keeps on increasing at order of n^2, where n is the number of elements. A compromise is reached for 4 elements in the radial direction and 400 elements in the circumferential direction. In the similar manner, for the strip, a mesh consisting of 400 elements is taken (80 elements in the length direction of the strip and 5 elements in the thickness direction).

Table 3.1. Material constants and geometric parameters for thermal analyses for roll (steel)

Parameter	Value
Inner roll radius (a)	0.23 m
Outer roll radius (b)	0.25 m
Convective heat transfer coefficient at outer periphery (h_e)	260 W/m^2-°C
Convective heat transfer coefficient at inner periphery (h_i)	2.6 W/m^2-°C
Thermal conductivity (k_r)	52 W/m-°C
Thermal diffusivity (α_r)	0.144×10^{-4} m^2/s
Initial temperature at the inner and outer periphery (T_i , T_e)	30 °C
Semi-bite angle (β)	8°
Heat flux ($\dot{q}$)	5×10^6 W/m^2

Table 3.2. Maximum temperature of roll for different mesh size

Divisions of roll		Maximum temperature (°C) in the roll		
Radial direction	Circumferential direction	after 20 revolution	after 40 revolution	after 60 revolution
1	400	1093	1101	1111
2	400	1259	1260	1277
3	400	1233	1334	1351
4	400	1359	1360	1377
5	400	1370	1371	1388
4	100	1321	1322	1339
	200	1345	1346	1363
	800	1361	1362	1379

3.8.2 Steady-State Temperature Distribution in Roll for Specified Heat Input

The results of the two-dimensional thermo-mechanical analysis to obtain the steady-state temperature distribution of the roll and the strip are described. First, the temperature distribution in the roll is obtained by three different methods *viz*., approximate method based on Laplace transform, series solution using integral transform technique (Yiannopoulos *et al*., 1997) and FEM using ABAQUS. A number of numerical experiments were conducted for different roll geometry and thermal properties to determine the appropriate number of terms of series expansions— m and n. Here, m=30 and n=15 is considered to find out the temperature distribution in roll within less than 1% accuracy. For the sake of simplicity in the analysis, the average thermal properties of the roll and strip are

considered. However, a few runs with the temperature dependent material properties of a typical steel showed insignificant error in the results. The material properties and the dimensions of the roll are tabulated in Table 3.1.

Figure 3.9 shows the temperature distribution on the surface of the roll at different angular velocities based on the input data of Table 3.1. This data is the same as taken by Yiannopoulos *et al*. (1997) for analyzing the temperature distribution in roll. It is observed that the peak temperature of the roll decreases with increasing angular velocity in a steady-state. The result of the approximate method is compared with the results of the (Yiannopoulos *et al*., 1997) and FEM by taking only the thermal module. The FEM simulations were carried out by using ABAQUS. The results obtained by FEM based procedure have been taken as the basis for assuring the accuracy of the present approximate method. Transient temperature distribution in the form of a series solution using integral transform technique is obtained. Approximate method employing the closed form expression for temperature calculation is mathematically simpler compared to Yiannopoulos *et al*. (1997).

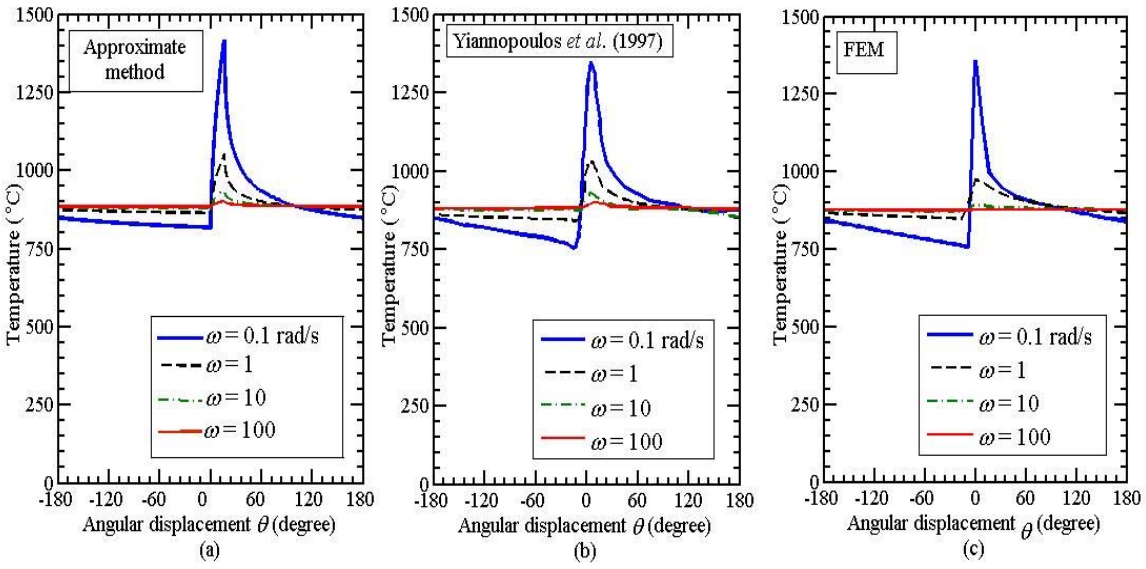

Fig. 3.9. Steady state temperature distributions in a rotating roll at the outer surface for heat input rate of 5 MW/m^2: (a) Approximate method based on Fischer *et al*. (2004) (b) Yiannopoulos *et al*. (1997) and (c) FEM

Figure 3.9 compares the temperature distribution predicted from the approximate method with that predicted by Yiannopoulos *et al*. (1997) and FEM. The difference of predicted peak temperatures by three methods is less than 8% at ω = 0.1 rad/s. The difference decreases with increasing ω. The maximum temperature of roll decreases with increasing angular velocity. Figure 3.10 shows the temperature distributions on the inner and outer surface of the roll at the angular velocity of 0.314 rad/s. It is observed that at the outer radius of the roll, the temperature variation on the periphery is more as compared to the inner radius. The agreement between temperature distributions obtained from three methods is good.

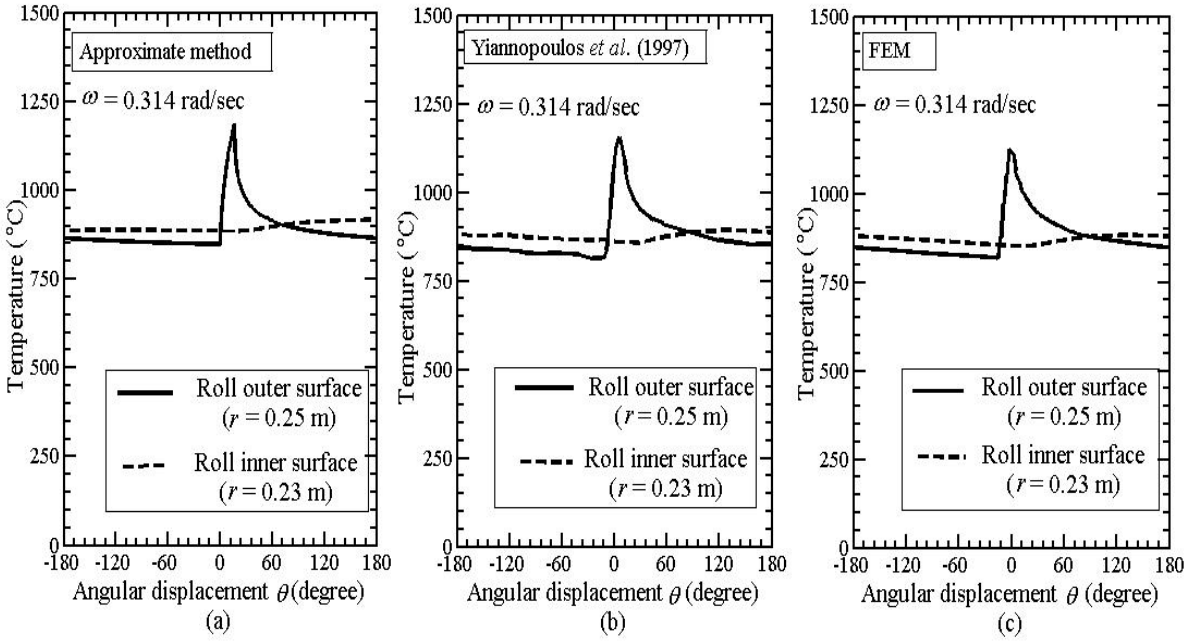

Fig. 3.10. Steady-state temperature distribution in a rotating roll at the inner and outer radii for heat input rate of 5MW/m^2: (a) Approximate method based on Fischer *et al*. (2004) (b) Yiannopoulos *et al*. (1997) and (c) FEM

Table 3.3 shows the comparison of peak temperature for all three methods at different angular velocities of roll. It is observed that at high angular speed of the rolls, the peak temperature is nearly the same in all the three cases. In all the cases, deviation between predictions is less than 10%.

Table 3.3. Comparison of the maximum steady-state temperature at different angular velocities

S. No	Angular velocity (ω rad/s)	Peak surface temperature in roll (°C)		
		Approximate method	Yiannopoulos *et al.* (1997)	FEM
1.	0.1	1420	1348	1360
2.	1	1055	1028	975
3.	10	940	931	896
4.	100	903	900	878

Figure 3.11 shows the temperature distributions on the inner and outer surface of the roll at the angular velocity of 1 rad/s. Here, the inner roll radius a is 0.25 m and the outer roll radius b is 0.30 m. The other parameters are given in Table 3.1. It is observed that the approximate method predicts the larger error than the series solution using integral transform technique in comparison to the FEM predictions which are considered to be the reference values. However, the maximum error is less than 6%.

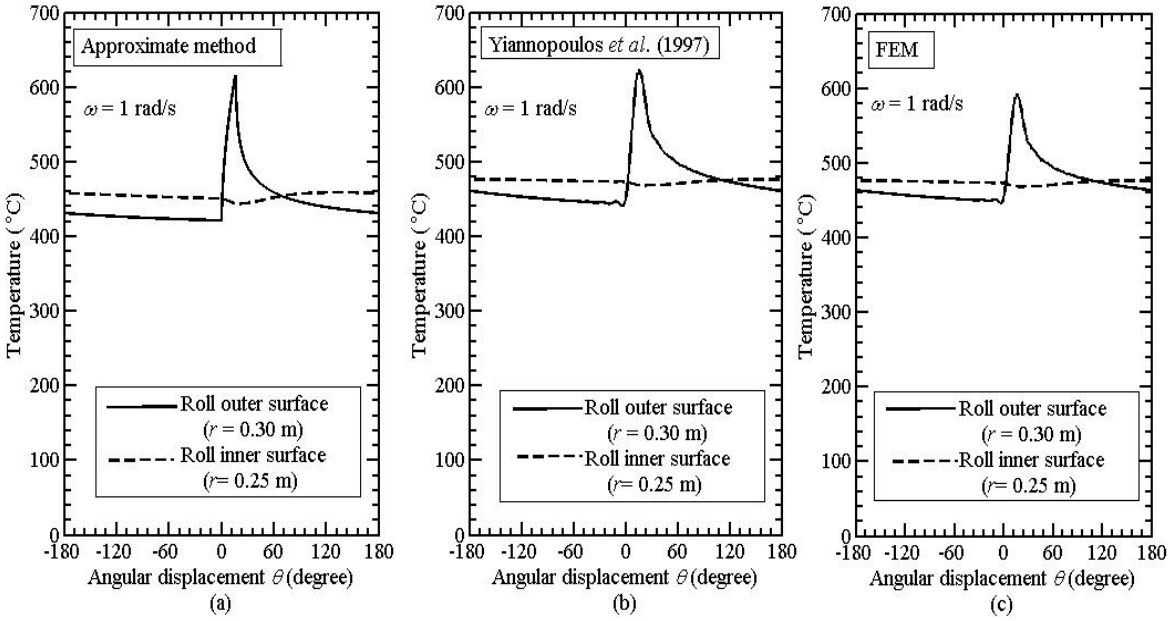

Fig.3.11. Steady-state temperature distributions in a rotating roll at the inner and outer radii for heat input of 5 MW/m^2, h_i = 5.2 W/m^2-°C and h_e = 520 W/m^2-°C: (a) Approximate method based on Fischer *et al.* (2004) (b) Yiannopoulos *et al.* (1997) and (c) FEM

The approximate method takes the minimum computational time compared with other two methods. The series solution using integral transform technique given by Yiannopoulos *et al*. (1997) involves the roots from the transcendental equation. These roots are function of the roll dimensions, thermal conductivity and convective heat transfer coefficient of the roll and need to be evaluated for different sets of parameters.

Table 3.4. Comparison of three methods for carrying out the thermal analysis of the roll

S.No.	Method	Computational screen time	Remarks
1.	Approximate Method based on Fischer *et al*. (2004)	less than 10 second	• Steady-state temperature is obtained. • Constant initial temperature of roll (T_0) is used to obtain a closed form solution. • No provision for incorporating temperature dependent material property data. • The roll is assumed to be made of homogeneous material.
2.	Yinnopoulos *et al*. (1997) (transient as well as steady-state)	about 25–30 minutes	• Transient as well as steady-state temperature is obtained. • Initial temperature of roll can be considered as function of radial and circumferential coordinates. • Incremental analysis can be carried out (by this time varying heat input into the roll may be considered). • No provision for taking temperature dependent material property data. • Homogeneous material of the roll is assumed.
3.	FEM	about 10 minutes for steady-state analysis by the fast FEM (described in Section 3.7) about 2 hours for transient analysis.	• Initial temperature of roll can be considered as function of radial and circumferential coordinates. • Temperature dependent material property data can be considered. • Composite or functionally graded material (FGM) can be considered.

Table 3.4 shows the comparison of results with three methods. Three methods for determining the temperature distribution in the roll are proposed in the present thesis. These three methods are approximate method, series solution using integral transform technique and an FEM model. The strip temperature distribution is calculated by an analytical method and an FEM model. The FEM model results are considered as a benchmark for the other two methods while making comparisons. The determination of temperature distribution through analytical method for the roll as well as strip is advantageous in terms of computational time. The analytical solutions are incorporated along with FEM deformation module to alleviate the complexity of the process and faster prediction of the temperature distribution in the roll and the strip.

3.8.3 A Comparison of Approximate Method and FEM Results with the Experimental Results of Jeswiet and Rice (1975)

The thermo-mechanical analysis of strip and roll is carried out to calculate the rise in temperature at the roll-strip interface. It is required to find out the power due to plastic deformation and friction power by FEM and choose an appropriate partition factor for heat transfer between the roll and the strip. This was carried out here with the roll and strip properties as shown in Table 3.5. The ambient temperature is always taken as 30 °C. The roll-strip interface temperature is compared from the experiments of Jeswiet and Rice (1975). The material of the strip is Alloy 1100-H141 of dimensions $280 \times 23 \times 9.8$ mm^3. The material properties of Alloy 1100-H141 and the roll are taken from Wilson *et al*. (1989). The strain-rate is kept constant for validating the results of the present model with the experiments of Jeswiet and Rice (1975).

Table 3.5. Aluminum alloy strip and steel roll properties

Parameter	Alloy 1100-H141 (strip)	Roll
Conductivity (W/m-°C)	284	54
Density (kg/m^3)	2707	7833
Specific heat (J/kg-ºC)	896	465
Flow stress (MPa)	$\sigma_y = 100\left(1+0.9\varepsilon^{0.355}\right)$	

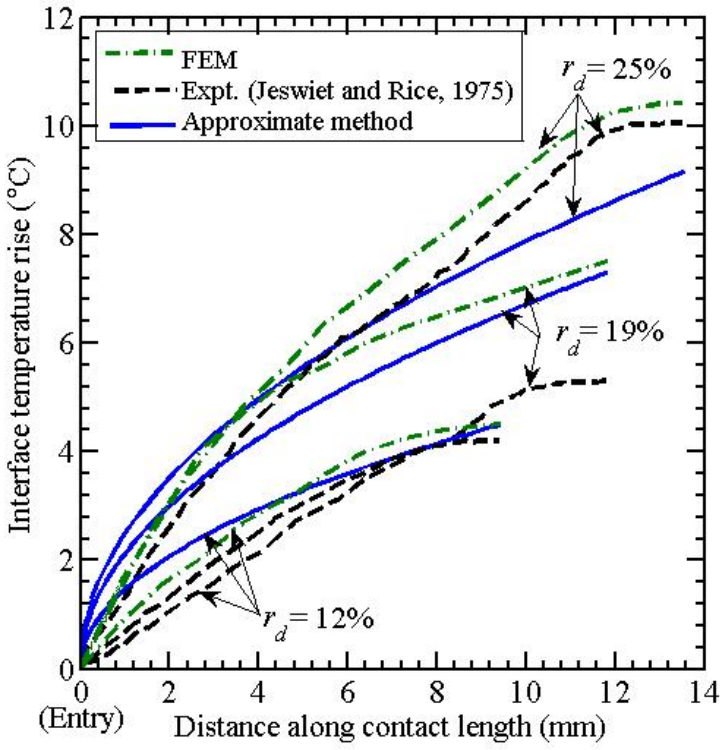

Fig. 3.12. Comparison of the present method with experiments of Jeswiet and Rice (1975) and FEM for Alloy 1100-H141

Roll radius and exit speed of strip are 75 mm and 0.096 m/s respectively. With this data, simulations were carried out for different reductions in strip, and the temperatures of roll and strip are recorded. The value of heat partition factor was determined by matching the average temperature of roll and strip at the roll bite. The quantity of heat distributed between the roll and the strip was obtained by one dimensional search. Figure 3.12 compares the predictions of present model and experimental measurements of interface temperature rise for different percentage of reductions. It is seen from Fig. 3.12 that the approximate method and FEM predictions are in good agreement with experiments except for the case of 19% reduction. The same observation is also reported in Wilson *et al*. (1989) based on finite difference method. Wilson *et al.* (1989) suspected that the deviation for 19% reduction case may be due to experimental results. Wilson *et al*. (1989) did not provide the details about the deformation modelling, for which they developed a FORTRAN 77 code entitled THERMAL for the estimation of temperature. The

exact detail of computational time has not been provided by them. The information could have been any way only indicative due to large difference in computer hardware in 1989 and at present in 2016. The present method carries out the deformation analysis by FEM, but due to convergence acceleration techniques adopted, it takes less than 10 minutes of screen time in 2.6 GHz processor and 3.25 GB RAM AMD Phenom II PC.

3.8.4 Further Comparison of FEM based and Approximate Methods

In this subsection, a comparison of the results obtained by approximate method and by an FEM based model is presented. This comparison is essential to throw light on certain aspects such as the effect of roll radius and exit velocity of strip. Approximate and FE methods were used for carrying out thermal analysis as described in the previous sections. However, deformation analysis is carried out solely by FEM. The output from deformation analysis subsequently forms the input to the thermal analysis for estimating average temperature under steady-state condition at the roll-strip interface. This temperature is estimated by taking into account the heat partition factor between the roll and the strip which is also evident from the approximate method. It can be reasonably argued that the average temperature at the roll-strip interface depends on the temperature gradient between the roll and the strip which is the driving factor of heat flow across the interface.

In order to further assess the accuracy of the proposed model, the new set of numerical experiments was carried out under cold rolling conditions by taking into account the thermal properties of strip and roll as per Table 3.6. The thickness of the roll cylinder was kept constant at 20 mm. It was assumed that the actual flow stress of strip is governed by the following empirical relation (Dixit and Dixit, 2008) considering strain-rate kept constant:

$$\sigma_y = (\sigma_Y)_0 \left\{1 + \frac{\varepsilon}{b}\right\}^n, \tag{3.52}$$

where $(\sigma_Y)_0$ is the yield stress of the material and b and n are material hardening parameters.

Table 3.6. Steel strip and roll properties

Parameter	Strip	Roll
Conductivity (W/m-°C)	30	52
Density(kg/m^3)	7800	7850
Specific heat (J/kg-ºC)	470	460
Diffusivity (m^2/sec)	0.82×10^{-5}	0.144×10^{-4}

Tables 3.7 and 3.8 show the comparison of the results obtained by approximate method and FEM for two different exit velocities of the strip. The mechanical properties of the strip and other required process parameters are provided in the captions of tables. The maximum error in the average interface temperature estimated by the approximate method and by FEM is 11%. In many cases, the error is much lesser than this. Thus, the proposed model in this work is in good agreement with both an approximate method and an FEM. The computational time with the approximate method is less than 10 seconds, whereas the FEM analysis takes about 10 minutes. The reduction in computational time is highly significant for online and offline optimization of the process. Assume that the process parameters are to be adjusted based on 10 function evaluations in an optimization routine. If the computational time is 10 second, the whole procedure takes less than 2 minutes. On the other hand, if the computational time is 10 minutes, the procedure takes about 1 hour and 40 minutes!

Table 3.7. Comparison of approximate method with FEM for exit velocity of 1 m/s (h_1 = 1mm, r_d = 24%, h_i = 2.6 W/m^2-°C, h_e = 260 W/m^2-°C, μ = 0.14, $(\sigma_Y)_0$ = 400 MPa, b = 0.052, n = 0.295, T_0 = 30 °C)

Roll radius R (mm)	Approximate method			FEM		
	Power (kW)		Average temperature at the interface (°C)	Power (kW)		Average temperature at the interface (°C)
	Plastic deformation (P_p)	Friction (P_f)		Plastic deformation (P_p)	Friction (P_f)	
35	81.64	19.04	72.51	81.13	20.12	75.21
65	82.08	29.54	91.41	81.99	32.53	94.5
130	84.12	67.98	159.3	84.21	68.32	178.72

Table 3.8. Comparison of approximate method with FEM for exit velocity of 2 m/s (h_1 = 1mm, r_d =24%, h_i = 2.6 W/m^2-°C, h_e = 260 W/m^2-°C, μ = 0.14, $(\sigma_Y)_0$ = 400 MPa, b = 0.052, n = 0.295, T_0 = 30 °C)

Roll radius R (mm)	Approximate method			FEM		
	Power (kW)		Average temperature at the interface (°C)	Power (kW)		Average temperature at the interface (°C)
	Plastic deformation (P_p)	Friction (P_f)		Plastic deformation (P_p)	Friction (P_f)	
35	163.27	38.08	91.82	162.25	40.24	94.82
65	164.15	59.08	102.12	163.97	65.075	111.25
130	187.89	152.98	182.63	168.56	136.49	197.85

The results presented in Table 3.7 and Table 3.8 show that the power required for plastic deformation and frictional work is linearly dependent on the exit velocity of the strip keeping the others parameter constant. It is observed that the exit velocity increases by 2 times, the power required due to plastic deformation and friction work becomes double approximately. This can also be inferred by comparing the power required for the plastic deformation (P_p) and the frictional work (P_f). Thus, the heat generation in the strip (due to plastic deformation as well as the friction work) is dependent on the exit velocity of strip. One observation is that the difference between approximate method and FEM is relatively higher for increased roll radius. With the increased roll radius, the contact area and periphery of the roll increases causing enhanced variation of temperature along the periphery. In the present work, the steady-state average temperature of the roll is superimposed on the analytical temperature calculated by Eqs. (3.19) and (3.20). Also, the interface roll temperature and strip temperature are matched based on the average temperature and point by point matching is not carried out. These approximations are valid for the small roll radius cases, where the periphery and contact length are smaller. Validity starts becoming weaker as the roll radius increases. Nevertheless for practical rolling conditions, in spite of the approximations employed, one can expect reasonable results with this method. A detailed parametric study has been carried out in Subsection 3.10.2 using

approximate method. Further, some results of parametric study using fast FEM model are presented in Appendix H.

3.9 Assessment of the Assumption of the Equality of Temperatures of Roll and Strip at the Interface

In the present work, the heat input into the roll is calculated on the basis of average temperature matching of roll and strip at the roll-strip interface. It is based on the assumption that the heat transfer coefficient at the roll-strip interface, h_c, is infinite, *i.e*., there is a perfect contact. Based on experimental finding, Hlady *et al*. (1995) proposed the following empirical expression for evaluating h_c:

$$\frac{h_c C}{k} = \left(\frac{P}{\sigma}\right)^{m_2}, \tag{3.53}$$

where k is the mean of the thermal conductivities of the roll and the strip, P is the mean roll pressure in kg/mm^2, σ is the flow stresses of the strip in MPa, m_2 is the constant of the strip material and C is a surface roughness parameter of the roll material. Here, one example is presented to give an estimate of h_c.

The material constant m_2 = 1.7 and surface roughness parameter C = 35 μm given by Hlady *et al*. (1995) is used to calculate the value of h_c with the input parameter given in Table 3.6. The flow stress of strip (steel) is governed by J-C model (Eq. 3.5), where the constants of J-C model are taken from Meslin and Hamann (2003) and are as follows: A=598 MPa, B=768 MPa, n_1 = 0.2092, C = 0.0137, m_1 = 0.807. The reference strain rate ($\dot{\varepsilon}_0$) is 0.001s^{-1} and melting temperature (T_m) is 1768 K. The initial temperature of roll and strip are taken as 15 °C and 250 °C, respectively. The outer radius of the roll (R) is 65 mm and the thickness of the roll is considered to be 20 mm. The computations are carried out for 28% reduction of inlet thickness of strip (h_1 = 1 mm), taking the equivalent Coulomb coefficient of friction as 0.20. The value of h_c is obtained as 19.6×10^6 W/m^2°C. The differences in the roll and the strip temperature at the interface is calculated using the following heat flux balance equation $q = h_c(T_s - T_r)$, where q denotes the heat input into roll

from the strip at the steady-state condition. The value of q is 6.5×10^6 W/m^2. The temperature differences in the roll and the strip temperature ($T_s - T_r$) is equal to 0.33 °C. This is very small. Hence, the assumption of the same strip and roll temperature is justified.

3.10 Typical Results Obtained from the Proposed Model

A thermo-mechanical model for warm flat rolling is developed using FEM for deformation analysis and an analytical methods for thermal analysis in Sections 3.3 and 3.4. The model is first validated by calculating the roll-force, roll-torque and steady-state temperature distribution in the deformation zone. A parametric study of the average temperature distribution at the roll-strip interface with two different roll radii for different reductions is carried out. The effect of yield stress of the material is also studied.

3.10.1 Validation

To test the validity of the model developed, the results obtained by model are compared with experimental data of Shirizly and Lenard (2000). They performed rolling experiments on cold rolled low carbon steel AISI 1018 with steel rolls. In their experimental work, the specimens were preheated in air at 850 °C for 60 min to ensure a homogeneous deformation temperature. The rolling speed is 157 mm/s and the coefficient of friction is 0.25. The strip dimension is taken as $(305\times44\times4.71)$ mm^3. The outer diameter of the work-roll is 150 mm. The inner diameter of the roll is not mentioned by Shirizly and Lenard (2000). Here, it is assumed as 130 mm, considering typical practical value. (Later on, the inner diameter of 120 mm was also chosen and it was found that results differ by an amount less than 1%. Thus, the inner diameter has an insignificant effect on roll torque and roll force in this case.) The convective heat losses at the outer and inner periphery roll are assumed as 260 W/m^2-°C and 2.6 W/m^2-°C respectively. The thermal properties of strip and roll are taken from Khalili *et al*. (2012).

The flow stress of the strip material is governed by modified J-C model. The modified J-C model material parameters are taken from Vural *et al*. (2003) for AISI 1018 cold rolled. In the modified J-C model, two separate J-C models are modeled for low and high strain rate cases. Vural *et al*. (2003) have suggested the smooth transition between two models over a narrow strain-rate zone. However, here discontinuous model is taken, as it does not pose any problem in FEM code. The parameters of J-C model given by Eq. (3.4) are A = 560 MPa, B = 300 MPa, n_1 = 0.32, m_1 = 0.55, T_m = 1773 K. For strain rate of less than $\dot{\varepsilon}_t$, C is given by

$$C = n_2 \left(\frac{\dot{\varepsilon}}{\dot{\varepsilon}_{01}} \right)^{n_2}, \tag{3.54}$$

and for strain rate of greater than $\dot{\varepsilon}_t$, C is given by

$$C = n_3 \left(\frac{\dot{\varepsilon}}{\dot{\varepsilon}_{02}} \right)^{n_3}, \tag{3.55}$$

where $\dot{\varepsilon}_{02}$ is calculated as

$$\dot{\varepsilon}_{02} = \left(\dot{\varepsilon}_{01} \right)^{n_2/n_3} \left(\dot{\varepsilon}_t \right)^{(n_3 - n_2)/n_3}. \tag{3.56}$$

For AISI 1018 cold-rolled steel (Vural *et al*., 2003), n_2 = 0.007, n_3 = 0.075, $\dot{\varepsilon}_{01} = 5 \times 10^{-6}$ s^{-1} and $\dot{\varepsilon}_t = 96$ s^{-1}.

Figures 3.13 and 3.14 compare experimental and simulated roll forces and roll torques, respectively with Shirizly and Lenard (2000). The input process parameters are given in the figures. It is seen from Fig. 3.14 that the roll torque gives the maximum 12.6% error with experimental results of Shirizly and Lenard (2000). However, the roll forces obtained from the proposed model were closed to experiment results obtained by Shirizly and Lenard (2000) as shown in Fig. 3.13.

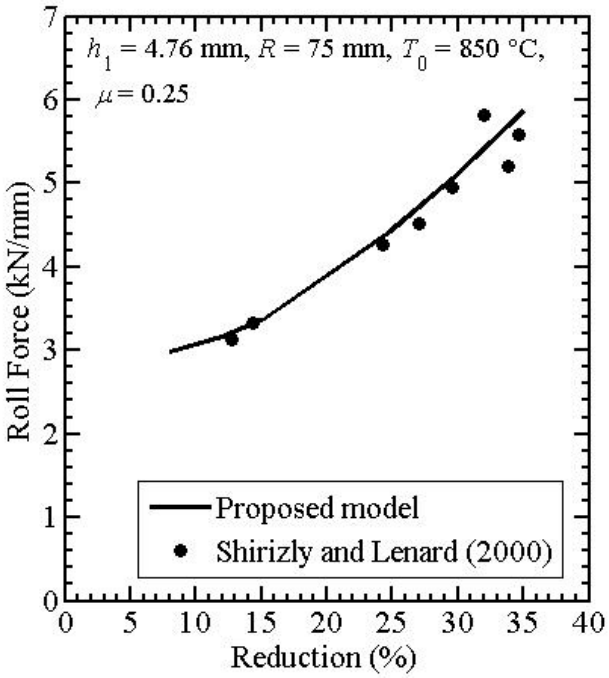

Fig. 3.13. Comparison of proposed model with experimental results of Shirizly and Lenard (2000) of roll force per unit width

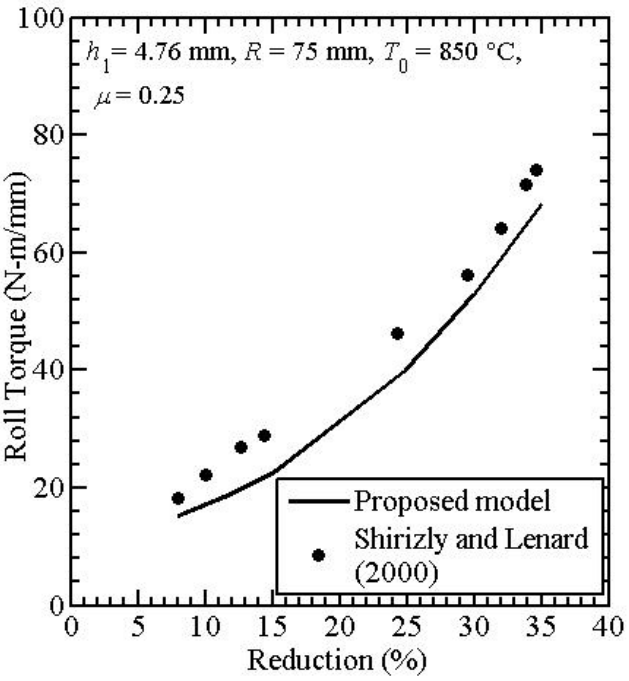

Fig. 3.14. Comparison of proposed model with experimental results of Shirizly and Lenard (2000) of roll torque per unit width

Further, an attempt was made to validate the roll surface temperature with the average temperature at the interfacing surface of the strip. The average temperatures at the deformation zone are compared with the experimental results of Serajzadeh and Mohammadzadeh (2007). Serajzadeh and Mohammadzadeh (2007) performed the warm rolling experiments of low carbon steel with steel rolls. They conducted the experiments with inlet strip temperature in the range of 500–750 °C for different rolling speed and percentage of reduction. The dimension of the strip was $(100\times5\times3)$ mm^3 and the work-roll diameter was 150 mm. The flow stress of the strip material is governed by the following power law given by Serajzadeh (2004):

$$\sigma_y = B\dot{\varepsilon}^m \varepsilon^n, \tag{3.57}$$

where B, m and n are the temperature dependent material constants expressed by

$$B = 1198 - 0.084T - 0.002T^2, \tag{3.58}$$

$$m = 0.788 - 0.0046T + 9.11\times10^{-6}T^2 - 7.04\times10^{-9}T^3 + 1.9\times10^{-12}T^4, \tag{3.59}$$

$$n = 0.36 - 2.96\times10^{-4}T, \tag{3.60}$$

where T is the temperature in °C. The inner diameter of the roll and convective heat transfer coefficients are assumed as in the previous example.

Table 3.9. Comparison of proposed model with experimental results of Serajzadeh and Mohammadzadeh (2007)

Initial temperature of strip (°C)	Inlet thickness of strip h_1(mm)	Reduction, r_d(%)	Revolution per minute (r.p.m) of the roll, ω	Average temperature at deformation zone (°C)	Expt. (Serajzadeh and Mohammadzadeh 2007) Temperature (°C)	% error
500	3	30	50	426.95	441	–3.19
650	3	15	50	599.62	595	0.78
650	3	30	50	577.16	530	8.89
750	3	15	65	692.52	700	3.28

For different values of the inlet temperature of strip, inlet thickness of strip, percentage of reduction and angular velocity of roll, results of the present work and

Serajzadeh and Mohammadzadeh (2007) are given in Table 3.9. It is observed that the error in the prediction of temperature is less than 9%.

3.10.2 Parametric Study

The parametric study has been carried out to obtain the average temperature at the roll-strip interface with different roll radius, flow stresses of the strip material, coefficient of friction and angular velocities of roll. Table 3.10 shows that the effect of roll radius becomes more predominant for higher reductions. It is observed that with increasing fractional reduction, the average temperature increases. It may be noted from Table 3.10 that friction power changes significantly on changing the roll radius although the power required for plastic deformation does not exhibit much variation. This is due to the increasing role played by the friction power. Table 3.11 shows the plastic power, friction power and temperature at the interface for two different sets of yield stresses and material hardening parameters. The yield stress in the second set is 10% higher than that in the first set. Similarly, the hardening parameters in the second set are 20% higher than those in the first set. As expected, the increase in flow stresses increases the temperature and this effect is more pronounced at higher reductions.

Table 3.10. Variation of average temperature at the interface with roll radii for different reductions (h_1 = 1mm, μ = 0.08, h_i = 2.6 W/m^2-°C, h_e = 260 W/m^2-°C, μ = 0.14, $(\sigma_Y)_0$ = 324 MPa, b = 0.052, n = 0.295, V_2 = 0.5 m/s, T_0 = 30 °C)

Reductions r_d (%)	R = 65 mm			R = 130 mm		
	Power (kW)		Average temperature at the interface (°C)	Power (kW)		Average temperature at the interface (°C)
	Plastic deformation (P_p)	Friction (P_f)		Plastic deformation (P_p)	Friction (P_f)	
8	9.45	0.91	34.51	9.406	1.54	35.25
12	14.62	1.95	37.37	14.55	2.97	38.12
16	20.15	3.14	40.53	19.93	4.92	42.35
20	25.53	4.73	44.02	23.49	9.42	48.23
24	31.01	6.61	47.87	30.79	10.67	52.07
28	36.72	8.94	52.31	36.41	14.31	58.23

Table 3.11. Variation of average temperature at the interface with different yield stresses and hardening parameters for different reductions (h_1 = 1mm, μ = 0.08, R = 65 mm, h_i =2.6 W/m^2-°C, h_e = 260 W/m^2-°C, V_2 = 0.5 m/s, T_0 = 30 °C)

Reductions r_d (%)	$(\sigma_Y)_0$ = 324 MPa, b = 0.052, n = 0.295			$(\sigma_Y)_0$ = 356.4 MPa, b = 0.0624, n = 0.354		
	Power (kW)		Average temperature at the interface (°C)	Power (kW)		Average temperature at the interface (°C)
	Plastic deformation (P_p)	Friction (P_f)		Plastic deformation (P_p)	Friction (P_f)	
8	9.45	0.91	34.51	10.52	1.05	35.54
12	14.62	1.95	37.37	16.34	2.21	39.12
16	20.15	3.14	40.53	22.62	3.68	42.68
20	25.53	4.73	44.02	28.98	5.45	47.61
24	31.01	6.61	47.87	35.42	7.68	52.34
28	36.72	8.94	52.31	42.2	10.39	58.6

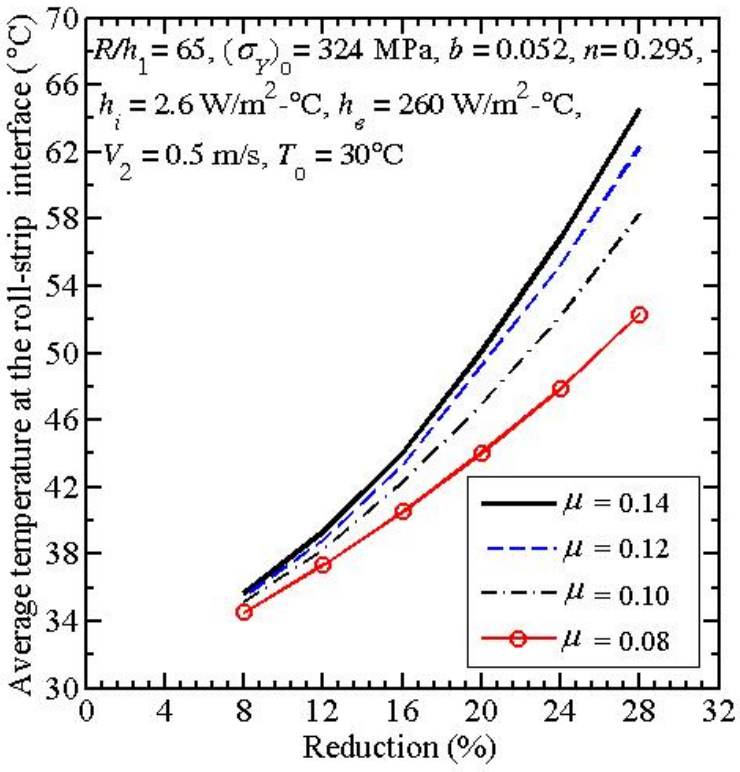

Fig. 3.15. Variation of average temperature at the interface with reduction for different coefficients of friction

The study is also extended to comprehend the effect of coefficient of friction, angular velocity of roll on average temperature of roll and strip at the roll-strip interface. It is observed from Fig. 3.15 that with increase in coefficient of friction at the interface, the average temperature increases. This effect is also more pronounced at higher reduction.

Figure 3.16 shows the variation of average temperature at the interface with angular velocity of roll for two different roll radii. It is observed that the temperature increases with increase in angular velocity, but the rate of increase of temperature with angular velocity decreases with increasing angular velocity. Increase in angular velocity increases the heat generation. It also tends to distribute the heat more evenly on the surface of the roll, making the temperature a weak function of the angular location on the periphery. Initially, the first effect dominates. As the angular speed increases, the influence of the second effect gets dominance. As a result, temperature versus ω plot typically follows the behaviour as shown in Fig. 3.16.

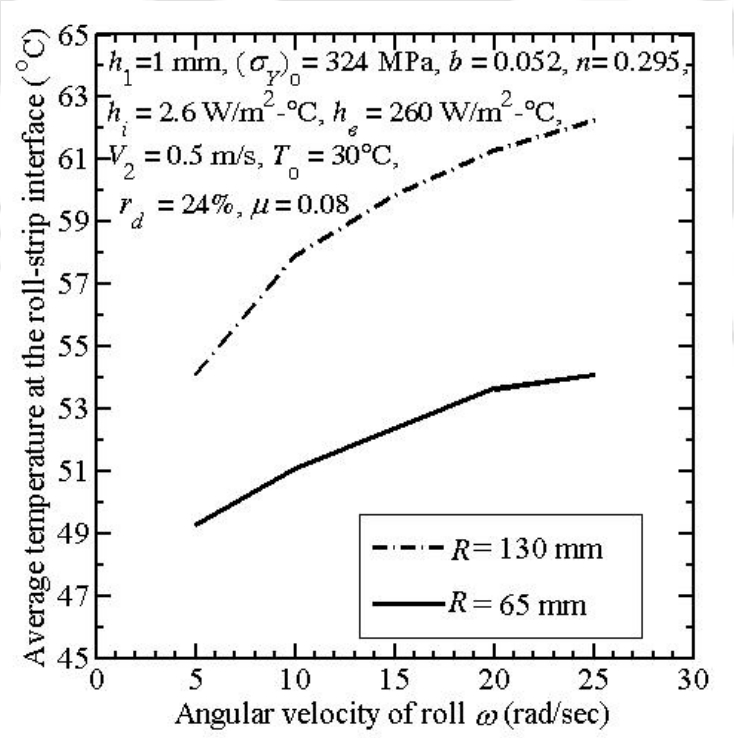

Fig. 3.16. Variation of average temperature at the interface with angular velocity of roll for different roll radii

In the cold rolling condition, the temperature increases because of heat generation due to plastic deformation and friction. A fraction of this heat goes into roll and the other portion goes into the strip. It is interesting to see the distribution of heat into roll and strip. Table 3.12 shows the rate of heat input at different reductions for different angular velocities of roll ω. It is observed that the fraction of heat input to the roll decreases with increasing ω. However, the temperature of the roll still increases, because the total power increases with ω.

Table 3.12. Heat distribution between the roll and the strip at different reductions for different ω

Reductions, r_d (%)	ω = 7.5 (rad/s)			ω = 15 (rad/s)			ω = 30 (rad/s)		
	Average temperature at the interface (°C)	Heat flux (W/m^2)		Average temperature at the interface (°C)	Heat flux (W/m^2)		Average temperature at the interface (°C)	Heat flux (W/m^2)	
		Roll	Strip		Roll	Strip		Roll	Strip
8	34.6	1.22	6.76	34.7	1.82	14.2	35	2.68	29.2
12	37.3	1.8	8.7	37.9	2.90	18.2	38.2	4.02	37.8
16	40.5	2.4	10.4	41	3.5	22	41.6	5.18	45.8
20	43.8	3	12	44.8	4.4	25.6	45.3	6.4	53.4
24	47.7	3.6	13.5	48.7	5.4	29	49.6	7.9	60.5
28	51.7	4.2	15	53.2	6.48	32	54.8	9.66	67.3

3.11 Conclusion

In this chapter, a steady-state thermo-mechanical model for warm flat rolling for obtaining the temperature of the exit strip using the FEM deformation module and separate thermal module is developed. The deformation analysis of the strip is carried out by an FEM model based on Eulerian flow formulation. The thermal analysis of the roll and the strip is carried out by an analytical method and FEM using ABAQUS. Three methods for determining the temperature distribution in the roll are presented. These three methods are approximate method, series solution using integral transform technique and an FEM model. The strip temperature distribution is calculated by an analytical method and an FEM model. The FEM model results are considered as a benchmark for the other two methods while

making comparisons. The determination of temperature distribution through analytical method for the roll as well as strip is advantageous in terms of computational time.

In the present work, the analytical solutions are incorporated along with FEM deformation module to alleviate the complexity of the process and faster prediction of the temperature distribution in the roll and the strip. The proposed steady-state thermo-mechanical warm flat rolling model is validated with the experimental results of Shirizly and Lenard (2000) and Serajzadeh and Mahammadzadeh (2007). Further, the parametric study is also carried out to see the consequence of the parameters such as rolling speed, roll radius, coefficient of friction and yield stress of the strip material considering cold rolling examples. It is found that the proposed model is suitable for cold rolling case by incorporating the constitutive relation in the FEM based deformation module.

Following are the salient contributions:-

- To predict the steady-state temperature distribution in the roll and the strip, a simplified and computationally faster, approximate method is proposed by adapting the model of Fischer *et al*. (2004).
- For calculating a steady-state temperature distribution in the roll and the strip by FEM, a methodology is proposed to calculate the temperature distribution in rolling for reducing the computational screen time. In the present work, FEM based software package ABAQUS is used, but the methodology can be employed with any package. The steady-state temperature distribution can also be obtained by carrying out a transient heat transfer analysis till the attainment of steady-state. However, this procedure takes about 2 hours of the screen time, whilst the FEM model requires about less than 10 minutes of the screen time by employing ABAQUS in the present case. If the problem is solved in a non-iterative way by writing a subroutine, the FEM model requires less than 1 minute. The FEM model uses a deformation module FOTRAN code based on Eulerian flow formulation and a thermal module implemented on an FEM based package ABAQUS for the fast estimation of the steady-state temperature distribution.

- Temperature distribution in the roll is determined by three different methods. These methods are approximate method (by adapting the model Fischer *et al*., 2004), series solution using integral transform technique (Yiannopoulos *et al*., 1997) and an FEM model. The comparative study of these three methods has been carried out to obtain the steady-state temperature distribution in roll for specified heat flux. It is observed that an approximate method takes the minimum computational time compared with other two methods. The series solution using integral transform technique involves the roots from the transcendental equation. The roots are the function of the roll dimensions, thermal conductivity and convective heat transfer coefficients of the roll and to be evaluated for change of these parameters. The FEM analysis is also computationally faster compared to the series solution using integral transform technique by employing the proposed methodology. It is found that an approximate method is most efficient as compared to the other two methods for obtaining the steady-state temperature distribution in the roll. Hence, the present model can be used for a quick estimation of steady-state temperature distribution in rolling.
- The comparison of approximate method and an FEM for thermal analysis is also carried out by calculating the temperature rise at the interface and compared with the experimental results. Further, the present model is validated with the experimental results by calculating the roll-force, roll-torque and average temperature at the roll-strip interface in warm rolling conditions. It is found that the present model predictions are well agreement with the experimental observations.
- Several authors proposed that the heat generated due to friction at the roll-strip interface is shared in a fixed proportion between the roll and the strip (Hwang *et al*., 1993; Hatta *et al*., 1980). In the present work, a heat partition factor λ is calculated by matching the average temperature of the roll and the strip at the roll-strip interface. The validity of the assumption of equal roll and strip temperature in the contact zone is assessed.

Chapter 4

Transient Thermal Analysis of Warm Flat Rolling

4.1 Introduction

The transient study of thermo-mechanical analysis of the flat rolling is essential in order to envisage the better understanding of the temperature distribution in the roll and the strip. This chapter deals with the transient analysis of warm flat rolling process. The transient analysis requires a time varying heat flux input into the roll from the warm strip. This brings the present analysis closer to the real time environment providing a better insight into the problem as the temperature during rolling is not steady at the beginning.

The transient behaviour of a rolling process requires a continuous change of the mechanical and thermal boundary conditions of the strip that enters and exits the bite zone. It is essential to study the transient behaviour of both the strip and roll including the constitutive modelling and friction behaviour (Lee *et al*., 2000). Due to transient nature of the problem, the analysis of the roll and strip together becomes complex. In order to avoid the complexities, many researchers have carried out the steady-state analysis of the rolling (Tseng *et al*., 1984; Hwang *et al*., 1990; Serajzadeh, 2004; Koohbor, 2015). A few researchers such as Guo (1998) and Lee *et al*. (2000) carried out the transient analysis of only the roll. Shahani *et al*. (2009) carried out two-dimensional thermo-mechanical analysis of hot rolling using FEM based package ANSYS. However, they did not consider the roll deformation. In the present work, a transient thermal analysis considering both the roll and the strip

together is carried out analytically. The roll deformation is taken into account by employing Hitchcock (1935) formula.

In this work, a mathematical model of warm flat rolling to find out the temperature distribution in the roll and the strip is presented. In-house warm rolling experiments were also conducted to validate the model for different process parameters. The deformation module of the strip uses Eulerian approach based on finite element method (FEM). The temperature distribution of the strip in the deformation zone and just after the deformation zone is obtained analytically as discussed in Section 3.6. The transient distribution in the roll is obtained analytically by integral transform technique. The present work employs a time varying heat flux input into the roll from the strip which extends the work of Yiannopoulos *et al*. (1997) who has considered a constant heat flux input into the roll with constant initial temperature T_0. An iterative procedure is carried out to obtain the temperature distribution assuming initial temperature as a function of radial and circumferential coordinates. The transient thermal analysis provides an inverse way of estimating the thermal parameters based on the temperature measurement of the exit strip.

The chapter is organized as follows. Section 4.2 presents the solution of transient heat conduction equation of the roll using integral transform technique. Section 4.3 provides a scheme of the transient thermal analysis of warm flat rolling process. The time varying heat input into the roll from the strip is studied in Section 4.4. Section 4.5 presents details of validation experiments on a laboratory mill. Results and discussion is presented in Section 4.6 including in-house experimental validation of the transient thermal analysis of warm flat rolling. Section 4.7 concludes the chapter.

4.2 Transient Temperature Distribution in Roll using Integral Transform Technique

In this section, the governing equation of the transient heat conduction with non-homogeneous boundary condition is solved. The heat input at the outer radius b in 2β angular zone is assumed to be $\dot{q}$ as shown in Fig. 4.1. Remaining outer surface of

the roll is subjected to convective heat loss. The inner surface at radius, a is subjected to convective heat loss only. The work roll is assumed to be rigid and fixed in space whereas the heat source is rotating with constant angular velocity ω.

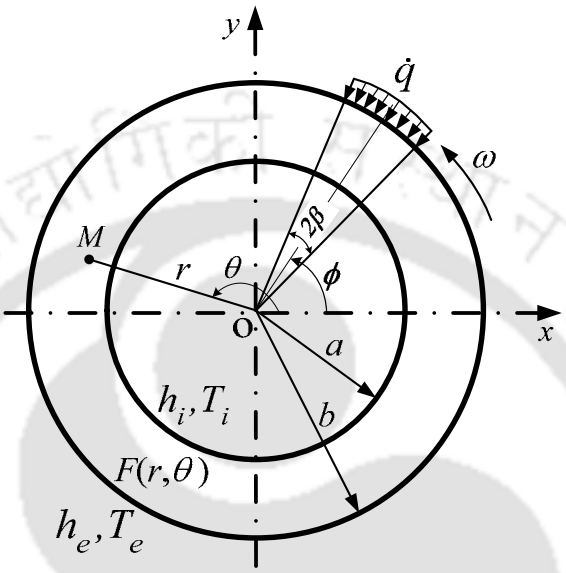

Fig. 4.1. A moving heat source with stationary roll

The two-dimensional governing differential equation for heat conduction is given by

$$\frac{\partial^2 T}{\partial r^2}+\frac{1}{r}\frac{\partial T}{\partial r}+\frac{1}{r^2}\frac{\partial^2 T}{\partial \theta^2}=\frac{1}{\alpha_r}\frac{\partial T}{\partial t}, \tag{4.1}$$

for the domain, $a \le r \le b$ with boundary conditions:

$$-k_r\frac{\partial T}{\partial r}+h_i\left(T-T_i\right)=0 \qquad \text{at } r = a, \tag{4.2}$$

$$k_r\frac{\partial T}{\partial r}+h_e\left(T-T_e\right)=q(\theta) \qquad \text{at } r = b, \tag{4.3}$$

where α_r is the thermal diffusivity of the roll material, k_r is the thermal conductivity of roll material, h_i is the convective heat transfer coefficient at the inner surface of the roll, h_e is the convective heat transfer coefficient at the outer surface of the roll, T_i is the ambient temperature at the inner periphery, T_e is the ambient temperature at the outer periphery and $q(\theta)$ is the heat flux at the outer surface. The heat source

position is expressed as a linear function of the angular velocity (ω) *i.e.*, $\phi = \omega t$. The rotating heat flux at the outer surface at any time is expressed as

$$q(\theta) = \begin{cases} \dot{q} & \text{for } (\phi-\beta) \le \theta \le (\phi+\beta) \\ 0 & \text{for } (\phi+\beta) \le \theta \le (2\pi+\phi-\beta) \end{cases}, \tag{4.4}$$

where t is time parameter. The initial condition is imposed as

$$T(r,\theta,t) = F(r,\theta) \quad \text{for } t = 0 \quad \text{in region } a < r < b, \tag{4.5}$$

where $F(r,\theta)$ is a specified function of r and θ.

The solution of the problem defined in Eqs. (4.1)–(4.5) is solved using Integral transform method. The procedure for obtaining the solution considering initial temperature as T_0 is described in Appendices C and D. For the general case of the initial temperature distribution $F(r,\theta)$ is considered in this section. The following expression of transient temperature distribution is obtained after employing the boundary as well as initial conditions from Eq. (C.83) (Appendix C) as

$$\begin{aligned} T_\alpha(r,\theta,t) = {} & \frac{\varepsilon}{\pi}\sum_{n=0}^{\infty}\sum_{m=1}^{\infty}\frac{R_n(\beta_m,r)}{N_n(\beta_m)}\exp\left(-\alpha_r\beta_m^2 t\right)\tilde{\tilde{F}}(\beta_m,n) \\ & + \frac{\varepsilon}{\pi}\sum_{n=0}^{\infty}\sum_{m=1}^{\infty}\frac{R_n(\beta_m,r)}{N_n(\beta_m)}\left(\frac{A_n(\beta_m,n,t)}{\alpha_r\beta_m^2}\right)\left(1-\exp\left(-\alpha_r\beta_m^2 t\right)\right), \end{aligned} \tag{4.6}$$

where

$$\tilde{\tilde{F}}(\beta_m,n) = \int_a^b \int_0^{2\pi} rR_n(\beta_m,r)\cos n(\theta-\phi)F(r,\theta)\,\mathrm{d}\theta\,\mathrm{d}r, \tag{4.7}$$

$$A_n(\beta_m,n,t) = \alpha_r\left(H_e\bar{T}_e b + \frac{\bar{\dot{q}}b}{k_r}\right)R_n(\beta_m,b) + \alpha_r\left(H_i\bar{T}_i a\right)R_n(\beta_m,a), \tag{4.8}$$

$$\bar{\dot{q}} = \int_0^{2\pi} q(\theta)\cos n(\theta-\phi)\,\mathrm{d}\theta, \tag{4.9}$$

$$\bar{T}_e = \int_0^{2\pi} T_e(\theta)\cos n(\theta-\phi)\,\mathrm{d}\theta, \tag{4.10}$$

$$\overline{T_i} = \int_0^{2\pi} T_i(\theta)\cos n(\theta-\phi)\,\mathrm{d}\theta. \tag{4.11}$$

$$H_i = \frac{h_i}{k_r}, \tag{4.12}$$

$$H_e = \frac{h_e}{k_r}, \tag{4.13}$$

and

$$\varepsilon = \begin{cases} \frac{1}{2} & \text{for } n = 0 \\ 1 & \text{for } n = 1,2,3,\ldots \end{cases}. \tag{4.14}$$

The functions $R_n(\beta_m, r)$ and $N_n(\beta_m)$ are obtained from Eqs. (D.38) and (D.73), respectively (Appendix D):

$$R_n(\beta_m, r) = L_n J_n(\beta_m r) - V_n Y_n(\beta_m r), \tag{4.15}$$

and

$$N_n(\beta_m) = \frac{2}{\pi^2\beta_m^2}\left[H_e^2 + \beta_m^2\left\{1-\left(\frac{n}{\beta_m b}\right)^2\right\}\right] - \frac{2}{\pi^2\beta_m^2}\frac{V_n^2}{K_n^2}\left[H_i^2 + \left\{1-\left(\frac{n}{\beta_m a}\right)^2\right\}\right], \tag{4.16}$$

where β_m are the positive roots of the transcendental characteristic equation given by

$$K_n L_n - V_n W_n = 0. \tag{4.17}$$

The expressions for the above terms L_n, K_n, V_n and W_n are derived in Appendix D:

$$L_n = \left(\frac{n}{b} + H_e\right) Y_n(\beta_m b) - \beta_m Y_{n+1}(\beta_m b), \tag{4.18}$$

$$K_n = \left(\frac{n}{a} - H_i\right) J_n(\beta_m a) - \beta_m J_{n+1}(\beta_m a), \tag{4.19}$$

$$V_n = \left(\frac{n}{b} + H_e\right) J_n(\beta_m b) - \beta_m J_{n+1}(\beta_m b), \tag{4.20}$$

and

$$W_n = \left(\frac{n}{a} - H_i\right) Y_n(\beta_m a) - \beta_m Y_{n+1}(\beta_m a). \tag{4.21}$$

Expanding the summation with index *n* in Eq. (4.6) as follows

$$T_\alpha(r,\theta,t)=\frac{1}{2\pi}\frac{R_0(\beta_m,r)}{N_0(\beta_m)}\left\{\exp\left(-\alpha_r\beta_m^2t\right)\tilde{\bar{F}}(\beta_m,0)+\left(\frac{A_0(\beta_m,0,t)}{\alpha_r\beta_m^2}\right)\left(1-\exp\left(-\alpha_r\beta_m^2t\right)\right)\right\}$$
$$+\frac{1}{\pi}\sum_{n=1}^{\infty}\sum_{m=1}^{\infty}\frac{R_n(\beta_m,r)}{N_n(\beta_m)}\left\{\exp\left(-\alpha_r\beta_m^2t\right)\tilde{\bar{F}}(\beta_m,n)+\left(\frac{A_n(\beta_m,n,t)}{\alpha_r\beta_m^2}\right)\left(1-\exp\left(-\alpha_r\beta_m^2t\right)\right)\right\},\tag{4.22}$$

Substituting Eqs. (4.7) and (4.8) in Eq. (4.22):

$$T_\alpha(r,\theta,t)=\frac{1}{2\pi}\frac{R_0(\beta_m,r)}{N_0(\beta_m)}\exp\left(-\alpha_r\beta_m^2t\right)\tilde{\bar{F}}(\beta_m,0)$$
$$+\frac{1}{2\pi}\frac{R_0(\beta_m,r)}{N_0(\beta_m)}\frac{1}{\beta_m^2}\left\{\left(H_e\bar{T}_eb+\frac{\bar{\dot{q}}b}{k_r}\right)R_0(\beta_m,b)+\left(H_i\bar{T}_ia\right)R_0(\beta_m,a)\right\}\left\{1-\exp\left(-\alpha_r\beta_m^2t\right)\right\}$$
$$+\frac{1}{\pi}\sum_{n=1}^{\infty}\sum_{m=1}^{\infty}\frac{R_n(\beta_m,r)}{N_n(\beta_m)}\left\{\exp\left(-\alpha_r\beta_m^2t\right)\tilde{\bar{F}}(\beta_m,n)+\left(\frac{A_n(\beta_m,n,t)}{\alpha_r\beta_m^2}\right)\left\{1-\exp\left(-\alpha_r\beta_m^2t\right)\right\}\right\}.\tag{4.23}$$

Using Eqs. (4.9), (4.10) and (4.11) in Eq. (4.23):

$$T_\alpha(r,\theta,t)=\frac{1}{2\pi}\sum_{m=1}^{\infty}\frac{R_0(\beta_m,r)}{N_0(\beta_m)}\exp\left(-\alpha_r\beta_m^2t\right)\tilde{\bar{F}}(\beta_m,0)$$
$$+\frac{1}{2\pi}\sum_{m=1}^{\infty}\frac{R_0(\beta_m,r)}{N_0(\beta_m)}\frac{\left\{\left(H_e2\pi T_eb+\frac{2\beta\dot{q}b}{k_r}\right)R_0(\beta_m,b)\right\}}{\beta_m^2}\left\{1-\exp\left(-\alpha_r\beta_m^2t\right)\right\}$$
$$+\frac{1}{2\pi}\sum_{m=1}^{\infty}\frac{R_0(\beta_m,r)}{N_0(\beta_m)}\frac{\left(H_i2\pi T_ia\right)R_0(\beta_m,a)}{\beta_m^2}\left\{1-\exp\left(-\alpha_r\beta_m^2t\right)\right\}$$
$$+\frac{1}{\pi}\sum_{n=1}^{\infty}\sum_{m=1}^{\infty}\frac{R_n(\beta_m,r)}{N_n(\beta_m)}\left\{\exp\left(-\alpha_r\beta_m^2t\right)\tilde{\bar{F}}(\beta_m,n)+\left(\frac{A_n(\beta_m,n,t)}{\alpha_r\beta_m^2}\right)\left(1-\exp\left(-\alpha_r\beta_m^2t\right)\right)\right\}.\tag{4.24}$$

Substituting Eqs. (4.7)–(4.11) in Eq. (4.24), the solution for the transient temperature distribution in the roll for stationary heat source is obtained as

$$T_\alpha(r,\theta,t)=\frac{1}{2\pi}\sum_{m=1}^{\infty}\frac{R_0(\beta_m,r)}{N_0(\beta_m)}\exp\left(-\alpha_r\beta_m^2 t\right)\tilde{\bar{F}}(\beta_m,0)$$
$$+\left(\pi H_e T_e+\frac{\dot{q}}{k_r}\beta\right)\sum_{m=1}^{\infty}\frac{R_0(\beta_m,r)}{F_0}\left\{1-\exp\left(-\alpha_r\beta_m^2 t\right)\right\}$$
$$+\frac{\pi^2}{2}H_i a T_i\sum_{m=1}^{\infty}\frac{R_0(\beta_m,r)}{F_0}R_0(\beta_m,a)\left\{1-\exp\left(-\alpha_r\beta_m^2 t\right)\right\}$$
$$+2\frac{\dot{q}}{k_r}\sum_{n=1}^{\infty}\sum_{m=1}^{\infty}\frac{R_n(\beta_m,r)}{F_n}\frac{\sin n\beta}{n}\cos n(\theta-\phi)\left\{1-\exp\left(-\alpha_r\beta_m^2 t\right)\right\}. \tag{4.25}$$

Equation (4.25) provides the transient temperature distribution in the hollow cylinder for the stationary heat source.

The solution of the heat conduction problem with time dependent boundary conditions can be related to the solution of the same problem with time independent boundary conditions by means of Duhamel's theorem (Özisik, 1993). Using Duhamel's Theorem the transient state temperature distribution for a rotating heat source is obtained. Then, Duhamel's theorem relates the solution $T(r,\theta,t)$ (Özisik, 1993):

$$T(r,\theta,t)=\frac{\partial}{\partial t}\int_{\tau=0}^{t}T_\alpha(r,\theta,t-\tau)\mathrm{d}\tau. \tag{4.26}$$

The rotating heat source position may expressed as

$$q(\theta)=\begin{cases}\dot{q} & \text{for } (\omega\tau-\beta)\le\theta\le(\omega\tau+\beta)\\ 0 & \text{for } (\omega\tau+\beta)<\theta<(2\pi+\omega\tau-\beta)\end{cases}, \tag{4.27}$$

where τ is a parameter.

Substituting Eq. (4.25) in Eq. (4.26), one obtain

$$T(r,\theta,t)=\frac{1}{2\pi}\sum_{m=1}^{\infty}\frac{R_0(\beta_m,r)}{N_0(\beta_m)}\exp\left(-\alpha_r\beta_m^2 t\right)\tilde{\tilde{F}}(\beta_m,0)$$
$$+\left(\beta\frac{\dot{q}}{k_r}+\pi H_e T_e\right)\sum_{m=1}^{\infty}\frac{R_0(\beta_m,r)}{F_0}\left\{1-\exp\left(-\alpha_r\beta_m^2 t\right)\right\}$$
$$+\frac{\pi^2}{2}aH_i T_i\sum_{m=1}^{\infty}\frac{R_0(\beta_m,r)}{F_0}R_0(\beta_m,a)\left\{1-\exp\left(-\alpha_r\beta_m^2 t\right)\right\}$$
$$+2\frac{\dot{q}}{k_r}\sum_{n=1}^{\infty}\sum_{m=1}^{\infty}\frac{R_n(\beta_m,r)}{F_n}\times\frac{\sin n\beta}{n}$$
$$\times\frac{\cos n(\theta-\omega t)-\lambda_n\sin n(\theta-\omega t)+\left(\lambda_n\sin n\theta-\cos n\theta\right)\exp\left(-\alpha_r\beta_m^2 t\right)}{1+\lambda_n^2}, \tag{4.28}$$

where

$$\lambda_n=\frac{\omega n}{\alpha_r\beta_m^2}, \tag{4.29}$$

$$F_n=\frac{\pi^2\beta_m^2 N_n(\beta_m)}{2} \tag{4.30}$$

and ω is the angular velocity of rotating heat source around the outer periphery of roll. In Eq. (4.28), the $\tilde{\tilde{F}}(\beta_m,0)$ in the first term is evaluated as follows:

$$\tilde{\tilde{F}}(\beta_m,0)=\int_a^b\int_0^{2\pi} rR_0(\beta_m,r)F(r,\theta)\,\mathrm{d}\theta\,\mathrm{d}r. \tag{4.31}$$

Remarks:

Note that Eq. (4.28) is exactly the same as Eq. (6) in the paper by Yiannopoulos *et al*. (1997) except for the first term. The initial temperature $F(r,\theta)$ is considered as a function of r–θ coordinates. The numerical integration is performed to evaluate the integration along with the function $F(r,\theta)$ in Eq. (4.31) using Gauss quadrature formula. After evaluating the term $\tilde{\tilde{F}}(\beta_m,0)$, Eq. (4.28) provides the incremental transient temperature distribution in the roll. In the present study, two-Gauss-point formula is used in the radial location between $r = a$ to $r = b$. In the circumferential

location, the range $-\pi$ to π is divided into three zones *viz*., $-\pi$ to $-\pi/3$, $-\pi/3$ to $\pi/3$ and $\pi/3$ to π assuming that the heat source is present at the location $\theta = 0°$. The four-Gauss-point formula is used for $-\pi/3$ to $\pi/3$ zone and two-Gauss-point formula is used for $-\pi$ to $-\pi/3$and $\pi/3$ to π. This differentiates the present approach from Yiannopoulos *et al*. (1997). Yiannopoulos *et al*. (1997) used a non-varying heat flux. In this study, a time varying heat flux is considered. Different values of heat flux are taken at the different incremental time. The solution of Yiannopoulos *et al*. (1997) considers the initial temperature as T_0.

The solution of the present problem involves an iterative procedure, in which the temperature is updated after each increment till the steady-state is achieved. The term $F(r,\theta)$ is updated after each time increment, Δt, taking initial temperature distribution of the roll. The temperature distribution $T(r,\theta,t')$ in the previous iteration is taken as initial temperature $F(r,\theta)$ in the current iteration. The temperature distribution $F(r,\theta)$ is used to evaluate the $\tilde{\tilde{F}}(\beta_m,0)$ term for obtaining the temperature distribution $T(r,\theta,t')$ at $t' = \Delta t$ using Eq. (4.28). In this work, the transient temperature distribution of roll is updated after small interval of time (after 5 revolution of the roll at a constant speed). During a small time interval, the heat flux input into the roll $\dot{q}$ is considered to be constant. In the present work, a time varying heat flux with different values of $\dot{q}$ at different increments is considered. Initial condition pertains to the condition at the beginning of the time interval.

4.3 Scheme of the Transient Thermal Analysis

The transient thermal analysis of warm flat rolling to obtain the temperature distribution in both the roll and the strip is carried out. In-house warm rolling experiments were also carried out to validate the model for different process parameters. Figure 4.2 shows the overview of the warm flat rolling model. The deformation analysis of the strip uses Eulerian approach based on finite element method (FEM). The FEM deformation module of the strip is described in Section

3.3. The temperature distribution of the strip is obtained analytically and provided in Section 3.6. The analytical solution of the transient temperature distribution in the roll is briefly described in Section 4.2.

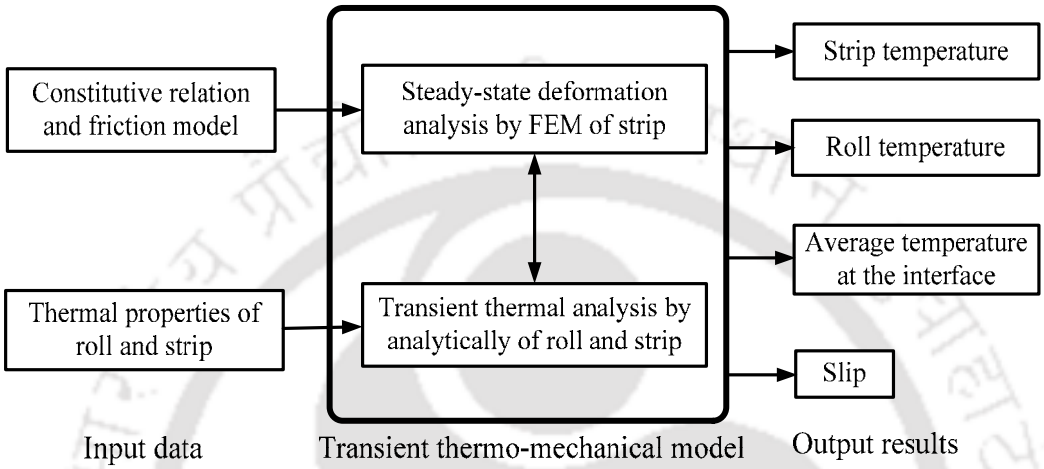

Fig. 4.2. Overview of transient thermal analysis of warm flat rolling

For the transient thermal analysis, the steady-state deformation analysis of the strip and the transient analysis of the roll and the strip together are carried out. To obtain the transient temperature distribution in both the roll and the strip, two sub-modules are described separately. One sub-module finds the temperature distribution in the strip. The other sub-module estimates the temperature distribution in rolls, when the heat transfer through the roll-strip interface is known. Exact value of the heat transfer along the roll-strip interface is not known.

In this work, the heat partition factor λ is inversely determined by matching the average temperature at the roll-strip interface in the following manner. If Q_T is the total heat (during incremental time Δt) due to friction work, plastic deformation work and the difference of temperature gradient between the roll and the strip, the quantity λQ_T is assumed to pass to the rolls and $(1-\lambda)Q_T$ remains in strip. The value of partition factor λ is obtained by matching the temperatures at the roll-strip interface from both the sub-modules. The sub-module for obtaining the transient

temperature of strip is described in Section 3.7 and that for transient temperature of roll is described in Section 4.2.

The algorithm of the whole procedure for obtaining the transient temperature distribution of the strip is as follows:

Step 1: Carry out the deformation analysis using FEM module based on Eulerian flow formulation taking temperature dependent mechanical properties and friction. Choose the incremental time step size for heat flux input into the roll from the strip.

Step 2: Carry out the transient thermal analysis of roll and strip together for fixed incremental time. Use modules for the estimation of roll and strip temperatures using temperature dependent thermal properties. Assuming that all the frictional heat goes into the roll and 90% of plastic deformation power goes as heat into the strip. A part of frictional heat may go into the strip as well depending on the relative temperature difference between the roll and the strip. However, it is better to begin the analysis by assuming that the roll is colder than strip due to forced or natural cooling, causing entire frictional heat to flow into the roll.

Step 3: If average temperature of the strip and roll are equal (with a tolerance of 0.1 °C) at the interface, go to Step 6.

If the average temperature of the strip at the interface is less than average temperature of roll, then go to Step 4.

If the average temperature of the strip at the interface is greater than average temperature of roll, then go to Step 5.

Step 4: Transfer the appropriate amount of heat from roll to strip for making the roll and strip average temperatures at the interface equal. This can be done using bisection method (Gerald and Wheatley, 1997). Go to Step 6.

Step 5: Transfer the appropriate amount of heat from strip to roll for making the roll and strip average temperatures at the interface equal. This can be done using bisection method. Go to Step 6.

Step 6: Record the exit strip temperature. Go to Step 2 after updating the temperature distribution of the roll. Updated temperature distribution of the roll is taken as the initial temperature of the roll for the next iteration.

Step 7: If the exit strip temperature is achieved steady-state, then stop. Else go to Step 2.

4.4 Typical Results of Transient Analysis with Varying Heat Flux

The transient temperature distribution of exit strip is obtained for the time varying heat input, $\dot{q}$ from the strip to the roll. In this work, $\dot{q}$ is taken as piecewise constant. The temperature of roll as well as $\dot{q}$ are updated after every increment using Eqs. (4.28) and (4.31). A typical example with ω = 7 rad/s and R = 65 mm is presented to examine the variation of exit strip temperature at 50 mm away from the roll bite for different increment of time. In this example, the strip and roll are considered to be made of steel. The flow stress of strip (steel) is governed by J-C model (Eq. 3.4), where the constants of J-C model are taken from Meslin and Hamann (2003) and these are as follows: A=598 MPa, B=768 MPa, n_1 = 0.2092, C = 0.0137, m_1 = 0.807. The reference strain rate ($\dot{\varepsilon}_0$) is 0.001 and melting temperature (T_m) is 1768 K. The initial temperature of roll and strip are taken as 15 °C and 250 °C, respectively. The outer radius of the roll (R) is 65 mm and the thickness of the roll is considered to be 20 mm. The thermal properties of the strip and the roll are given in Table 4.1 on the basis of property data provided by Steiner (1990). The computations are carried out for 28% reduction of 1 mm of strip (h_1 = 1 mm) taking the equivalent Coulomb coefficient of friction as 0.20.

Table 4.1. Thermal properties of roll and strip made of steel

Parameters	Roll	Strip
Thermal conductivity (W/m-°C)	50	40
Specific heat (J/kg-°C)	460	470
Density (kg/m^3)	7850	7800
Thermal diffusivity (m^2/s)	0.144×10^{-4}	0.11×10^{-4}

Figure 4.3 shows the transient temperature distribution as a function of time in the strip at a location of 50 mm from the exit of roll bite. The transient temperature of exit strip is obtained by updating the roll temperature after 5, 10 and 15

revolutions. The average temperature of the roll and the strip at the roll-strip interface is matched after each increment. One can observe that the time increment has an insignificant effect on the steady-state temperature of exit strip, whereas transient temperature distributions deviate by the maximum of 20°C with time. For the present analysis, the temperature of the roll is updated after completing 5 revolution of the roll.

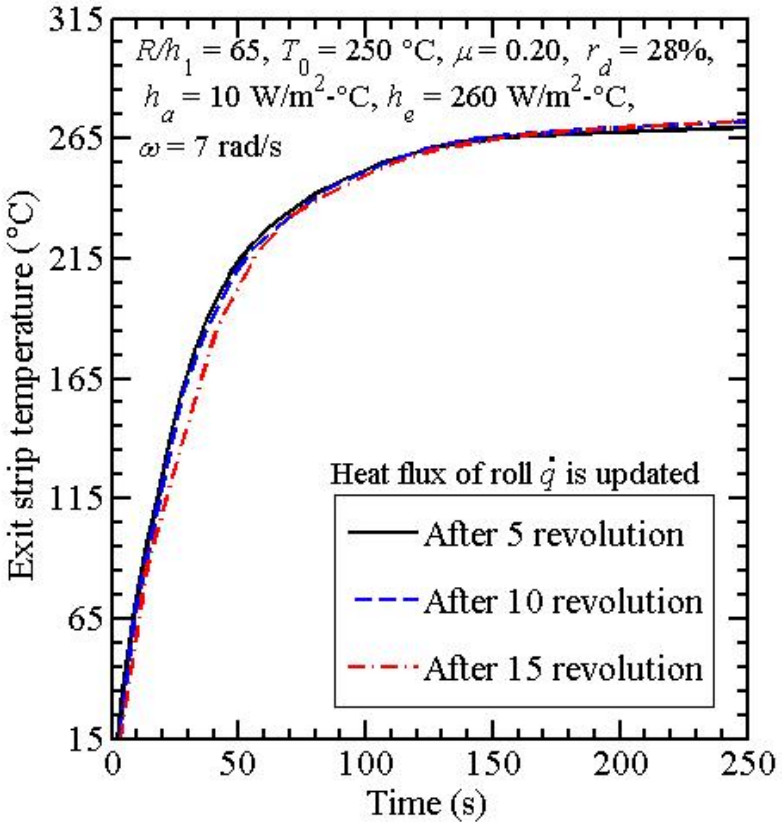

Fig. 4.3. Exit strip temperature with time at the distance 50 mm away from the roll bite for different increment time

Figure 4.4 shows the variation of heat flux input into the roll with the average temperature at roll-strip interface. The heat input into the roll is higher at the beginning due to high temperature difference between the roll and the strip at the interface. As the rolling time increases, the heat flux input into the roll keeps on reducing with increasing average temperature at the roll-strip interface.

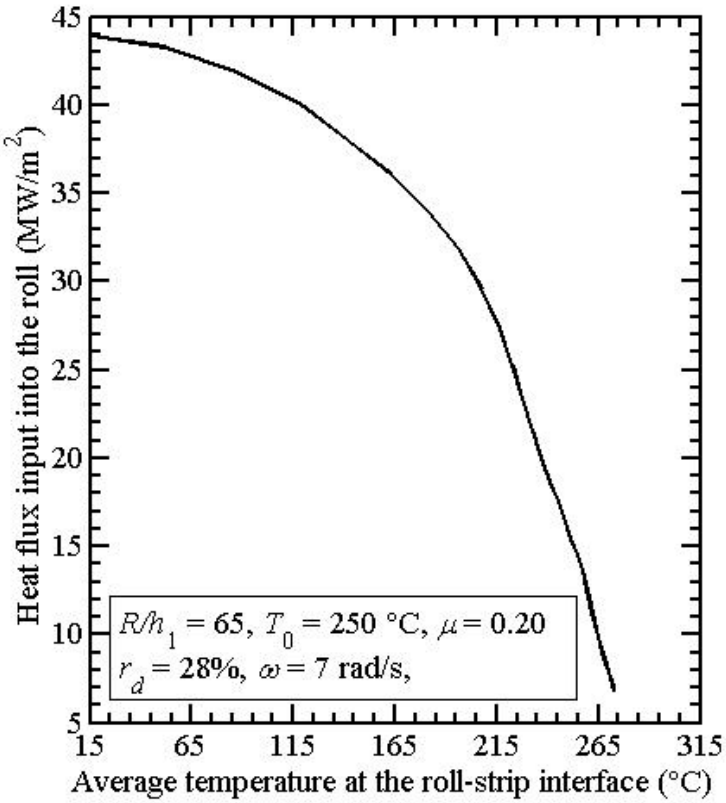

Fig. 4.4. Variation of heat input into the roll with temperature

4.5 Details of Validation Experiments

In this section, details of rolling mill and the method for the measurement of the exit strip temperature and slip is described. The rolling experiments were carried out in a laboratory rolling mill.

4.5.1 Equipment and Method

The experimental setup for the rolling conducted in the laboratory is shown in Fig. 4.5. The mill is driven by a 15 kW induction motor with no load speed of 1460 RPM. The commercially pure aluminum alloy strips were rolled in a two-high laboratory rolling mill with rolls of 200 mm diameter and 300 mm barrel length to various reductions. The roll gap was adjusted by a mechanical screw down system.

The feeler gauges were used to measure the roll gap. The details of the rolling mill are described in Dixit *et al*. (2002). The rolls were made of high carbon high chromium steel (D2 steel) and commercially pure aluminum alloy was used as strip material. The compositions of the strip and the roll materials are provided in Table 4.2. The Scanning Electron Microscope (SEM) equipped with an Energy Dispersive Spectrometer (EDS) was used to find out the chemical composition of the strip material. The chemical composition of the roll material is provided in the paper of Oliveira *et al*. (2006).

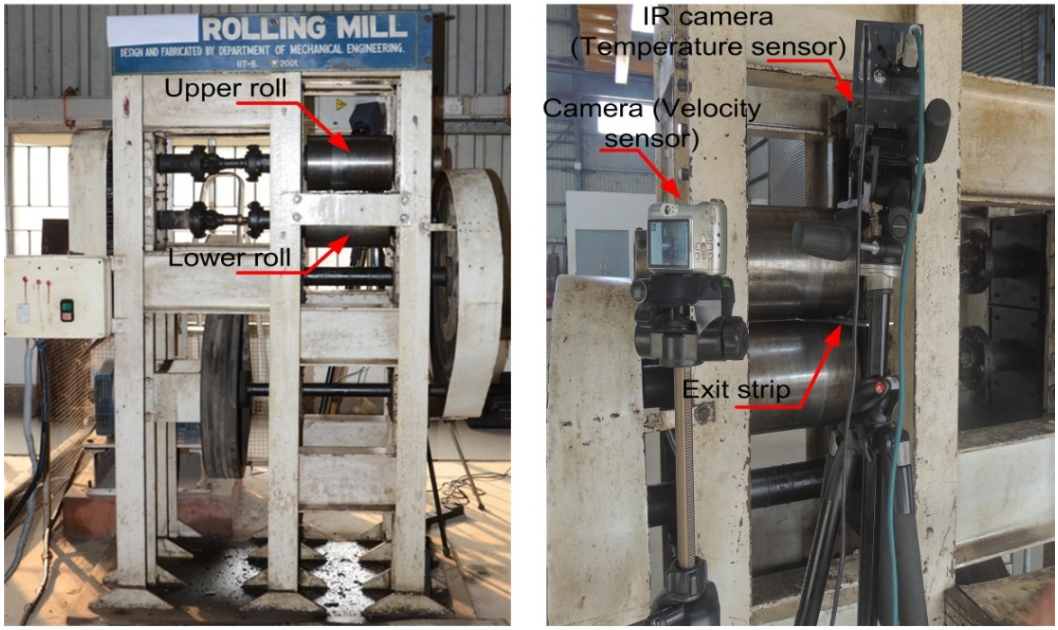

Fig. 4.5. A laboratory rolling mill (a) front view and (b) arrangement for measuring the temperature and velocity of exit strip at the rear side

Table 4.2. Chemical composition of the strip and the roll material

Material	Chemical composition								
	Mn	Si	Al	Fe	Cu	Cr	C	Mo	V
Strip (Aluminum alloy)	0.05	0.13	99.1	0.51	0.21	–	–	–	–
Roll (D2 steel) Oliveira *et al*. (2006)	0.4	0.96	–	83.51	–	11.91	1.48	0.98	0.76

The exit strip temperature is measured by a non contact sensor–IR Camera (Infra Tec hr Head Vario CAM 480SL) that captures the thermo-graphic image. IRBIS®3plus analysis software is used for processing the thermo-graphic image. The frequency of the thermo-graphic image is 8 frames per second (FPS). The strips were heated in a laboratory furnace and placed in the roll gap within 5s of taking it out from the furnace. The temperature was measured just after rolling at the exit from the roll bite and the data were stored for further processing.

The roll peripheral speed was measured by a tachometer. For measuring the exit velocity of strip, a Nikon D7000 Camera is used. This camera offers high-image-quality full HD movie recording of 1920×1080 for 7 FPS. In the present study, the video at the exit of the roll was captured. This video was further converted into images. The time required to capture a single frame was calculated by dividing the total time of video with FPS of camera. The number of frames in which the strip could be seen at the exit was counted. The product of numbers of frames and time required to capture a single frame yields the time taken by the strip to come out of the roll gap. Hence, the length of the rolled strip divided by this time results in exit velocity.

4.5.2 Method for Measuring the Centreline Temperature of the Strip

For measuring the centerline temperature of the strip, a small groove of the elliptical shape was drilled at the middle on the upper surface of the strip before rolling. The surface and centerline temperature of exit strip is measured by using IR Camera. For measuring the temperature at the center of the strip, a blind groove of the elliptical shape (major diameter of 10 mm along rolling direction and minor diameter of 6 mm along transverse direction) was drilled at the middle on the upper surface of the strip. The depth of the groove was equal to semi-thickness of the strip. After rolling, the depth gets changed but remains almost equal to the semi-thickness of rolled sheet. The reason for choosing the elliptical shape is that deformed shape of the elliptical groove was able to expose the surface at the center of the strip. This was not the case with a blind circular blind-hole which tends to get filled up after deformation.

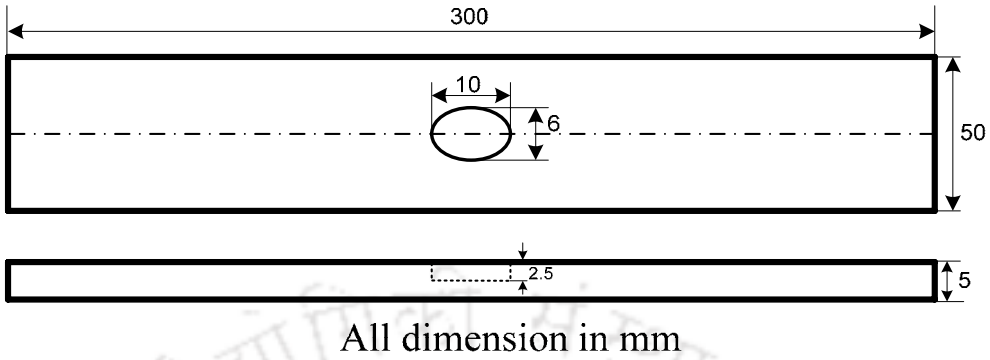

Fig. 4.6. A schematic diagram of strip for showing the elliptical groove

After the deformation of 5 mm thick sheet, the deformed elliptical groove had on an average (based on 3 replicates) major diameter of about 10.7 mm and minor diameter of 6.8 mm. The maximum depth was equal to semi-thickness of rolled sheet with less than 0.01 mm error. Thus, the bottom surface of the groove was at the level of strip center in thickness direction. The schematic diagram and initial dimension of the strip and the groove are shown in Fig. 4.6. As the volume of the groove is much smaller than overall size of the strip, it does not influence the temperature distribution of the strip significantly. The temperature of the strip on the surface and at the center (*i.e.*, bottom surface of groove) was measured just after the rolling by IR camera as described earlier. The IR camera provided the three-dimensional temperature distribution in the volume of 300 mm^3, which included the top surface of the strip as well as bottom surface of the blind groove.

4.5.3 Determination of Friction from Slip Measurement

During rolling, the exit speed of strip is higher than the roll speed (peripheral speed of work roll) due to deformation of the strip at bite zone. The relative difference of these speeds is defined as forward slip (f_s):

$$f_s = \frac{V_2 - V_R}{V_R} \times 100 \,, \tag{4.32}$$

where V_2 is the exit velocity of strip and V_R is the roll velocity. The forward slip is calculated by FEM. Velocity sensor may be used to measure the exit speed of strip and the roll speed may be measured by a tachometer. The slip measurement gives

the proper estimation of the coefficient of friction. The slip measurement requires the exit speed of strip and roll peripheral speed. The accuracy of the estimation is dependent on the accuracy of the measured parameters and the mathematical model considered. For better accuracy, the instruments should have better precision and accuracy. The coefficient of friction is also estimated by other two methods *viz*., the minimum roll gap measurement method and the inverse method based on the exit strip temperature measurement are presented in Chapter 5. It was found that the magnitude of slip is not very sensitive to material parameters among the other two methods. Hence, in the absence of material data, it can be used as an effective method to find out the coefficient of friction.

4.6 Results and Discussion for Transient Thermal Analysis of Roll-Strip System

To validate the present model, the temperature rise at the roll-strip interface is compared with the experimental results of cold and warm rolling described in the above Section. The cold rolling experimental results are taken from the available literature for comparison and are presented in Subsection 4.6.1. The warm rolling experimental validation of the present model is carried out by conducting in-house warm rolling experiment and discussed in Subsection 4.6.2. The details of rolling mill and the method for the measurement of the exit strip temperature and slip is described. The coefficient of friction is estimated based on slip measurement under warm rolling conditions.

4.6.1 Validation of the Proposed Model under Cold Rolling Condition

In this subsection, the proposed transient thermo-mechanical model for flat rolling is validated with the experimental results available in the literature. Jeswiet and Zhou (1992) and Liu (2002) conducted the experiments of aluminum alloy strip to measure the transient temperature of roll at different angular velocities. The effect of strain-rate was neglected by Jeswiet and Zhou (1992) and Liu (2002). Jeswiet and Zhou (1992) measured the roll temperature distribution at different angular velocities of roll considering the aluminum alloy strip with length, l = 305 mm,

width, w = 25 mm and thickness, t = 4 mm. The equivalent Coulomb coefficient of friction is taken as 0.08. The governing equation of the flow stress of the strip was taken as (Jeswiet and Zhou, 1992)

$$\sigma_y = 100\left(1+0.9\varepsilon^{0.355}\right) . \tag{4.33}$$

The thermal properties of roll and strip material are given in Table 4.3.

Table 4.3. Thermal properties of roll and strip material for validation of proposed model with the experimental results of Jeswiet and Zhou (1992)

Parameters	Roll (Steel)	Strip (Aluminum alloy)
Thermal conductivity (W/m°C)	48.9	177
Specific heat (J/kg°C)	443	875
Density (kg/m^3)	7836	2770
Thermal diffusivity (m^2/s)	0.141×10^{-4}	0.73×10^{-6}

Figures 4.7 and 4.8 show the temperature distribution of roll surface as a function of time at angular velocities ω = 0.59 and 1.46 rad/s respectively. It is observed that the results of the proposed model are in well agreement with the experimental results of Jeswiet and Zhou (2000). An error of less than 1°C is observed between the present and the experimental results.

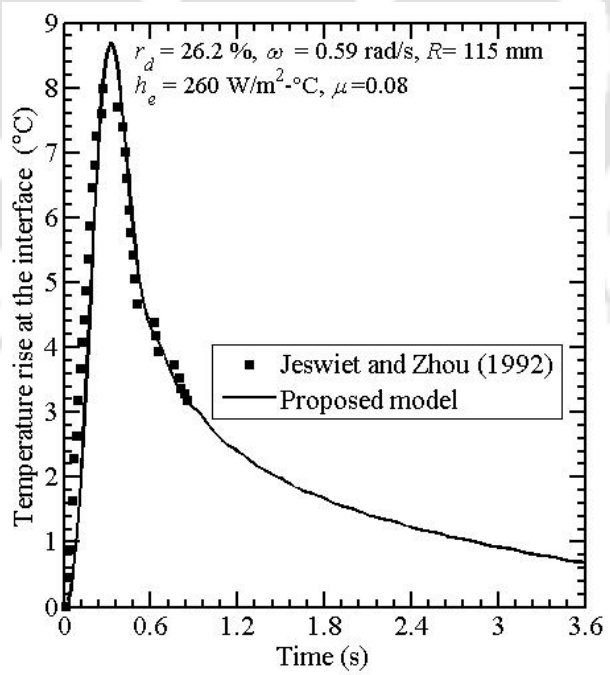

Fig. 4.7. Comparison of proposed model with the experimental results of Jeswiet and Zhou (1992) for ω = 0.59 rad/s

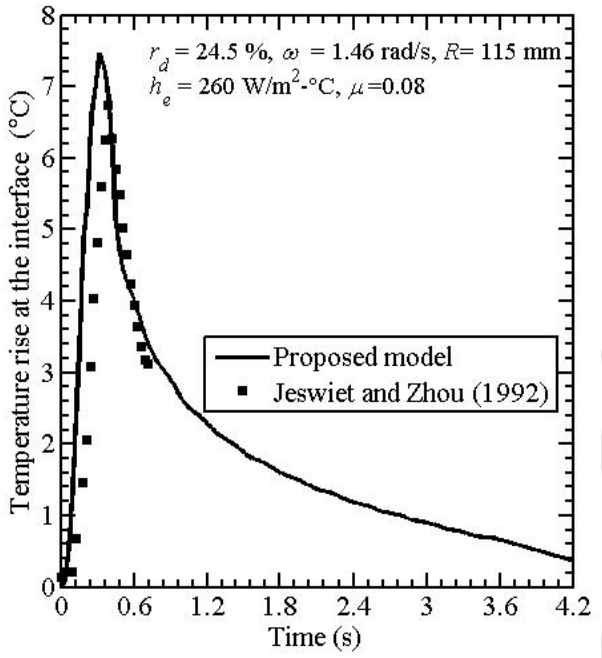

Fig. 4.8. Comparison of proposed model with the experimental results of Jeswiet and Zhou (1992) for ω = 1.46 rad/s

Another example is also considered to validate the proposed model with the experimental results of Liu (2002) in which temperature was recorded continuously with time for more than one revolution of roll. Liu (2002) performed the experiments on cold rolling without any lubricant at the roll-strip interface. (It is to be mentioned that the present model specifically developed for warm rolling may also be used for cold rolling. It can also be used for hot rolling by employing the appropriate friction model.) A strip of aluminum alloy was used with length, l = 100 mm, width, w = 1000 mm and thickness, t = 3 mm. The conductivity, density and specific heat were taken as 284 W/m-°C, 2707 kg/m^3 and 896 J/kg-°C, respectively for the strip and 54 W/m-°C, 7833 kg/m^3 and 465 J/kg-°C, respectively for the roll.

Figures 4.9–4.11 compare the temperature distribution of proposed model with the experimental results of Liu (2002) for different reductions of strip. The input data is shown in the figures. It is observed that temperatures increase with increasing reduction of the strip. This is due to the increase of heat generation at the roll-strip interface. However, the peak temperature at the interface almost coincides

with the experimental results. Hence, the present model provides a good approximation of the temperature distribution in the roll and the strip in rolling.

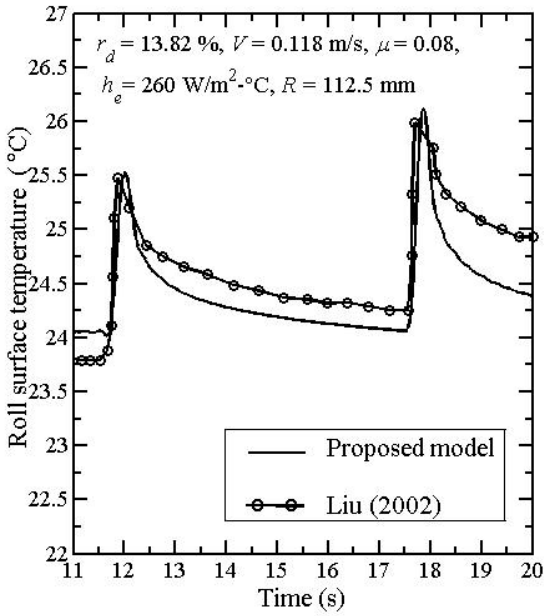

Fig. 4.9. Comparison of proposed model with the experimental results of Liu (2002) for r_d = 13.82 %

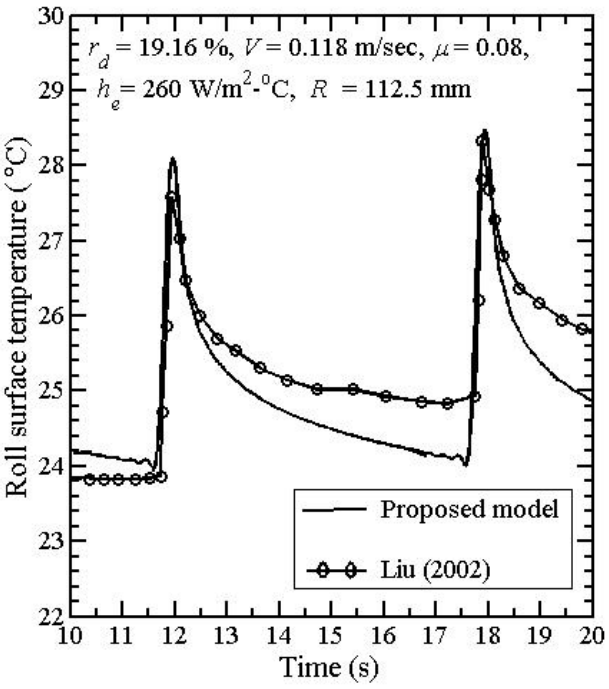

Fig. 4.10. Comparison of proposed model with the experimental results of Liu (2002) for r_d = 19.16 %

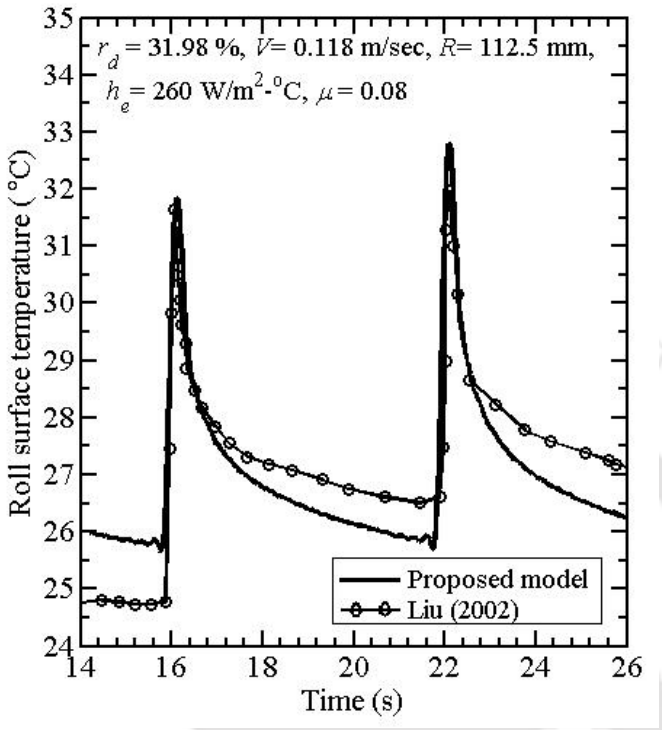

Fig. 4.11. Comparison of proposed model with the experimental results of Liu (2002) for r_d = 31.98 %

4.6.2 Validation of the Proposed Model under Warm Rolling Condition

In-house warm rolling experiments were conducted to measure the temperature of exit strip and slip at different reductions for different inlet temperature of the strip. Temperature was recorded at the surface of the strip at 50 and 150 mm away from the bite zone for different reductions for different inlet temperatures. The slip was also recorded for each case. The strip length was 300 mm, width 50 mm and thickness 5 mm before rolling. Three replicates were performed at each rolling condition and the averaged temperature is taken for validating the proposed model. The equivalent Coulomb's coefficient of friction in rolling is obtained experimentally by the slip measurement. The thermal properties of roll and strip material are provided in Table 4.4.

During rolling the heat is lost from the surface of the strip to air by convection. The convective heat transfer loss takes place on the surface of the strip.

The convective heat transfer coefficient of air, h_a can be calculated from the Nusselt number, $\bar{\mathrm{N}}_{ux}$ defined as

$$\bar{\mathrm{N}}_{ux} = \frac{h_a L}{k_a} \ , \tag{4.34}$$

where k_a is the thermal conductivity of air and L is the distance between two sensor location of strip. The Nusselt number can be calculated as (Incropera *et al*., 2003)

$$\bar{\mathrm{N}}_{ux} = 0.664\,\mathrm{Re}_x^{1/2}\,\mathrm{Pr}^{1/3} \qquad \mathrm{Pr} \geq 0.6, \tag{4.35}$$

where $\bar{\mathrm{N}}_{ux}$ is the Nusselt number, Re_x is the Reynold number and Pr is the Prandtl number. Equation (4.35) is valid for $3\times10^3 < \mathrm{Re}_x < 5\times10^8$ and $0.6 < \mathrm{Pr} < 50$. The Reynold number of air, Re_x and Prandtl number, Pr are evaluated using the following relations

$$\mathrm{Re}_x = \frac{uL}{\nu}, \tag{4.36}$$

$$\mathrm{Pr} = \frac{\mu c_{pa}}{k_a} \tag{4.37}$$

where u is the velocity of air, ν is the kinematic viscosity of air, c_{pa} is the specific heat of air, μ is the dynamic viscosity of air at temperature T_a. The approximate value of convective heat transfer coefficient of air is calculated as h_a = 10 W/m^2°C based on the relation given in Eqs. (4.34), (4.35), (4.36) and (4.37). The flow stress of the strip is governed by (Lenard and Malinowski, 1993):

$$\sigma_y = \sigma_1 + n_4\varepsilon \quad \text{for} \ \ \varepsilon \geq 0.1, \tag{4.38}$$

$$\sigma_y = \sigma_2\left(\frac{\varepsilon}{0.1}\right)^{n_5} \quad \text{for} \ \ \varepsilon < 0.1, \tag{4.39}$$

where σ_1, σ_2, n_4 and n_5 are temperature-dependent parameters as per Table 4.5. The warm rolling experiments of aluminum alloy sheets were carried out at a constant speed of the rolling mill. Thus, the strain-rate dependency is not taken into account for validating the experimental results with the proposed model.

Table 4.4. Thermal properties for the roll and strip in the proposed model

Material	Thermal conductivity k (W/m-°C)	Specific heat c_p (J/kg-°C)	Density ρ (kg/m^3)	Thermal diffusivity, α (m^2/s)	Reference
Strip(Aluminum)	218	904	2710	0.890×10^{-6}	Davies (1992)
Roll (Steel)	52	460	9850	0.144×10^{-4}	Steiner (1990)

Table 4.5. Temperature dependent parameters for calculating flow stress of the strip (Lenard and Malinowski, 1993)

Temperature (°C)	σ_1 (MPa)	σ_2 (MPa)	n_4	n_5
22	153.78	150.38	34.065	0.256
100	149.64	146.23	34.090	0.195
200	138.56	135.90	26.637	0.175
300	113.85	111.29	25.623	0.363

The experiments were conducted for three different inlet strip temperatures at different percentage reductions. The coefficient of friction is obtained experimentally for each case based on forward slip measurement as shown in Table 4.5. Although the results of the coefficient of friction are not getting validated quantitatively in the present study, the slip (and consequently friction) increases with temperature as observed by Lenard and Malinowski (1993). This also agrees with the correlation provided by Roberts (1978). The coefficient of frictions obtained in Table 4.6 are used in the proposed model to calculate the exit strip temperature at two location *viz*., 50 and 150 mm away from the roll bite. The exit strip temperatures at these two locations are also measured experimentally. Table 4.7 shows the comparison of the exit strip temperature obtained experimentally and computationally. The experimental results are in good agreement with the proposed model. The maximum error between the experimental results and the proposed model is less than 7%.

Table 4.6. Measured forward slip and averaged coefficient of friction for the rolling experiments for h_1 = 5 mm, R = 100 mm

Inlet temperature of strip (°C)	Reduction, r_d (%)	Forward slip, f_s (%)	Friction, μ
150	39.6	30.36	0.21
200	37.7	35.68	0.24
250	35.5	39.13	0.27

Table 4.7. Comparison of exit strip surface temperature of proposed model with experimental results for h_1 = 5 mm, R = 100 mm (Values in bracket are standard deviations)

Inlet temperature of strip (°C)	Reduction, r_d (%)	Exit strip temperature (°C) away from the roll bite					
		50 mm			150 mm		
		Experiment	Proposed model	% error	Experiment	Proposed model	% error
150	39.6	129 (1.5)	133.85	–3.76	83 (1.1)	84.39	–1.67
200	37.7	170 (3.2)	177.56	–4.45	105 (1.9)	101.82	3.03
250	35.5	228 (2.6)	239.11	–4.87	178 (2.1)	165.95	6.77

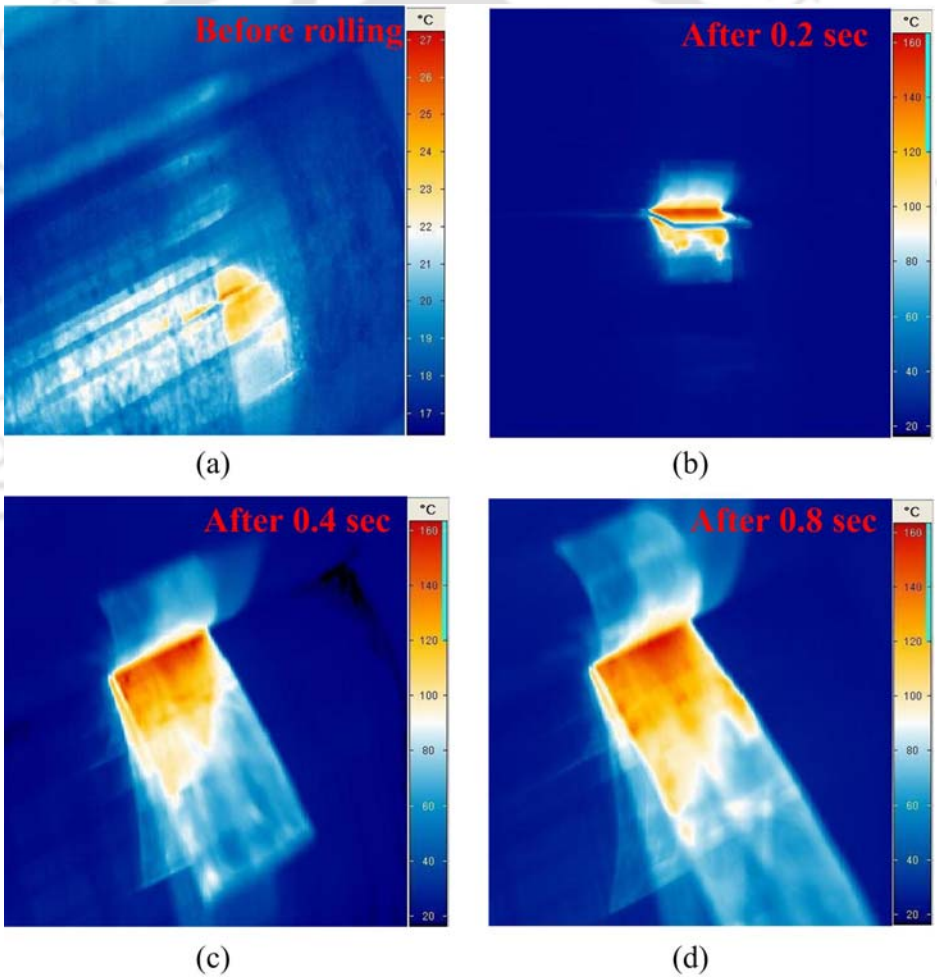

Fig. 4.12. Thermogram of the steel roll and the aluminum strip surface temperature (a) Before rolling, (b) exit strip after 0.2 sec, (c) exit strip after 0.4 sec and (d) exit strip after 0.8 sec

Figure 4.12 shows the IR camera recorded temperature profile across the surface of the roll and the strip at the inlet strip temperature of 150 °C. It is seen from Fig. 4.12a that the roll surfaces are at room temperature before rolling. Figures 4.12b, 4.12c and 4.12d show the surface temperature distribution of the roll and the strip at different time periods during rolling.

The temperature of exit strip at the surface as well as centerline at the same location is also compared with experimentally measured temperature. The surface and centerline temperature of exit strip was measured 50 mm from the exit of the roll bite at different reductions in strip for different inlet temperatures. It was found that the temperature variation is about 8–13 °C from the center to the surface of the strip. Table 4.8 provides the comparison between the experimentally measured temperatures and the proposed model results. There is a variation less than 5%. Another example is also considered, in which the temperature was measured for different reductions in the strip at same inlet temperature. The experimentally measured temperature was at 50 and 150 mm away from the roll bite for different reductions in strip. Table 4.9 shows the comparison of proposed model results with the experimentally measured temperature at two places, 50 and 150 mm from the exit of the roll bite on the surface of the exit strip. It is seen from Table 4.8 that the exit strip temperatures predicted by the model differ by less than 6% from experimental results.

Table 4.8. Comparison of proposed model with experimental results at centerline and surface of strip for h_1 = 5 mm, R = 100 mm (Values in bracket are standard deviations)

Inlet temperature of strip (°C)	Reduction, r_d (%)	Exit strip temperature (°C) at 50 mm away from the roll bite					
		At centerline			At surface		
		Experiment	Proposed model	% error	Experiment	Proposed model	% error
150	20	145 (1.8)	151.52	–4.49	132 (2.5)	128.91	2.34
150	35	147 (3.9)	153.83	–4.65	136 (3.6)	132.68	2.44
200	13	182 (2.1)	188.38	–3.51	163 (1.6)	168.18	–3.18
200	37	195 (1.7)	196.58	–0.81	187 (1.9)	184.29	1.49

Table 4.9. Comparison of exit strip surface temperature of proposed model with experimental results for h_1 = 5 mm, R = 100 mm, T_0 = 200 °C (Values in bracket are standard deviations)

Reduction, r_d (%)	At 50 mm away from the roll bite			At 150 mm away from the roll bite		
	Experiment	Proposed model	% error	Experiment	Proposed model	% error
12.4	172 (1.6)	175.2	–1.86	110 (1.6)	104.3	5.23
19.2	183 (2.9)	188.4	–2.95	139 (3.1)	132.2	4.86
25.4	198 (3.8)	199.8	–0.91	158 (2.5)	162.4	–2.78
32.4	228 (3.4)	219.3	3.82	175 (3.8)	178.3	–1.88

4.7 Conclusion

In the present work, a transient thermal model for warm flat rolling is validated with the experiments. In-house warm rolling experiments were conducted at different reductions for different inlet strip temperatures. The exit strip temperature was measured experimentally at two different locations, 50 and 150 mm from the exit of the roll bite at the surface as well as at the centerline. It is found that the temperature predicted by the proposed model deviates by less than 7% from the experimentally measured temperature. The coefficient of friction is estimated based on slip measurement. Thus, the present model can be used to predict reasonable result with good accuracy.

Chapter 5

Estimation of the Friction in Cold and Warm Flat Rolling

5.1 Introduction

Friction is one of the most influential parameters in the rolling process. In fact, the rolling of sheets is accomplished by means of friction. For reducing the thickness of the sheet, the rolls feed the sheet as they rotate in the opposite directions. It is essential to estimate the frictional behaviour between the roll and the strip at the roll-strip interface. The rolling industry needs reliable and accurate mathematical models for the improved predictions of friction as well as surface finish (Le and Sutcliffe, 2002). This enhances the productivity and the quality of the rolled sheet. The estimation of friction requires the measurement of roll pressure and interfacial shear stress along the roll-strip contact length. For this, a number of load sensors needs to be inserted into the rolls (Roberts, 1978). Many researchers estimated the friction at the roll-strip interface both theoretically and experimentally (Siebel and Lueg, 1933; Al-Salehi *et al*., 1973; Roberts, 1978). A simplified model to estimate the friction at the roll-strip interface by measuring the roll-force and strip material data is described in the book by Roberts (1978). In most of the early mathematical modelling of cold rolling processes, Coulomb's friction model or Wanhiem and Bay's friction model (Zhang and Bay, 1977; Christensen *et al*., 1986) is used. In the hot rolling, the use of constant friction factor model is preferred. For low pressure in rolling, Wanhiem and Bay model coincides with the Coulomb's friction model (Kobayashi *et al*., 1989; Richelsen, 1994).

The effects of the friction and surface roughness on the edge crack initiation and growth is studied by Xie *et al*. (2011). They stated that the coefficient of friction

is an important parameter, which controls the initiation of microcracks and their propagation during rolling process.

In this chapter, the possibility of online determination of the coefficient of friction in rolling is proposed. The measurement of friction can give the idea about the quality as well as surface finish of the strip. However, the measurement of friction by no means is an easy task. In the literature, various methods have been employed for measuring the friction in rolling. Some of these methods require damaging of the surface of the rolls (Al-Salehi *et al*., 1973). The methods based on the measurement of roll force, roll torque and the shear stress can be easily used, but their reliability is dependent on reliability of measuring devices and the mathematical model. A possible way of measuring the average coefficient of friction in rolling is to measure the exit temperature of the strip. It can be easily done by means of temperature sensors. In this work, an inverse method of estimating the average value of coefficient of friction is proposed based on the exit temperature measurement. For a given exit temperature, the inverse model searches the appropriate value of using a one-dimensional search technique *i.e*., bisection method. The estimated coefficient of friction is also compared with other two methods. In total, three different methods for the estimation of friction are compared. Firstly, a simple online procedure is used to estimate the friction based on the slip measurement. In the second method, the friction is estimated based on the maximum inlet strip thickness that can enter the roll-gap unaided. In the third method, an inverse estimation is carried out for determining the coefficient of friction based on the exit strip surface temperatures at one specified location. The exit strip surface temperatures can be easily measured experimentally in warm rolling.

The rest of the chapter is organized as follows. Section 5.2 deals with estimation of friction based on slip measurement. The estimation of the coefficient of friction on the basis of minimum roll gap measurement is presented in Section 5.3. Section 5.4 presents the comparison of the coefficients of friction estimated from slip and minimum roll gap measurement. Section 5.5 deals with inverse

estimation of the coefficient of friction by measuring the exit strip temperature. Section 5.6 concludes the chapter.

5.2 Determination of Friction from Slip Measurement

The friction plays a significant role in the relative speed between the strip and the rolls during rolling. During rolling, the exit speed of strip is higher than the roll speed (peripheral speed of work roll) due to the deformation of the strip in the bite zone. The velocity sensor is used to measure the exit speed of strip, and the roll speed is measured by a tachometer. The procedure for obtaining the friction is already explained in Subsection 4.5.3.

5.3 Determination of Friction from Minimum Roll Gap Measurement

At the beginning, the rolling requires minimum coefficient of friction to drag the strip into the roll gap. The following relation estimates the required minimum coefficient of friction (Dixit and Dixit, 2008):

$$\mu_{\min} = \sqrt{\frac{h_1 - h}{R}}, \tag{5.1}$$

where h_1 is the inlet thickness of the strip, h is the gap between the rolls and R is the roll radius of the roll. Figure 5.1 shows the schematic diagram of the strip entering into the roll gap.

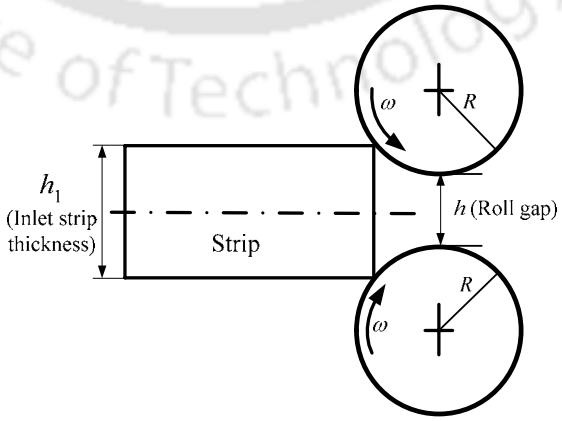

Fig. 5.1. Schematic diagram of the strip entry into the roll gap

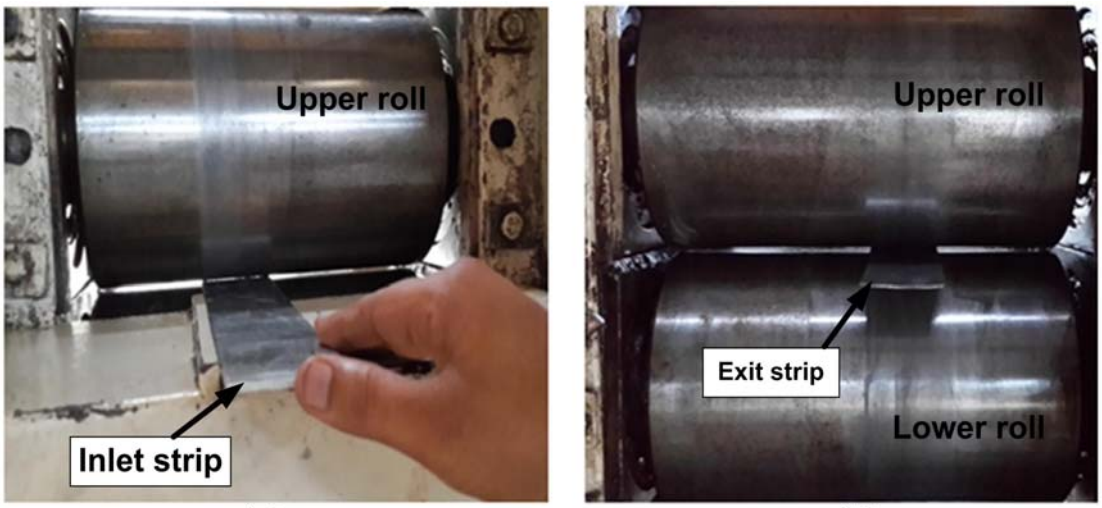

Fig. 5.2. A photograph of (a) strip getting inserted into the roll gap and (b) strip coming out of the roll

The commercially pure aluminum alloy strips were rolled in a two-high laboratory rolling mill. Before carrying out the experiments, the rolls and the strips are cleaned thoroughly with acetone in order to remove grease and lubricants. It is necessary to have the same surface roughness both at the upper and lower surfaces of the strip. For measuring the CLA surface roughness values (R_a), Pocket Surf (Mahr, GMBH) was used. Its measuring range is 0.03−6.35 μm and accuracy is ±0.01 micron. The rolls have the average surface roughness, R_a = 0.45 μm and the strip has the surface roughness, R_a = 0.48 μm. The experiments were carried out for different inlet thickness of the strip. A one dimensional technique *viz*., bisection method (Gerald and Wheatley, 1997) was employed to get the minimum roll gap for different inlet strip thickness. The bisection method provides the minimum interval of the roll gap at which the strip is self-drawn into the roll gap. This value of roll gap (h) is then used in Eq. (5.1) to find out the minimum coefficient of friction. The initial range in bisection method is from 0.05 mm to the inlet thickness of the strip. The strip is inserted between the rolls by aligning it longitudinally along the roll gap as shown in Fig. 5.2a. The rolled strip coming out from the roll gap is shown in Fig. 5.2b.

5.4 Comparison of the Coefficients of Friction Obtained from Slip and Minimum Roll Gap Measurement

The coefficient of friction is calculated by slip measurement and minimum roll gap measurement under cold rolling condition. The total seven experiments were conducted with different thicknesses of the strip at various reductions. Three replicates were done for each case. The minimum roll gap and slip were measured experimentally in all the cases. Table 5.1 shows the comparison of the estimated coefficient of friction based on slip measurement and minimum roll gap measurement. It is observed that the coefficient of friction predicted by slip is lower than the minimum roll gap measurement. This is due to the fact that starting friction is more and once the rolling process is sustained, the coefficient of friction reduces. The comparative study is useful for getting confidence of the coefficient of friction by the temperature measurement. In cold rolling case, the coefficient of friction was estimated by Yadav *et al*. (2011b) and it was reported that the coefficient of friction increases with increasing reduction. The similar trend is also observed from Table 5.1 in estimated friction values by both the methods. Figure 5.3 compares the coefficient of friction with reductions estimated by slip and minimum roll gap measurement methods. It is to be noted that the inlet thickness of the strip is different for all reductions. It is seen from Fig. 5.3 that the variation of the coefficient of frictions are similar by both the methods.

Table 5.1. Comparison of coefficient of friction in cold rolling condition

Strip dimension $l\times w\times t$ (mm^3)		Minimum roll gap (mm)	Reduction, r_d (%)	Estimated coefficient of friction, μ	
Before rolling	After rolling			By Eq. (4.32)	By Eq. (5.1)
300×50×3.0	475.8×50.3×1.88	1.09	37.3	0.129	0.140
300×50×3.5	497.1×50.3×2.10	1.19	40.0	0.148	0.152
300×50×4.0	499.2×50.5×2.38	1.38	40.5	0.158	0.162
300×50×4.5	552.3×50.5×2.42	1.91	46.2	0.155	0.161
300×50×5.0	559.2×50.6×2.65	2.09	47.1	0.159	0.170
300×50×5.5	552.4×50.8×2.94	2.35	46.6	0.165	0.173
300×50×6.0	562.4×50.8×3.15	2.78	47.5	0.165	0.179

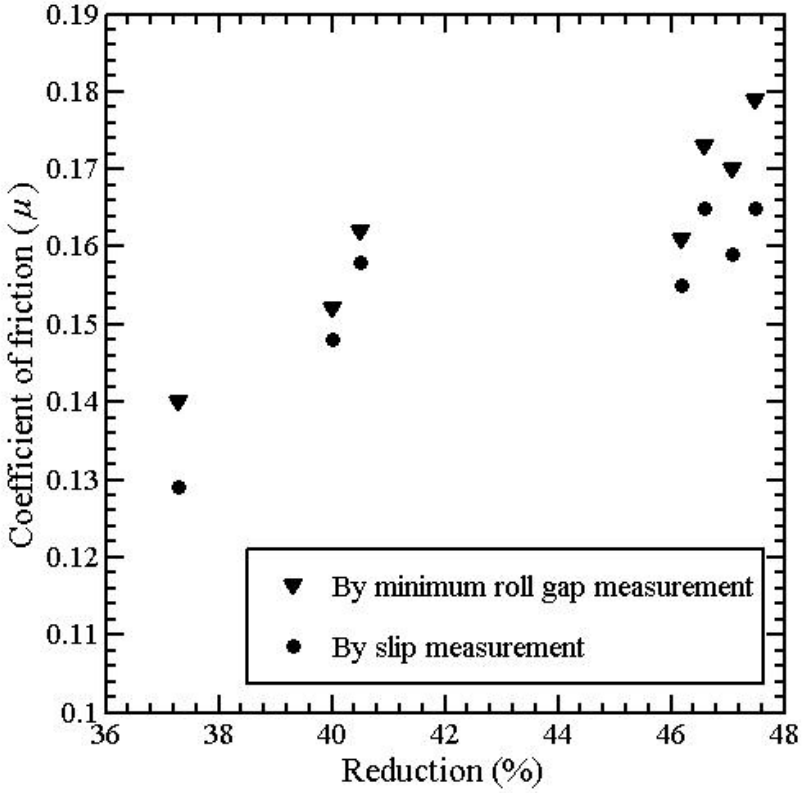

Fig. 5.3 Comparison of coefficient of friction with reductions in cold rolling condition for different thickness of the strip

5.5 Inverse Estimation of the Friction Based on the Exit Strip Temperature Measurement

In this section, the procedure of inverse estimation of the friction by the measurement temperature of exit strip at one specified location. For this a methodology described by Yadav *et al*. (2011a) based on exit strip temperature measurement, is employed to estimate the coefficient of friction. However, Yadav *et al*. (2011a) presented the results for cold rolling case and assuming the rolls as insulated (thermal analysis of the roll was not carried out). In the present work, the coefficient of friction is obtained based on the exit strip temperature in warm flat rolling considering the coupled thermo-mechanical analysis of the roll and the strip. If the material and thermal properties of the strip and the roll are known, then the

coefficient of friction is determined based on exit strip surface temperature at one point. This methodology can be implemented for the online determination of coefficient of friction, where rolling of the known material is carried out. The exit strip surface temperature is measured experimentally at different reductions conducting in-house warm rolling experiments.

The flow stress of strip as a function of strain and temperature of strip are obtained by performing tensile test at different temperatures. The tests were performed according to ASTM E8/E8M–15. Two replicates were carried out at each testing condition. A 100 kN capacity universal testing machine (Make: Instron, Model: 8801) was used for carrying out the tensile test. The ram velocity was kept constant at 1 mm/min for all the experiments. It is assumed that the material behaves as per the power law neglecting the effect of strain-rate. The flow stresses of the strip is the function of strain and temperature as given by

$$\sigma_y = \sigma_0 \varepsilon_{eq}^{n} \left(\frac{T}{T_{\mathrm{m}}} \right)^{-\gamma} . \tag{5.2}$$

The multiple regression analysis is carried out to find out the unknown parameters of power law given by Eq. (5.2) for the temperature dependent flow stress. The following material parameters are obtained as σ_0 = 85.75 MPa, n = 0.0387, γ = 0.2351 using multiple regression analysis. Figure 5.4 compares the flow stresses predicted by Eq. (5.2) with the experimentally obtained flow stresses at different temperatures.

The temperature of exit strip at 50 mm away from the roll bite was measured experimentally at different reductions in strip for two different inlet temperatures. The roll radius was 100 mm and the rolling mill speed was 0.5 m/s. Figure 5.5 shows the experimentally measured temperature of exit strip with the variation of upper and lower limits. It was observed that the temperature differs by 3–8 °C at the same rolling conditions during experiments. At each condition three replicates were done. There were more variations in temperature at higher inlet temperatures of strip. For employing an inverse method, the averaged temperature of the exit strip based on the replicates is considered.

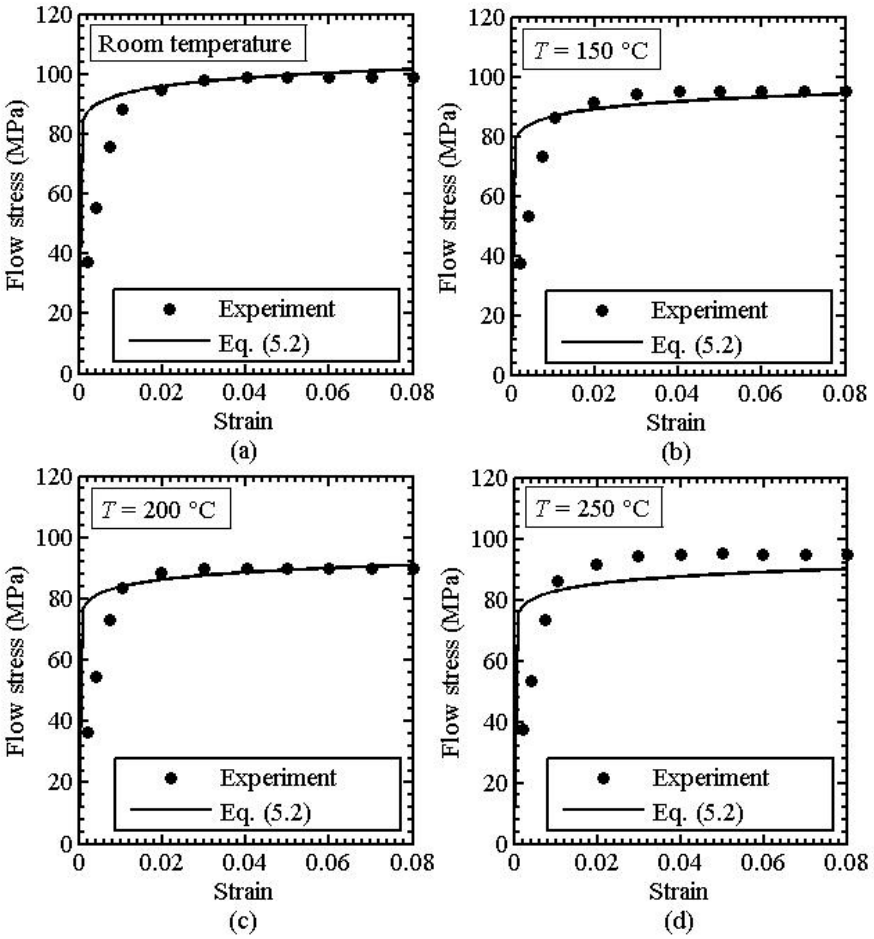

Fig. 5.4 Comparison of flow stresses with strain at different temperatures with experiments and multiple regression analysis

Employing a reverse procedure, the coefficient of friction is estimated using one-dimensional search technique *e.g.*, bisection method between the upper and lower bounds. The temperature $T(\mu)$ being the function of coefficient of friction is calculated by using the theoretical model described in Section 4.3. The following optimization problem is solved:

Find μ that minimizes

$$F = \left\{T\left(\mu\right) - T_{sm}\right\}^2, \tag{5.3}$$

$$\mu_l < \mu < \mu_u,$$

where T_{sm} is the experimentally measured temperature at the surface of the exit strip. The corresponding computed exit strip temperatures at the surface $T_s(\mu)$ from the theoretical model. As the theoretical model has been already validated in Subsection 4.6.2, this procedure is enough for establishing the confidence in the methodology. The lower and upper limits of the coefficient of friction are μ_l and μ_u, respectively. The coefficient of friction is estimated by measuring the temperature of exit strip surface at one specified location. The thermal properties of the roll and the strip material are given in Table 4.2.

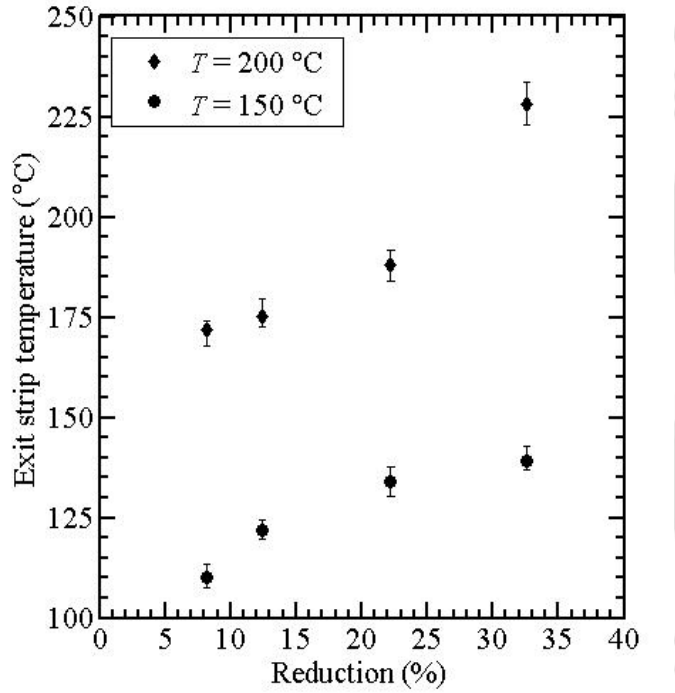

Fig. 5.5. Experimentally measured temperature as a function of reductions at 50 mm away from the roll bite

The inverse analysis is carried out with different inlet temperatures of the strip and the percentage reductions under warm rolling condition. The convergence is obtained in 12–13 functions evaluation taking the lower and upper limit of coefficient of friction as 0.08 to 0.30, respectively. The algorithm is terminated after getting the value of coefficient of friction upto 0.001 accuracy. The coefficient of friction is also calculated based on the slip measurement taking the same rolling conditions and presented in Table 5.2. It is found that the inlet strip temperature

affects the coefficient of friction. Table 5.2 shows the comparison of friction at two different inlet strip temperature by slip measurement and inverse estimation. The coefficient of friction estimated by the inverse analysis is well within 4% error with the slip measurement. The deviation is lesser for higher inlet strip temperature as shown in Table 5.2. Figure 5.6 shows the coefficients of friction estimated based on the slip and exit strip temperature measurement at two different inlet strip temperatures. The comparative study is useful for getting confidence in estimating the coefficient of friction by the exit strip temperature measurement.

Table 5.2. Comparison of the coefficient of friction estimated by slip and temperature measurement in warm rolling

Reduction, r_d (%)	Friction (μ) at T = 150 °C			Friction(μ) at T = 200 °C		
	By slip (Eq. 4.32)	By temperature	% error	By slip (Eq. 4.32)	By temperature	% error
8.2	0.135	0.138	–2.22	0.143	0.144	–0.70
12.4	0.172	0.169	1.74	0.167	0.172	–2.99
22.2	0.191	0.198	–3.67	0.198	0.197	–1.01
32.6	0.199	0.203	–2.01	0.223	0.218	2.15

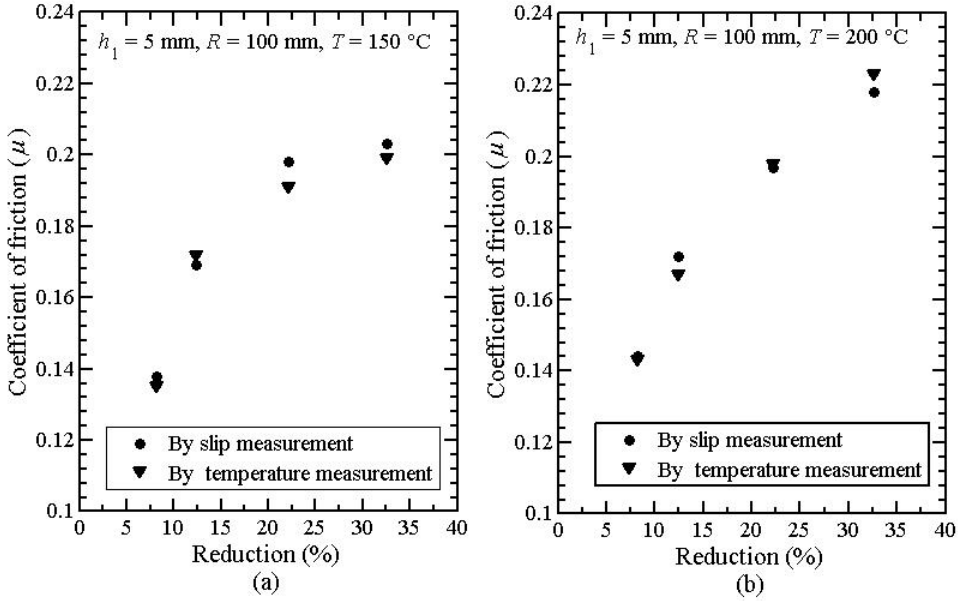

Fig. 5.6. Comparison of the coefficients of friction with reduction based on slip and temperature measurement (a) T = 150 °C and (b) T = 200 °C

5.6 Conclusion

In the present work, the coefficient of friction is determined by three methods. These three methods employed to determine the coefficients of friction are the slip measurement, the minimum roll gap measurement and the exit strip temperature measurement. The slip measurement requires the exit speed of strip and roll peripheral speed. There is a good agreement in all the methods. If the thermal and material properties of strip and roll are known, then the exit temperature of the strip measurement method can be used as a quick estimate of the coefficient of friction in rolling. Hence, in the absence of material data, it can be used as an effective method to find out the coefficient of friction.

Chapter 6

Inverse Estimation of the Mechanical Properties and the Coefficient of Friction

6.1 Introduction

For proper control and optimization of the process, modelling of the process is essential. Modelling of the process requires input data about material properties and friction. In batch production mode of rolling with newer materials, it may be difficult to determine the input parameters offline. In view of it, the present work proposes a methodology to determine these parameters online by the measurement of exit temperature and slip. The proposed methodology is validated with experimentally measured temperature of exit strip temperature of warm flat rolling. The warm flat rolling provides economical and processing advantages over the cold as well as the hot rolling process. For example, warm rolling requires less energy compared to the cold rolling and provides improved surface roughness, quality of the rolled sheet and close tolerance as compared to the hot rolling (Xie *et al*., 2011).

Li and Ghosh (2003) conducted experimental study to measure the flow stress with strain at different strain-rates range of 0.015–1.5 s^{-1} and temperature range of 200–350 °C. By conducting the uniaxial tensile test, the authors found that the elongation increases with increasing temperature and decreases with increasing strain-rate. The sensitivity study of strain hardening rate and strain-rate sensitivity constants are also presented and it is found that strain hardening rate decreases and strain-rate sensitivity increases with increasing the temperature. Further, they assessed the warm formability of three different materials *viz*., Al 5754, Al 5182+Mn and Al 6111-T4 interms of elongation, fracture strain and strain-rate

sensitivity parameter. It is found that Al 5754 and Al 5182+Mn (strain hardenable alloys) are superior to the Al 6111-T4 (precipitation hardened alloy). Smerd *et al.* (2005) measured the tensile strength of aluminum alloy sheets (AA 5754 and AA 5182) at high strain rates by tensile split Hopkinson bar test. The authors published number of experimental data on high strain-rate tensile test, which can be used to assess the accuracy of the mathematical models.

The formability of Al-alloys can be increased by warm forming (Cho and Altan, 2005). It is essential to optimize the process parameters with the better insight of the flow behaviour of the material and formability. However, the measurement of the flow stresses of the strip and the coefficient of friction at the interface requires a series of separate uniaxial tests and friction tests (Byon *et al.*, 2008). In the present work, an inverse analysis is carried out to predict the mechanical parameters and coefficient of friction during warm flat rolling. The methodology requires the measurement of the slip and temperature distribution of strip at the exit at one location. The heuristic algorithm is used to identify the unknown mechanical properties and the friction. The main contributions of this chapter are as follows. Firstly, a simple computationally and experimentally efficient algorithm has been adopted for minimization of the objective function. Secondly, a method is proposed for estimating process parameters-dependent coefficient of friction as well as mechanical properties based on the measurement of slip and temperature of strip at exit. The experimental validation of the proposed methodology to estimate the friction as well as mechanical properties is provided in the separate section based on the slip and the temperature measurement.

The rest of the chapter is organized as follows. Section 6.2 describes the direct model concisely to estimate the exit strip temperature. Section 6.3 deals with the inverse estimation of parameters methodology. Section 6.4 presents the results obtained from inverse modelling. Section 6.5 presents the sensitivity study on the parameters of power law and friction based on the exit strip temperature measurement. The experimental validation of strategy for the inverse estimation of mechanical properties and coefficient of friction in warm flat rolling is presented in Section 6.6. Section 6.7 concludes the chapter.

6.2 Direct Model

The direct model of warm flat rolling uses two separate modules *viz*., deformation module and thermal module. The deformation module uses finite element method (FEM) based on Eulerian flow formulation for the strip. Subsequently, thermal analysis of roll and strip is carried out analytically. The procedure is repeated in an iterative manner till the convergence is obtained. The direct model has been described in Sections 3.2–3.6 to obtain the temperature distribution of the strip using an approximate method for the estimation of roll temperature. The inverse model needs the exit strip surface temperature at one specified location and slip measurement. The schematic arrangement for the measurement of temperature of exit strip and exit velocity of strip is shown in Fig. 6.1.

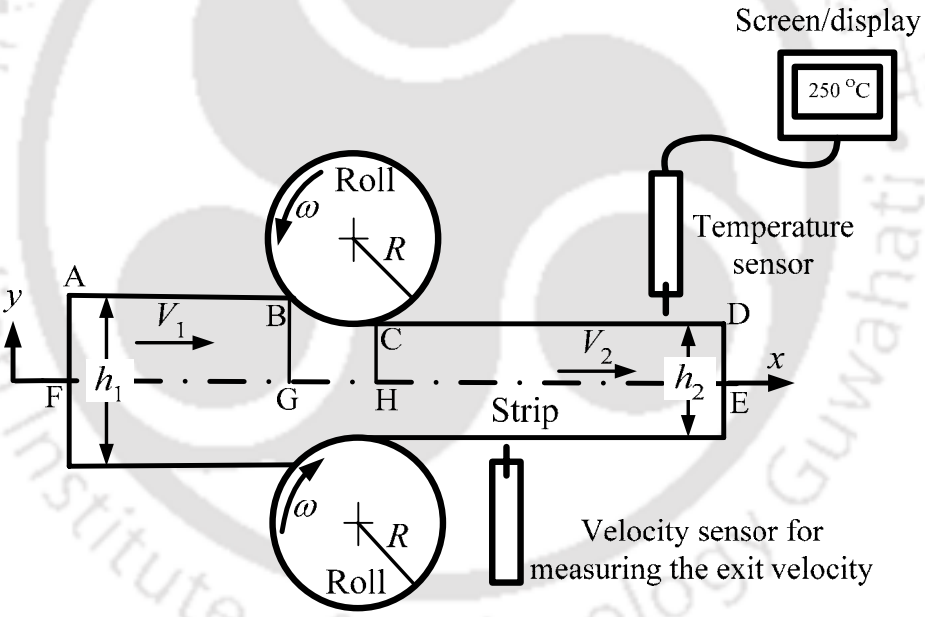

Fig. 6.1. Schematic arrangements of forward slip and temperature measurement during rolling process

6.3 Inverse Model

In this section, inverse methodology for estimating the mechanical properties and the coefficient of friction is described. The unknown mechanical properties as well as the coefficient of friction are estimated by the measurement of the surface temperature of exit strip at one specified location and slip measurement. Two

models of flow stress are used in this work. One is the Johnson-Cook (J-C) model (Johnson and Cook, 1983) given by

$$\sigma_y = \left(A + B\varepsilon_{eq}^{n_1}\right)\left[1 + C\ln\frac{\dot{\varepsilon}_{eq}}{\dot{\varepsilon}_0}\right]\left[1 - \left(\frac{T - T_{amb}}{T_{\mathbf{m}} - T_{amb}}\right)^{m_1}\right], \tag{6.1}$$

where $\dot{\varepsilon}_0$, T_{amb} and $T_{\mathbf{m}}$ are the reference strain rate, the ambient temperature and the melting temperature, respectively. A, B, C, n_1 and m_1 are the material parameters. The other is a power law given by

$$\sigma_y = \sigma_0 \varepsilon_{eq}^{n}\left(\frac{\dot{\varepsilon}}{\dot{\varepsilon}_r}\right)^{\beta_1}\left(\frac{T}{T_{\mathrm{m}}}\right)^{-\gamma}, \tag{6.2}$$

where σ_0, n, β_1 and γ are the material parameters. The J-C model has a fairly wide range of applicability. Hence, it is used for carrying out the master simulations of warm rolling and these simulations are taken in lieu of real shop floor experiments. It is to be noted that J-C model is used for testing the methodology by numerical experiments. Later, the experimental validation of the methodology with the actual shop floor data of warm flat rolling is presented in Section 6.5. The power law model is used for the inverse estimation of material parameters in somewhat restricted range of parameters. It is assumed that the material behaves as per the power law material model given in Eq. (6.2). This model may not be valid over wide ranges of strain, strain-rate and temperature. However, it is always possible to select smaller domains for fitting this model. A number of such models in various smaller domains collectively can model the behaviour in a wider zone.

The root mean squared (RMS) fractional error, E of the estimated and the measured quantity (exit temperature, roll force or roll torque) is taken as the objective function, which is minimized with respect to the decision variables σ_0, n, β_1, γ and μ. Mathematically,

$$E = \sqrt{\frac{1}{n}\times\sum_{i=1}^{n}\left(\frac{\text{measured parameter} - \text{estimated parameter}}{\text{measured parameter}}\right)^2}, \tag{6.3}$$

where n is the number of experimental observations. It was found that any one parameter among exit temperature, roll force and roll torque can be the basis for calculating E, although the exit temperature measurement is the most convenient from a practical point of view. Figure 6.1 shows the schematic representation of arrangement for temperature measurement. Alternatively, one can measure as many parameters as convenient for better reliability. Minimization of the objective function is carried out by a heuristic method inspired by the similar method used by Chandrasekeran *et al*. (2012) and Eideh and Dixit (2013).

6.3.1 Details of the Algorithm

The methodology for finding out the material parameter and friction during rolling is as follows:

Step 1: Decide the ranges of strain, strain-rate and temperature in which the power law model has to be fitted. The total domain can be represented as a rectangular parallelepiped in a three-dimensional space with strain, strain-rate and temperature as axes. Carry out 8 experiments approximately corresponding to eight corners of rectangular parallelepiped. The number of experiments is decided on the basis of 2-level two full factorial of design of experiments (DOE). It is not possible to carry out the experiments at exact desired values of strain, strain-rate and temperature. Actual controllable parameters are percentage reduction, rolling speed and initial temperature. The computational model of the rolling guides in the proper selection of controllable parameters.

Step 2: Choose suitable ranges for material parameters, σ_0, n, β_1, and γ of power law and the coefficient of friction μ.

Step 3: For each parameter the range is divided into three linguistic zones *viz*., low (L), medium (M) and high (H) as shown in Fig. 6.2 for two parameters. Thus, the entire domain gets divided into $3^5 = 243$ cells.

Step 4: Select the middle (M) values of all the parameters as initial guess parameters. Calculate E using (Eq. 6.3). The E is first calculated only on the basis of two measurements— one corresponding to high reduction, low temperature and high strain rate and other corresponding to low reduction, high temperature and low strain rate. If $E \geq 0.1$, the error is considered very high and there is no need to calculate

errors for other experimental points. If E< 0.1, then gradually other experimental points are included in the error calculation for finding out E subject to maximum of 8 experimental points. This strategy helps in reducing the computational time involved in function evaluation.

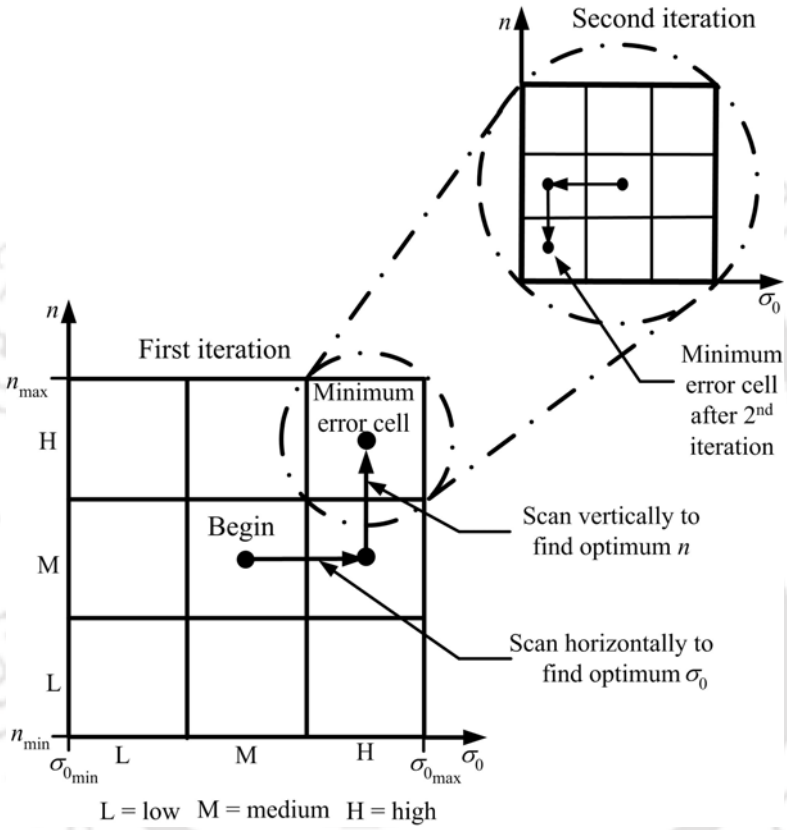

Fig. 6.2. Two-dimensional graphical representation of search procedure

Step 5: Keeping 4 other parameters (n, β_1, γ and μ) constant, carry out one dimensional search for optimum σ_0 in the following manner:

- If the estimated temperature at the current point is greater than the measured temperature, then decrease the value of σ_0 by jumping to the center of adjacent cell. If reduction in E is significant based on test of significance, then the center of adjacent cell becomes the current point. If the reduction in E is insignificant, both points are taken as current point and further exploration is

carried out in a parallel manner from both points. If E increases, then σ_0 is not changed.

- If the estimated temperature at the current point is lesser than the measured temperature, then increase the value of σ_0 by jumping to the center of adjacent cell. If reduction in E is significant based on test of significance, then the center of adjacent cell becomes the current point. If the reduction in E is insignificant, both points are taken as current point and further exploration is carried out in a parallel manner from both points. If E increases, then σ_0 is not changed.
- Else do not change the value of σ_0.

Step 6: The similar methodology as discussed in Step 5 is repeated for optimizing other parameters *i.e.*, one parameter at a time is changed keeping other four parameters constant. After completing an iteration consisting of five one-dimensional searches, the search domain gets reduced to one cell.

Step 7: For the further refinement, the optimum cell is further divided as in Step 3. Repeat the procedure of Step 4 to Step 6. A graphical representation for reducing sizes of the search domain towards optimum is shown in Fig. 6.2.

After carrying out this procedure, if the E could not be reduced significantly, then the ranges of strain rate, temperature and strain need to be reduced.

6.3.2 Modification of the Algorithm for Variable Friction Case

In many cases, the friction is a function of process parameters and it cannot be considered constant. Most predominantly, it depends on the temperature. The friction can be measured by measuring the slip at each experimental point. For each experimental point, the coefficient of friction may be different. The algorithm developed in Subsection 6.3.1 can be used for this case also. Now, the number of decision variables reduces from 5 to 4. However, in each cell, while estimating the observable parameter (temperature, roll force and roll torque), the proper value of coefficient of friction as estimated based on slip measurement needs to be considered.

6.4 Results and Discussion

In the following subsections, inverse estimation of material parameters and coefficient of friction and inverse estimation of material parameters with considering the coefficient of friction is variable. The inverse estimation have been carried out for different strip materials namely, AISI 4142 steel, copper and Aluminum alloy considering roll material to be steel.

6.4.1 Inverse Estimation of Mechanical Properties and Friction

In this subsection, actual shop floor experiments have not been carried out. For validating the proposed procedure, numerical experiments have been carried out. It is assumed that the actual flow stress is governed by the well known J-C relation. The constants of different material of J-C model are given in Table 6.1.

Table 6.1. Constants of J-C model for different materials

Material	A (MPa)	B (MPa)	n_1	C	m_1	$\dot{\varepsilon}_0$	T_m (K)	References
Steel (AISI 4142)	598	768	0.2092	0.0137	0.807	0.001	1768	Meslin and Hamann (2003)
Copper	90	292	0.31	0.025	1.09	1	1338	Raczy *et al.* (2004)
Aluminum Alloy AI6061-T6)	293	121.3	0.23	0.002	1.34	1	925	Shang *et al.* (2012)

Table 6.2. Thermal properties of strip material

Material	Thermal Conductivity (W/m-°C)	Heat Capacity (J/kg-°C)	Density (kg/m^3)	References
Steel (AISI 4142)	43	470	7800	Steiner (1990)
Copper	400	385	8960	Zhang *et al.* (2011)
Aluminum Alloy (AI6061-T6)	237	900	2700	Davies (1992)

The actual coefficient of friction is assumed to be 0.20. The roll radius (R) is 65 mm and inlet thickness of the strip (h_1) is 1 mm. With these data, virtual simulations are carried out using the FEM analysis for different initial temperature of strip, percentage of reduction and exit velocity of strip. Forward slip is recorded.

The mechanical properties are obtained by the inverse analysis using the thermal properties of material as given in Table 6.2. The work-roll material is considered as steel only for the entire analysis. The thermal properties of roll are given in Khalili *et al*. (2012).

Inverse analysis provides the material parameters σ_0, n, β_1, γ and the coefficient of friction μ of different materials *viz*., AISI steel, Copper and Aluminum Alloy AI6061-T6 as given in Table 6.3. The convergence is obtained in 32–42 function evaluation *i.e*., in 3–4 iterations for all three different materials of strip. The convergence depends on the initial hypercube size of the unknown parameters. Starting with a large range of domain is better, but the number of iterations required for convergence will be large.

Table 6.3. Values of material parameters and friction by inverse analysis

Obtained material and process parameters	Steel (AISI 4142)		Copper		Aluminum Alloy (AI6061-T6)
Temperature range (°C)	175–375	375–575	175–375	375–575	150–275
σ_0 (MPa)	461.1	408	117	124	202
n	0.085	0.0966	0.155	0.174	0.0567
β_1	0.013	0.0122	0.0468	0.0065	0.0032
γ	0.565	0.83	0.8	0.967	0.75
μ	0.2005	0.1995	0.2005	0.2005	0.1875
Range: strain-rate: 10–100 s^{-1} and strain: 0.02–0.4					

Figures 6.3 and 6.4 show the variation of flow stresses with strain at the estimated and the actual mechanical properties for work material (steel) of strip. It is assumed that the power law gives the better results for smaller range of process parameter. Hence, temperature is defined in the two ranges *i.e.* 175–375 °C and 375–575 °C. Later on the larger range is also considered. Figures 6.3a and 6.3b show the variation of flow stresses with strain for temperatures of 250 and 325 °C, respectively, at different strain rates. The parameters of power law were fitted in the range of 175–375 °C and are tabulated in Table 6.3. Similar graphs have been plotted for the temperature range (375–575 °C) in Figs. 6.4a and 6.4b. For display purpose 450 °C and 525 °C temperatures are chosen. It is observed that the estimated flow stresses are in good agreement with actual material flow stresses; the maximum error is less than 1%.

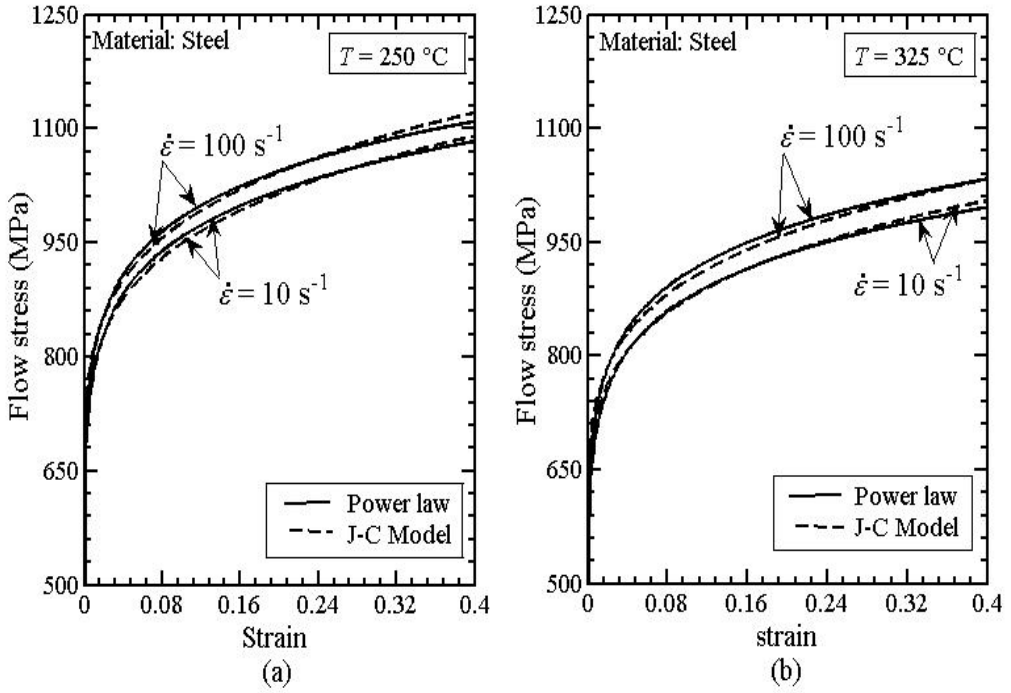

Fig. 6.3. Variation of flow stresses with strain for steel (strip) at actual and estimated material properties (a) 250 °C (b) 325 °C

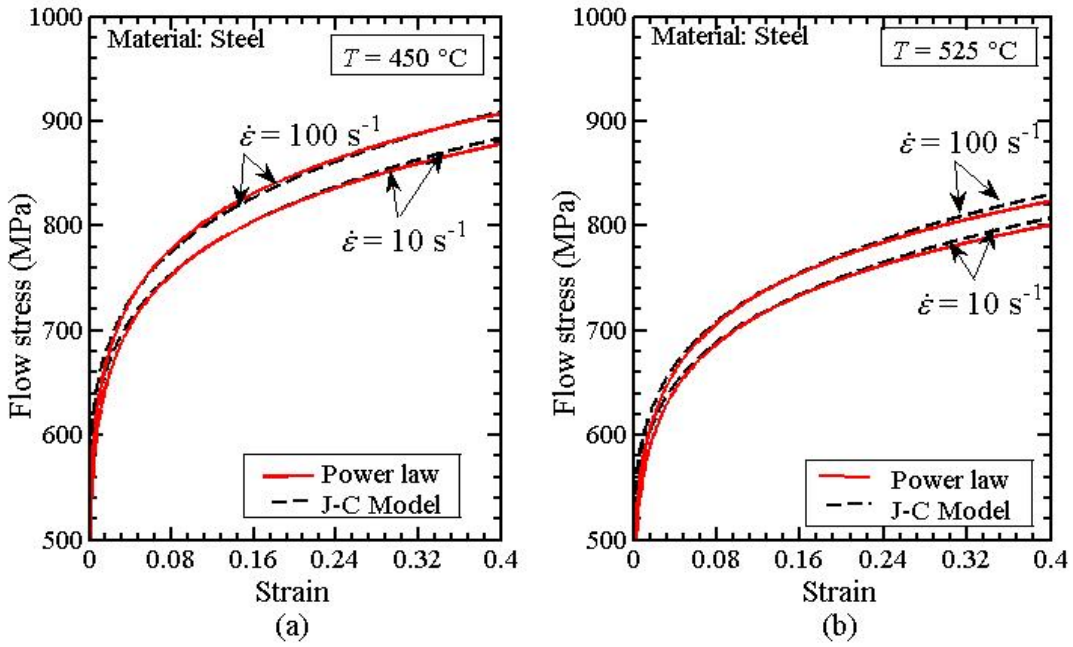

Fig. 6.4. Variation of flow stresses with strain for steel (strip) at actual and estimated material properties for temperature (a) 450 °C (b) 525 °C

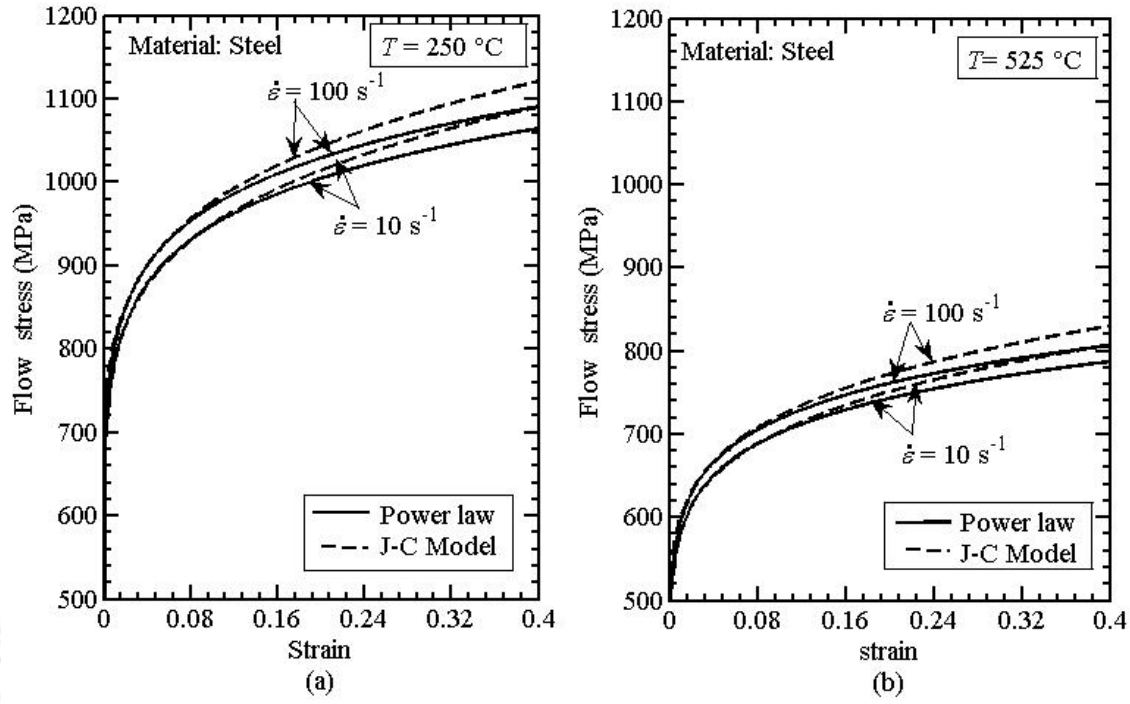

Fig. 6.5. Variation of flow stresses with strain for steel (strip) at actual and estimated material properties for temperature (a) 250 °C (b) 525 °C

Figure 6.5 show the variation of flow stress with strain at different strain rates for the temperature range of 175–580 °C. Figure 6.5a corresponds to 250 °C and Fig. 6.5b corresponds to 525 °C. Here, the inverse estimation of mechanical properties have been carried out for larger range of temperature. The same inverse methodology is used to obtain the following material parameters: σ_0 = 443 MPa, n = 0.0835, β_1 = 0.0105, γ = 0.701 and coefficient of friction μ = 0.1995. It is observed that in this case, there is somewhat larger deviation with J-C model.

For the work material copper, the same inverse methodology is implemented to obtain the optimum material and process parameters. Figure 6.6 and 6.7 show the variation of flow stresses with strain for different temperatures at different strain rates. It is seen from Figs. 6.6a, 6.6b, 6.7a and 6.7b that the flow stresses are in good agreement with actual material parameters. The maximum error between actual flow stresses and estimated flow stresses is lesser than 1%.

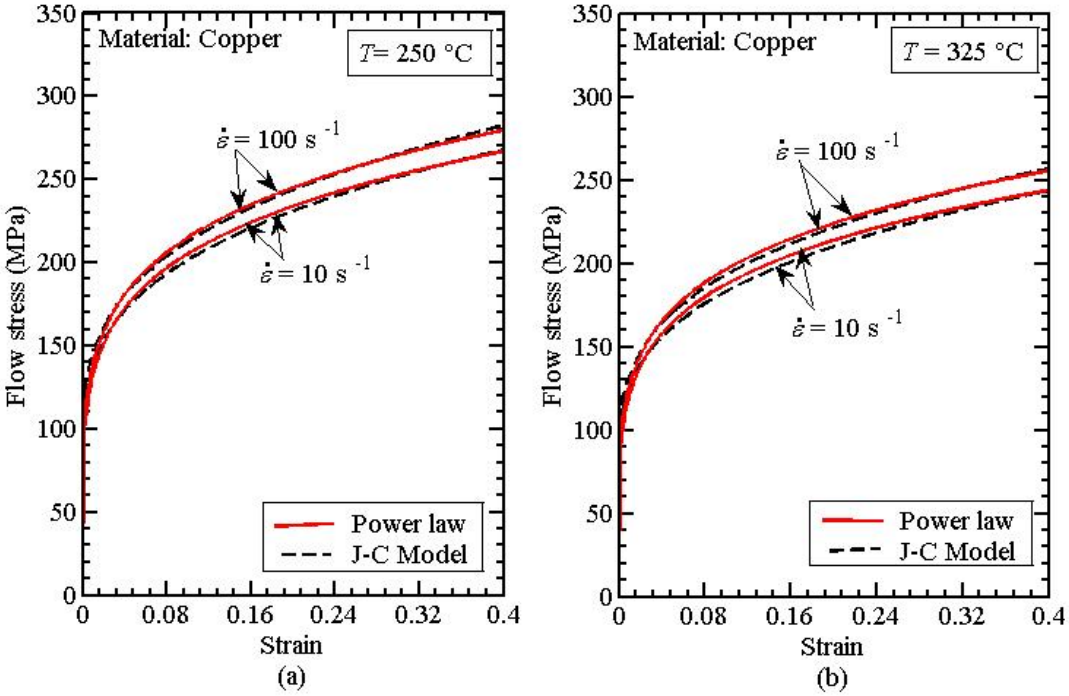

Fig. 6.6. Variation of flow stresses with strain for copper (strip) at actual and estimated material properties for temperature (a) 250 °C (b) 325 °C

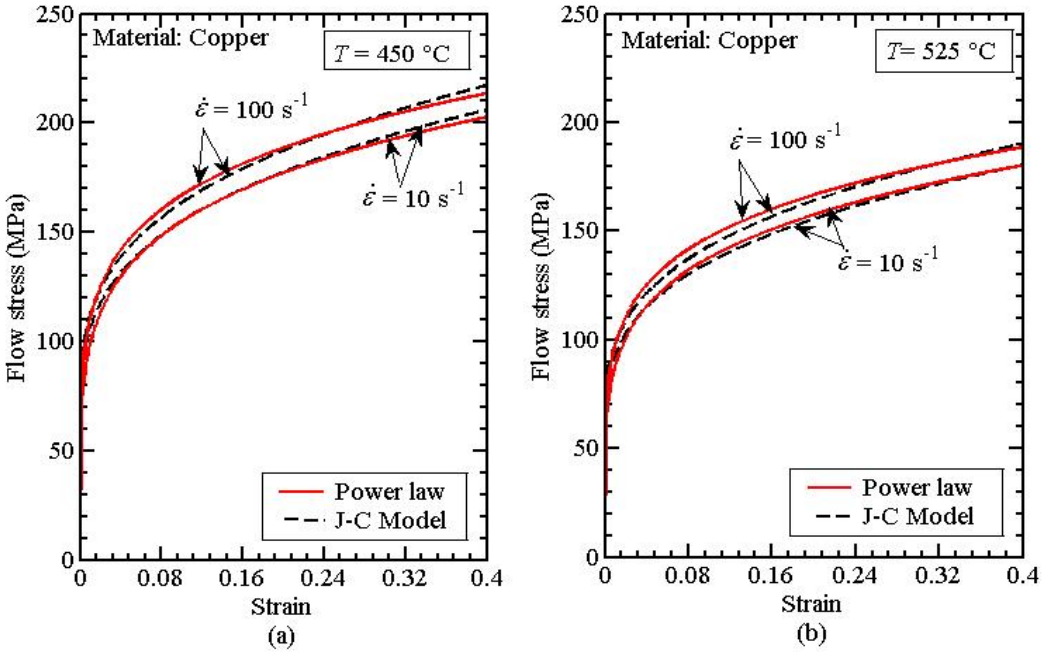

Fig. 6.7. Variation of flow stresses with strain for copper (strip) at actual and estimated material properties for temperature (a) 450 °C (b) 525 °C

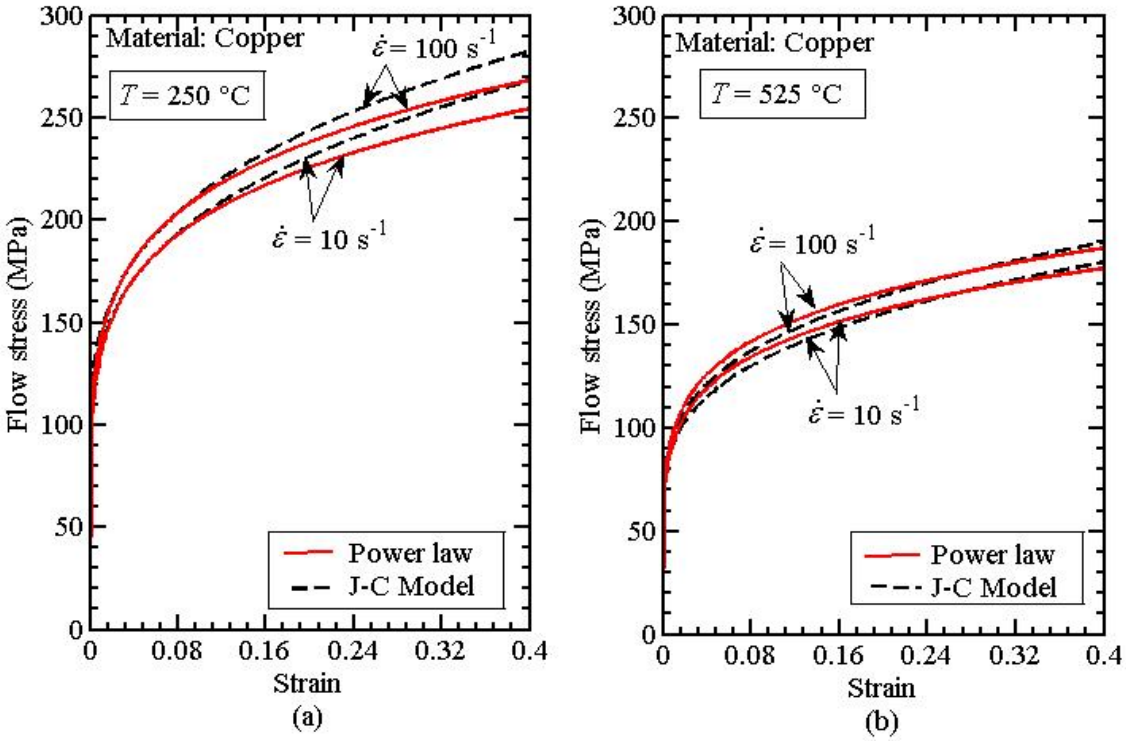

Fig. 6.8. Variation of flow stresses with strain for copper (strip) at actual and estimated material properties for temperature (a) 250 °C (b) 325 °C

Figure 6.8 shows the variation of flow stress with strain of copper at different strain rates for the temperature range of 175–575 °C. The inverse methodology is used to obtain the unknown material parameters as σ_0 = 128.14 MPa, n = 0.172, β_1 = 0.0233, γ = 0.837 and coefficient of friction μ = 0.1895. Although larger error compared to smaller temperature ranges is obtained, the error is lesser than 5%.

A similar methodology of inverse analysis has been used for aluminum AI6061-T6. Figure 6.9 shows the variation of flow stress with strain for actual and estimated material parameters for aluminum strip. Here, the temperature range considered is 125–275 °C. For the case of aluminum strip material, the inverse estimated coefficient of friction and parameters of power law shows the good agreement with J-C model at high strain compared to the low strain as shown in Fig. 6.9.

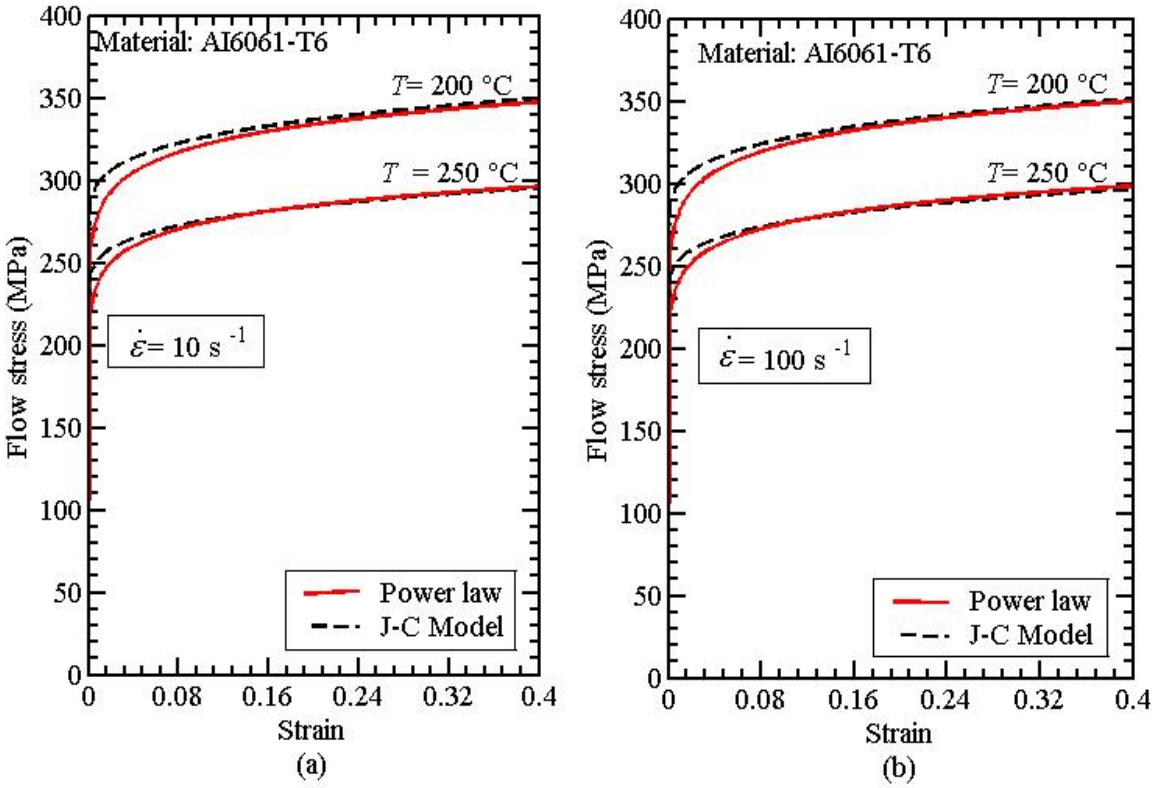

Fig. 6.9. Variation of flow stresses with strain for aluminum (strip) at actual and estimated material properties for temperature (a) 150 °C (b) 250 °C

6.4.2 Inverse Estimation of Mechanical Properties and Friction for Variable Friction Case

In this subsection, the coefficient of friction is assumed to vary with temperature. The coefficient of friction is determined on the basis of forward slip measurement. The exit speed of strip is higher than the speed roll (peripheral speed of work-roll) during rolling due to reduction in strip at deformation zone. The forward slip is calculated by deformation FEM module. The roll speed may be measured by a tachometer and velocity of exit speed may be measured by velocity sensor as shown in Fig. 6.1. Yadav *et al*. (2011b) also used the velocity sensor and the temperature sensor for estimating the coefficient of friction and flow stress of the strip material by measuring the forward slip and the exit strip temperature for cold flat rolling.

The coefficient of friction is assumed for dry rolling cases to follow the following relation (Lenard and Kalpakjian, 1991):

$$\mu = 0.41 - 0.00025T - 0.028V_R \tag{6.4}$$

where T is the average temperature at the deformation zone in °C and V_R is the roll speed in m/s. Table 6.4 shows the estimated coefficient of frictions for different cases.

Table 6.4. Optimum coefficient of friction

Case	Inlet temperature, T (°C)	Exit velocity, V_2 (m/s)	Reduction, r_d (%)	Optimum coefficient of friction, μ
1.	325	0.5	4	0.243
2.	325	0.5	28	0.232
3.	325	3	4	0.235
4.	325	3	28	0.227
5.	245	0.5	4	0.252
6.	245	0.5	28	0.263
7.	245	3	4	0.241
8.	245	3	28	0.234

The coefficient of frictions is determined at different rolling process parameters using an empirical formula (Lenard, 2000) expressed in Eq. (6.4) for steel as a material of the roll and strip. It is found that the coefficient of friction decreases with increasing inlet temperature of strip. It may be due to insignificant effect of temperature softening and oxide layer. The behaviour of the coefficient of friction depends upon the combination of the materials of the roll and the strip during rolling process. The optimum material parameters for power law are obtained as σ_0 = 456 MPa, n = 0.077, β_1 = 0.0035, γ = 0.735. Figure 6.10 shows the variation of flow stresses with strain for actual and estimated material parameters. The difference between the actual and estimated flow stresses is less than $\pm 3\%$.

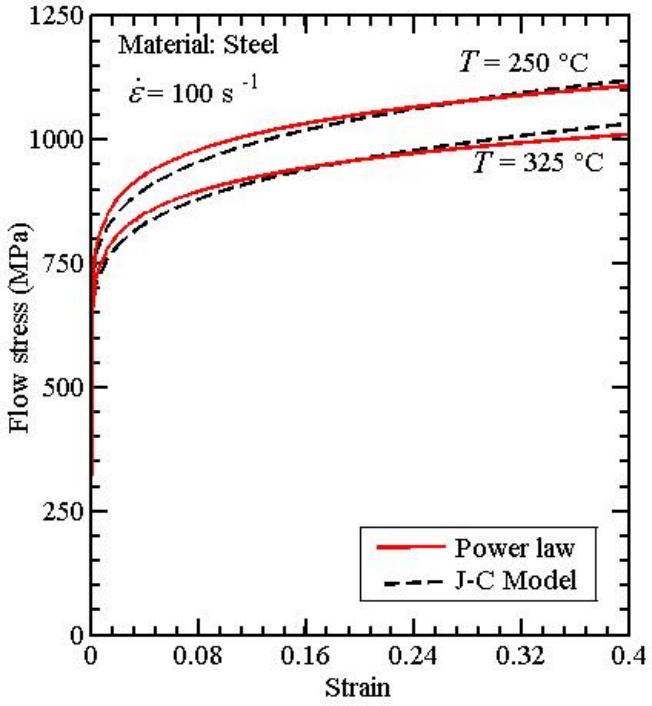

Fig. 6.10. Variation of flow stresses with strain at actual and estimated material properties of steel for strain-rate 100 s^{-1}

6.5 Sensitivity Analysis

A sensitivity study is carried out for the material parameters and the coefficient of friction obtained by an inverse analysis for steel (strip) at 250 °C and 375 °C inlet temperature of strip. Table 6.5 shows the temperature difference in the exit strip temperature computed at the coefficient of friction and estimated material parameters of power law obtained by inverse estimation. Here, the actual temperature was obtained using J-C model. Computational results have been obtained by taking inverse estimated parameters as well as perturbing them one-by-one. The error in temperature at 150 mm from the exit of roll bite has been calculated for the two cases *i.e.*, E_{I} for high inlet temperature, low reduction and low roll speed and E_{II} for low inlet temperature, high reduction, high roll speed. Instead of roll speed, the exit velocities are specified for providing a better feel.

Table 6.5. Error in the temperature estimation at optimum values and at $\pm 5\%$ variation in the material parameters and coefficient of friction for steel work-material

Material Parameters and coefficient of friction used to estimate the temperature	Error in exit strip temperature	
	Case I E_I (T = 375 °C, V_2 = 0.5 m/s, r_d = 4%) °C	Case II E_{II} (T = 250 °C, V_2 = 3 m/s, r_d = 28%) °C
$(\sigma_0, n, \beta, \gamma, \mu)$ = (461.11 MPa, 0.085, 0.013, 0.565, 0.2005)	+0.98	–1.51
$(1.05\sigma_0, n, \beta_1, \gamma, \mu)$	+1.27	+30.3
$(0.95\sigma_0, n, \beta_1, \gamma, \mu)$	–0.68	–4.48
$(\sigma_0, 1.05n, \beta_1, \gamma, \mu)$	–0.84	–32.65
$(\sigma_0, 0.95n, \beta_1, \gamma, \mu)$	+1.1	+19.35
$(\sigma_0, n, 1.05\beta_1, \gamma, \mu)$	+0.96	+16.19
$(\sigma_0, n, 0.95\beta_1, \gamma, \mu)$	–0.90	–40.68
$(\sigma_0, n, \beta_1, 1.05\gamma, \mu)$	+1.07	+58.61
$(\sigma_0, n, \beta_1, 0.95\gamma, \mu)$	–0.77	–62.08
$(\sigma_0, n, \beta_1, \gamma, 1.05\mu)$	+0.89	+35.26
$(\sigma_0, n, \beta_1, \gamma, 0.95\mu)$	–1.25	–6.05
The exit temperature of strip at 150 mm from the exit of the roll bite is obtained by J-C model: T_{exit} = 248.85 °C for case I and T_{exit} = 294.93 °C for case II.		

The sensitivity of error in temperature with respect to error in the estimation of material parameter *viz*., $\sigma_0, n, \beta_1, \gamma$ and μ is estimated. This information helps in determining the permissible errors in $\sigma_0, n, \beta_1, \gamma$ and μ. The convergence criteria can be chosen accordingly. E_I and E_{II} for the inversely determined parameters along with $\pm 5\%$ material and process parameters variation are listed. The exit strip temperature measurement is more sensitive for low inlet temperature, high reduction, and high exit velocity as shown in Table 6.5. It is observed that temperature estimates are very sensitive to γ.

Sensitivity derivatives are calculated using the central difference method. Table 6.5 can be used to estimate partial derivatives of E_{I} and E_{II} with respect to parameters. For example, $\partial E_{II} / \partial \sigma_0$ comes out to be 0.754 °C/MPa by central

difference method. Similarly, $\partial E_{II}/\partial n = -5.20\,^{\circ}\mathrm{C}$, $\partial E_{II}/\partial \beta_1 = 5.68\,^{\circ}\mathrm{C}$, $\partial E_{II}/\partial \gamma = 12.06\,^{\circ}\mathrm{C}$, and $\partial E_{II}/\partial \mu = 4.13\,^{\circ}\mathrm{C}$. It is noted that the derivatives of error in temperatures at actual and estimated parameters with respect to γ are high. Hence, the most sensitive parameter is γ. This type of analysis helps in determining the convergence criteria.

6.6 Experimental Validation of Strategy for the Inverse Estimation of Mechanical Properties and the Coefficient of Friction

To validate the strategy for finding out the mechanical properties and coefficient of friction, an experimental study is conducted to measure the flow stresses. The mechanical properties of the strip material calculated through tensile tests are presented in Subsection 6.6.1. The experimental verification of the inverse modelling is presented in Subsection 6.6.2. Subsection 6.6.3 deals with correlation coefficient developed between flow stresses with different inlet strip temperatures/reduction.

6.6.1 Direct Measurement of Mechanical Properties through Tensile Test

The mechanical properties were evaluated by means of tensile tests at different temperature (Due to isotropic nature of the material, compression test is also likely to give the same results, albeit the compression test can be carried out upto much larger strain.). The tests were performed according to ASTM E8/E8M–15. Two replicates were carried out at each testing condition. A 100 kN capacity universal testing machine (Make: Instron, Model: 8801) was used for carrying out the tensile test. The specimen was made of commercially pure aluminium alloy as per standard ASTM design. The tensile test of the specimen at different temperatures was carried out in a universal testing machine to find out the stress-strain relationship. Figures 6.11a and 6.11b show the engineering stress-strain curve and true stress-strain curve at different temperatures with approximately constant strain-rate, respectively. The ram velocity was kept constant at 1 mm/min for all the experiments. This corresponds to a strain-rate less than 3×10^{-3} s^{-1}. It is to be noted that the yield point

of the tested material is obtained from the true stress-strain relation rather than the engineering stress-strain curve for different temperatures.

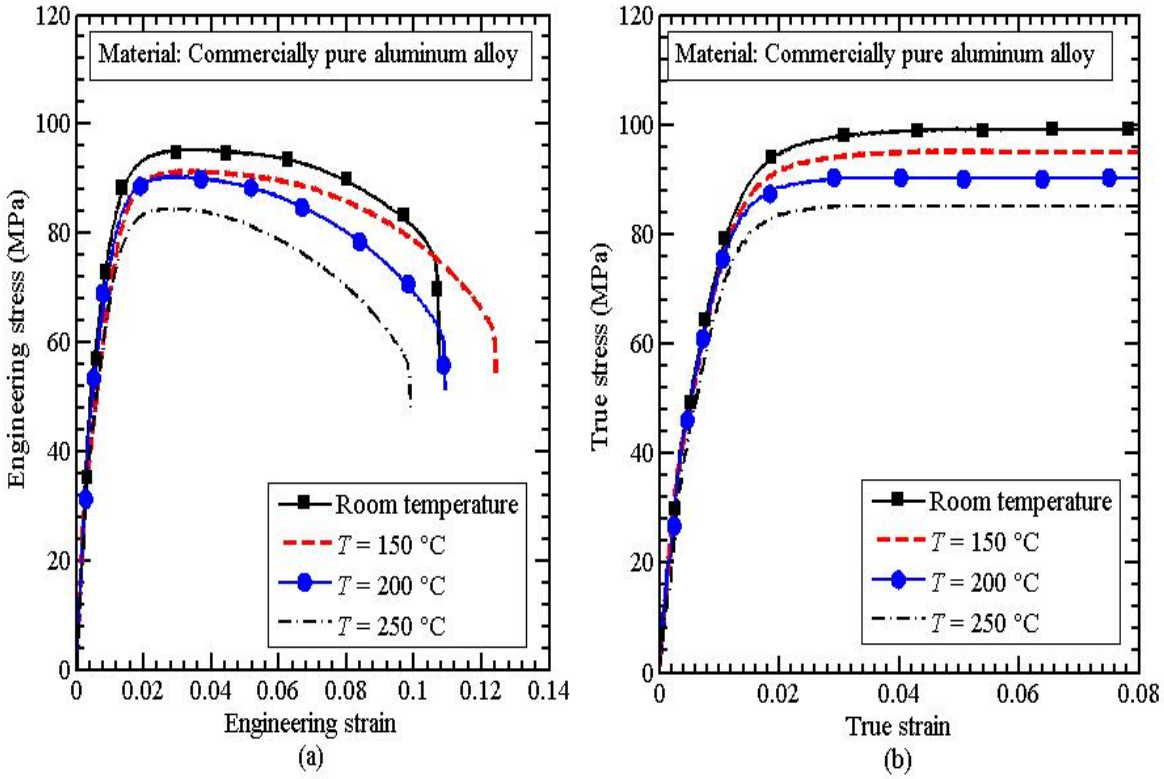

Fig. 6.11. Measured stress-strain curve at different temperatures experimentally: (a) Engineering stress–strain curve and (b) True stress–strain curve

The following relation is fitted from the stress-strain data obtained at different temperatures considering constant strain-rate,

$$\sigma_y = K\varepsilon_{eq}^n \ , \tag{6.5}$$

where σ_y is the flow stress in MPa and ε_{eq} is the equivalent strain. The material constants K and n are considered to be temperature dependent. Table 6.1 shows the optimum values of K and n obtained from the least squared curve fitting technique and a quasi-Newton method for error minimization at different temperatures. The MATLAB® inbuilt function FMINUNC is employed to obtain the value of K and n by minimizing the error with the experimental data. The coefficient of determination R^2 is close to 1 indicating good fitting.

Table 6.6. Proper values of K and n at different temperatures

Temperature (°C)	By the least square method			By optimization method		
	K (MPa)	n	R^2 value	K (MPa)	n	R^2 value
Room temperature	115.35	0.0497	0.991	113.58	0.0498	0.993
150	108.71	0.0437	0.992	108.6	0.0438	0.993
200	98.36	0.0281	0.998	98.69	0.2871	0.995
250	94.35	0.0329	0.998	95.04	0.338	0.986

The multiple regression analysis is also carried out to find out the unknown parameters of power law for the temperature dependent flow stress. It is assumed that the material behaves as per the power law material model neglecting the effect of strain-rate. The flow stresses of the strip is the function of strain and temperature as given by

$$\sigma_y = \sigma_0 \varepsilon_{eq}^n \left(\frac{T}{T_m} \right)^{-\gamma} . \tag{6.6}$$

The following fitted material parameters are obtained as σ_0 = 85.75 MPa, n = 0.0387, γ = 0.2351. Further, the material paramters of power law are also calculated using optimization method. For this, an optimization problem may be approximated by a quadratic program. An upper bound and lower bound estimating formula are also obtained using a sequential quadratic programming (SQP) method. A Quadratic program (QP) is a nonlinear programming problem having quadratic objective function and linear constraints. SQP solves a QP at each iteration till the convergence is obtained. There are several variants of SQP method. The principle of SQP method is briefly described in Appendix I. The MATLAB® inbuilt functions FMINCON is used in this work which uses SQP for constrained optimization of nonlinear function. The three problems are solved to estimate the unknown variables σ_0, n and γ from the experimental true stress–strain data. The objective functions with constaints and obtained optimum values are tabulated in Table 6.7. The lower bound and upper bound fits of the flow stresses with strain are obtained by solving the problem II and problem III, respectively.

Table 6.7. Different optimization problems for estimating optimum values of σ_0, n and γ

Optimization Problem	Objective function to be minimized	Constraint	Optimum value			
			σ_0 (MPa)	n	γ	R^2 value
Problem-I (most likely estimate)	$F=\sum_{i=1}^{n}\left\{(\sigma_f)_{\text{expt}}-\sigma_0\varepsilon^n\left(\frac{T}{T_{\text{m}}}\right)^{-\gamma}\right\}^2$,	Nil	89.25	0.0417	0.2051	0.923
Problem-II (lower bound estimate)	$F=\sum_{i=1}^{n}\left\{(\sigma_f)_{\text{expt}}-\sigma_0\varepsilon^n\left(\frac{T}{T_{\text{m}}}\right)^{-\gamma}\right\}^2$,	$(\sigma_f)_{\text{expt}}\geq\sigma_0\varepsilon^n\left(\frac{T}{T_{\text{m}}}\right)^{-\gamma}$	78.63	0.0298	0.0298	0.829
Problem-III (upper bound estimate)	$F=\sum_{i=1}^{n}\left\{(\sigma_f)_{\text{expt}}-\sigma_0\varepsilon^n\left(\frac{T}{T_{\text{m}}}\right)^{-\gamma}\right\}^2$,	$(\sigma_f)_{\text{expt}}\leq\sigma_0\varepsilon^n\left(\frac{T}{T_{\text{m}}}\right)^{-\gamma}$	102.35	0.0548	0.2151	0.843

6.6.2 Determination of Mechanical Properties and the Coefficient of Friction Based on Temperature and Slip Measurements

In-house warm rolling experiments were conducted to measure the temperature of exit strip and slip at different reductions for different inlet temperatures of the strip. Temperature was recorded at the surface of the strip at 50 mm away from the bite zone for different reductions. The details of the experimental procedure were described in Section 4.5. The inverse estimation requires surface temperature of exit strip at the specified location. The forward slip was also recorded for different reductions at different inlet temperature of the strip are shown.

The experimentally measured temperatures of the strip at surface for different reductions are shown in Table 6.8. The number of experiments is decided on the basis of 2-level full factorial of design of experiments considering two parameters *viz*., inlet strip temperatures and reductions at constant rolling speed. The total four different reductions at two different inlet temperatures have been decided to carry out the experiments. Three replicates were performed at each rolling condition and the averaged temperature is taken for the inverse analysis. There was a variation of 3–8 °C within replicates. The coefficient of friction is estimated by an FEM model based on slip measurement as given in Table 6.9. The estimated friction values at different reductions with different inlet temperatures of strip.

Table 6.8. Measured average temperature of exit strip at different reductions for different inlet strip temperatures for h_1 = 5 mm, R = 100 mm (Values in bracket are standard deviations)

Reduction, r_d (%)	Averaged exit strip surface temperature (°C) at 50 mm from the bite zone	
	Inlet strip temperature, T = 100 °C	Inlet strip temperature, T = 200 °C
8.2	97.7 (1.5)	172.1 (3.5)
12.4	98.7 (2.5)	175.7 (2.1)
22.2	104.6 (3.1)	189.6 (2.1)
32.6	107.7 (3.8)	227.9 (4.4)

Table 6.9. Experimentally measured forward slip and estimated averaged coefficient of friction for different rolling temperature with different reductions at h_1 = 5 mm, R = 100 mm

Reduction, r_d (%)	Inlet strip temperature, T = 100 °C		Inlet strip temperature, T = 200 °C	
	Forward slip, f_s (%)	Friction, (μ)	Forward slip, f_s (%)	Friction, (μ)
8.2	12.4	0.125	13.4	0.143
12.4	15.3	0.165	16.9	0.167
22.2	24.3	0.180	28.7	0.198
32.6	35.1	0.188	36.8	0.223

The results presented in Table 6.9 are considered for the strip made of commercially pure aluminum alloy and the roll material is made of high carbon and high chromium steel. The coefficient of friction increases with increasing the inlet strip temperature. It may be due to temperature softening in the strip before rolling which results in sticking phenomenon. Due to softening of the asperities, the real area of contact increases, thus increasing the friction. The inverse methodology is employed by taking the shop floor experimental data. The methodology proposed in Section 6.3 is validated by measuring the exit strip temperature and slip. The thermal properties for the roll and the strip used in the direct model to find out the temperature of exit strip are provided in Table 4.3. The convective heat transfer coefficients of the roll at the inner and outer periphery are 2.6 and 260 W/m^2-°C, respectively in the direct model. The convective heat transfer coefficient of strip surface just after the bite zone is taken as 10 W/m^2-°C.

The basic concept of an inverse method for parameters identification is to compute a set of unknown material parameters based on initial guess. The methodology described in Section 6.3 is adopted to find out the mechanical properties and coefficient of friction. The mechanical properties of strip and coefficient of friction at the interface are obtained by the measurement of temperature and slip. The material behaves as per the power law material model neglecting the effect of strain-rate as expressed in Eq. (6.6). Figure 6.12 shows the inverse methodology for estimating mechanical properties and coefficient of friction.

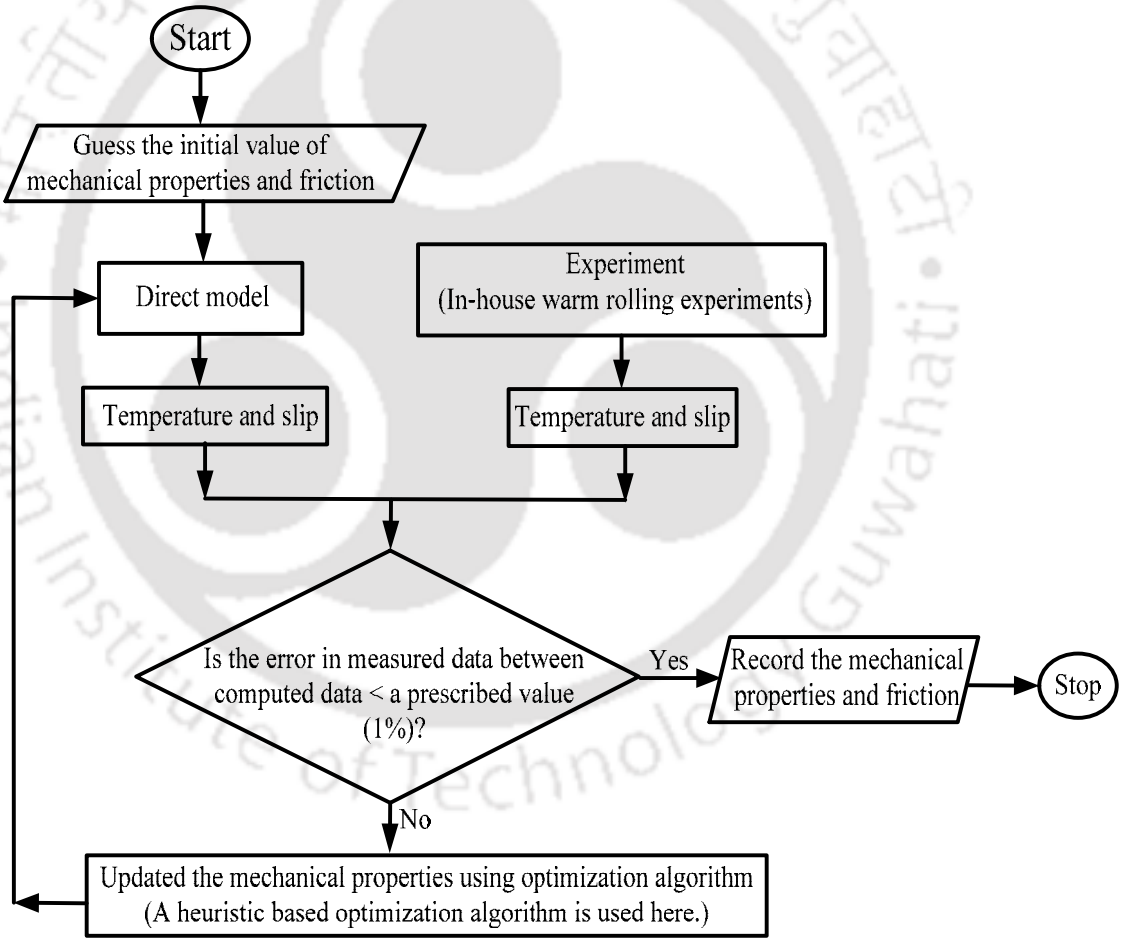

Fig. 6.12. Flow chart of the inverse model for mechanical properties and the coefficient of friction determination

The following objective function is to be minimized with respect to the decision variables σ_0, n, γ and μ such as

$$E_1 = \sqrt{\frac{1}{n} \times \sum_{i=1}^{n} \left(\frac{T_{ism} - T_{isc}}{T_{ism}} \right)^2}, \tag{6.7}$$

where n is the number of experimental observations, T_{ism} is the measured temperature at the strip surface experimentally and T_{isc} is the computed temperature from the direct model at the strip surface.

The constant of power law obtained from the inverse estimation are as follows: σ_0 = 84.56 MPa, n = 0.0372, γ = 0.2358. The convergence is obtained in 10–13 function evaluation *i.e.*, in 4–5 iterations. However, the convergence of the optimization alogrithm depends on the initial hypercube size of the unknown parameters. Starting with a large range of domain is better, but the number of iterations required for convergence will be large.

Figure 6.13 shows the comparison of the flow stress–strain curve. The upper bound fit, lower bound fit and inversely estimated flow stresses–strain curve with experimental stress-strain curve is shown at different temperatures. It is found that the deviation of the inversely estimated flow stresses is 5–10% from the experimental flow stress. Fig. 6.13a shows the comparison of flow stresses with strain at room temperatures. Figures 6.13b, 6.13c and 6.13d show the comparison of flow stress-strain curve at three diffeternt temperatures *viz*., 150, 200 and 250 °C, respectively. It is observed that barring low strain data, the experimental values match with estimated values. In all the cases, the experimental data lies between the upper and lower bound estimates. It is to be noted that the power law fits well only in the pastic deformation region, which is dominant in the metal forming. Hence, the poor matching of low strain data is not a major concern. The experimental data is based on tensile test. For most of the metals including aluminium, tensile and compressive behaviour is resonably the same. The proper matching of the model with experimental data further confirms it.

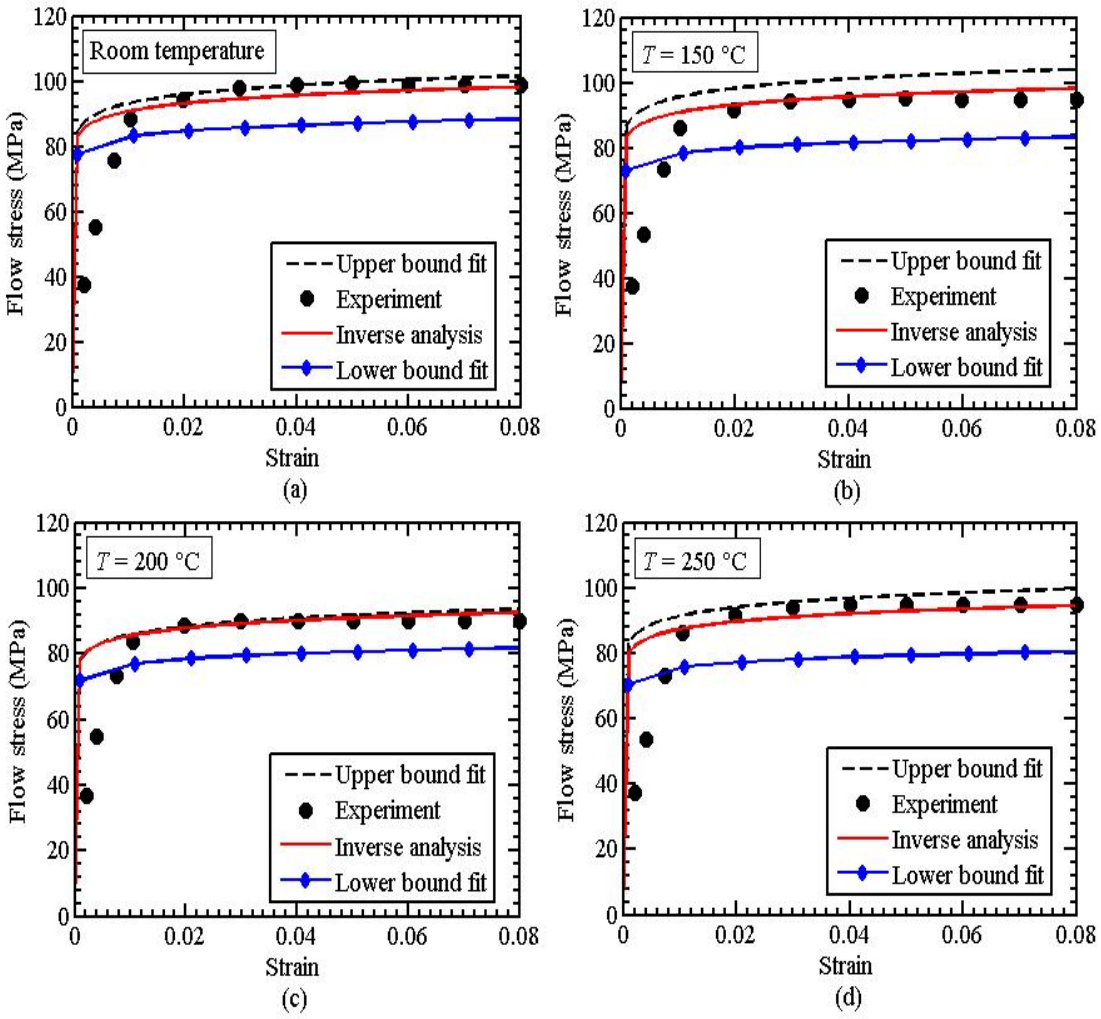

Fig. 6.13. Comparison of the experimental stress-strain curves and inversely estimated stress-strain curves at different temperatures with upper and lower bound fit data (a) Room temperature, (b) 100 °C, (c) 150 °C and (d) 250 °C

Once the mechanical properties of the strip and the coefficient of friction are obtained from an inverse analysis, their ability to predict the temperature is validated experimentally by measuring the temperature at different locations of the exit strip. The exit strip temperature at any location is evaluated theoretically from the direct model by using the friction and mechanical properties obtained from the inverse model. The theoretical predictions of the exit strip temperature are compared with the experimentally measured temperatures at the surface as well as at the centerline of the exit strip. Figure 6.14 compares the inversely obtained exit strip temperatures with experimentally measured temperatures at the surface as well as at the

centerline. For comparison, two different inlet strip temperatures–100 and 200 °C were considered. The strip exit temperature shows a sudden upward trend at higher reductions and higher temperature of 200 °C. This is due to the interaction between high temperature and high reductions compared to the other cases. The experiments were carried out for different reductions in the strip. The temperature was measured at the surface and centerline of the strip at 150 mm away from the bite zone. Further, the exit strip temperatures were measured at 50 and 150 mm away from the bite zone both at the surface and centerline and compared with the theoretical results. The comparison is shown in Fig. 6.15. In this case, the inlet strip temperature was taken as 150 °C. It is observed that the theoretical predictions are in close agreement with the experimental results with a variation of ±5%.

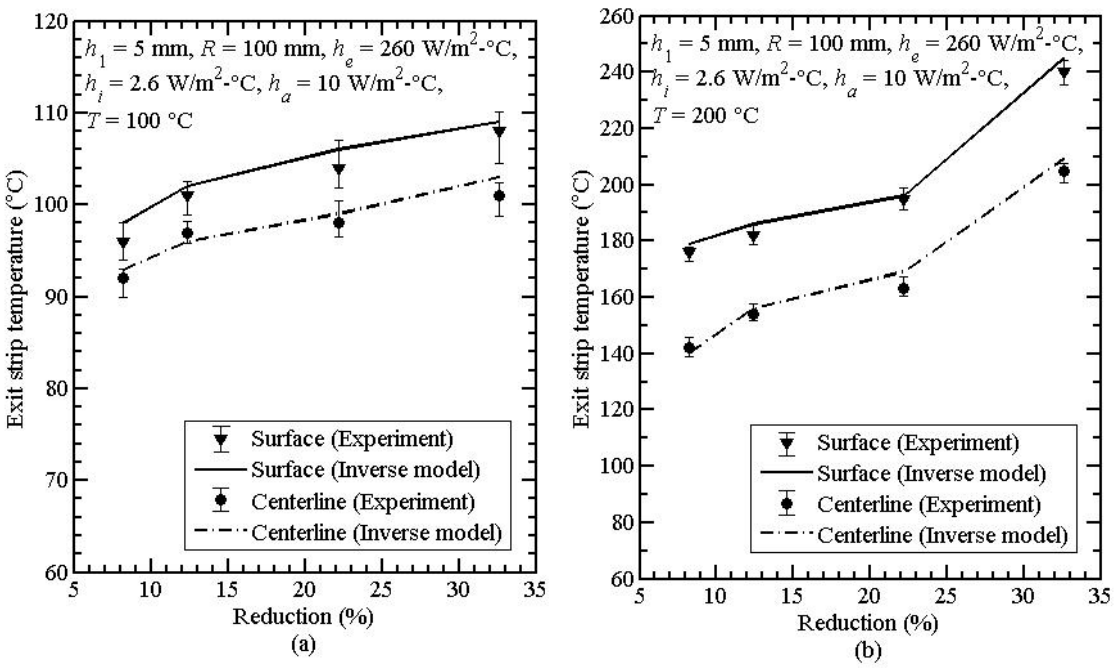

Fig. 6.14. Comparison of exit strip temperature predictions of inverse model with experiments at 150 mm from the bite zone for different inlet temperatures: (a) T = 100 °C and (b) T = 200 °C

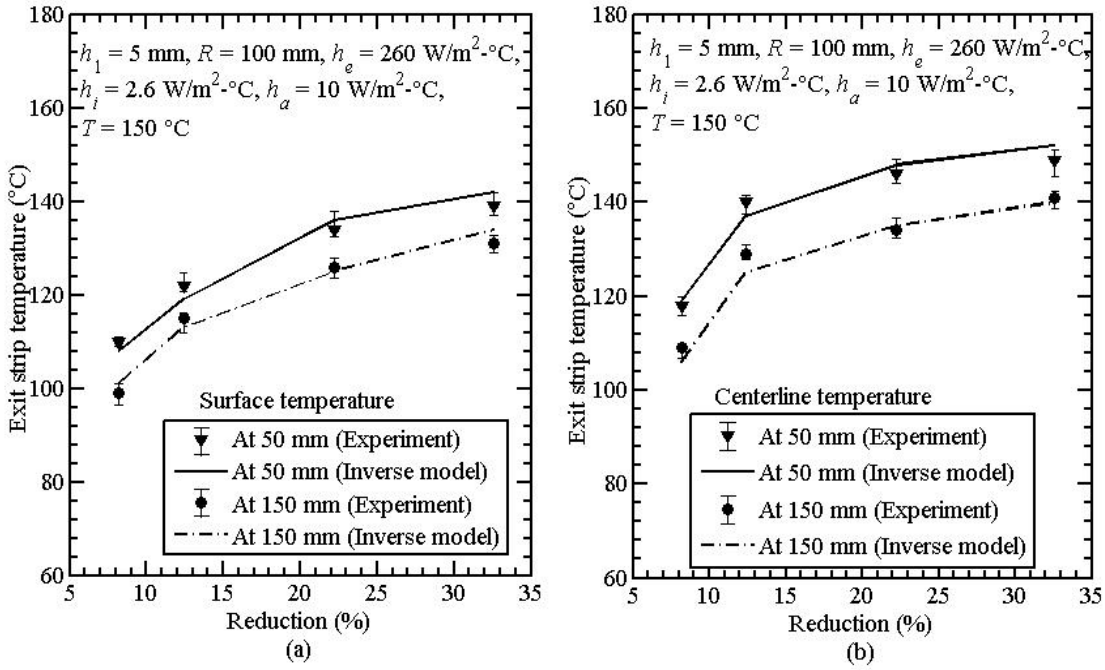

Fig. 6.15. Comparison of exit strip temperature predictions of inverse model with experiments at 50 and 150 mm from the bite zone for inlet temperature of strip 150 °C (a) at surface and (b) at centerline

6.6.3 Correlation of Surface Roughness and Hardness on Flow Stresses and the Coefficient of Friction

In this section, as a part of the study on mechanical properties, the micro hardness tests and surface roughness measurement of the strip after rolling were carried out. Three replicates were carried out at different conditions. For analyzing the quality of rolled sheet, the surface roughness and the coefficient of friction are the most important controllable parameters. In the present work, the surface roughness and hardness of the strip material variation is studied at different rolling temperatures for different reductions. Surface roughness of the rolled strip was measured using the surface roughness measuring instrument (Pocket Surf). The centre line average value (CLA) surface roughness value (R_a) is measured for three replicates. The surface roughness was measured along the rolling and transverse directions of strip. The averaged surface roughness was 0.48 μm of all the samples before rolling. In each replicate, the measurement was taken at 10 points. The combined data of all measurements was used to make inference about average quality attribute along with

the standard error in the estimate. Table 6.10 shows the surface roughness values of the strip after cold rolling of commercially pure aluminum alloy. Tables 6.11 and 6.12 show the estimated coefficient of friction and the average measured surface roughness of the rolled strip at different inlet strip temperatures in warm rolling. In the case of cold rolling, the surface roughness decreases with reduction. This may be due to burnishing action in the presence of friction. It was found that the surface quality of strip deteriorates with increasing the inlet temperature of strip and it increases with reduction. This may be due to change in the nature of the friction (sliding to sticking) and extra softness of the material due to increased temperature.

Table 6.10. Estimated coefficient of friction and averaged measured surface roughness in cold rolling at different reductions for h_1 = 5 mm, R = 100 mm (Values in bracket are standard deviations)

Reduction, r_d (%)	Friction based on slip measurement, (μ)	Measured surface roughness after cold rolling, R_a (μm)	
8.2	0.06	0.411 (0.026)	0.379 (0.014)
12.4	0.09	0.368 (0.024)	0.349 (0.025)
22.2	0.11	0.336 (0.033)	0.299 (0.018)
32.6	0.12	0.288 (0.012)	0.281 (0.021)

Table 6.11. Estimated coefficient of friction and averaged measured surface roughness in warm rolling for T = 150 °C at different reductions for h_1 = 5 mm, R = 100 mm (Values in bracket are standard deviations)

Reduction, r_d (%)	Friction based on slip measurement, (μ)	Measured surface roughness after warm rolling R_a (μm) at T = 150 °C	
8.2	0.124	0.521 (0.022)	0.512 (0.012)
12.4	0.169	0.541 (0.037)	0.510 (0.021)
22.2	0.184	0.557 (0.054)	0.531 (0.027)
32.6	0.192	0.571 (0.039)	0.541 (0.044)

Table 6.12. Estimated coefficient of friction and averaged measured surface roughness in warm rolling for T = 200 °C at different reductions for h_1 = 5 mm, R = 100 mm (Values in bracket are standard deviations)

Reduction, r_d (%)	Friction based on slip measurement, (μ)	Measured surface roughness after warm rolling R_a (μm) at T = 200 °C	
8.2	0.143	0.532 (0.021)	0.545 (0.015)
12.4	0.167	0.556 (0.032)	0.534 (0.029)
22.2	0.198	0.598 (0.045)	0.551 (0.035)
32.6	0.223	0.561 (0.039)	0.495 (0.016)

Figure 6.16 shows the three-dimensional surface plots of the strip before and after rolling for different reductions. The three-dimensional topography of aluminum strip is taken by using non-contact profilometer/3D/surface roughness (M/S Taylor Hobson®) machine. It is seen from Fig. 6.16 that surface asperities deform with increasing the reductions. Thus, the surface roughness decreases with reductions. The average surface roughness of the rolled strip values are reported in Table 6.10 for different reductions.

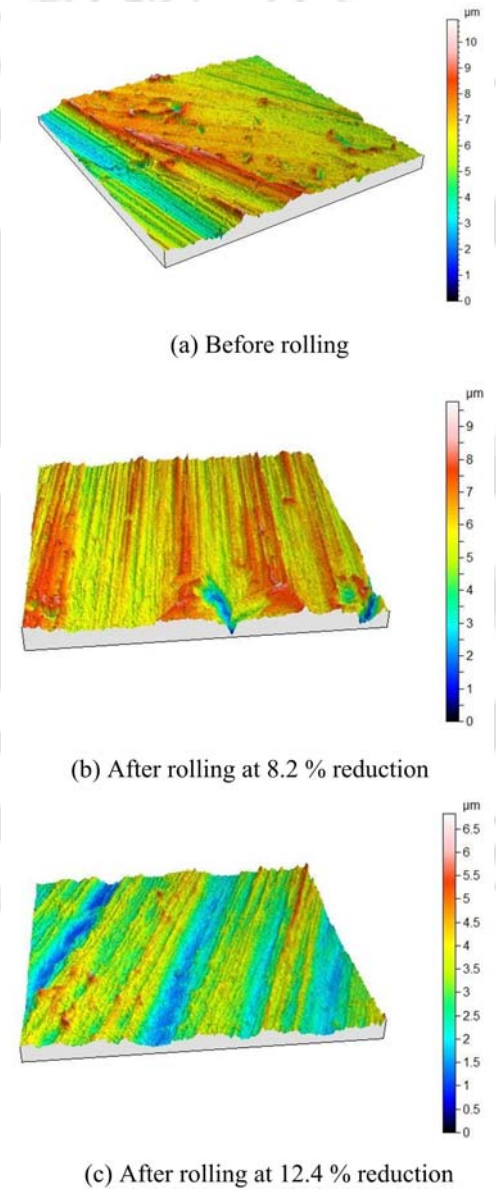

Fig. 6.16. Three-dimensional topography of aluminum strip in cold rolling (a) before rolling, (b) after rolling at 8.2 % reduction and (c) after rolling at 12.4 % reduction

The correlation coefficients between the coefficient of friction and the surface roughness are determined for the cold and warm rolling cases at four different reductions. The surface roughness was measured in the longitudinal and transverse directions and the coefficient of friction was estimated based on the slip measurement. The correlation coefficients are determined between the coefficient of friction and the surface roughness at different reductions in strip are –0.967and –0.981 along the longitudinal and transverse directions, respectively for cold rolling case. In warm rolling cases, the correlation coefficients are determined for inlet temperature of strip is 150 °C between the coefficient of friction and the averaged surface roughness at different reductions in strip is 0.957 and 0.754 along the longitudinal and transverse directions, respectively. Further, the correlation coefficients are determined for inlet temperature of strip is 200 °C between the coefficient of friction and the averaged surface roughness at different reductions in strip is 0.624 and –0.661 along the longitudinal and transverse directions, respectively.

At each replicate, micro hardness measurements were carried out at 8–10 places along rolling and transverse directions. The combined data of all measurements were used to make inference about the average quality attribute along with standard deviation. The average hardness values of strip at the surface are measured and provided in Table 6.13. The experiments were conducted under dry rolling condition keeping the speed of the rolling mill constant. The hardness of strip material increases from 39.98 to 52.2 VHN after rolling. More deviations in hardness values are observed for the reduction in strip of 32.6 as compared to 8.2, 12.4 and 22.2 at 100 °C inlet temperature, which is expected as high reduction in strip causes more strain hardening and proportionately more non-uniformity.

The correlation coefficients between the hardness and flow stress are determined for different inlet temperatures of strip at four different reductions. The flow stresses are calculated using inversely estimated material properties corresponding to the average equivalent strain evaluated from the FEM model. The correlation coefficients between the hardness and flow stress at different reductions

in strip are 0.949, 0.897 and 0.833 at 100, 150 and 200 °C inlet temperatures, respectively.

Table 6.13. Average hardness value of strip after rolling for h_1 = 5 mm, R = 100 mm (Values in bracket are standard deviations). The average hardness value of strip before rolling is 39.98 (2.21)

Reduction, r_d (%)	Inlet temperature of strip (°C)		
	T = 100 °C	T = 150 °C	T = 200 °C
8.2	40.6 (1.61)	41.2 (1.64)	39.8 (1.77)
12.4	43.8 (1.39)	42.9 (0.96)	41.2 (1.31)
22.2	46.7 (0.71)	44.9 (1.66)	42.7 (1.38)
32.6	52.2 (1.50)	49.6 (1.95)	47.9 (0.92)

6.7 Conclusion

In the present work, a methodology for the inverse estimation is developed and validated with the experiments is carried out. The methodology requires the estimation of the exit strip surface temperature and slip. A heuristic method is used for the minimization of the error between the experimentally measured and the estimated temperature of exit strip. The inversely estimated flow stresses are compared with the experimentally measured flow stresses. The experimental flow stresses are obtained by conducting tensile tests at different temperatures. A good agreement between the inversely estimated and experimental flow stresses is observed. It is observed that the parameters obtained by inverse analysis based on temperature measurement at the low and high inlet strip temperatures can be used for the intermediate temperatures. The slip measurement gives the proper estimation of coefficient of friction. If the coefficient of friction is assumed constant for different process conditions, then only the measurement of temperature can be carried out. It has been observed that in place of the exit temperature, the roll torque or roll force can also be measured. A sensitivity analysis is also carried out and it is found that γ is the most sensitive parameter among σ_0, n and β_1 of the power law. It is observed that the drop in exit strip temperature is more in case of higher inlet strip temperatures. The forward slip increases with increasing percentage reduction in the strip. As a result, coefficient of friction increases with the reduction. The surface roughness and hardness measurement is also carried out to assess the quality of the rolled strip. It is observed that the average measured surface roughness of the rolled

strip increases with reduction in warm rolling. However, in cold rolling cases the surface roughness decreases with increasing reductions. This may be due to burnishing action in the presence of friction. On the other hand, the surface quality of strip deteriorates with increasing inlet temperature of strip and it increases with reduction. It is observed that the micro-hardness of the surface of the rolled strip increases with increasing reductions. However, with increases the inlet strip temperature, the hardness is decreased.

Chapter 7

Inverse Estimation of the Thermal Parameters and the Coefficient of Friction

7.1 Introduction

For finding out the temperature distribution in the roll and the strip, one needs to know their mechanical and thermal properties as well as the friction at the roll-sheet interface. One difficulty is unavailability of property data, especially when they are temperature-dependent *e.g.*, thermal conductivity and thermal diffusivity of the roll and strip. The thermal analysis of warm flat rolling can be useful for the estimation of the thermal properties of the roll and the strip based on the transient temperatures distribution. In view of it, the present work proposes to estimate the (1) thermal properties of materials of the sheet and the roll, (2) the convective heat transfer coefficients and (3) the coefficient of friction by measuring the temperature of outgoing sheet at two specified places and slip.

Özisik (1993) stated that inverse analysis can be employed to estimate the thermal properties of the material by the measurement of time-temperature data. However, the inverse solutions are very sensitive to changes in input data resulting from the measurement and modelling errors. It is essential to study the uniqueness of the parameters which are inversely estimated. The present chapter deals with the inverse estimation of thermal parameters of the roll as well as strip and the coefficient of friction based on the transient temperature distribution in strip at two locations and the slip measurements. The inverse analysis provides the following unknown thermal parameters such as the thermal conductivity of the roll (k_r), thermal diffusivity of the roll (α_r), thermal conductivity of the strip (k_s), thermal diffusivity of the strip (α_s), convective heat transfer losses of the roll outer periphery

(h_e), convective heat transfer loss at the inner periphery (h_i), convective heat transfer losses of the strip surface (h_a). The coefficient of friction (μ) is determined based on slip measurement.

As reported by earlier researchers (Tseng, 1999; Jiang *et al*., 2011; Yu *et al*., 2012; Min *et al*., 2012), the influence of oxide layer or scale takes place in hot strip rolling when temperature is in the range of 850–1100 °C. In the present work, an inverse methodology is proposed to estimate the thermal parameters of the roll and the strip by the measurement of exit strip temperature in warm flat rolling. In warm flat rolling, the oxidation of the roll and the strip may occur. The influence of oxide layer on the thermal parameters is taken into account by inverse estimation. The proper estimation of the thermal parameters can be estimated even after oxidation as the inverse procedure updates the material properties of the roll and the strip continuously (at the corresponding average temperature of the deformation zone) till the steady-state is achieved.

The rest of the chapter is organized as follows: The direct model to find out the transient temperature distribution in the strip and the roll is briefly presented in Section 7.2. Section 7.3 presents the detailed parametric study and inference of inverse modelling. Section 7.4 deals with the inverse estimation of the thermal parameters and the coefficient of friction in warm flat rolling. Results obtained from inverse modelling are presented in Section 7.5. Section 7.6 concludes the chapter.

7.2 Direct Model for Transient Temperature Distribution

In this section, a direct model of transient thermal analysis of the roll and the strip is briefly discussed for obtaining the transient temperature distribution in warm flat rolling. The steady-state deformation analysis of the strip is based Eulerian flow formation using finite element method (FEM). The transient thermal analysis of the roll and strip is carried out analytically. For estimating the temperature distribution in the roll uses series solution using integral transform method is presented in Section 4.3. The transient temperature distributions of the strip is obtained using eigenfunctions and separation of variables methods in the bite zone and just after the

bite zone are presented in Section 3.6. The experimental validation of the direct model considering warm flat rolling is provided in Subsection 4.6.2. It is to be mentioned that in actual shop floor, the temperature and slip data need to be collected online for the estimation of thermal parameters and the coefficient of friction. However, in this chapter, the actual experiments have been replaced by virtual simulations-experiments based on direct model with temperature dependent thermal and mechanical properties. As the direct model has been already validated, the inverse procedure is enough for establishing the confidence in the methodology. Figure 7.1 shows the schematic arrangement of the temperature sensors and velocity sensor in warm flat rolling process. The purpose of temperature sensors is to record the temperature of exit strip at any specified locations and the velocity sensor provides the exit velocity of the moving strip.

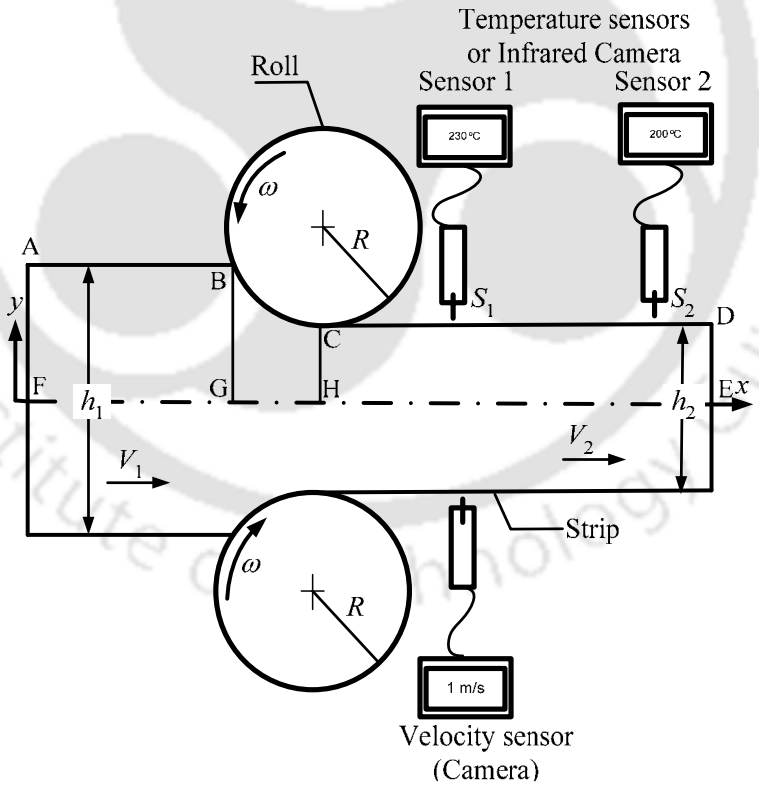

Fig. 7.1. Schematic arrangement of temperature and velocity of exit strip measurement

7.3 Parametric Study and Inference of Inverse Modelling

In this section, an extensive parametric study is carried out for studying the sensitivity of thermal parameters. The surface temperatures of the exit strip are measured at two locations: 50 mm and 500 mm away from the roll exit point (The locations of temperatures sensor 1 and sensor 2 are determined on the basis of numerical experiments. The distance between two temperatures sensors is sufficient for getting the unique solution in the inverse estimation of the thermal parameters.). Figure 7.2 shows that the distribution of temperature with time is slightly dependent on the thermal conductivity of the roll. However, the steady-state temperature is not affected by thermal conductivity.

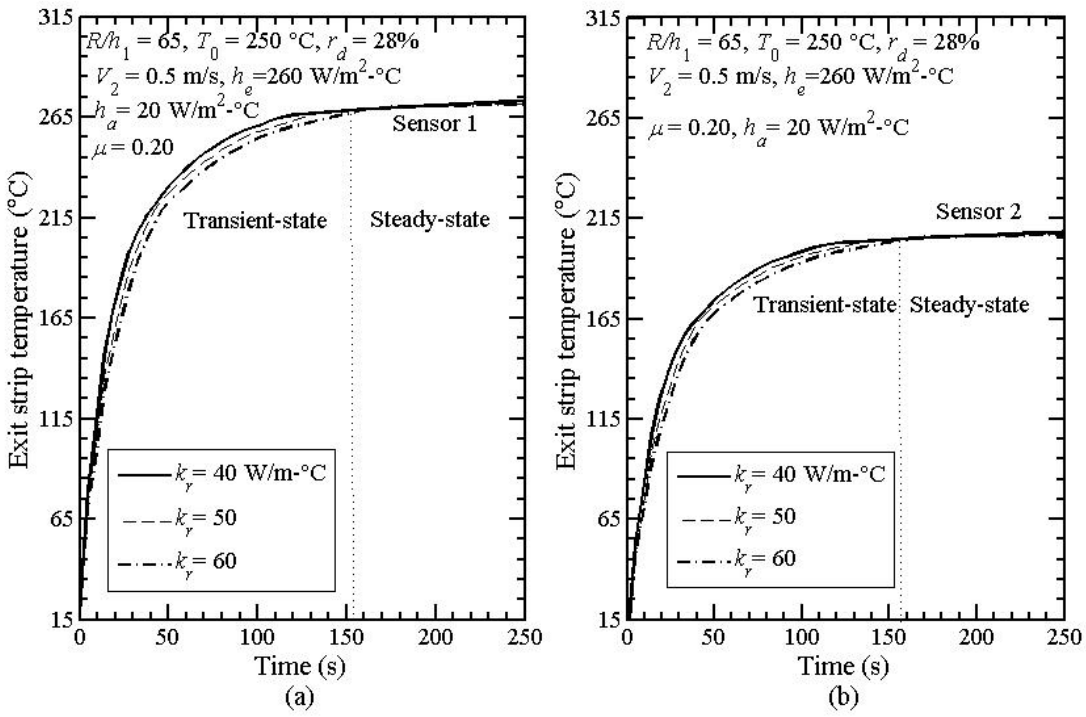

Fig. 7.2. Effect of thermal conductivity of roll material (k_r) on surface temperature of strip (a) Sensor 1 (b) Sensor 2

Figure 7.3 shows the effect of thermal diffusivity of roll material (α_r) on the surface temperature at the two locations (50 mm and 500 mm away from roll exit).

Here, also the steady-state temperatures are unaffected by thermal diffusivity of the roll, but distribution of transient temperature with time is strongly dependent on the thermal diffusivity. Fortunately, the patterns of time-temperature distribution do not vary in similar style for k_r and α_r. Hence, it is possible to extract the k_r and α_r from the time-temperature distribution. Some parametric study was carried out to ascertain that a particular time-temperature can be obtained only by a unique k_r and α_r combination.

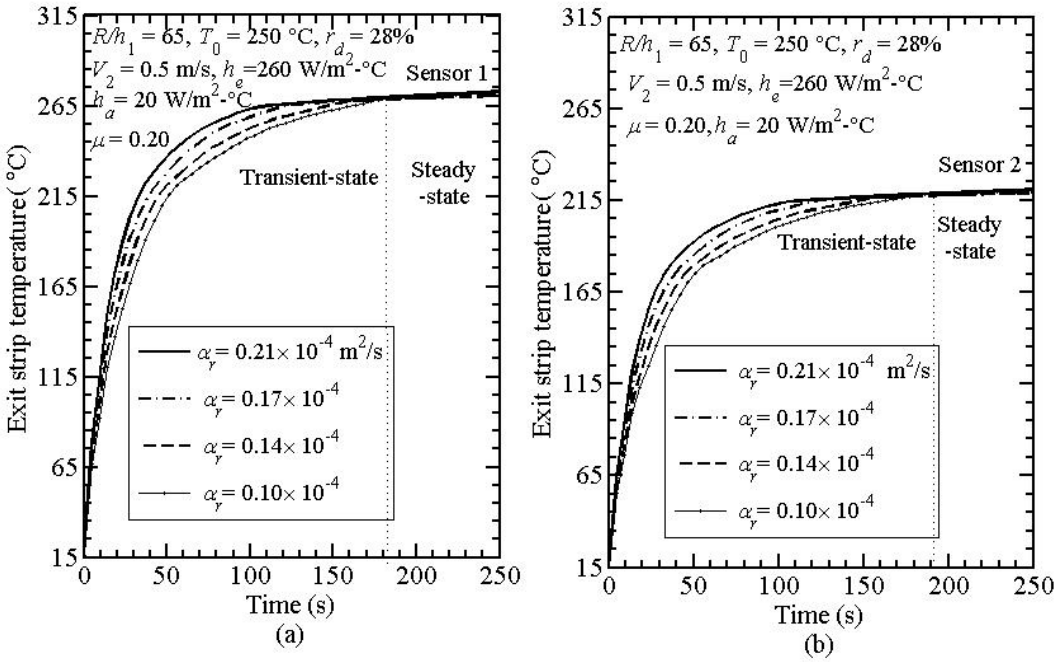

Fig. 7.3. Effect of thermal diffusivity of roll material (α_r) on surface temperature of strip (a) Sensor 1 (b) Sensor 2

Figure 7.4 shows the dependency of strip surface temperature on the thermal conductivity of the strip (k_s). It is observed that transient as well as steady-state temperatures at the two locations are strongly dependent on k_s. Moreover, the temperature difference between two locations increases as k_s decreases. Figure 7.5 shows that thermal diffusivity of strip influences the temperature distribution at the first location, but does not affect the temperature at the second location due to sufficient amount of diffusion already taken place.

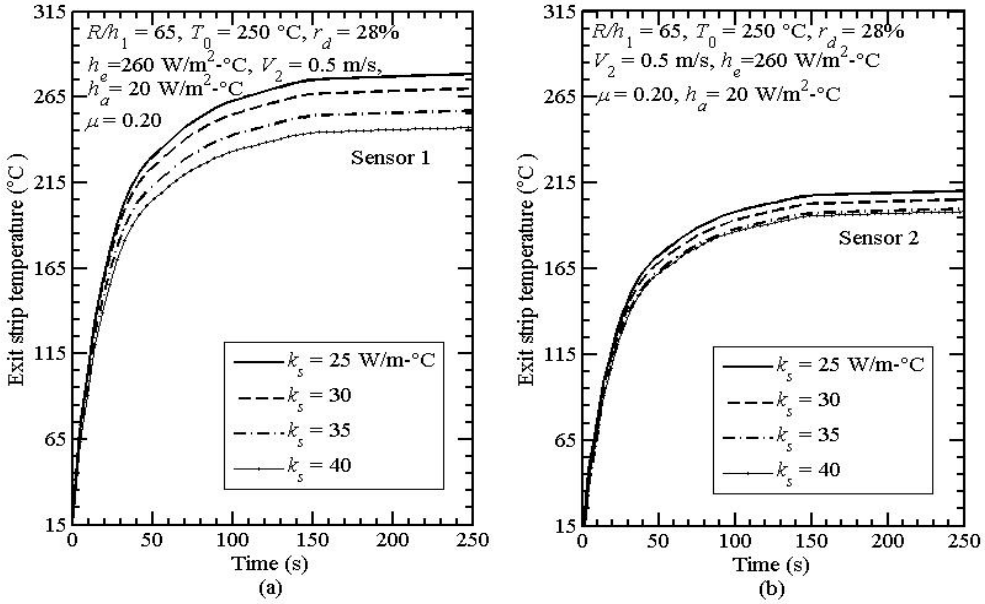

Fig. 7.4. Effect of thermal conductivity of strip material (k_s) on surface temperature of strip (a) Sensor 1 (b) Sensor 2

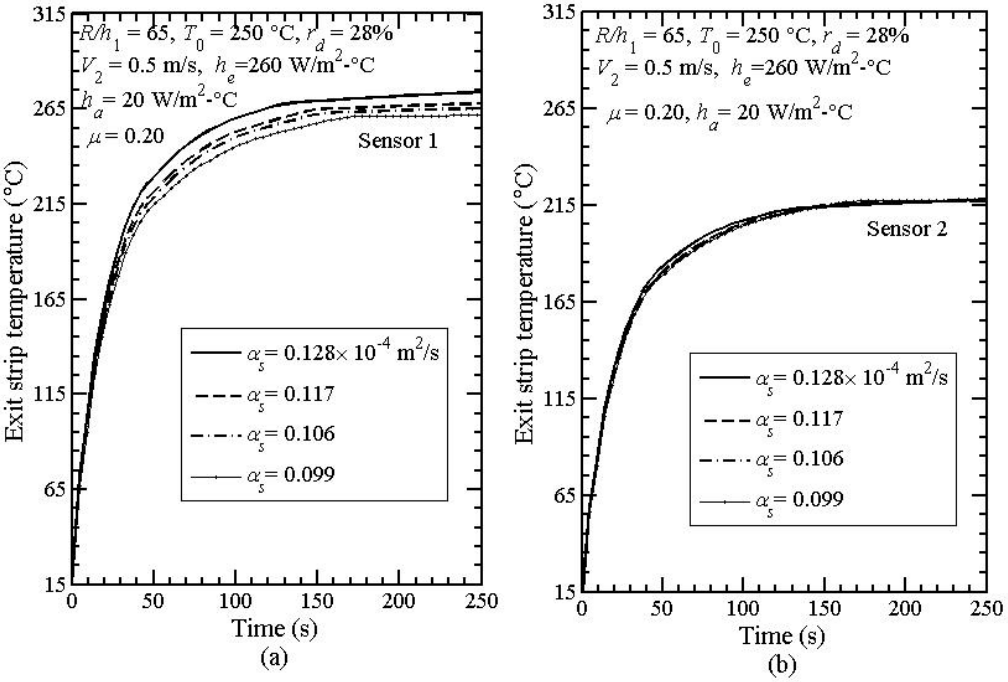

Fig. 7.5. Effect of thermal diffusivity of strip material (α_s) on surface temperature of strip (a) Sensor 1 (b) Sensor 2

Figure 7.6 shows that convective heat transfer coefficient at the roll outer surface (h_e) influences the temperature distribution at both locations. However, the variation of temperature differences between two locations for h_e follows a different pattern than that for k_s. This can be ascertained by comparing Fig. 7.4 with Fig. 7.5. Figure 7.7 shows the influence of convective heat transfer coefficient (h_a) at the strip surface. Here, the temperatures at two locations are prominently affected by h_a. This dependency follows a different pattern than other parameters. Here, the steady state as well as transient components are significantly affected by the variation of h_a. Figure 7.8 shows the influence of convective heat transfer coefficient at the inner surface of the roll periphery. Here, the effect of h_i on temperatures at two locations is insignificant. It is observed that the temperature distribution at 50 mm from the roll bite deviates slightly as the convective heat transfer coefficient of roll at the inner periphery is increased. Moreover, the exit strip temperature is almost invariant to the inner convective heat transfer coefficient at 500 mm from the roll bite. Hence, it can be assumed that the convective heat transfer coefficient at the inner periphery of the roll does not have significant effect on the exit strip temperature.

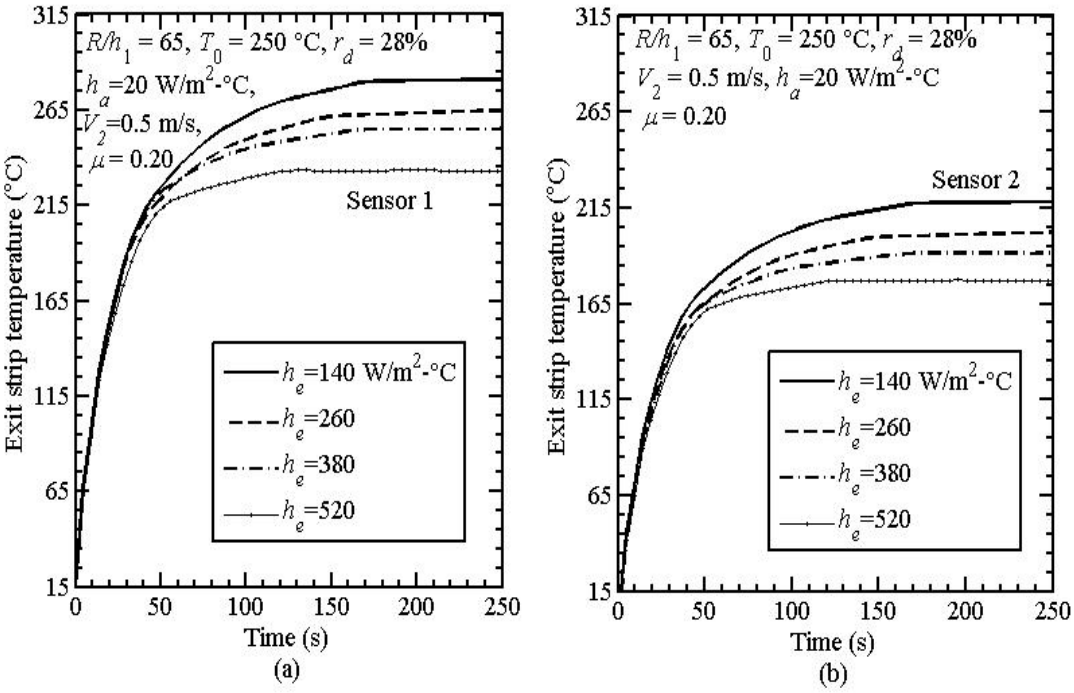

Fig. 7.6. Effect of convective heat transfer losses of roll at outer periphery (h_e) on surface temperature of strip (a) Sensor 1 (b) Sensor 2

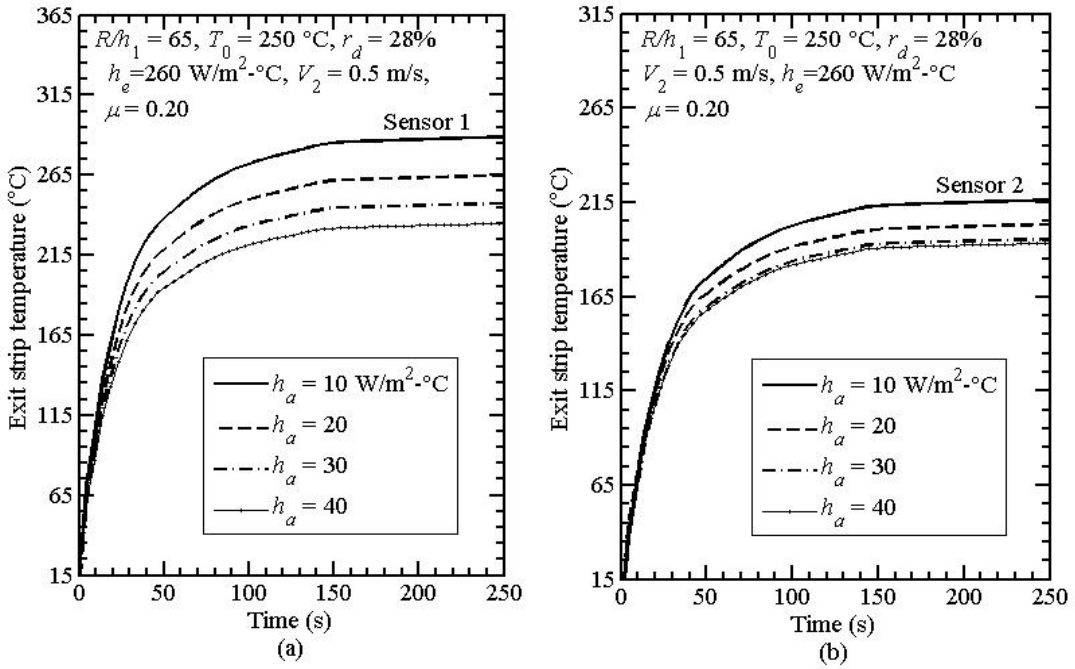

Fig. 7.7. Effect of convective heat transfer losses of strip surface (h_a) at interstand zone (a) Sensor 1 (b) Sensor 2

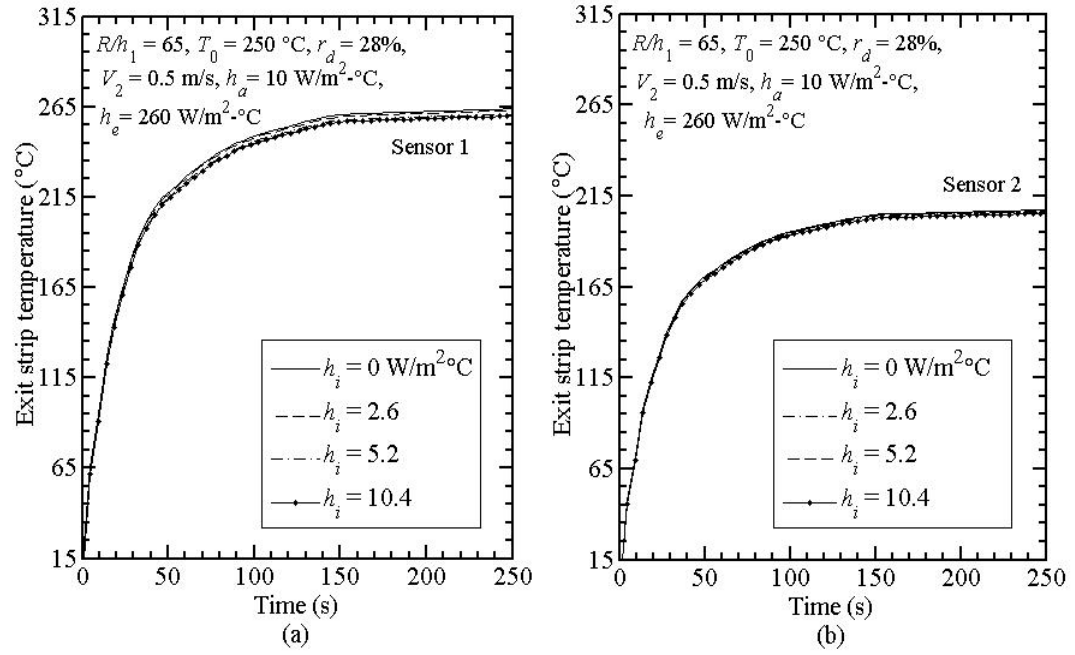

Fig.7.8. Effect of convective heat transfer losses of inner periphery of the roll (h_i) on surface temperature of strip (a) Sensor 1 (b) Sensor 2

Keeping this fact into consideration, the determination of h_i by inverse analysis is not carried out. In any case, the h_i is low due to the mounting of the roll on a rigid shaft without any forced cooling. It was observed that for a fixed value of coefficient of friction μ, the slip is unaffected by thermal parameters due to their insignificant effect on the kinematics of rolling. Hence, the coefficient of friction can be obtained by the measurement of the slip. Based on the parametric study, Table 7.1 lists the identifying signals for various parameters. From Table 7.1, it is seen that there are sufficient numbers of signals to predict the seven parameters uniquely. However, apart from the slip, it is essential to measure transient as well as steady-state temperatures at two locations.

Table 7.1. Procedure to identify the parameters by inverse analysis

S. No	Parameters	Identifying signal	Remarks
1.	μ	Slip	It does not depend significantly on thermal parameters
2.	k_r (W/m-°C)	Temperature-time distributions at two sensor locations	
3.	α_r (m^2/s)	Temperature-time distributions at two sensor locations	It is possible to extract k_r and α_r from this signal.
4.	k_s (W/m-°C)	Steady-state temperatures at two sensors location and their difference	
5.	α_s (m^2/s)	Temperature distribution at first sensor location	
6.	h_e (W/m^2-°C)	Steady-state temperature at two sensors location	
7.	h_a (W/m^2-°C)	Steady-state and transient temperatures at two sensors location	

7.4 Methodology for Inverse Estimation

The exit strip temperatures at two locations are measured at a number of discrete times and are compared with the calculated temperature obtained from the direct model. The direct model uses temperature dependent material properties. The mean squared fractional errors (MSFE) at two locations are taken as E_1 and E_2. The

objective function is to minimize max(E_1, E_2) with respect to the decision (design) variables k_r, α_r, k_s, α_s, h_e, h_a and μ. Mathematically,

$$E_1 = \frac{1}{n} \times \sum_{i1=1}^{n} \left(\frac{T_{i1m} - T_{i1c}}{T_{i1m}} \right)^2, \tag{7.1}$$

$$E_2 = \frac{1}{n} \times \sum_{i2=1}^{n} \left(\frac{T_{i2m} - T_{i2c}}{T_{i2m}} \right)^2. \tag{7.2}$$

In the above expressions, T_{i1m} and T_{i2m} denote measured temperatures at two sensor locations *i.e.*, at S_1 and S_2. The corresponding computed temperatures are denoted by T_{i1c} and T_{i2c} and n denotes the number of observations. The minimization is carried out by a heuristic method similar to that illustrated in Section 6.3 for estimating the mechanical properties and friction at constant thermal parameters of flat rolling. A general outline of the method is illustrated in Fig. 7.9.

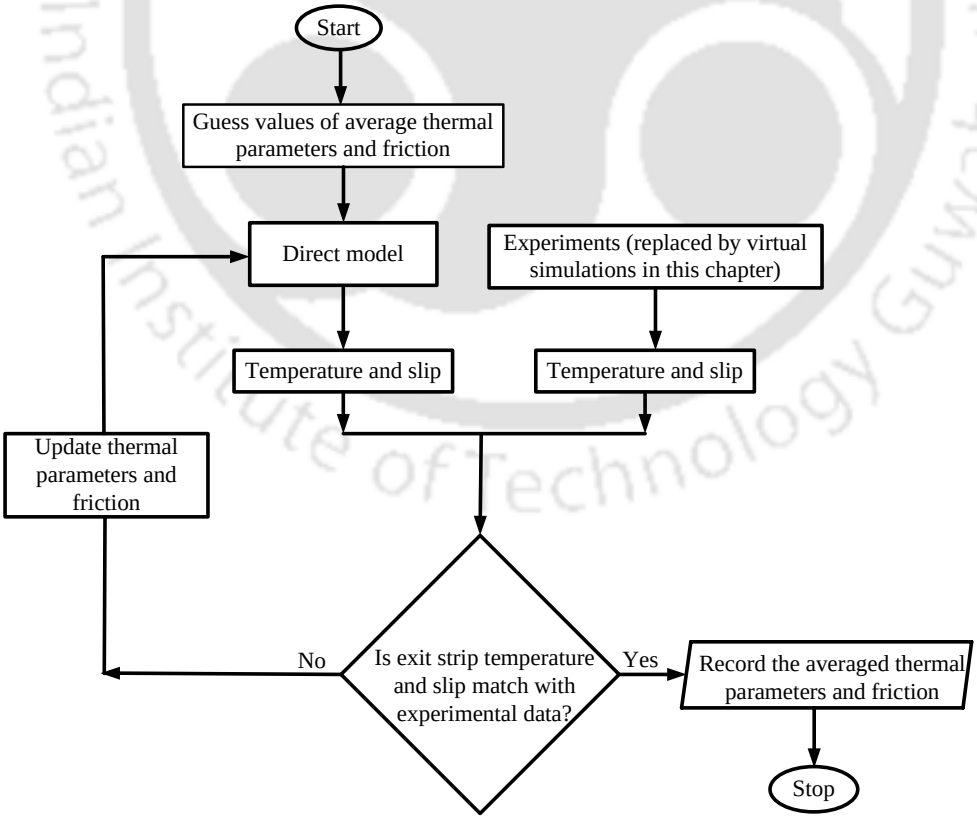

Fig. 7.9. Flow chart illustrating the methodology of inverse model

7.4.1 Methodology

The methodology for finding out the average thermal properties of roll and strip and the coefficient of friction during rolling is as follows:

Step 1: Choose suitable ranges for the thermal parameters k_r, α_r, k_s, α_s, h_e, h_a of the roll and the strip and the coefficient of friction μ.

Step 2: For each thermal parameter the range is divided into three linguistic zones *viz*., low (L), medium (M) and high (H) as shown in Fig. 7.10 for two parameters. Thus, the entire domain gets divided into $3^6 = 729$ cells.

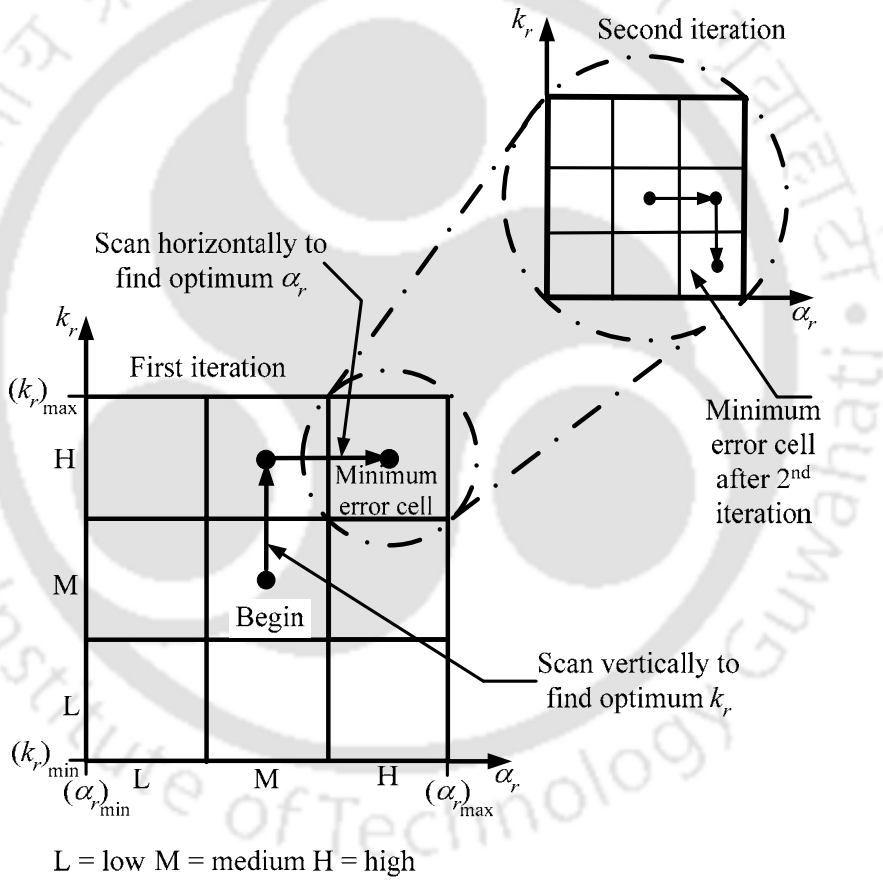

Fig. 7.10. Two-dimensional graphical representation of search procedure

Step 3: Select the middle (M) values of all the thermal parameters as initial guess values.

Step 4: Find out the coefficient of friction based on the slip measurement in the selected cell. For this, carry out a one-dimensional search technique *eg*., bisection

section method (Gerald and Wheatley, 1997) to get the true friction value. The obtained values of coefficient of friction are used in direct model. Estimate E_1 and E_2 using the true value of μ. The E_1 corresponds to the Sensor 1 (S_1) and E_2 corresponds to the Sensor 2 (S_2).

Step 5: Keeping 5 other parameters (α_r, k_s, α_s, h_e and h_a) constant, carry out one-dimensional search for optimum k_r in the following manner:

- If at the current point, the computed temperatures at two locations S_1 and S_2 are smaller than the measured temperatures, then decrease the value of k_r by jumping to the center of adjacent cell.
- If at the current point, the computed temperatures at two locations S_1 and S_2 are greater than the measured temperatures, then increase the value of k_r by jumping to the center of adjacent cell.
- Else do not change the value of k_r.

Step 6: The similar methodology as discussed in Step 4 and Step 5 is repeated for optimizing other parameters *i.e*., change the one parameter at a time keeping other five parameters to be constant. After completing an iteration consisting of six one-dimensional searches, the search domain gets reduced to one cell. Figure 7.10 shows how the one optimum cell is further reduced to three linguistic zones *viz*., low (L), medium (M) and high (H) in one iteration. Go to Step 2.The procedure continues till E_1 and E_2 are less than 0.001.

7.5 Results from Inverse Modelling

For validating the proposed procedure, a number of numerical experiments have been conducted. The actual thermal parameters of the roll and strip material are temperature dependent. Table 7.2 provides the temperature dependent material properties of the roll and the strip. The actual equivalent Coulomb coefficient of friction is assumed to be 0.20.The inner and outer roll radii are 45 and 65 mm, respectively and the inlet thickness of strip (h_1) is 1 mm. The schematic arrangement of sensors in the rolling mill is shown in Fig. 7.1. The distance between the

temperature sensors S_1 and S_2 from the exit of roll bite are 50 mm and 500 mm, respectively. With this data, virtual simulations are carried out using the direct model for different inlet temperatures, percentage reductions and exit velocities of strip. The results of virtual simulations are taken as actual experimental results as the direct model has already been validated. For inverse analysis, the steel roll and the steel strip with the flow stress governed by J-C model (given by Eq. 3.5) are considered.

Table 7.2. Parameters and value used in the direct model

Parameters		References
k_r steel (W/m-°C)	$42.284-3.01\times10^{-2}T-1.35\times10^{-5}T^2-4.43\times10^{-8}T^3$	Khalili *et al*. (2012)
ρ_r steel (kg/m^3)	7850	
c_{pr} steel (J/kg-°C)	$429.47+0.2575T-5\times10^{-5}T^2$	
k_s steel (W/m-°C)	$44-0.0067T-2\times10^{-5}T^2$	Tszeng and Saraf (2003)
$\rho_s c_{ps}$ steel (J/m^3-°C)	$4\times10^6-1.8\times10^{-3}T+6.3T^2+0.018T^3-2.7\times10^{-5}T^4$	

The inverse analysis provides the average thermal parameters of roll and strip and the coefficient of friction. The analysis is carried out with different inlet temperatures of the strip, percentage reductions and exit velocities of strip. The convergence is obtained in 25–31 function evaluation *i.e*., in 4–5 iterations. The convergence depends on the initial hypercube size of the unknown parameters. Starting with a large range of domain is better, but the number of iterations required for convergence will be large. Table 7.3 shows the percentage error between the actual (virtual simulations) and estimated average thermal parameters and the coefficient of friction for two different initial temperatures of 250°C and 450 °C, keeping R, $\%r$ and V_2 constant. It is observed that the deviation of estimated and actual parameters is less than $\pm$ 7%.The accuracy of the estimated parameters is improved at higher inlet temperature as observed from Table 7.3.

Table 7.3. Comparison of the actual and the estimated values of thermal parameters for h_1 = 1 mm, R = 65 mm, r = 28% and V_2 = 0.5 m/s

Parameter	T_0 = 250 °C			T_0 = 450 °C		
	Estimated parameter	Actual parameter	% error	Estimated parameter	Actual parameter	% error
k_r (W/m-°C)	33.07	33.23	0.48	26.11	26.14	0.12
α_r (m^2/s)	0.088×10^{-4}	0.086×10^{-4}	–2.33	0.062×10^{-4}	0.061×10^{-4}	–1.64
k_s (W/m-°C)	39.44	41.08	3.99	36.01	35.12	–2.53
α_s (m^2/s)	0.092×10^{-4}	0.09×10^{-4}	–2.22	0.08×10^{-4}	0.081×10^{-4}	1.23
h_e (W/m^2-°C)	255	260	1.92	277	260	–6.54
h_a (W/m^2-°C)	20.84	20	–4.2	18.98	20	5.10
μ	0.212	0.20	–5.66	0.198	0.20	1.01

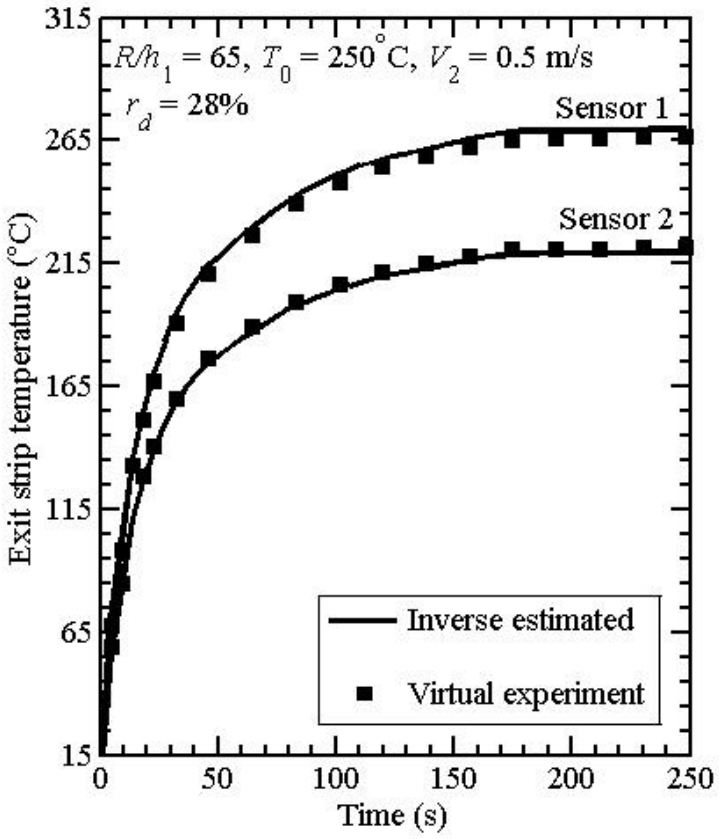

Fig. 7.11. Comparison of actual (virtual simulation) and inverse estimated temperature profiles of exit strip at locations Sensor 1 and Sensor 2

The actual temperature distribution from the direct model is compared with the inverse estimation for inlet strip temperature of 250 °C (Fig. 7.11). This comparison corresponds to calculated mean squared fractional error E_1 = 0.00014 and E_2 = 0.00011. It is observed that the exit strip temperature distribution from the direct model is in excellent agreement with the inverse estimation. The similar results are obtained for inlet strip temperature of 450 °C but are not shown for the sake of brevity. Figure 7.12 compares the maximum temperature distribution at the interface for different cases computed from the direct and inverse model and a good agreement is observed.

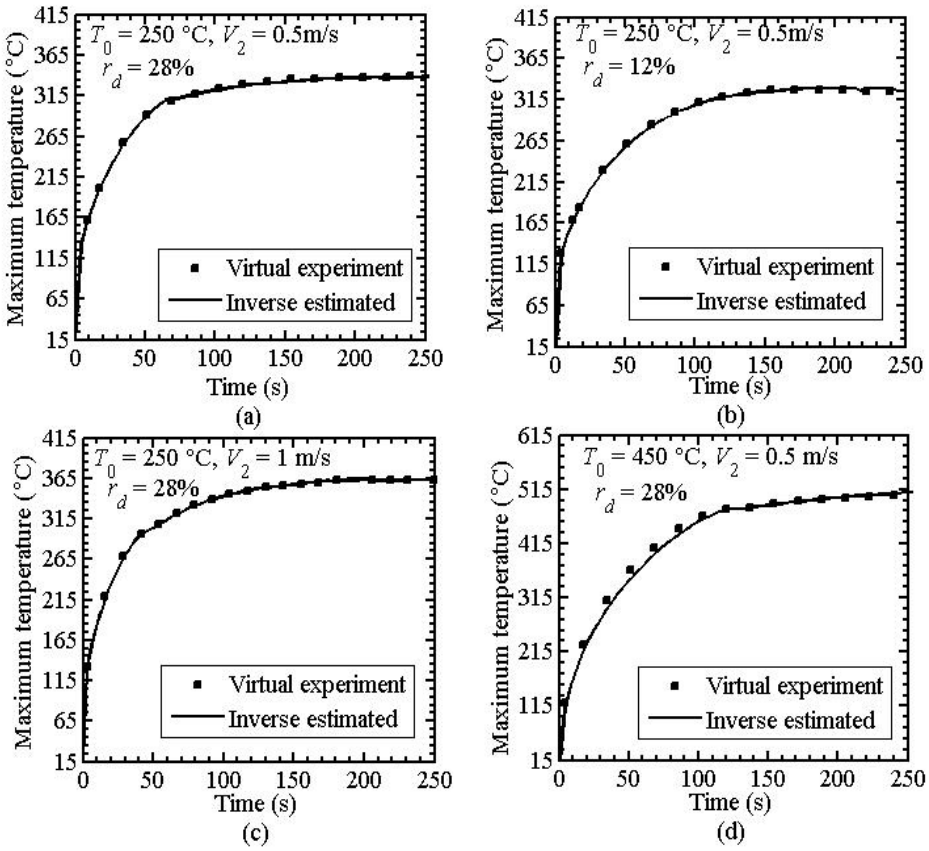

Fig. 7.12. Comparison of the maximum temperature obtained from the actual (virtual simulation) and the inverse estimated parameters for (a) r_d = 28%, V_2 = 0.5 m/s, T_0 = 250 °C (b) r_d = 12%, V_2 = 0.5 m/s, T_0 = 250 °C (c) r_d = 28%, V_2 = 1 m/s, T_0 = 250 °C and (d) r_d = 28%, V_2 = 0.5 m/s, T_0 = 450 °C

Figures 7.12a and 7.12b show the maximum temperature computed at the deformation zone using the actual and the estimated parameters. This comparison is

carried out for two percentage reductions in strip *viz*., r_d = 12 and 28%. A similar comparison has been done for V_2 = 1 m/s and T_0 = 450 °C as shown in Fig. 7.12c and 7.12d. The estimated thermal parameters and coefficient of frictions are obtained on the basis of exit strip temperature and slip. In Fig. 7.13, the variation of maximum temperatures at the interface between the actual and inverse estimation is presented for four sets of rolling parameters *viz*., (%r_d, V_2, T_0) = (12, 0.5, 250), (%r_d, V_2, T_0) = (28, 0.5, 250), (%r_d, V_2, T_0) = (12, 1, 250) and (%r_d, V_2, T_0) = (12, 0.5, 450). The average thermal parameters and coefficient of friction obtained at (%r_d, V_2, T_0) = (12, 0.5, 250) are used to compare the maximum temperature at the interface for other three cases.

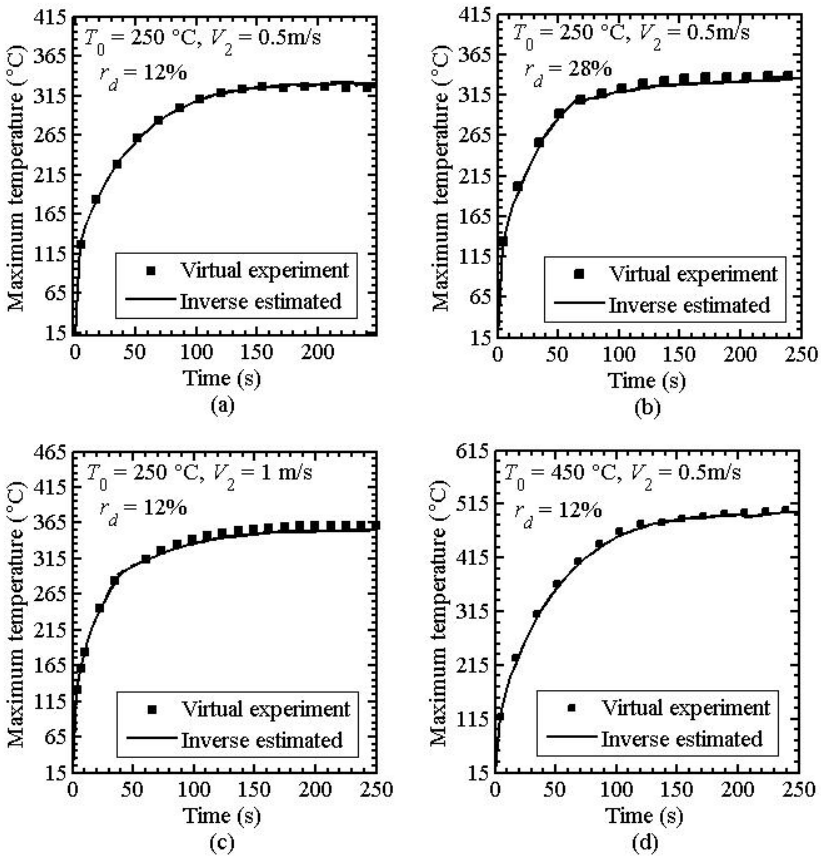

Fig. 7.13. Comparison of the maximum temperature obtained from the actual (virtual simulation) and the inverse estimated parameters at this condition (r_d = 12%, V_2 = 0.5 m/s, T_0 = 250 °C) for (a) r_d = 12%, V_2 = 0.5 m/s, T_0 = 250 °C (b) r_d = 28%, V_2 = 0.5 m/s, T_0 = 250 °C (c) r_d = 12%, V_2 = 1 m/s, T_0 = 250 °C and (d) r_d = 12%, V_2 = 0.5 m/s, T_0 = 450 °C

From Figs. 7.13a and 7.13b, it is observed that if the percentage reduction is increased from 12 to 28%, then the maximum temperature at the interface deviates by only 5 °C. It is observed from Fig. 7.13c that when V_2 is increased from 0.5 to 1 m/s the temperature at the interface deviates by less than 10 °C. It is seen from Fig. 7.13d that if the thermal parameters and the coefficient of friction obtained at (%r_d, V_2, T_0) = (12, 0.5, 250) are used for (%r_d, V_2, T_0) = (12, 0.5, 450), the maximum temperature changes by 5 °C only. Hence, the thermal parameters obtained at condition: (%r_d, V_2, T_0) = (12, 0.5, 250), may be used for higher reduction in strip, rolling speed and inlet strip temperature. The maximum temperature can be predicted within 1% accuracy.

In order to study the effect of the temperature distribution in roll at different radial distances, a comparison of the temperature distribution in roll at the actual and the estimated parameters is carried out. The comparison corresponds to the E_1 = 0.00014 & E_2 = 0.00011 and is shown in Fig. 7.14.

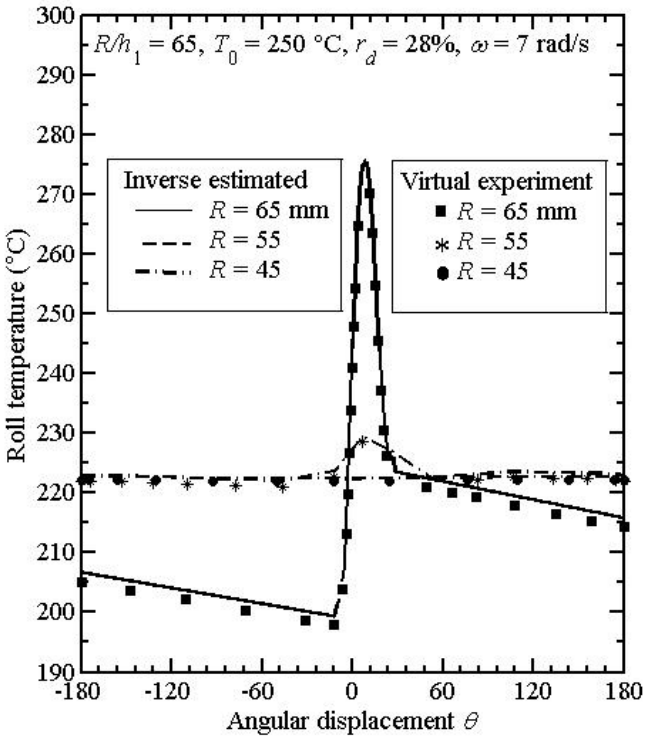

Fig. 7.14. Comparison of temperature distribution in roll at different radial distances (R) after 50 revolutions completed with actual (virtual simulation) and the inverse estimated parameters

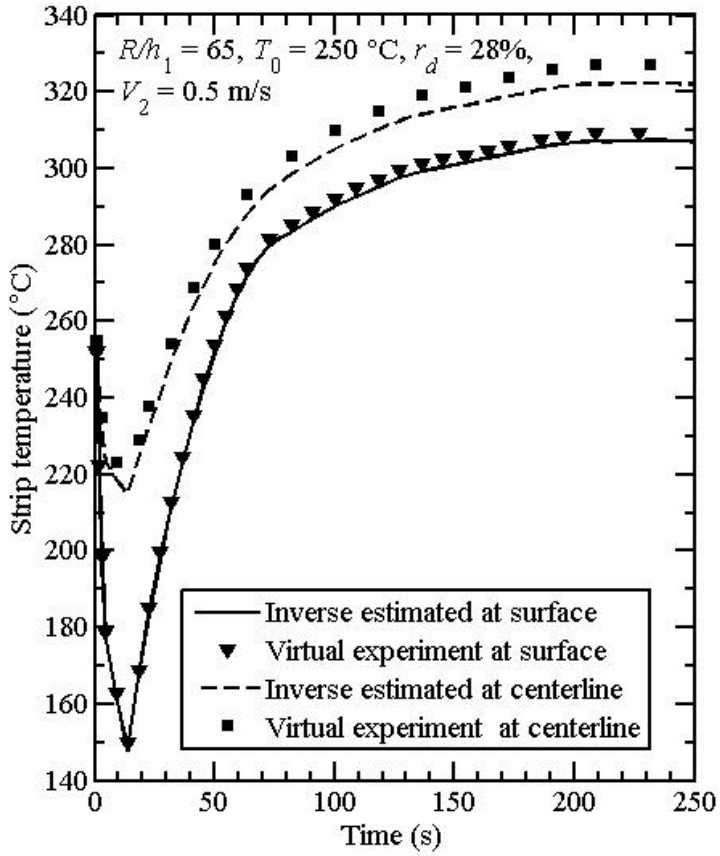

Fig. 7.15. Comparison of temperature distribution in strip at deformation zone with actual (virtual simulation) and the inverse estimated parameters

It is observed that the peak temperature occurs at the exit of contact region and the maximum difference in the temperature is found to be 5 °C with the actual and estimated material parameters. A good agreement is observed between the temperatures of roll at actual parameters and inverse estimated parameters. Further the effect of temperature distribution for strip at the deformation zone is also studied for the same rolling conditions. It can be seen from Fig. 7.15 that the temperature at the surface estimated by inverse method almost matched with direct model. However, the temperature at the centre deviates by upto 8 °C from the actual (virtual simulations) temperature.

For studying the error of estimation in steady-state temperature distribution, three different rolling process parameters, *viz*., $\%r_d$, V_2 and T_0, are considered. Table

7.4 shows the percentage error in the maximum and average temperatures (roll-strip interface) for the actual parameters and the parameters estimated by inverse method. Note that the inverse estimation was carried out for 12% reduction in the strip to obtain the thermal parameters and the coefficient of friction. These thermal parameters and the coefficient of friction are used for comparing the steady-state maximum and average temperatures at the interface at two other percentage reductions (20% and 28%). It is observed that the percentage error between the temperatures obtained at the actual parameters and the temperature obtained at the estimated parameters is within $\pm 2\%$ when percentage reduction varies from 12 to 28.

Table 7.4. Percentage error in steady-state temperature with actual (virtual simulation) and inverse estimated parameters for different reductions in strip at R/h_1 = 65, V_2 = 0.5 m/s, T_0 =250 °C

Reduction, r_d (%)	Maximum Temperature at the interface (°C)		% error	Average temperature at the interface (°C)		% error
	By actual parameters	By estimated parameters		By actual parameters	By estimated parameters	
12	325.37	328.76	1.04	269.98	272.14	0.80
20	330.25	332.56	0.78	276.34	279.52	1.15
28	338.54	336.97	–0.46	282.46	285.14	0.95

Similarly, the analysis is also carried out by varying the exit velocity and inlet temperature of strip and the results are shown in Tables 7.5 and 7.6. Here, the inverse estimation is carried out for 0.5 m/s exit velocity of strip with T_0 = 250 °C and r_d = 28% to obtain the thermal parameters and the coefficient of friction. These thermal parameters and the coefficient of friction are used for comparing the steady-state maximum and average temperatures at the interface at exit velocities of strip (V_2), 1 m/s and 1.5 m/s. It is observed from Table 7.5 that the percentage error in the maximum and average temperatures at the interface increases with the increase in exit velocity of strip at estimated and actual values of parameters. Table 7.6 shows the percentage error in the maximum and average temperatures at the interface with varying inlet strip temperature at estimated and actual values of parameters. Here, the inverse estimated parameters are obtained at T_0 = 250 °C, V_2 = 0.5 m/s and r_d =

28% and are used to compare the steady-state maximum and the average temperatures at the interface for the inlet strip temperatures of 350 °C and 450 °C. It is observed that the percentage error increases upto the maximum 2.05 % when T_0 varies from 250 to 450 °C.

Table 7.5. Percentage error in steady-state temperature with actual (virtual simulation) and inverse estimated parameters for different exit velocity of strip at $R/h_1 = 65$, $r_d = 28$ %, $T_0 = 250$ °C

Exit velocity V_2 (m/s)	Maximum Temperature at the interface (°C)		% error	Average temperature at the interface (°C)		% error
	By actual parameters	By estimated parameters		By actual parameters	By estimated parameters	
0.5	338.54	336.97	–0.46	282.46	285.14	0.95
1	362.31	363.33	0.28	332.14	335.34	0.96
1.5	405.52	410.23	1.16	381.56	372.52	–2.36

Table 7.6. Percentage error in steady-state temperature with actual (virtual simulation) and inverse estimated parameters for different inlet temperature of strip at $R/h_1 = 65$, $r_d = 28$ %, $V_2 = 0.5$ m/s

Inlet temperature of strip T_0 (°C)	Maximum Temperature at the interface (°C)		% error	Average temperature at the interface (°C)		% error
	By actual parameters	By estimated parameters		By actual parameters	By estimated parameters	
250	338.54	336.97	–0.46	282.46	285.14	0.95
350	395.85	396.52	0.17	371.74	364.11	–2.05
450	504.15	506.63	0.50	474.15	468.81	–1.13

7.6 Conclusion

In the present work, an inverse method is proposed for the estimation of the thermal parameters and the coefficient of friction in a warm flat rolling process. The methodology requires the estimation of the exit temperature of strip at two locations and the forward slip. The slip measurement gives the proper estimation of the coefficient of friction. The inverse method employs a heuristic method for the minimization of the error between measured and computed temperatures at two locations of exit strip. The thermal parameters *viz*., thermal conductivity of the roll (k_r), thermal diffusivity of the roll (α_r), thermal conductivity of the strip (k_s), thermal

diffusivity of the strip (α_s), convective heat transfer losses of the roll outer periphery (h_e), convective heat transfer losses of the strip surface (h_a) and the coefficient of friction (μ) are simultaneously estimated and they are compared with their exact values used in virtual simulation. It is to be noted that thermal and mechanical parameters used in the simulation-experiments have been taken as temperature dependent, but the inverse method predicts their average values. A comparison of the maximum temperatures computed using the inverse estimated parameters with the temperatures computed using the actual parameters is also carried out. The accuracy of the estimated parameters is also assessed by comparing the temperature distributions obtained using the actual parameters used in direct method. The proposed inverse method can be used as a quick estimate of the thermal parameters and the coefficient of friction. The method requires only the exit strip temperature at two locations and velocity measurement by a velocity sensor. The uniqueness of the solution has been studied heuristically and numerically.

Chapter 8

Conclusions and Scope for Future Work

8.1 Conclusions

The inverse estimation of material properties and the process parameters in rolling is important for controlling the process and assessing the quality of the product. In this thesis, the inverse estimation of material properties, convective heat transfer coefficients and friction in warm flat rolling has been carried out. The following parameters are determined by inverse method: four constants of power law model, thermal conductivity of the roll (k_r), thermal diffusivity of the roll (α_r), thermal conductivity of the strip (k_s), thermal diffusivity of the strip (α_s), convective heat transfer losses of the roll at the outer periphery (h_e), convective heat transfer losses of the strip surface (h_a) and the coefficient of friction (μ). The inverse analysis requires the measurements of the exit strip temperature and the slip. For finding out the temperature distribution of the exit strip and the slip, a thermo-mechanical model for warm flat rolling is proposed. The deformation analysis uses finite element method (FEM) based on the Eulerian flow formulation and the thermal analysis is based on the analytical methods. The determination of temperature distribution through the analytical methods for the roll as well as the strip has the advantage in terms of computational time.

The salient findings of the thesis can be summarized as follows:

- An approximate method has been proposed for the estimation of temperature distributions in the roll and strip in a rolling process. To predict the steady-state temperature distribution in the roll, a simplified and computationally

efficient approximate method is proposed by adapting the model of Fischer *et al*. (2004). The temperature distribution in the strip is obtained analytically. The method uses simplified mathematical models for heat transfer analysis, which are used in conjunction with a computationally efficient FEM code for deformation analysis. The method is validated with the experimental results available in the literature and a good agreement is found. Thus, this methodology can facilitate control and design engineers for the quick estimation of the steady-state temperature distribution in rolling processes. The proposed model can be used for the inverse estimation of the mechanical properties and the coefficient of friction by the measurement of exit strip temperature and slip.

- A fast FEM analysis has been carried out for the estimation of steady-state temperature distribution in rolling process. The input into the thermal analysis is taken from the deformation module based on Eulerian flow formulation. A computationally efficient methodology is developed for finding out the steady-state temperature distribution in rolling. The finite element based software package ABAQUS is used for implementing the proposed methodology. The steady-state temperature can also be obtained by carrying out a transient heat transfer analysis till the steady-state is achieved. However, the FEM procedure takes about 2 hours of the screen time, whilst the fast FEM model proposed in the present work requires less than 10 minutes of the screen time in ABAQUS. It has been observed that if the problem is solved in a non-interactive way by writing a subroutine code, *viz*. DFLUX, the method requires less than 1 minute. Thus, the proposed methodology provides the quick estimation of the steady-state temperature distribution in the rolling by FEM. The FEM results ensure the accuracy of the proposed model using an approximate method to find out the temperature distribution in the roll and the strip.

- The transient thermal analysis of the roll and strip together for warm flat rolling has been carried out. The analysis employs a time varying heat flux

input into the roll from the strip. An iterative procedure is carried out to obtain the temperature distribution assuming initial temperature as a function of radial and circumferential coordinates. In-house warm rolling experiments were also carried out to validate the proposed model by measuring the exit strip temperature at the surface as well as at the centerline. The exit strip temperature was measured experimentally by using an IR Camera and the exit velocity of the strip by normal video recording camera. The experimentally measured slip matching with the computed slip by FEM provides the coefficient of friction at the corresponding process parameters. It is observed that for different inlet strip temperatures and percentage reductions in strip, the proposed model is in well agreement with the experimental results with an error of about less than 8%. The transient thermal analysis provides an inverse way of estimating the thermal parameters based on the temperature measurement of the exit strip.

- The possibility of online determination of the coefficient of friction in the rolling is explored. Three different approaches are employed *viz*., minimum roll gap measurement method, slip measurement method and inverse method based on the temperature measurement. The first two methods are the classical methods and they are considered for the comparison purpose. The third approach deals with the inverse estimation of the coefficient of friction based on the exit strip surface temperatures with the known material properties. It has been observed that slip is not very sensitive to material parameters. Hence, in the absence of material data, it can be used as an effective method to find out the coefficient of friction.
- An efficient inverse methodology has been developed to estimate the mechanical properties and the coefficient of friction based on the exit strip temperature and the slip measurements. Instead of the exit strip temperature, the roll-torque or roll-force can also be measured for carrying out the inverse analysis. However, the measurement of the exit strip temperature is the most convenient. A heuristic method is used for the minimization of the error

between the actual and the estimated temperature of exit strip. The inverse model requires only 4-5 iterations to estimate the material parameters. A sensitivity analysis of the material parameters and the coefficient of friction based on the exit strip temperature measurement has also been carried out. It is observed that the temperature softening parameters is the most sensitive material parameters for estimating the temperature.

- The proposed inverse methodology is validated by conducting in-house experiments to estimate the mechanical properties of strip material and the coefficient of friction at the roll-strip interface. The coefficient of friction is estimated based on the slip measurement. The flow stress of the strip is estimated based on the temperature measurement and is compared with the experimentally measured flow stresses at different temperature. The surface roughness and micro-hardness measurements are carried out to assess the quality of the rolled strip. It is observed that the average measured surface roughness of the rolled strip at different inlet strip temperatures increases in warm rolling. However, in cold rolling, the surface roughness decreases with increasing reductions. This may be due to burnishing action in the presence of friction. The micro-hardness of the surface of the rolled strip increases with increasing the reductions. However, with increase in the inlet strip temperature, the micro-hardness decreases.
- An inverse method is proposed for finding out the average thermal properties of the roll and the strip. The methodology requires the transient temperature distribution at the exit strip at two locations. The coefficient of friction is estimated based on slip measurement. For a fixed value of the coefficient of friction, the slip is unaffected by thermal parameters. Based on the sensitivity study, a procedure to identify the parameters by inverse analysis is illustrated. It is seen that there are sufficient number of signals to predict the seven parameters uniquely. However, apart from the slip, it is essential to measure the transient as well as the steady-state temperatures at two locations. The uniqueness of the solution has been studied heuristically and numerically.

8.2 Scope for Future Work

- In the present work, an inverse methodology for the estimation of the mechanical and the thermal parameters has been developed separately. This work can be extended for the inverse estimation of the mechanical properties, thermal parameters and the coefficient of friction together.
- The study of the strain-rate dependency on the coefficient of friction in rolling is not carried out in the present thesis. The proposed thermo-mechanical model of warm flat rolling can be used to explore the effect of strain-rate on the friction.
- The plane strain thermo-mechanical model for warm flat rolling is developed to analyze the rolling process in this thesis. The deformation analysis is carried out by FEM and analytical solutions are used for thermal analysis. Further, this work can be extended to three-dimensional FEM modelling to analyze the rolling behaviour of different materials, for example, composite and functionally graded material.
- The three-dimensional analytical modelling for the temperature distribution in a rolling process does not exist in the literature. The development of such a model will benefit the rolling industry greatly.
- In the present work, an experimental study is carried out to see the effect of inlet temperatures of strip and percentage reductions in strip on the exit strip temperature. Further, experiments can be carried out to study the effect of different thickness of the sheet at different rolling speeds, which will provide a better insight of the metallurgical behaviour of the rolled sheet. Further, heat partition factor can be determined by carrying out the combined analysis of the roll and the strip.
- The effect of lubrication on the exit strip temperature and roll pressure distribution can be studied theoretically as well as experimentally. The proposed method can be extended to incorporate the effect of lubrication for analyzing the warm flat rolling. The experimental study can also be conducted to measure the pressure distribution in the roll and the friction hill

in the bite zone by embedding sensors in the roll at different lubricants. Further, the effect of lubricants on friction and surface oxidation in the roll and the strip in rolling can be explored.

- In the present thesis, the experimental study has been carried out to measure the exit strip upper surface temperature distribution for validating the inverse methodology to find out the material and process parameters. However, inverse methodology can also be employed by measuring the bottom surface temperature of the strip.
- In the present work, a 100 kN capacity universal testing machine was used for carrying out the tensile test. The tensile test of aluminum alloy is carried out at different temperatures for the constant strain-rate to validate the inverse estimation of mechanical properties in warm flat rolling. In future, the servo hydraulic testing machine, Dynamic System Inc. (DSI) can be used to determine the mechanical properties of the metal at different temperatures for different strain-rates. This is mainly used to determine experimental data for the simulation of high temperature material properties in manufacturing. This provides the validation of the inverse method for different combinations of the strains, strain-rates and temperature in flat rolling.
- The present work can be extended to estimate the residual stresses in the deformation zone based on the obtained material and thermal parameters from the inverse modelling.
- The proposed thermo-mechanical model of warm flat rolling presented in this thesis can be extended to estimate the various defects by using micro-mechanics and continuum damage mechanics. Further, the proposed model can be extended to analyze the behaviour of the microstructure evolution during hot flat rolling as well as other metal forming processes.

References

- Abo-Elkhier, M., (1997), Elasto-plastic finite element modelling of strip cold rolling using Eulerian fixed mesh technique, Finite Elements in Analysis and Design, **27**, pp. 323–334.
- Al-Salehi, F.A.R., Firbank, T.C. and Lancaster, P.R., (1973), An experimental determination for the roll pressure distributions in cold rolling, International Journal of Mechanical Sciences, **15**, pp. 693–710.
- Arif, A.F.M., Khan, O. and Zubair, S.M., (2004), Prediction of roll temperature with a non- uniform heat flux at tool and workpiece interface, Heat and Mass Transfer, **41**, pp. 75–94.
- Alexander, J.M., (1955), A slip line field for the hot rolling process, Proceedings of the Institution of Mechanical Engineers, **169**, pp. 1021–1030.
- Alexander, J.M., (1972), On the theory of rolling, Proceeding of The Royal Society (London), **159**, pp. 144–163.
- Atreya, A. and Lenard, J.G., (1979), A study of cold rolling, Transactions of the ASME, Journal of Engineering Materials and Technology, **101**, pp. 129–134.
- Avitzur, B., (1964), An upper-bound approach to cold-strip rolling, Transactions of the ASME, Journal of Engineering for Industry, Series B, **86**, pp. 31–48.
- Belyakov, A., Kaibyshev, R. and Torganchuk, V., (2016), Microstructure and mechanical properties of 18%Mn TWIP/TRIP steels processed by warm or hot rolling, Steel Research International, **87**, pp. 1–5, DOI: 10.1002/srin.201600123.

- Bland, D.R. and Ford, H., (1948), The calculations of roll force and torque in cold strip rolling with tensions, Proceedings of Institution of Mechanical Engineers Part B: Journal of Engineering Manufacture, **159**, pp. 144–163.
- Bland, D.R. and Sims, R.B., (1953), A note on the theory of rolling with tensions, Proceedings of Institution of Mechanical Engineers Part B: Journal of Engineering Manufacture, **167**, pp. 371–372.
- Byon S. M., Kim S. I. and Lee Y., (2008), A numerical approach to determine flow stress-strain curve of strip and friction coefficient in actual cold rolling mill, Journal of Materials Processing Technology, **201**, pp. 106–111.
- Chandra, S. and Dixit, U.S., (2004), A rigid-plastic finite element analysis of temper rolling process, Journal of Materials Processing Technology, **152**, pp. 9–16.
- Chandrasekaran, M., Muralidhar, M., Krishna, C.M. and Dixit, U.S., (2012), Online machining optimization with continuous learning, in Computational Methods for Optimizing Manufacturing Technology: Models and Techniques 2012; J. Paulo Davim (editior), IGI Global, Hershey, PA.
- Chang, D.F., (1999), Thermal stresses in work rolls during the rolling of metal strip, Journal of Materials Processing Technology, **94**, pp. 45–51.
- Chen, W.L. and Yang, Y.C., (2010), Inverse problem of estimating the heat flux at the roll/workpiece interface during rolling process, Applied Thermal Engineering, **30**, pp. 1247–1254.
- Chen, S., Li, W., Liu, X., (2014), Calculation of rolling pressure distribution and force based on improved Karman equation for hot strip mill, International Journal of Mechanical Sciences, **89**, 256–263.
- Cho, H. and Ngaile, G., (2003), Simultaneous determination of flow stress and interface friction by finite element based inverse analysis technique, CIRP Annals–Manufacturing Technology, **52**, pp. 221–224.

- Cho H. and Altan T., (2005), Determination of flow stress and interface friction at elevated temperatures by inverse analysis technique, Journal of Materials Processing Technology, **170**, pp. 64–70.
- Christensen, P., Everfelt, K. and Bay, N., (1986), Pressure distributions in plate rolling, Annals of CIRP, **35**, pp. 141–146.
- Chun, M., Biglou, J., Lenard, J.G. and Kim, J., (1999), Using neural networks to predict parameters in the hot working of aluminum alloys, Journal of Materials Processing Technology, **86**, pp. 245–251.
- Collins, I.F., (1968), The algebraic-geometry of slip line fields with applications to boundary value problems, Proceedings of the Royal Society (London), A, **303**, pp. 317–338.
- Collins, I.F., (1969), Slip-line field solution for compression and rolling with slipping friction, International Journal of Mechanical Sciences, **11**, pp. 971–978.
- Davies, J., (1992), Properties and Selection: Nonferrous Alloys and Special-Purpose Materials. ASM International Handbook, **2**: The Materials International Society, Material Park, Ohio, USA.
- DesRuisseaux, N.R. and Zerkle, R.D., (1970), Temperature in semi-infinite and cylindrical bodies to moving heat sources and surface cooling, Journal of Heat and Mass Transfer, **92**, pp. 456–464.
- Dewhurst, P., Collins, I.F. and Johnson, W., (1973), A class of slip-line field solutions for the hot rolling of strip, Proceedings of the Institution of Mechanical Engineers, Part C: Journal of Mechanical Engineering Science, **15**, pp. 439–447.
- Dixit, U.S. and Dixit, P.M., (1996), A finite element analysis of flat rolling and application of fuzzy set theory, International Journal of Machine Tools and Manufacture, **36**, pp. 947–969.

- Dixit, U.S., (1997), Cold Flat Rolling: Modelling with Fuzzy Parameters, Anisotropic Effects and Residual Stresses, PhD Thesis, Department of Mechanical Engineering, IIT Kanpur, India.
- Dixit, U.S. and Dixit, P.M., (1997a), Finite element analysis of flat rolling with inclusion of anisotropy, International Journal of Mechanical Sciences, **39**, pp. 1237–1255.
- Dixit, U.S. and Dixit, P.M., (1997b), A study on residual stresses in rolling, International Journal of Machine Tools and Manufacture, **37**, pp. 837–853.
- Dixit, U.S., Robi, P.S. and Sarma, D.K., (2002), A systematic procedure for the design of a cold rolling mill, Journal of Materials Processing Technology, **121**, pp. 69–72.
- Dixit, U.S. and Chandra, S., (2003), Neural network based methodology for the prediction of roll force and roll torque in fuzzy form for cold flat rolling process, International Journal of Advanced Manufacturing Technology, **22**, pp. 883–889.
- Dixit, P.M. and Dixit, U.S., (2008), Modeling of Metal Forming and Machining Processes: By Finite Element and Soft Computing Methods. Springer, London.
- Doğruoğlu, A.N., (2001), On constructing kinematically admissible velocity fields in cold sheet rolling, Journal of Materials Processing Technology, **110**, pp. 287–299.
- Domanti, S.A. and McElwain, D.L.S., (1998), Cold rolling of flat metal products: Contribution of mathematical modelling, Proceedings of the Institution of Mechanical Engineers, Part B: Journal of Engineering Manufacture, **212**, pp. 73–86.
- Drucker, D.C., (1954), Coulomb friction, plasticity and limit loads, Transactions of the ASME, Journal of Applied Mechanics, **21**, pp. 71–74.

- Eideh, A. and Dixit, U.S., (2013), A robust and efficient inverse method for determining the thermal parameters during laser forming, Proceedings of National conference on Recent Advancements in Mechanical Engineering NERIST, Nirjuli, India, November 8-9, 2013.
- Eklund, E., (1933), The analysis of factors influencing rolling pressure and power consumption in the hot rolling of steel, Steel, pp. 8–14, (Translated from Jerkontorets Ann. Feb. 1927, by B. Blomquist).
- Fleck, N. A. and Johnson, K. L., (1987), Towards a new theory of cold rolling thin foil, International Journal of Mechanical Sciences, **29**, 507–524.
- Fleck, N.A., Johnson, K.L., Mear, M.E. and Jhang, L.C., (1992), Cold rolling of foil, Proceedings of Institution of Mechanical Engineers Part B: Journal of Engineering Manufacture, **206**, pp. 119–131.
- Firbank, T.C. and Lancaster, P.R., (1965), A suggested slip-line field for cold rolling with slipping friction, International Journal of Mechanical Sciences, **7**, pp. 847–852.
- Firbank, T.C. and Lancaster, P.R., (1966), Note: On some aspects of the cold rolling problem, International Journal of Mechanical Sciences, **8**, pp. 653–656.
- Firbank, T.C. and Lancaster, P.R., (1967), A proposed slip-line field for lubricated cold rolling, International Journal of Mechanical Sciences, **9**, pp. 65–67.
- Fischer, F.D., Werner, E.A. and Knothe, K., (2001), The surface temperature of a halfplane heated by friction and cooled by Convection. ZAMM, Journal of Applied Mathematics and Mechanics, **81**, pp. 78–81.
- Fischer, F.D., Schreiner, W.E., Werner, E.A. and Sun, C.G., (2004), The temperature and stress fields developing in rolls during hot rolling, Journal of Materials Processing Technology, **150**, pp. 263–269.

- Galantucci, L.M. and Tricarico, L., (1999), Thermo-mechanical simulation of a rolling process with an FEM approach. Journal of Materials Processing Technology. **92-93**, pp. 494–501.
- Gelton, C.J.M. and Koter, A.W.A, (1982), Application of mesh rezoning in the updated Lagrangian method to metal forming analysis, In: Numerical Methods in Industrial Forming Processes, (J.F.T. Pittman *et al*. Eds.), Pineridge press, Swansea, U.K., pp. 511–521.
- Gerald, C. F. and Wheatley, P. O., (1997), Applied Numerical Analysis. 5th edition, Addison-Westey, England.
- Gratacos, P., Montmitonnet, P., Fromholz, C. and Chenot, J.L., (1992), A plane-strain elastoplastic finite-element model for cold rolling of thin strip, International Journal of Mechanical Sciences, **34**, pp. 195–210.
- Green, J.W. and Wallace, J.F., (1962), Estimation of load and torque in the hot rolling process, Journal of Mechanical Engineering Science, **4**, pp. 136–142.
- Green, J.W., Sparling, L.G.M. and Wallace, J.F., (1964), Shear plane theories of hot and cold rolling, Journal of Mechanical Engineering Science, **6**, pp. 219–235.
- Gudur, P.P. and Dixit, U.S., (2008a), A neural network-assisted finite element analysis of cold flat rolling, Engineering Applications of Artificial Intelligence, **21**, pp. 43–52.
- Gudur, P.P. and Dixit, U.S., (2008b), A combined finite element and finite difference analysis of cold flat rolling, Transaction of the ASME, Journal of Manufacturing Science and Engineering, **130**, pp. 01107-1–01107-6.
- Guo, R., (1998), Two-dimensional transient thermal behavior of work rolls in rolling process, Transaction of the ASME, Journal of Manufacturing Science and Engineering, **120**, pp. 28–33.

- Gunasekera, J.S., Jia, Z., Malas, J.C. and Rabelo, L., (1998), Development of a neural network model for a cold rolling process, Engineering Applications of Artificial Intelligence, **11**, pp. 597–603.
- Han H., (2005), Determination of mean flow stress and friction coefficient by modified two- specimen method in cold rolling, Journal of Materials Processing Technology, **159**, pp. 404–408.
- Hartley, P., Sturgess, C.E.N., Liu, C. and Rowe, G.W., (1989), Experimental and theoretical studies of work-piece deformation, stress and strain during flat rolling, International Materials Reviews, **34**, pp. 19–34.
- Hatta, N., Kokado, J. and Nishimura, H., (1980), Analysis of slab temperature change and rolling mill line length in quasi continuous hot strip mill equipped with two roughing mils and six finishing mills, The Iron and Steel Institute of Japan, **21**, pp. 270–277.
- Hawkins, D.N. and Tsinopoulos, G., (1978), Effect of warm extrusion on the structure and properties of low-carbon steels, Journal of Mechanical Working Technology, **2**, pp. 161–177.
- Hawkins, D.N., (1981), An etchant for revealing the substructure in low-carbon steels, Metallography, **14**, pp. 61–68.
- Hawkins, D.N., (1985), Warm working of steels, Journal of Mechanical Working Technology, **11**, pp. 5–21.
- Heeg, R., Kiefer, T., Kugi, A., Fichet, O. and Irastorza, L., (2007), Feedforward control of plate thickness in reversing plate mills, IEEE Transactions on Industry Applications, **43**, pp. 386–394.
- Hlady, C.O., Brimacombe, J.K., Samarasekera, I.V. and Hawbolt, E.B., (1995), Heat transfer in the hot rolling of metals, Metallurgical and Materials Transaction B, **26B**, pp. 1019–1027.
- Hill, R., (1963), A general method of analysis for metal-working processes, Journal of the Mechanics and Physics of Solids, **11**, pp. 305–326.

- Hirschvogel, M., (1979), Recent developments in industrial practice of warm working, Journal of Mechanical Working Technology, **2**, pp. 317–332.
- Hitchcock, J.H., (1935), Elastic deformation of rolls during cold rolling, American Society of Mechanical Engineers: Report of special research committee on roll neck bearings, pp. 33–41.
- Hsu, P.T., Yang, Y.T., Chen, C.K., (2000), A three dimensional inverse problem of estimating the surface thermal behavior of the working roll in rolling process, Transaction of the ASME, Journal of Manufacturing Science and Engineering, **122**, pp. 76–82.
- Huang, C.H., Ju, T.M. and Tseng, A.A., (1995), The estimation of surface thermal behavior of the working roll in hot rolling process, International Journal of Heat and Mass Transfer, **38**, pp. 1019–1031.
- Hwang, S.M. and Joun, M.S., (1992), Analysis of hot-strip rolling by a penalty rigid-viscoplastic finite element method, International Journal of Mechanical Sciences, **34**, pp. 971–984.
- Hwang, S.M., Joun, M.S. and Kang, Y.H., (1993), Finite element analysis of temperatures, metal flow, and roll pressure in hot strip rolling, Transaction of the ASME Journal of Manufacturing Science, **115**, pp. 290–298.
- Hwang, S. M., Sun, C.G., Ryoo, S.R. and Kwak, W. J., (2002), An integrated FE process model for precision analysis of thermo-mechanical behaviors of rolls and strip in hot strip rolling, Computational Methods of Application in Mechanics Engineering, **191**, pp. 4015–4033.
- Incropera, F.P., Dewitt, D.P., Bergman, T.L. and Lavine, A.S., (2003), Fundamentals of Heat Mass Transfer, 7th edition, John Wiley & Sons, New York.
- Jeswiet, J. and Cao, X., (1994), The effect of aspect ratio upon friction and normal forces in strip rolling, Journal of Materials Processing Technology, **45**, pp. 99–104.

- Jeswiet, J. and Rice, W. B., (1975), Measurement of strip temperature in the roll gap during cold rolling, CIRP Annals–Manufacturing Technology, **24**, pp. 153–161.
- Jeswiet, J. and Zhou, S., (1992), Temperature, heat flux and conductivity in bar rolling, CIRP Annals–Manufacturing Technology, **41**, pp. 299–302.
- Jeswiet, J., Arentoft, M. and Henningsen, P., (2006), Methods and devices used to measure friction in rolling, Proceedings of the Institution of Mechanical Engineers, Part B: Journal of Engineering Manufacture, **220**, pp. 49–57.
- Johnson, W. and Kudu, H., (1960), The use of upper-bound solutions for the determination of temperature distribution in fast hot rolling and axi-symmetric extrusion processes, International Journal of Mechanical Sciences, **1**, pp. 175–191.
- Johnson, G.R. and Cook, W.H., (1983), A constitutive model and data for metals subjected to large strains, high strain rates and high temperatures, In: Proceedings of the 17th International Symposium on Ballistics, **21**, International Ballistics committee, The Hague, Netherlands, 19-21 April 1983, pp. 541–547.
- Jiang, Z.Y., Tieu, A.K., Lu, C., Sun, W.H., Zhang, X.M. and Liu, X.H., (2004), Three dimensional thermomechanical finite element simulation of ribbed strip rolling with friction variation, Finite Element in Analysis and Design, **40**, pp. 1139–1155.
- Jiang, Z.Y., Xiong, S.W., Tieu, A.K. and Wang, Q.J., (2008), Modelling of the effect of friction on cold strip rolling, Journal of Materials Processing Technology, **201**, pp. 85–90.
- Jiang. Z.Y., Wei, D.B., Tieu, K., Huang, J.X., Zhang, A.W., Shi, X. and Jiao, S.H., (2011), Study on oxidation of stainless steels during hot rolling, International Journal of Manufacturing, Materials, and Mechanical Engineering, **1**, pp. 31–42.

- Kalpakjian, S. (2008), Manufacturing Engineering and Technology, 5th Edition Addison-Wesley, London.
- Karman, T. von, (1925), On the theory of rolling, Zeitschrift für Angewandte Mathematik und Mechanik (ZAMM), **5**, pp. 139–141.
- Khan, O.U., Jamal, A., Arshed, G.M. Arif, A.F.M. and Zubair, S.M., (2004), Thermal analysis of a cold rolling process—A numerical approach, Numerical Heat Transfer, Part A: Application, **46**, pp. 613–632.
- Khalili, L., Serajzadeh, S. and Koohbor, B., (2012), Thermomechanical behavior of work rolls during warm strip rolling. Metallurgical and Materials Transactions B, **43B**, pp. 1638–1648.
- Kim, N., Kobayashi, S. and Altan, T., (1991), Three-dimensional analysis and computer simulation of shape rolling by the finite and slab element method, International Journal of Mechanical Sciences, **31**, pp. 553–563.
- Kim, L., Lee, J. and Hwang, S.M., (2009), An analytical model for the prediction of strip temperatures in hot strip rolling, International Journal of Heat and Mass Transfer, **52**, pp. 1864–1874.
- Kiuchi, M., Yanagimoto, J. and Wakamatsu, E., (2000), Overall thermal analysis of hot plate/sheet rolling, CIRP Annals–Manufacturing Technology, **49**, pp. 209–213.
- Kobayashi, S., Oh, S. and Altan, T., (1989), Metal forming and the finite-element method, Oxford University Press, New York.
- Koohbor, B., (2015), Finite element modeling of thermal and mechanical stresses in work-rolls of warm strip rolling process, Proceedings of the Institution of Mechanical Engineers, Part B: Journal Engineering Manufacture, doi: 10.1177/0954405414564807.
- Komanduri, R. and Hou, Z.B. (2001), Analysis of heat partition and temperature distribution in sliding systems, Wear, **251**, pp. 925–938.

- Kreyszig, E., (1999), Advanced Engineering Mathematics, 8th edition, John Wiley & Sons, Inc, New York.
- Kumar, D. and Dixit, U.S., (2006), A slab method study of strain hardening and friction effects in cold foil rolling process, Journal of Materials Processing Technology, **171**, pp. 331–340.
- Kusiak, J., Kawalla, R., Pietrzyk, M. and Pircher, H., (1996), Inverse analysis applied to the evaluation of material parameters in the history dependent flow stress equation in hot forming of metals, Journal of Materials Processing Technology, **60**, pp. 455–461.
- Min, K., Kim, K., Kim, S.K. and Lee, D.J., (2012), Effects of oxide layers on surface defects during hot rolling processes, Metallurgical and Material International, **18**, pp. 341–348.
- Lahoti, G.D., Shah, S.N. and Altan, T., (1978), Computer-aided analysis of the deformations and temperatures in strip rolling, Transactions of the ASME, Journal of Engineering for Industry, **100**, pp.159–166.
- Lahoti, G.D., Akgerman, N., Oh, S.I. and Altan, T., (1980), Computer-aided analysis of metal flow and stresses in plate rolling, Journal of Mechanical Working Technology, **4**, pp. 105–119.
- Larkiola, J., Myllykoski, P., Nylander,J. and Korhonen, A.S., (1996), Prediction of rolling force in cold rolling by using physical models and neural computing, Journal of Materials Processing Technology, **60**, pp. 381–386.
- Le, H.R. and Sutcliffe, M.P.F., (2001), A robust model for rolling of thin strip and foil, International Journal of Mechanical Sciences, **43**, pp. 1405–1419.
- Le, H.R. and Sutcliffe, M.P.F., (2002), Rolling of thin strip and foil: application of a tribological model for ‘‘mixed’’ lubrication, Transaction of ASME, Journal of Tribology, **124**, pp. 129–136.

- Lee, C.H. and Kobayashi, S., (1973), New solutions to rigid-plastic deformation problems using a matrix method, Transactions of the ASME, Journal of Engineering for Industry, **95**, pp. 865–873.
- Lee, J.D., (1998), A large-strain elastic-plastic finite element analysis of rolling process, Computer Methods in applied Mechanics and Engineering, **161**, pp. 315–347.
- Lee, J.D., Manzari, M.T. Shen, Y.L. and Zeng, W., (2000), A finite element approach to transient thermal analysis of work rolls in rolling process, Transaction of the ASME, Journal of Manufacturing Science and Engineering, **122**, pp. 706–715.
- Lee, J.H., Kwak, W.J., Sun, C.G., Kim, K.H., Ko, K.H. and Hwang, S.M., (2004), Precision online model for prediction of strip temperature in hot strip rolling, Ironmaking and Steelmaking, **31**, pp. 153–168.
- Lenard, J.G., (1991), Measurement of friction in cold flat rolling, Journal of Material Shaping Technology, **9**, pp. 171–180.
- Lenard, J.G. and Kalpakjian, S., (1991), The effect of temperature on the coefficient of friction in flat rolling, CIRP Annals–Manufacturing Technology, **40**, pp. 223–226.
- Lenard, J.G., (1992), Friction and forward slip in cold strip rolling, Transactions of the ASME, Journal of Engineering for Industry, **104**, pp. 55–64.
- Lenard, J.G. and Malinowski, Z., (1992), Measurements of friction during the warm rolling of aluminum, Journal of Materials Processing Technology, **39**, pp. 357–371.
- Lenard J. G. and Zhang S., (1997), A study of friction during the lubricated cold rolling of an aluminum alloy, Journal of Materials Processing Technology, **72**, pp. 293–301.

- Lenard, J.G., (2000), Tribology in metal rolling, Keynote Presentations, CIRP Annals–Manufacturing Technology, **49/2**, pp. 567–590.
- Lenard J.G. and Nad L.B., (2002), The coefficient of friction during hot rolling of low carbon steel strips, Transactions of ASME, Journal of Tribology, **124**, pp. 840–846.
- Li, G.J. and S. Kobayashi, (1982), Rigid-plastic finite element analysis of plane strain rolling, Transactions of the American Society of Mechanical Engineers; Journal of Engineering for Industry, **104**, pp.55–64.
- Li, E.B., Tieu, A.K. and Yuen, W.Y.D., (2003), Application of digital image correlation technique to dynamic measurement of the velocity field in the deformation zone in cold rolling, Optics and Lasers in Engineering, **39**, pp. 479–488.
- Li, D. and Ghosh, A., (2003), Tensile deformation behavior of aluminum alloys at warm forming temperatures, Materials Science and Engineering A, **352**, pp. 279–286.
- Liu, Y., (2002), Friction at Strip-Roll Interface in Cold Rolling, PhD Thesis, Faculty of Engineering, University of Wollongong 2002; http://ro.uowedu.au/theses/1827 accessed on dated July 31, 2014.
- Lindgren, L.E. and Edberg, J., (1990), Explicit versus implicit finite element formulation in simulation of rolling, Journal of Materials Processing Technology, **24**, pp. 85–94.
- Liu, C., Hartley, P., Sturgess, C.E.N. and Rowe, G.E., (1985), Elastic-plastic finite element modelling of cold rolling of strip, International Journal of Mechanical Sciences, **27**, pp. 531–541.
- Louaisil, K., Dubar, M., Deltombe, R., Dubois, A. and Dubar, L., (2009), Analysis of interface temperature, forward slip and lubricant influence on friction and wear in cold rolling, Wear, **266**, pp. 119–128.
- Luo, C. and Keife, H., (1998), A thermal model for the foil rolling process, Journal of Materials Processing Technology, **74**, pp.158–173.

- Malinowski, Z. and Lenard, J.G., (1992), A study of the state of stress during cold strip rolling, Journal of Materials Processing Technology, **33**, pp. 273–288.
- Marques Barata, M.J.M and Martins, P.A.F., (1990), A solution to plane strain rolling by the weighted residuals method, International Journal of Mechanical Sciences, **32**, pp. 817–827.
- Maslen, S.H. and Tseng, A.A., (1981), Program Rolling User's Manual, Report No. MMLTR818, Martin Marietta Laboratories, Baltimore, MD.
- Meslin, F.H. and Hamann, J.C., (2003), The problem of constitutive equations for the modelling of chip formation: towards inverse methods. pp. 123–142. In: Boisse, P., T. Altan, and K. Luttervelt, (editors.), Friction and Flow Stress in Forming and Cutting. First South Asian Edition, London, UK.
- Min, K., Kim, K., Kim, S.K. and Lee, D.J., (2012), Effects of oxide layers on surface defects hot rolling processes, Metallurgical and Materials International, **18**, pp. 341–348.
- Mori, K., Osakada, K. and Oda, T., (1982), Simulation of plane-strain rolling by the rigid-plastic finite element method, International Journal of Materials Processing Technology, **24**, pp. 519–527.
- Nepershin, A., (1999), Plane strain hot rolling of slab and strip, International Journal of Mechanical Sciences, **141**, pp. 1401–1421.
- Oliveira, C.K.N., Benassi, C.L. and Casteletti, L.C., (2006), Evaluation of hard coatings obtained on AISI D2 steel by thermo-reactive deposition treatment, Surface & Coatings Technology, **201**, pp. 1880–1885.
- Oluwole, O.O. and Olaogun, O., (2011), Slip line field solution for second pass in lubricated 4 high reversing cold rolling sheet mill, Engineering, **3**, pp. 1225–1233.

- Orowan, E., (1943), The calculation of roll pressure in hot and cold flat rolling, Proceedings of Institution of Mechanical Engineers, **150**, pp. 140–167.
- Özişik, M.N., (1993), Heat Conduction, John Wiley & Sons. New York.
- Park, J.J. and Kobayashi, S., (1984), Three-dimensional finite element analysis of block compression, International Journal of Mechanical Sciences, **26**, pp. 165–176.
- Patula, E.J., (1981), Steady-state temperature distribution in a rotating roll subject to surface heat fluxes and convective cooling, Transactions of the ASME, Journal of Heat Transfer, **103**, pp. 36–41.
- Pietrzyk, M. and Lenard, J.G., (1990), The effect of the temperature rise of the roll on the simulation of the flat rolling process, Journal of Materials Processing Technology, **22**, pp. 177–190.
- Prakash, R.S., Dixit, P.M. and Lal, G.K., (1995), Steady-state plane strains cold rolling of a strain-hardening material, Journal of Materials Processing Technology, **47**, pp. 201–229.
- Raczy, A., Altenhof, W.J. and Alpas, A.T., (2004), An Eulerian finite element model of the metal cutting process, Proceedings of 8th International LS-DYNA Users Conference, Detroit, USA, May 2-4, 2004, pp. 9–25.
- Rao, R.S. and Kumar, A., (1979), A finite element solution of strip rolling, International Journal of Machine Tool Design and Research, **17**, pp. 157–168.
- Rao, R.S. and Lee, H.Y., (1989), A finite element solution of strip rolling, Journal of Mechanical Working Technology, **20**, pp. 453–461.
- Rao, S.S., (2013), Engineering Optimization: Theory and Practice, New Age International Publishers, New Delhi, India.
- Richelson, A.B., (1991), Viscoplastic analysis of plane-strain rolling using different friction models, International Journal of Mechanical Sciences, **33**, pp. 761–774.

- Richelson, A.B., (1994), Interface element modelling of friction in rolling, Journal of Materials Processing Technology, **42**, pp. 209–216.
- Rigler, G.W., Aberl, H.R., Staufer, W., Aistleitner, K. and Weinberger, K.H., (1996), Improved rolling mill automation by means of advanced control techniques and dynamic simulation, IEEE Transactions on Industry Applications, **32**, pp. 599–607.
- Roberts, W.L., (1965), A simplified cold rolling, Iron and Steel Engineer Year Book, pp. 925–937.
- Roberts, W.L., (1976), Computing the coefficient of friction in the roll bite from mill data, Blast Furnace and Steel Plant, **55**, pp. 499–508.
- Roberts, W.L., (1978), Editor, Cold rolling of steel. New York, Marcel Dekker.
- Rooyen, G.T.V. and Backofen, W.A., (1957), Friction in cold rolling, Journal of the Iron and Steel Institute, **6**, pp. 235–244.
- Roychoudhary, R. and Lenard, J.G., (1984), A mathematical model for cold rolling–Experimental Substantiation, Proceedings of 1st International Conference on Technology and Plasticity, Tokyo, pp. 1138–1143.
- Serajzadeh, S., Taheri, A.K., Mucciardi, F., (2002), Unsteady state work-roll temperature distribution during continuous hot slab rolling, International Journal of Mechanical Sciences, **44**, pp. 2447–2462.
- Serajzadeh, S., (2004), Modelling the warm rolling of a low carbon steel, Materials Science and Engineering A, **371**, pp. 318–323.
- Serajzadeh, S., (2006), A model for prediction of flow behavior and temperature distribution during warm rolling of a low carbon steel, Materials and Design, **27**, pp. 529–534.
- Serajzadeh, S. and Mohammadzadeh, M., (2007), Effects of deformation parameters on the final microstructure and mechanical properties in warm

rolling of a low-carbon steel, International Journal of Advanced Manufacturing Technology, **34**, pp. 262–269.

- Sezek, S., Akaskal, B. and Can, Y., (2008), Analysis of cold and hot plate rolling using dual stream functions, Materials and Design, **29**, pp. 584–596.
- Shahani, A.R., Setayeshi, S., Nodamaie, S.A., Asadi, M.A. and Rezaie, S., (2009), Prediction of influence parameters on the hot rolling process using finite element method and neural network, Journal of Materials Technology, **209**, pp. 1920–1935.
- Shang, J., Hatkevich, S. and Wilkerson, L., (2012), Experimental study and numerical simulation of electromagnetic tube expansion, Proceedings of the 5th International Conference on High Speed Forming, 24-26 April 2012, pp. 83–92.
- Shangwu, X., Rodrigues, J.M.C. and Martins, P.A.F., (2003), Three-dimensional modelling of the vertical-horizontal rolling process, Finite Elements in Analysis and Design, **39**, pp. 1023–1037.
- Sheikh, H., (2009), Thermal analysis of hot strip rolling using finite element and upper bound methods, Applied Mathematical Modelling, **33**, pp. 2187–2195.
- Shi, J., McEwain, D.L.S. and Langlands, T.A.M., (2001), A comparison of methods to estimate the roll torque in thin strip rolling, International Journal of Mechanical Sciences, **43**, pp. 611–630.
- Shirizly, A. and Lenard, J.G., (2000), The effect of lubrication on mill loads during hot rolling of low carbon steel strips, Journal of Materials Processing Technology, **97**, pp. 61–68.
- Shivpuri, R. and Chou, P.C., (1989), A comparative study of slab, upper bound and finite element methods for predicting force and torque in cold rolling, International Journal of Machine Tools and Manufacture, **29**, pp. 305–322.

- Siebel, E. and Lueg, W., (1933), Investigations into the distribution of pressure at the surface of the material in contact with rolls, Mitteilungen aus dem Kaiser-Wilhem-Institut Fŭr Eisenforschung, **15**, pp. 1–15.
- Smerd, R., Winkler, S., Salisbury, C., Worswick, M., Lloyd, D. and Finn, M., (2005), High strain rate tensile testing of automotive aluminum alloy sheet, International Journal of Impact Engineering, **32**, pp. 541–560.
- Steiner, R., (1990), ASM Handbook: Properties and Selection: Irons, Steels, and High-Performance Alloys, ASM International Handbook. **1**: The Materials International Society, Material Park, Ohio, USA.
- Stephenson, D.A., (1983), Friction in cold strip rolling, Wear, **92**, pp. 293–311.
- Stevans, P.G., Ivens, K.P. and Harper, P., (1971), Increasing work roll life by improved roll-cooling practice, Journal of Iron and Steel Institute, **209**, pp. 1–11.
- Subramanian, E.V. and Bourell, D.L., (1984), Roll pressure modeling of mutlipass warm rolling of carbon steel, Journal of Applied Metal Working, **3**, pp. 264–271.
- Sun, C.G., Yun, C.S. Chung, J.S. and Hwang, S.M., (1998), Investigation of thermomechanical behavior of a work roll and a roll life in hot strip rolling, Metallurgical and Materials Transactions A. **29A**, pp. 2407–2424.
- Taha, H.A., (2000), Operations Research An Introduction, Prentice-Hall of India Pvt. Ltd., New Delhi, India.
- Tamano, T., (1973), Finite element analysis of steady metal flow problems, Journal of the Japan Society of Technology Plasticity, **14**, pp. 766–769.
- Tamano, T. and Yangimoto, S., (1975), Finite element analysis of steady metal flow problems, Journal of the Japan Society of Mechanical Engineers, **41**, pp. 1130–1135.

- Thomson, P.E., (1982), A combined viscoplasticity and finite element analysis of cold rolling, Numerical Methods in Industrial Forming Processes, (editor: Pittman), Pineridge Press, Swansea, U.K., pp. 757–765.
- Tieu, A.K. and Liu, Y.J., (2004), Friction variation in the cold-rolling processes, Tribology International, **37**, pp. 177–183.
- Tseng, A.A., (1984), A numerical heat transfer analysis of strip rolling, Transactions of the ASME, Journal of Heat Transfer, **106**, pp. 512–517.
- Tseng, A.A., Tong, S.X., Maslen, S.H. and Mills, J.J., (1990), Thermal behavior of aluminum rolling, Transactions of the ASME, Journal of Heat Transfer, **112**, pp. 301–308.
- Tszeng, T.C. and Saraf, V., (2003), A study of fin effects in the measurement of temperature using surface-mounted thermocouples, Transactions of the ASME Journal of Heat Transfer, **125**, pp. 926–935.
- Tudball, A. and Brown, S.G.R., (2006), Practical finite element heat transfer modelling for hot rolling of steels, Ironmaking and Steelmaking, **33**, pp. 61–66.
- Tuncer, C. and Dean, T.A., (1987), A new pin design for pressure measurement in metal forming processes, International Journal of Machine Tools and Manufacture, **27**, pp. 325–331.
- Vural, M., Rittel, D. and Ravichandran, G., (2003), Large strain mechanical behavior of 1018 cold-rolled steel over a wide range of strain rates, Metallurgical and Materials Transactions A, **34**, pp. 2873–2885.
- Wanheim, T. and Bay, N., (1978), A model for friction in metal forming processes, Annals of CIRP, **27**, pp. 189–194.
- Weisz-Patrault, D., Ehrlacher ,A. and Legrand, N., (2011), A new sensor for the evaluation of contact stress by inverse analysis during steel strip rolling, Journal of Materials Processing Technology, **211**, pp. 1500–1509.

- Weisz-Patrault, D., Ehrlacher ,A. and Legrand, N., (2012), Evaluation of temperature field and heat flux by inverse analysis during steel strip rolling. International Journal of Heat and Mass Transfer, **55**, pp. 629–641.
- Weisz-Patrault, D., Ehrlacher, A. and Legrand, N., (2013), Analytical inverse solution for coupled thermoelastic problem for the evaluation of contact stress during steel strip rolling, Applied Mathematical Modelling, **37**, pp. 2212–2229.
- Weisz-Patrault, D., Ehrlacher, A. and Legrand, N., (2014), Temperature and heat flux fast estimation during rolling process, International Journal of Thermal Sciences, **75**, pp. 1–20.
- Wilson,W. R. D., Chang, C. T. and Sa, C. Y., (1989), Interface temperatures in cold rolling, Journal of Material Shaping Technology, **6**, pp. 229–240.
- Xie, H.B., Jiang, Z.Y. and Yuen, W.Y.D., (2011), Analysis of friction and surface roughness effects on edge crack evolution of thin strip during cold rolling, Tribology International, **44**, pp. 971–979.
- Yadav, V., Singh, A.K., Joshi, S.N. and Dixit, U.S., (2011a) Comparison of the performance of lubricants in rolling based on temperature measurement. Proceedings of the 14th International Conference on Material Forming-ESAFORM2011, Belfast, United Kingdom, 27-29, 1353, pp. 357–361.
- Yadav, V., Singh, A.K. and Dixit, U.S., (2011b), Online determination of material parameters and coefficient of friction in cold flat rolling process. Proceedings of the International Conference on Computational Methods in Manufacturing (ICCMM2011), IIT Guwahati, India, 5-16 December 2011, pp. 35–42.
- Yang, Y.Y., Linkens, D.A. and Tolamantes-Silva, J., (2004), Roll load prediction–data collection, analysis and neural network modelling, Journal of Materials Processing Technology, **152**, pp. 304–315.

- Yanushkevich, Z., Lugovskaya, A., Belyakov, A. and Kaibyshev, R., (2016), Deformation microstructures and tensile properties of an austenitic stainless steel subjected to multiple warm rolling, Materials Science & Engineering A, **667**, pp. 279–285.
- Yiannopoulos, A.C., Anifantis, N.K. and Dimarogonas, A.D., (1997), Thermal stress optimization in metal rolling, Journal of Thermal Stresses, **20**, pp. 569–590.
- Yoneyama T, Asaoka H, Kimura H, Hoshino I, Kokubo M., (1999), Heat transfer and roll surface temperature in the hot rolling of aluminum sheet, Transactions of the ASME, Journal of Tribology, **121**, pp. 753–760.
- Yu, H., Yu, Q., Kang, J. and Liu, X., (2012), Investigation on temperature change of cold magnesium alloy strips rolling process with heated roll, Journal of Materials Engineering and Performance, **21**, pp.1841–1848.
- Yu, X., Jiang, Z., Wang, X., Wei, D. and Yang, D., (2012), Effect of coiling temperature on oxide scale of hot-rolled strip, Advanced Materials Research, 415-417, pp. 853–858.
- Yuan, W.Y.D., (1985), On the heat transfer of a moving composite strip compressed by two rotating cylinders, Transactions of the ASME, Journal of Heat Transfer, **107**, pp. 541–548.
- Yuen, W.Y.D., Dixon, A., Nguyen, D.N., (1996), The modeling of mechanics of the deformation in flat rolling, Journal of Materials Processing Technology, **60**, pp. 87–94.
- Zhang, W. and Bay, N., (1997), Numerical analysis of cross shear plate rolling, CIRP Annals–Manufacturing Technology, **46/1**, pp. 195–200.
- Zhang, S.H., Zhang, G.L., Liu, J.S., Li, C.S. and Mei, R.B., (2010), A fast rigid-plastic finite element method for online application in strip rolling, Finite Elements in Analysis and Design, **46**, pp. 1146–1154.

- Zhang, Y., Zhang, H.L., Wu, J.H. and Wang, X.T. (2011), Enhanced thermal conductivity in copper matrix composites reinforced with titanium-coated diamond particles, Scripta Materialia, **65**, pp. 1097–1100.
- Zhu, Y.D. and Avitzur, B., (1988), Criterion for the prevention of split ends, Transactions of ASME, Journal of Engineering for Industry, **110**, pp. 162–172.
- Zienkiewicz, O.C. and Godbole, P.N., (1974), Flow of plastic and visco-plastic solids with special reference to extrusion and forming processes, International Journal of Numerical Methods in Engineering, **8**, pp. 3–16.
- Zienkiewicz, O.C., Jain, P.C. and Onate, E., (1978), Flow of solids during forming and extrusion: some aspects of numerical solution, International Journal of Solids and Structures, **14**, pp. 15–38.
- Zyczkowski, M., (1981), Combined Loadings in the Theory of Plasticity, PWN-Polish Scientific, Warsaw.

Appendices

Appendix A

FEM Formulation of Deformation Analysis of Flat Rolling (Dixit, 1997)

In this work, the deformation analysis of warm flat rolling is carried out by finite element method (FEM) based on Eulerian flow formulation. The continuity equation and equation of motion along with mesh and boundary condition of strip is provided in Section 3.3. The procedure of FEM Galerkin formulation is briefly described here. Before that boundary conditions are discussed in detail.

A.1 Boundary Condition

The boundary conditions are shown in Fig. 3.3. Here, they are described in the text. Along AF and DE, the essential boundary conditions are given as

$$v_1 = V_1, v_2 = 0 \quad \text{on AF}, \tag{A.1}$$

$$v_1 = V_2, v_2 = 0 \quad \text{on DE}, \tag{A.2}$$

where v_1 and v_2 are the components of velocity in x_1 and x_2 directions, respectively. The inlet and exit velocities, V_1 and V_2, respectively, are related as

$$V_1 = V_2\left(1 - r_d\right), \tag{A.3}$$

where r_d is the fractional reduction given by

$$r_d = \frac{h_1 - h_2}{h_1}. \tag{A.4}$$

The roll velocity corresponding to V_2 is obtained as the velocity at the neutral point (a point at which shear stress changes its sign). The neutral point, in this formulation

is found by minimizing the total power with respect to the position of neutral point which is based on generalized upper bound theorem (Collins, 1969).

On the plane of symmetry EF and on the surface AB and CD (as shown in Fig. 3.3), the following boundary conditions are used,

$$t_1 = 0 \ , v_2 = 0, \tag{A.5}$$

where t_1 is the traction component in longitudinal direction. However, in the nodes adjacent to B and C, the boundary condition v_2=0 is replaced by t_2=0. On the roll-strip interface (boundary BC), the normal component of velocity, v_n = 0. This leads to

$$v_2 + v_1 \tan\phi = 0 \quad \text{on BC}, \tag{A.6}$$

where ϕ is the angular position of the point on the interface, the angular position of point C being zero. The frictional traction t_s on BC is related to normal traction t_n by Coulomb's friction model subjected to a limit on its maximum value as

$$|t_s| = f|t_n|, \tag{A.7}$$

where f is obtained from the model of Wanheim and Bay. At low pressures, f corresponds to equivalent Coulomb coefficient of friction and t_s and t_n are tangential and normal components of stress vector $\boldsymbol{t}$, whose components in the Cartesian system are obtained as

$$t_i = \sigma_{ij} n_j . \tag{A.8}$$

Here, n_j is the unit normal to the surface. The radius of curvature of BC is R'. According to the Hitchcock's formula, the radius of the deformed arc of contact R' to the roll radius R is given by

$$\frac{R'}{R} = \left(1 + \frac{F_\gamma}{C\delta}\right), \tag{A.9}$$

where F_r is the roll force and δ= (h_1–h_2) is the draft (difference in initial and final thickness). The constant C depends on the materials of rolls, its value for steel rolls being 4.62×10^4 MN m^{-2}.

A.2 Galerkin Formulation

In this work, Galerkin weak formulation has been used. Let v_1, v_2 and p be the functions that satisfy the essential boundary condition exactly. Thus, the continuity and momentum equation will becomes

$$\int_A \left[\left(\dot{\varepsilon}_{11} + \dot{\varepsilon}_{22} \right) w_p + \left(\frac{\partial \sigma_{11}}{\partial x_1} + \frac{\partial \sigma_{12}}{\partial x_2} \right) w_1 + \left(\frac{\partial \sigma_{21}}{\partial x_1} + \frac{\partial \sigma_{22}}{\partial x_2} \right) w_2 \right] \mathrm{d}x_1 \mathrm{d}x_2 = 0, \quad \text{(A.10)}$$

where A denotes the domain of a typical area element, and w_p, w_1 and w_2 are the weight functions that satisfies the boundary conditions, respectively. In index notations, Eq. (A.10) can be written as

$$\int_A \left[\dot{\varepsilon}_{ii} w_p + \sigma_{ij,j} w_i \right] \mathrm{d}x_1 \mathrm{d}x_2 = 0. \quad \text{(A.11)}$$

Using the divergence theorem, second integral can be simplified as

$$\int_A \sigma_{ij,j} w_i \mathrm{d}x_1 \mathrm{d}x_2 = \int_A \left(\sigma_{ij} w_i \right)_{,j} \mathrm{d}x_1 \mathrm{d}x_2 - \int_A \left(\sigma_{ij} w_{i,j} \right) \mathrm{d}x_1 \mathrm{d}x_2, \quad \text{(A.12)}$$

Using Gauss divergence theorem for two-dimensions, Eq. (A.12) yields

$$\begin{aligned} \int_A \sigma_{ij,j} w_i \mathrm{d}x_1 \mathrm{d}x_2 &= \oint_\Gamma \sigma_{ij} w_i n_j \mathrm{d}\Gamma - \int_A \left(\sigma_{ij} w_{i,j} \right) \mathrm{d}x_1 \mathrm{d}x_2, \\ &= \oint_\Gamma t_i w_i \mathrm{d}\Gamma - \int_A \left(\sigma_{ij} w_{i,j} \right) \mathrm{d}x_1 \mathrm{d}x_2. \end{aligned} \quad \text{(A.13)}$$

The last term of the right hand side of Eq. (A.13) can be written as

$$\int_A \left(\sigma_{ij} w_{i,j} \right) \mathrm{d}x_1 \mathrm{d}x_2 = \int_A \sigma_{ij} \frac{1}{2} \left[\left(w_{i,j} + w_{j,i} \right) + \left(w_{i,j} - w_{j,i} \right) \right] \mathrm{d}x_1 \mathrm{d}x_2. \quad \text{(A.14)}$$

Interchanging the dummy index and making use of symmetry yields

$$\int_A \sigma_{ij} \frac{1}{2} \left[\left(w_{i,j} - w_{j,i} \right) \right] \mathrm{d}x_1 \mathrm{d}x_2 = 0. \quad \text{(A.15)}$$

Therefore Eq. (A.14) becomes

$$\int_A \left(\sigma_{ij} w_{i,j} \right) \mathrm{d}x_1 \mathrm{d}x_2 = \int_A \sigma_{ij} \frac{1}{2} \left[\left(w_{i,j} + w_{j,i} \right) \right] \mathrm{d}x_1 \mathrm{d}x_2. \quad \text{(A.16)}$$

The symmetric part can be denoted as $\dot{\varepsilon}_{ij}(w)$. Thus,

$$\int_A \left(\sigma_{ij} w_{i,j}\right) \mathrm{d}x_1 \mathrm{d}x_2 = \int_A \sigma_{ij} \dot{\varepsilon}_{ij}(w)\, \mathrm{d}x_1 \mathrm{d}x_2. \tag{A.17}$$

Using Eq. (A.13) in Eq. (A.11) provides

$$\int_A \dot{\varepsilon}_{ii} w_p \mathrm{d}A + \int_A \sigma_{ij} \dot{\varepsilon}_{ij}(w) \mathrm{d}A - \int_{\Gamma i} t_i w_i \mathrm{d}\Gamma = 0. \tag{A.18}$$

For incompressible material deforming by Levy-Mises flow rule, the following equation is obtained:

$$\sigma_{ij} \dot{\varepsilon}_{ij}(w) = -p\dot{\varepsilon}_{ii}(w) + 2\eta_1 \dot{\varepsilon}_{ij} \dot{\varepsilon}_{ij}(w), \tag{A.19}$$

where η_1 is the Levy-Mises coefficient.

Incorporating Eq. (A.19) into Eq. (A.18), the weak weighted residual form is obtained as

$$\int_A I_a dA + \int_A I_b dA - \int_{\Gamma_1} I_c d\Gamma - \int_{\Gamma_2} I_d d\Gamma = 0, \tag{A.20}$$

where

$$I_a = \dot{\varepsilon}_{ii} w_p = \left[\dot{\varepsilon}_{11} + \dot{\varepsilon}_{22}\right] w_p ,$$

$$I_b = -p\left[\dot{\varepsilon}_{11}(w) + \dot{\varepsilon}_{22}(w)\right] + 2\eta_1 \left[\dot{\varepsilon}_{11}\dot{\varepsilon}_{11}(w) + 2\dot{\varepsilon}_{12}\dot{\varepsilon}_{12}(w) + \dot{\varepsilon}_{22}\dot{\varepsilon}_{22}(w)\right],$$

$$I_c = t_1 w_1,$$

$$I_d = t_2 w_2 . \tag{A.21}$$

Γ_1 and Γ_2 are the respectively those part of the boundaries where tractions t_1 and t_2 are specified.

A.3 Finite Element Approximation

Seeing the form Eq. (A.20), C^0 continuity is sufficient since pressure is of zero order derivative and the first order derivatives of velocity are present. Bilinear approximation and bi-quadric approximation have been adopted for pressure and velocity, respectively. Figure A.1 shows a typical quadrilateral element in natural coordinates that are selected to descretize the domain.

The approximation for v_1 and v_2 will be

$$\begin{Bmatrix} v_1 \\ v_2 \end{Bmatrix} = \left[N_v\right]\left\{v^e\right\}, \tag{A.22}$$

Here, weight functions for velocity and pressure are approximated using the same shape function as that of velocity and pressure, respectively:

$$\left\{w_v\right\} = \left[N_v\right]\left\{w_v^e\right\}. \tag{A.23}$$

The approximation for pressure will be

$$p = \left\{N_p\right\}^{\mathrm{T}}\left\{p^e\right\}. \tag{A.24}$$

The weight function for pressure is given as

$$\left\{w_p\right\} = \left\{N_p\right\}^{\mathrm{T}}\left\{w_p^e\right\}. \tag{A.25}$$

For geometry approximation, a nine noded element is used having the same shape function as the velocity. Thus,

$$x_1 = \left\{N\right\}^{\mathrm{T}}\left\{x_1^e\right\}, \tag{A.26}$$

$$x_2 = \left\{N\right\}^{\mathrm{T}}\left\{x_2^e\right\}, \tag{A.27}$$

where $\left\{x_1^e\right\}$ and $\left\{x_2^e\right\}$ are the vectors containing the nodal x_1 and x_2 coordinates respectively.

Since the nine noded elements were taken for velocity approximation, therefore the boundary element should be a three noded element. Figure A.1 shows a typical elements and nodes. The weight functions at the boundary will be given as

$$w_1 = \left\{w_1^b\right\}^{\mathrm{T}}\left\{N^b\right\}, \tag{A.28}$$

$$w_2 = \left\{w_2^b\right\}^{\mathrm{T}}\left\{N^b\right\}, \tag{A.29}$$

For the traction, the approximation is given as

$$t_1 = \left\{N^b\right\}^{\mathrm{T}}\left\{t_1^b\right\}, \tag{A.30}$$

$$t_2 = \left\{N^b\right\}^{\mathrm{T}}\left\{t_2^b\right\}, \tag{A.31}$$

where t_1 and t_2 are the nodal traction values of the traction. The expressions for N_i^b are given as

$$N_1^b = \frac{1}{2}\left(\varsigma^2 - \varsigma\right),\ N_2^b = \frac{1}{2}\left(\varsigma^2 + \varsigma\right),\quad N_3^b = \frac{1}{2}\left(1 - \varsigma^2\right), \tag{A.32}$$

where ς is the natural coordinate on the boundary.

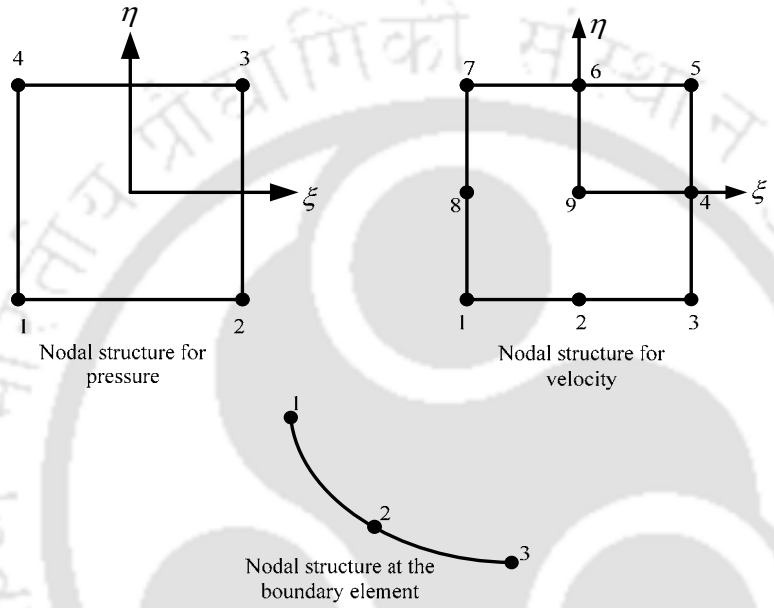

Fig. A.1. A typical diagram of the nodal structure of pressure, velocity and boundary element considered in the approximation

A.4 Finite Element Equations

The expressions of Eq. (A.21) can be expressed in matrix form to obtain the solution. Let us assume that $\{\dot{\varepsilon}\}$ is a vector given as

$$\{\dot{\varepsilon}\} = \begin{Bmatrix} \{\dot{\varepsilon}_{11}\} \\ \{\dot{\varepsilon}_{22}\} \\ \sqrt{2}\{\dot{\varepsilon}_{12}\} \end{Bmatrix} = \begin{Bmatrix} \dfrac{\partial v_1}{\partial x_1} \\ \dfrac{\partial v_2}{\partial x_2} \\ \dfrac{1}{\sqrt{2}}\left(\dfrac{\partial v_1}{\partial x_2} + \dfrac{\partial v_2}{\partial x_1}\right) \end{Bmatrix}. \tag{A.33}$$

Similarly $\{\dot{\varepsilon}(w)\}$ will be

$$\{\dot{\varepsilon}(w)\} = \begin{Bmatrix} \{\dot{\varepsilon}_{11}(w)\} \\ \{\dot{\varepsilon}_{22}(w)\} \\ \sqrt{2}\{\dot{\varepsilon}_{12}(w)\} \end{Bmatrix} = \begin{Bmatrix} \dfrac{\partial w_1}{\partial x_1} \\ \dfrac{\partial w_2}{\partial x_2} \\ \dfrac{1}{\sqrt{2}}\left(\dfrac{\partial w_1}{\partial x_2} + \dfrac{\partial w_2}{\partial x_1}\right) \end{Bmatrix}. \tag{A.34}$$

Using the approximation for velocities and weights, the strain rate vectors $\{\dot{\varepsilon}\}$ and $\{\dot{\varepsilon}(w)\}$ can be approximated as

$$\{\dot{\varepsilon}\} = [B]\{v^e\}, \tag{A.35}$$

$$\{\dot{\varepsilon}(w)\} = [B]\{w_v^e\}, \tag{A.36}$$

where

$$[B] = \begin{bmatrix} \dfrac{\partial N_1}{\partial x_1} & 0 & \dfrac{\partial N_2}{\partial x_1} & 0 & ---- & \dfrac{\partial N_9}{\partial x_1} & 0 \\ 0 & \dfrac{\partial N_1}{\partial x_2} & 0 & \dfrac{\partial N_2}{\partial x_2} & ---- & 0 & \dfrac{\partial N_9}{\partial x_2} \\ \dfrac{1}{\sqrt{2}}\dfrac{\partial N_1}{\partial x_2} & \dfrac{1}{\sqrt{2}}\dfrac{\partial N_1}{\partial x_1} & \dfrac{1}{\sqrt{2}}\dfrac{\partial N_2}{\partial x_2} & \dfrac{1}{\sqrt{2}}\dfrac{\partial N_2}{\partial x_1} & ---- & \dfrac{1}{\sqrt{2}}\dfrac{\partial N_9}{\partial x_2} & \dfrac{1}{\sqrt{2}}\dfrac{\partial N_9}{\partial x_1} \end{bmatrix}_{3\times 18} \tag{A.37}$$

From Eq. (A.33), the following form can be written:

$$\dot{\varepsilon}_{11} + \dot{\varepsilon}_{22} = \{1 \quad 1 \quad 0\}\begin{Bmatrix} \{\dot{\varepsilon}_{11}\} \\ \{\dot{\varepsilon}_{22}\} \\ \sqrt{2}\{\dot{\varepsilon}_{12}\} \end{Bmatrix} = \{1 \quad 1 \quad 0\}\{\dot{\varepsilon}\}, \tag{A.38}$$

Substituting Eq. (A.35) in Eq. (A.38) yields

$$\dot{\varepsilon}_{11} + \dot{\varepsilon}_{22} = \{1 \quad 1 \quad 0\}[B]\{v^e\} = \{m\}^T[B]\{v^e\} = \lfloor m \rfloor [B]\{v^e\}, \tag{A.39}$$

where

$$\{m\} = \begin{Bmatrix} 1 \\ 1 \\ 0 \end{Bmatrix}. \tag{A.40}$$

Similarly,

$$\dot{\varepsilon}_{11}(w)+\dot{\varepsilon}_{22}(w)=\lfloor m\rfloor[B]\{w_v^e\}=\{w_v^e\}^{\mathrm{T}}[B]^{\mathrm{T}}\{m\}, \tag{A.41}$$

Using Eqs. (A.25), (A.28), (A.29), (A.30), (A.31), (A.35), (A.36), (A.39) and (A.40), Eq. (A.20) becomes

$$\begin{aligned}
&\int_A \{w_p^e\}^{\mathrm{T}}\{N_p\}\lfloor m\rfloor[B]\{v^e\}\,\mathrm{d}x_1\mathrm{d}x_2\\
&+\int_A -\{w_v^e\}^{\mathrm{T}}[B]^{\mathrm{T}}\{m\}\{N_p\}^{\mathrm{T}}\{p^e\}\\
&+\int_A 2\eta_1\{w_v^e\}^{\mathrm{T}}[B]^{\mathrm{T}}[B]\{v^e\}\,\mathrm{d}x_1\mathrm{d}x_2\\
&=\int_{\Gamma_1}\{w_1^b\}^{\mathrm{T}}\{N_b\}\{N_b\}^{\mathrm{T}}\{t_1^b\}\,\mathrm{d}\Gamma+\int_{\Gamma_2}\{w_2^b\}^{\mathrm{T}}\{N_b\}\{N_b\}^{\mathrm{T}}\{t_2^b\}\,\mathrm{d}\Gamma.
\end{aligned} \tag{A.42}$$

On incorporating the following notation, we have

$$\begin{aligned}
\int_A -\{N_p\}\lfloor m\rfloor[B]\mathrm{d}x_1\mathrm{d}x_2&=[K_{pv}^e],\\
\int_A -[B]^T\{m\}\{N_p\}^{\mathrm{T}}\mathrm{d}x_1\mathrm{d}x_2&=[K_{vp}^e]=[K_{pv}^e]^{\mathrm{T}},\\
\int_A 2\eta_1[B]^{\mathrm{T}}[B]\,dxdy&=[K_{vv}^e],\\
\int_{\Gamma_1}\{N_b\}\{N_b\}^{\mathrm{T}}\{t_1^b\}d\Gamma&=\{f_1^b\},\\
\int_{\Gamma_2}\{N_b\}\{N_b\}^{\mathrm{T}}\{t_2^b\}d\Gamma&=\{f_2^b\},
\end{aligned} \tag{A.43}$$

The above integrals can be solved by transforming to the natural coordinates. On substituting Eq. (A.22) into Eq. (A.33) and assembling all the expressions with notations, the final finite element equation becomes

$$\sum_{e=1}^{ne}\{w^e\}^{\mathrm{T}}[K^e]\{\delta^e\}=\sum_{e=1}^{nb_1}\{w_1^b\}^{\mathrm{T}}\{f_1^b\}+\sum_{e=1}^{nb_1}\{w_2^b\}^{\mathrm{T}}\{f_2^b\}, \tag{A.44}$$

where n_e is the number of area elements and nb_1 and nb_2 are the number of boundary elements on Γ_1 and Γ_2, respectively. Further

$$\left\{w^e\right\}=\begin{Bmatrix}\left\{w_p^e\right\}\\ \left\{w_v^e\right\}\end{Bmatrix},\quad \left\{\delta^e\right\}=\begin{Bmatrix}\left\{p^e\right\}\\ \left\{v^e\right\}\end{Bmatrix} \text{ and } \left[K^e\right]=\begin{bmatrix}[0] & \left[K_{pv}^e\right]\\ \left[K_{vp}^e\right] & \left[K_{vv}^e\right]\end{bmatrix}, \quad \text{(A.45)}$$

For numerical evaluation, the variables of the area integral are transformed to natural coordinates (ξ,η) using following transformation

$$\int_A(----)\,\mathrm{d}x_1\mathrm{d}x_2=\int_{-1}^{+1}\int_{-1}^{+1}(----)|J|\mathrm{d}\xi\mathrm{d}\eta, \quad \text{(A.46)}$$

$$|J|=\begin{bmatrix}\frac{\mathrm{d}x_1}{\mathrm{d}\xi} & \frac{\mathrm{d}x_2}{\mathrm{d}\xi}\\ \frac{\mathrm{d}x_1}{\mathrm{d}\eta} & \frac{\mathrm{d}x_2}{\mathrm{d}\eta}\end{bmatrix}, \quad \text{(A.47)}$$

where $|J|$ is the elemental Jacobian matrix. Similarly, the boundary integrals are transformed by the relation

$$\int_\Gamma(---)\,\mathrm{d}\Gamma=\int_{-1}^{+1}(----)|J|\,\mathrm{d}\xi, \quad \text{(A.48)}$$

where $|J_b|$ is the Jacobian for boundary element and is given by

$$|J_b|=\sqrt{\left(\frac{\mathrm{d}x_1}{\mathrm{d}\xi}\right)^2+\left(\frac{\mathrm{d}x_2}{\mathrm{d}\xi}\right)^2}, \quad \text{(A.49)}$$

Along the boundary the coordinates (x_1,x_2) are approximated using 1-D quadrature shape function. All element matrices are evaluated using 3×3 Gauss quadrature. On considering a typical element, the finite element residual form becomes

$$\left\{w^e\right\}^T\left[K^e\right]\left\{\delta^e\right\}=\left\{w_1^b\right\}^T\left\{f_1^b\right\}+\left\{w_2^b\right\}^T\left\{f_2^b\right\}, \quad \text{(A.50)}$$

The assembled finite element weighted residual form is

$$\left\{W\right\}^T\left[K^e\right]\left\{\Delta\right\}=\left\{W\right\}^T\left\{F\right\}, \quad \text{(A.51)}$$

where $\{W\}$ is the global vector of nodal values of weight functions of pressure and velocity, $[K]$ is the global coefficient elemental matrix, $\{\Delta\}$ is the global vector of nodal values of pressure and velocity and $\{F\}$ is the global right hand side vector. After removing the arbitrary weight function, the FEM expression will be

$$[K]\{\Delta\} = \{F\}, \tag{A.52}$$

A.5 Application of Boundary Conditions

The velocity condition at the roll-strip interface can be given as

$$v_2 + v_1 \tan\phi = 0, \tag{A.53}$$

From Fig. (A.2), t_s and t_n can be written as

$$t_s = t_1 \cos\phi - t_2 \sin\phi, \tag{A.54}$$

$$t_n = -t_1 \sin\phi - t_2 \cos\phi, \tag{A.55}$$

The friction at a typical node on the work-roll interface is shown in Fig. A.2.

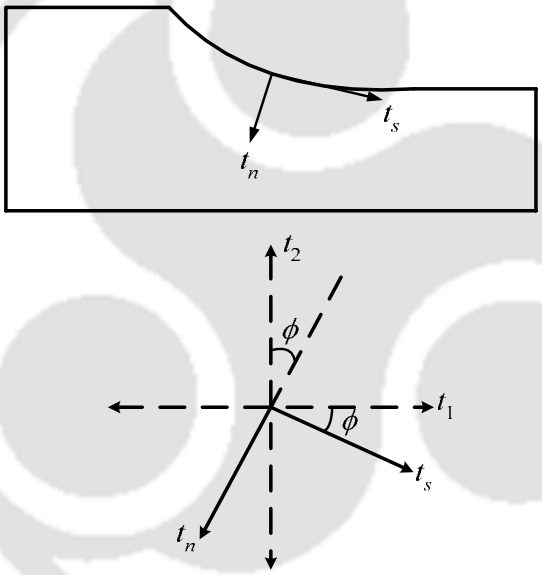

Fig. A.2. Shear and normal component of traction at work-roll interface

Substituting Eqs. (A.54) and (A.55) in Eq. (A.7) provides

$$t_1(1 + f\tan\phi) - t_2(\tan\phi - f) = 0. \tag{A.56}$$

Replacing $f = ck_s$ in Eq. (A.56) where k_s is –1 before neutral point and +1 after neutral point. Eq. (A.56) for a boundary element of FEM can be written as

$$\begin{Bmatrix} (t_{b_1}^1) \\ (t_{b_1}^2) \\ (t_{b_1}^3) \end{Bmatrix} (1 + ck_s \tan\phi) - \begin{Bmatrix} (t_{b_2}^1) \\ (t_{b_2}^2) \\ (t_{b_2}^3) \end{Bmatrix} (\tan\phi - ck_s) = 0. \tag{A.57}$$

In terms of the global right hand side vector, Eq. (A.57) can be written as

$$\{F\}_{(d_p+2k-1)}\left(1+ck_s\tan\phi\right)-\{F\}_{(d_p+2k)}\left(\tan\phi-ck_s\right)=\{0\}, \qquad \text{(A.58)}$$

where d_p is the total number of pressure nodes.

Procedure adopted for the application of the boundary condition at the node '*k*' is as follows:

- Change the $(d_p+2k-1)^{th}$ row of global coefficient matrix [*K*] by the following linear combination: $(1+ ck_s \tan\varphi)$ time $(d_p+2k-1)^{th}$ row of [*K*] – $(\tan\alpha- ck_s)$ time $(d_p+2k)^{th}$ row of [*K*].
- Make the $(d_p+2k-1)^{th}$ row of global right hand vector {*F*} zero.
- Change $(n_p+2k)^{th}$ of [*K*] as zero.
- The velocity boundary condition at the node is applied (Eq. A.6), set $(d_p+2k, d_p+2k-1)^{th}$ element of [K] to $\tan\phi$ and $(d_p+2k, d_p+2k)^{th}$ element of [K] to 1.

Procedures for applying essential boundary conditions at the other boundaries are as follows

- All the elements of stiffness matrix corresponding to specified degree of freedom are made zero except the diagonal terms.
- Replace the diagonal elements by 1.
- For specified degree of freedom, the right hand side vector elements are replaced and other elements are changed by subtracting the products of the corresponding coefficient element and the specified value.

After imposing the boundary condition, the final matrix equation is solved iteratively by the House holder method, because the resulting matrix of the mixed formulation is ill-conditioned. Once the solution is obtained in the form of primary variables for nodal pressure and velocity for any assumed position of neutral point, the secondary variables such as roll-force, roll-torque and slip can be calculated. This calculation is termed as post processing of the FEM.

Appendix B

Finite Difference Representation of Temperature Gradients

Assuming the heat flow from outer radius *b* to inner radius *a* as one-dimensional axi-symmetric, heat balance provides

$$2\pi a k_r \left(\frac{\partial T}{\partial r}\right)_{r=a} = 2\pi b k_r \left(\frac{\partial T}{\partial r}\right)_{r=b}, \tag{B.1}$$

or

$$a\left(\frac{\partial T}{\partial r}\right)_{r=a} = b\left(\frac{\partial T}{\partial r}\right)_{r=b}. \tag{B.2}$$

Average temperature gradient is approximately along the radial location of the roll given by

$$\left(\frac{\partial T}{\partial r}\right)_{avg} = \frac{\left(\frac{\partial T}{\partial r}\right)_{r=a} + \left(\frac{\partial T}{\partial r}\right)_{r=b}}{2} \simeq \frac{T_b - T_a}{b-a}, \tag{B.3}$$

Equations (B.2) and (B.3) provide

$$\left(\frac{\partial T}{\partial r}\right)_{r=a} = 2b\frac{T_b - T_a}{b^2 - a^2}, \tag{B.4}$$

$$\left(\frac{\partial T}{\partial r}\right)_{r=b} = 2a\frac{T_b - T_a}{b^2 - a^2}. \tag{B.5}$$

Appendix C

Derivation of Eq. (3.33) for Moving Heat Source by Integral Transform Technique

C.1 Temperature Distribution in Roll for Stationary Heat Source

Temperature distribution in the roll is obtained by solving governing heat conduction equation with the given boundary and initial conditions. An integral transform technique is employed for finding out the temperature distribution of the roll in the radial as well as circumferential direction. Figure C.1 shows the schematic location of heat input into roll. Let the heat input be given at outer radius b in the zone 2β angular displacement as shown in Fig. C.1. Remaining outer surface of the roll is subjected to convective heat loss. The inner surface at radius a is subjected to convective loss only. The work roll is assumed to be rigid and fixed in space.

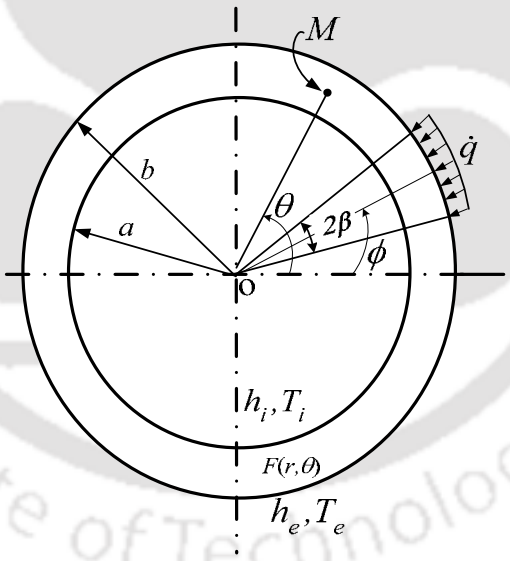

Fig. C.1. A stationary uniform heat source with stationary roll

The heat conduction equation is solved using the integral transform method consisting of the following steps (Özişik,1993):

(i) Appropriate formula for the integral transform and corresponding inversion formula are developed.

(ii) By the application of integral transformation, the partial derivatives with respect to the space variables are removed from the heat conduction equation, thus reducing it to an ordinary differential equation for the transform of temperature.

(iii) The resulting ordinary differential equation is solved subject to the transformed initial condition. The desired solution is obtained by inverting the solution, available as the transform of the temperature.

Step 1: Development of Integral-Transform Pair

To solve the heat conduction problems assuming polar coordinate system with the integral transform technique, appropriate integral-transform pairs are needed in the r and θ variables. The following two-dimensional heat conduction equation in polar coordinates involving $T(r,\theta,t)$ variables is given as

$$\frac{\partial^2 T}{\partial r^2}+\frac{1}{r}\frac{\partial T}{\partial r}+\frac{1}{r^2}\frac{\partial^2 T}{\partial \theta^2}=\frac{1}{\alpha_r}\frac{\partial T}{\partial t}, \tag{C.1}$$

$$-k_r\frac{\partial T}{\partial r}+h_i\left(T-T_i\right)=0 \qquad \text{at } r=a\,, \tag{C.2}$$

$$k_r\frac{\partial T}{\partial r}+h_e\left(T-T_e\right)=q(\theta) \qquad \text{at } r=b\,, \tag{C.3}$$

where $q(\theta)$ is the heat flux at the outer surface, h_e is the convective heat transfer coefficient at the outer surface, h_i is the convective heat transfer coefficient at the inner surface, α_r is the thermal diffusivity of the roll, T_i is the ambient temperature at inner periphery of the roll and T_e is the ambient temperature at the outer periphery of the roll. The heat flux at the outer surface at any location, ϕ is expressed as

$$q\left(\theta\right)=\begin{cases}\dot{q} & \text{for } \left(\phi-\beta\right)\le\theta\le\left(\phi+\beta\right)\\ 0 & \text{for } \left(\phi+\beta\right)\le\theta\le\left(2\pi+\phi-\beta\right)\end{cases}. \tag{C.4}$$

The initial condition is considered as

$$T\left(r,\theta,t\right)=F\left(r,\theta\right) \quad \text{for } t=0 \quad \text{in region, } a<r<b, \tag{C.5}$$

where $F\left(r,\theta\right)$ is the initial temperature distribution of the roll.

Employing the method of separation of variables, the temperature distribution can be expressed as

$$T\left(r,\theta,t\right)=\Psi\left(r,\theta\right)\Gamma\left(t\right). \tag{C.6}$$

Using Eq. (C.6) and Eq. (C.1), the following differential equation is obtained:

$$\frac{1}{\Psi}\left(\frac{\partial^2\Psi}{\partial r^2}+\frac{1}{r}\frac{\partial\Psi}{\partial r}+\frac{1}{r^2}\frac{\partial^2\Psi}{\partial\theta^2}\right)=\frac{1}{\alpha_r\Gamma(t)}\frac{\partial\Gamma(t)}{\partial t}=-\beta_m^2 \tag{C.7}$$

or,

$$\frac{1}{\Psi}\left(\frac{\partial^2\Psi}{\partial r^2}+\frac{1}{r}\frac{\partial\Psi}{\partial r}+\frac{1}{r^2}\frac{\partial^2\Psi}{\partial\theta^2}\right)+\beta_m^2=0 \tag{C.8}$$

$$\frac{\mathrm{d}\Gamma(t)}{\mathrm{d}t}+\alpha_r\beta_m^2\Gamma(t)=0. \tag{C.9}$$

Equation (C.9) is called the Helmholtz equation. Using separation of variables in r and θ, $\Psi(r,\theta)$ is decomposed as

$$\Psi(r,\theta)=R(r)\Phi(\theta). \tag{C.10}$$

Substitution of Eq. (C.10) into Eq. (C.8) provides

$$\frac{1}{R}\left(\frac{\mathrm{d}^2R}{\mathrm{d}r^2}+\frac{1}{r}\frac{\mathrm{d}R}{\mathrm{d}r}\right)+\frac{1}{r^2}\left(\frac{1}{\Phi}\frac{\mathrm{d}^2\Phi}{\mathrm{d}\theta^2}\right)+\beta_m^2=0. \tag{C.11}$$

The above equality is satisfied if each group of functions is equal to an arbitrary separation constant such that

$$\frac{1}{\Phi}\frac{\mathrm{d}^2\Phi}{\mathrm{d}\theta^2}=-n^2, \tag{C.12}$$

or,

$$\frac{\mathrm{d}^2\Phi}{\mathrm{d}\theta^2}+n^2\Phi=0. \tag{C.13}$$

Substituting Eq. (C.12) into Eq. (C.11), the following differential equation is obtained:

$$\frac{\mathrm{d}^2R}{\mathrm{d}r^2}+\frac{1}{r}\frac{\mathrm{d}R}{\mathrm{d}r}+\left(\beta_m^2-\frac{n^2}{r^2}\right)R=0 \tag{C.14}$$

Let $R\equiv R_n(\beta_m,r)$ *i.e.*, R is a function of r, but contains the constant β_m.

$$\frac{\mathrm{d}^2R_n(\beta_m,r)}{\mathrm{d}r^2}+\frac{1}{r}\frac{\mathrm{d}R_n(\beta_m,r)}{\mathrm{d}r}+\left(\beta_m^2-\frac{n^2}{r^2}\right)R_n(\beta_m,r)=0. \tag{C.15}$$

Equation (C.15) is the Bessel differential equation of the order n (Özisik, 1993).

Representation of $T(r,t)$ over $a \le r \le b$

The representation of an arbitrary function $T(r,t)$ defined in a finite interval $a \le r \le b$ in terms of the eigenfunctions is of the following eigenvalue problem:

$$\frac{\mathrm{d}^2 R_n(\beta_m, r)}{\mathrm{d}r^2} + \frac{1}{r}\frac{\mathrm{d}R_n(\beta_m, r)}{dr} + \left(\beta_m^2 - \frac{n^2}{r^2}\right) R_n(\beta_m, r) = 0 \ , \qquad \text{(C.16)}$$

with boundary conditions:

$$-\frac{\mathrm{d}R_n(\beta_m, r)}{\mathrm{d}r} + H_i R_n(\beta_m, r) = 0 \qquad \text{at } r = a, \qquad \text{(C.17)}$$

$$\frac{\mathrm{d}R_n(\beta_m, r)}{\mathrm{d}r} + H_e R_n(\beta_m, r) = 0 \qquad \text{at } r = b, \qquad \text{(C.18)}$$

where

$$H_i = \frac{h_i}{k_r}, \quad H_e = \frac{h_e}{k_r}. \qquad \text{(C.19)}$$

Equation (C.16) is a special case of Sturm−Liouville problem (Özisik, 1993). Hence, the functions, $R_n(\beta_m, r)$ have the following orthogonality property:

$$\int_a^b r R_n(\beta_m, r) R_n(\beta_{n_1}, r)\,\mathrm{d}r = \begin{cases} 0 & \text{for } m \ne n_1 \\ N_n(\beta_m) & \text{for } m = n_1 \end{cases}, \qquad \text{(C.20)}$$

where the norm $N_n(\beta_m)$ is defined by

$$N_n(\beta_m) = \int_a^b r \left\{R_n(\beta_m, r)\right\}^2 \mathrm{d}r \,. \qquad \text{(C.21)}$$

The representation of an arbitrary function, $T(r,t)$ defined in the interval $a \le r \le b$ in terms of eigenfunctions, $R_n(\beta_m, r)$ of the eigenvalue problem defined by Eq. (C.16) in the form

$$T(r,t) = \sum_{m=1}^{\infty} c_m R_n(\beta_m, r) \qquad \text{in} \quad a \le r \le b \qquad \text{(C.22)}$$

where c_m is an arbitrary constant. The unknown coefficient c_m is obtained by multiplying $rR_n(\beta_m, r)$ on both sides of Eq. (C.22) and integrating from $r = a$ to $r = b$. This provides,

$$\int_a^b T(r,t)\, rR_n(\beta_m,r)\,\mathrm{d}r = \int_a^b rR_n(\beta_m,r)\sum_{m=1}^{\infty} c_m R_n(\beta_m,r)\,\mathrm{d}r. \tag{C.23}$$

Using the orthogonality relation (Özisik, 1993), the constant c_m can be expressed as

$$c_m = \frac{1}{N_n(\beta_m)}\int_a^b rR_n(\beta_m,r)T(r,t)\,\mathrm{d}r. \tag{C.24}$$

Use of Eq. (C.24) into Eq. (C.22) provides

$$T(r,t) = \sum_{m=1}^{\infty}\frac{R_n(\beta_m,r)}{N_n(\beta_m)}\int_a^b rR_n(\beta_m,r)T(r,t)\,\mathrm{d}r. \tag{C.25}$$

The integral transform pair of Eq. (C.25) can be expressed as follows:

Inverse relation: $$T(r,t) = \sum_{m=1}^{\infty}\frac{R_n(\beta_m,r)}{N_n(\beta_m)}\tilde{T}(\beta_m,t) \tag{C.26}$$

Direct relation: $$\tilde{T}(\beta_m,t) = \int_a^b rR_n(\beta_m,r)T(r,t)\,\mathrm{d}r \tag{C.27}$$

where $\tilde{T}(\beta_m,t)$ is the integral transform of the function $T(r,t)$ with respect to the r variable, $N_n(\beta_m)$ is the norm and $R_n(\beta_m,r)$ is the eigenfunctions of the Bessel differential equation of order n given by Eq. (C.16). The detailed derivation of $N_n(\beta_m)$ and $R_n(\beta_m,r)$ are given in Appendix D.

Representation of $T(\theta)$ over $0 \le \theta \le 2\pi$

The representation of an arbitrary function $T(\theta)$ defined in the interval $0 \le \theta \le 2\pi$ in terms of the eigenfunctions of the eigenvalue problem associated with Eq. (C.13), the following eigenvalue problem

$$\frac{\mathrm{d}^2\Phi}{\mathrm{d}\theta^2} + n^2\Phi = 0\,. \tag{C.28}$$

The solution of Eq. (C.28) provides

$$\Phi(n,\theta) = \sum_{n=0}^{\infty}\left(A_n \sin n\theta + B_n \cos n\theta\right). \tag{C.29}$$

The function $T(\theta)$ is periodic in θ with a period of 2π in terms of functions in the form

$$T(\theta)=\sum_{n=0}^{\infty}\left(A_n\sin n\theta+B_n\cos n\theta\right) \qquad \text{in } 0\le\theta\le 2\pi \tag{C.30}$$

This requires the separation constants n to be taken as integers *i.e.*, $n = 0, 1, 2, 3\ldots$. Multiplying $\sin n\theta$ on both sides of Eq. (C.29) and integrating between $\theta=0$ to $\theta=2\pi$,

$$\int_0^{2\pi} T(\theta)\sin n\theta\ \mathrm{d}\theta = A_n\int_0^{2\pi}\sin^2 n\theta\ \mathrm{d}\theta + B_n\int_0^{2\pi}\sin n\theta\cos n\theta\ \mathrm{d}\theta = A_n\pi+0. \tag{C.31}$$

Hence, A_n is obtained as

$$A_n=\frac{1}{\pi}\int_0^{2\pi} T(\theta)\sin n\theta\mathrm{d}\theta \qquad \text{for } n=0,1,2,3,... \tag{C.32}$$

Similarly, for obtaining the coefficient B_n, both sides of Eq. (C.30) is multiplied by $\cos n\theta$ and integrating between $\theta=0$ to $\theta=2\pi$. Hence, the expression for B_n is obtained as

$$B_n=\begin{cases}\dfrac{1}{\pi}\displaystyle\int_0^{2\pi} T(\theta)\cos n\theta\mathrm{d}\theta & \text{for } n=1,2,3,...\\[2ex] \dfrac{1}{2\pi}\displaystyle\int_0^{2\pi} T(\theta)\ \mathrm{d}\theta & \text{for } n=0\end{cases}. \tag{C.33}$$

Note that θ in Eqs. (C.32) and (C.33) can be replaced by ϕ, as it is a dummy variable. Inserting Eqs. (C.32) and (C.33) into Eq. (C.30), the arbitrary function of temperature $T(\theta)$ can be written as

$$T(\theta)=\frac{\varepsilon}{\pi}\sum_{n=0}^{\infty}\int_0^{2\pi} T(\phi)\cos n(\theta-\phi)\mathrm{d}\phi, \tag{C.34}$$

where

$$\varepsilon=\begin{cases}\dfrac{1}{2} & \text{for } n=0\\[2ex] 1 & \text{for } n=1,2,3,...\end{cases}. \tag{C.35}$$

The complete solution for $T(r,\theta,t)$ is constructed by the product of theses elementary solutions is given as

$$T(r,\theta,t)=T(r,t)\times T(\theta). \tag{C.36}$$

Inserting Eqs. (C.25) and (C.34) into Eq. (C.35), the auxiliary temperature distribution can be expressed as

$$T(r,\theta,t)=\left(\sum_{m=1}^{\infty}\frac{R_n(\beta_m,r)}{N_n(\beta_m)}\int_a^b rR_n(\beta_m,r)T(r,t)\,\mathrm{d}r\right)\times\left(\frac{\varepsilon}{\pi}\sum_{n=0}^{\infty}\int_0^{2\pi}T(\phi)cos\,n(\theta-\phi)\;\mathrm{d}\phi\right),\tag{C.37}$$

or,

$$T(r,\theta,t)=\frac{\varepsilon}{\pi}\sum_{n=0}^{\infty}\sum_{m=1}^{\infty}\frac{R_n(\beta_m,r)}{N_n(\beta_m)}\int_a^b\int_0^{2\pi}rR_n(\beta_m,r)\;cos\,n(\theta-\phi)T(r,\phi,t)\,\mathrm{d}\phi\mathrm{d}r.\tag{C.38}$$

The integral transform pair of Eq. (C.38) can be written into following forms:

Inverse relation: $$T(r,\theta,t)=\frac{\varepsilon}{\pi}\sum_{n=0}^{\infty}\sum_{m=1}^{\infty}\frac{R_n(\beta_m,r)}{N_n(\beta_m)}\tilde{\bar{T}}(\beta_m,n,t).\tag{C.39}$$

Direct relation: $$\tilde{\bar{T}}(\beta_m,n,t)=\int_a^b\int_0^{2\pi}rR_n(\beta_m,r)\;cos\,n(\theta-\phi)T(r,\phi,t)\,\mathrm{d}\phi\mathrm{d}r\tag{C.40}$$

n is positive integer 0, 1, 2, 3,… and β_m is the positive roots of the transcendental characteristics equations. The transcendental characteristics equation is given in Appendix D.

Step 2: Integral Transform of Heat Conduction Problem

Once the integral transform pair is obtained the partial derivatives with respect to the space variables r and θ is to be removed from the governing heat conduction equation. The removal of the partial derivative with respect to the variable, θ from Eq. (C.1) is accomplished using integral-transform pair equation.

The integral-transform pair of the variable θ for the function $T(r,\theta,t)$ is given by Eq. (C.34) as

Inverse relation: $$T(r,\theta,t)=\frac{\varepsilon}{\pi}\sum_{n=0}^{\infty}\bar{T}(r,n,t),\tag{C.41}$$

Direct relation: $$\bar{T}(r,n,t)=\int_0^{2\pi}cos\,n(\theta-\phi)T(r,\phi,t)\,\mathrm{d}\phi.\tag{C.42}$$

The following time-dependent heat conduction problem for a hollow cylinder of inner radius, a and outer radius, b is considered with varying temperature with respect to the variables r and θ.

The integral transform of Eq. (C.1) with respect to θ is given by the application of Eq. (C.42) as

$$\frac{\partial^2 \overline{T}}{\partial r^2}+\frac{1}{r}\frac{\partial \overline{T}}{\partial r}+\frac{1}{r^2}\int_0^{2\pi}\cos n\left(\theta-\phi\right)\frac{\partial^2 \overline{T}}{\partial \theta^2}\,\mathrm{d}\theta=\frac{1}{\alpha_r}\frac{\partial \overline{T}}{\partial t} \tag{C.43}$$

where bar over T denotes the integral transform with respect to θ. Note that in Eq. (C.43) integration of cosine function is performed with respect to θ, instead of ϕ. In the integral term of Eq. (C.43), the partial differential is transformed into ordinary differential by integrating by parts in the following manner with notation $\Phi\left(\theta\right)\equiv\cos n\left(\theta-\phi\right)$:

$$\begin{aligned}\int_0^{2\pi}\Phi\left(\theta\right)\frac{\partial^2 T}{\partial \theta^2}\,\mathrm{d}\theta&=\Phi\left(\theta\right)\frac{\partial T}{\partial \theta}\bigg|_0^{2\pi}-\int_0^{2\pi}\frac{\mathrm{d}\Phi\left(\theta\right)}{\mathrm{d}\theta}\frac{\partial T}{\partial \theta}\,\mathrm{d}\theta\\&=\Phi\left(\theta\right)\frac{\partial T}{\partial \theta}\bigg|_0^{2\pi}-T\frac{\mathrm{d}\Phi\left(\theta\right)}{\mathrm{d}\theta}\bigg|_0^{2\pi}+\int_0^{2\pi}T\frac{\mathrm{d}^2\Phi\left(\theta\right)}{\mathrm{d}\theta^2}\,\mathrm{d}\theta\\&=\left[\Phi\left(\theta\right)\frac{\partial T}{\partial \theta}-T\frac{\mathrm{d}\Phi\left(\theta\right)}{\mathrm{d}\theta}\right]_0^{2\pi}+\int_0^{2\pi}T\frac{\mathrm{d}^2\Phi\left(\theta\right)}{\mathrm{d}\theta^2}\,\mathrm{d}\theta\end{aligned} \tag{C.44}$$

The first term of Eq. (C.44) vanishes as the functions are cyclic with a period of 2π. This yields

$$\int_0^{2\pi}\Phi\left(\theta\right)\frac{\partial^2 T}{\partial \theta^2}\,\mathrm{d}\theta=\int_0^{2\pi}T\frac{\mathrm{d}^2\Phi\left(\theta\right)}{\mathrm{d}\theta^2}\mathrm{d}\theta. \tag{C.45}$$

Use of Eq. (C.12) into Eq. (C.45), the following equation is obtained

$$\int_0^{2\pi}T\frac{\mathrm{d}^2\Phi\left(\theta\right)}{\mathrm{d}\theta^2}\,\mathrm{d}\theta=-n^2\int_0^{2\pi}\Phi\left(\theta\right)T\mathrm{d}\theta=-n^2\overline{T}\,. \tag{C.46}$$

Using Eqs. (C.45) and (C.46) into Eq. (C.43) provides

$$\frac{\partial^2 \overline{T}}{\partial r^2}+\frac{1}{r}\frac{\partial \overline{T}}{\partial r}-\frac{n^2}{r^2}\overline{T}=\frac{1}{\alpha_r}\frac{\partial \overline{T}}{\partial t}\qquad \text{in } a\le r\le b\quad t>0\,, \tag{C.47}$$

Similarly, the boundary conditions as well as the initial condition can be written using integral transform with respect to θ as

Boundary conditions:

$$-\frac{\partial \overline{T}}{\partial r}+H_i\left(\overline{T}-\overline{T}_i\right)=0 \qquad \text{at } r=a, \tag{C.48}$$

$$\frac{\partial \overline{T}}{\partial r}+H_e\left(\overline{T}-\overline{T}_e\right)=\overline{\dot{q}} \qquad \text{at } r=b, \tag{C.49}$$

Initial condition:

$$\overline{T}\left(r,n,t\right)=\overline{F}\left(r,n\right) \qquad \text{for } t=0\,. \tag{C.50}$$

Now, the integral transform with respect to variable r for the function, $\overline{T}\left(r,n,t\right)$ is obtained from the transform pair given in Eqs. (C.26) and (C.27), as follows:

Inverse formula:
$$\overline{T}\left(r,n,t\right)=\sum_{m=1}^{\infty}\frac{R_n\left(\beta_m,r\right)}{N_n\left(\beta_m\right)}\tilde{\overline{T}}\left(\beta_m,n,t\right), \tag{C.51}$$

Direct formula:
$$\tilde{\overline{T}}\left(\beta_m,n,t\right)=\int_a^b rR_n\left(\beta_m,r\right)\overline{T}\left(r,n,t\right)\mathrm{d}r, \tag{C.52}$$

where tilde over $\tilde{\overline{T}}$ denotes the integral transform with respect to the r variable. The integral transform with respect to r is obtained by using Eqs. (C.51) and (C.52) into Eq. (C.47). The following expression is obtained:

$$\int_a^b rR_n\left(\beta_m,r\right)\left(\frac{\partial^2\overline{T}}{\partial r^2}+\frac{1}{r}\frac{\partial\overline{T}}{\partial r}-\frac{n^2}{r^2}\overline{T}\right)\mathrm{d}r=\frac{1}{\alpha_r}\frac{\partial\tilde{\overline{T}}}{\partial t}. \tag{C.53}$$

The integral term in Eq. (C.53) is evaluated by integrating by parts twice and utilizing the properties of the eigenvalue problem for the function $R_n\left(\beta_m,r\right)$ along with the boundary conditions as (Özisik, 1993)

$$I\equiv\int_a^b rR_n\left(\beta_m,r\right)\left(\frac{\partial^2\overline{T}}{\partial r^2}+\frac{1}{r}\frac{\partial\overline{T}}{\partial r}-\frac{n^2}{r^2}\overline{T}\right)\mathrm{d}r$$

$$=\int_a^b rR_n\left(\beta_m,r\right)\frac{\partial^2\overline{T}}{\partial r^2}\mathrm{d}r+\int_a^b R_n\left(\beta_m,r\right)\frac{\partial\overline{T}}{\partial r}\mathrm{d}r-\int_a^b rR_n\left(\beta_m,r\right)\frac{n^2}{r^2}\overline{T}\mathrm{d}r$$

$$=rR_n\left(\beta_m,r\right)\frac{\partial\overline{T}}{\partial r}\bigg|_a^b-\int_a^b\left(r\frac{\mathrm{d}R_n\left(\beta_m,r\right)}{\mathrm{d}r}+R_n\left(\beta_m,r\right)\right)\frac{\partial\overline{T}}{\partial r}\mathrm{d}r$$

$$+\int_a^b R_n\left(\beta_m,r\right)\frac{\partial\overline{T}}{\partial r}\mathrm{d}r-\int_a^b rR_n\left(\beta_m,r\right)\frac{n^2}{r^2}\overline{T}\mathrm{d}r$$

$$= rR_n(\beta_m,r)\frac{\partial \bar{T}}{\partial r}\bigg|_a^b - \int_a^b r\frac{\mathrm{d}R_n(\beta_m,r)}{\mathrm{d}r}\frac{\partial \bar{T}}{\partial r}\mathrm{d}r - \int_a^b R_n(\beta_m,r)\frac{\partial \bar{T}}{\partial r}\mathrm{d}r$$
$$+\int_a^b R_n(\beta_m,r)\frac{\partial \bar{T}}{\partial r}\mathrm{d}r - \int_a^b rR_n(\beta_m,r)\frac{n^2}{r^2}\bar{T}\mathrm{d}r$$
$$= rR_n(\beta_m,r)\frac{\partial \bar{T}}{\partial r}\bigg|_a^b - \int_a^b r\frac{\mathrm{d}R_n(\beta_m,r)}{\mathrm{d}r}\frac{\partial \bar{T}}{\partial r}\mathrm{d}r - \int_a^b rR_n(\beta_m,r)\frac{n^2}{r^2}\bar{T}\mathrm{d}r$$
$$= rR_n(\beta_m,r)\frac{\partial \bar{T}}{\partial r}\bigg|_a^b - r\bar{T}\frac{\mathrm{d}R_n(\beta_m,r)}{\mathrm{d}r}\bigg|_a^b$$
$$+\int_a^b\left(r\frac{\mathrm{d}^2R_n(\beta_m,r)}{\mathrm{d}r^2}+\frac{\mathrm{d}R_n(\beta_m,r)}{\mathrm{d}r}\right)\bar{T}\mathrm{d}r - \int_a^b rR_n(\beta_m,r)\frac{n^2}{r^2}\bar{T}\mathrm{d}r$$
$$= rR_n(\beta_m,r)\frac{\partial \bar{T}}{\partial r}\bigg|_a^b - r\bar{T}\frac{\mathrm{d}R_n(\beta_m,r)}{\mathrm{d}r}\bigg|_a^b$$
$$+\int_a^b\left(r\frac{\mathrm{d}^2R_n(\beta_m,r)}{\mathrm{d}r^2}+\frac{\mathrm{d}R_n(\beta_m,r)}{\mathrm{d}r}-\left(rR_n(\beta_m,r)\right)\frac{n^2}{r^2}\right)\bar{T}\mathrm{d}r$$
$$= \left[r\left(R_n(\beta_m,r)\frac{\partial \bar{T}}{\partial r}-\bar{T}\frac{\mathrm{d}R_n(\beta_m,r)}{\mathrm{d}r}\right)\right]_a^b$$
$$+\int_a^b r\left(\frac{\mathrm{d}^2R_n(\beta_m,r)}{\mathrm{d}r^2}+\frac{1}{r}\frac{\mathrm{d}R_n(\beta_m,r)}{\mathrm{d}r}-\frac{n^2}{r^2}R_n(\beta_m,r)\right)\bar{T}\mathrm{d}r$$

$$I = b\left(R_n(\beta_m,r)\frac{\partial \bar{T}}{\partial r}-\bar{T}\frac{\mathrm{d}R_n(\beta_m,r)}{\mathrm{d}r}\right)\bigg|_{r=b}$$
$$-a\left(R_n(\beta_m,r)\frac{\partial \bar{T}}{\partial r}-\bar{T}\frac{\mathrm{d}R_n(\beta_m,r)}{\mathrm{d}r}\right)\bigg|_{r=a}$$
$$+\int_a^b r\left(\frac{\mathrm{d}^2R_n(\beta_m,r)}{\mathrm{d}r^2}+\frac{1}{r}\frac{\mathrm{d}R_n(\beta_m,r)}{\mathrm{d}r}-\frac{n^2}{r^2}R_n(\beta_m,r)\right)\bar{T}\mathrm{d}r. \qquad \text{(C.54)}$$

Now, multiplying by $r\bar{T}$ on both sides of Eq. (C.15) and integrating between $r = a$ to $r = b$, provides

$$\int_a^b r\left(\frac{\mathrm{d}^2R_n(\beta_m,r)}{\mathrm{d}r^2}+\frac{1}{r}\frac{\mathrm{d}R_n(\beta_m,r)}{\mathrm{d}r}-\frac{n^2}{r^2}R_n(\beta_m,r)\right)\bar{T}\mathrm{d}r = -\beta_m^2\int_a^b rR_n(\beta_m,r)\bar{T}\mathrm{d}r, \qquad \text{(C.55)}$$

Use of Eq. (C.27) into Eq. (C.55) provides

$$\int_a^b r\left(\frac{\mathrm{d}^2 R_n(\beta_m,r)}{\mathrm{d}r^2}+\frac{1}{r}\frac{\mathrm{d}R_n(\beta_m,r)}{\mathrm{d}r}-\frac{n^2}{r^2}R_n(\beta_m,r)\right)\bar{T}\,\mathrm{d}r=-\beta_m^2\tilde{\bar{T}}(\beta_m,n,t). \tag{C.56}$$

Using Eqs. (C.56) and (C.54) into Eq. (C.53), the following equation is obtained:

$$\begin{aligned}\frac{\mathrm{d}\tilde{\bar{T}}(\beta_m,n,t)}{\mathrm{d}t}+\alpha_r\beta_m^2\tilde{\bar{T}}(\beta_m,n,t)=\alpha_r b\left(R_n(\beta_m,r)\frac{\partial\bar{T}}{\partial r}-\bar{T}\frac{\mathrm{d}R_n(\beta_m r)}{\mathrm{d}r}\right)\Bigg|_{r=b}\\ -\alpha_r a\left(R_n(\beta_m,r)\frac{\partial\bar{T}}{\partial r}-\bar{T}\frac{\mathrm{d}R_n(\beta_m r)}{\mathrm{d}r}\right)\Bigg|_{r=a}.\end{aligned} \tag{C.57}$$

From the boundary conditions at $r = b$, given in Eqs. (C.49) and (C.18) the following equation is obtained:

$$\frac{\partial\bar{T}}{\partial r}+H_e\left(\bar{T}-\bar{T}_e\right)=\frac{\bar{\dot{q}}}{k_r} \qquad \text{at } r=b \tag{C.58}$$

$$\frac{\mathrm{d}R_n(\beta_m,r)}{\mathrm{d}r}+H_eR_n(\beta_m,r)=0 \qquad \text{at } r=b \tag{C.59}$$

Multiplying Eq. (C.58) by $R_n(\beta_m,r)$ and Eq. (C.59) by $\bar{T}$, one can obtain

$$R_n(\beta_m,r)\left(\frac{\partial\bar{T}}{\partial r}+H_e\left(\bar{T}-\bar{T}_e\right)=\frac{\bar{\dot{q}}}{k_r}\right), \tag{C.60}$$

$$\bar{T}\left(\frac{dR_n(\beta_m,r)}{dr}+H_eR_n(\beta_m,r)=0\right), \tag{C.61}$$

Subtracting Eq. (C.60) from Eq. (C.61):

$$\begin{aligned}\left(R_n(\beta_m,r)\frac{\partial\bar{T}}{\partial r}-\bar{T}\frac{\mathrm{d}R_n(\beta_m,r)}{\mathrm{d}r}\right)\Bigg|_{r=b}\\ +H_eR_n(\beta_m,b)\left(\bar{T}-\bar{T}_e\right)-H_e\bar{T}R_n(\beta_m,b)=\frac{\bar{\dot{q}}}{k_r}R_n(\beta_m,b),\end{aligned} \tag{C.62}$$

Simplifying Eq. (C.62), the following equation is obtained:

$$\left(R_n(\beta_m,r)\frac{\partial\bar{T}}{\partial r}-\bar{T}\frac{\mathrm{d}R_n(\beta_m,r)}{\mathrm{d}r}\right)\Bigg|_{r=b}=H_e\bar{T}_eR_n(\beta_m,b)+\frac{\bar{\dot{q}}}{k_r}R_n(\beta_m,b). \tag{C.63}$$

Similarly, from the boundary conditions at $r = a$ given in Eqs. (C.48) and (C.17), the following equation is obtained:

$$-\frac{\partial \bar{T}}{\partial r}+H_i\left(\bar{T}-\bar{T}_i\right)=0 \qquad \text{at } r=a, \tag{C.64}$$

$$-\frac{\mathrm{d}R_n\left(\beta_m,r\right)}{\mathrm{d}r}+H_iR_n\left(\beta_m,r\right)=0 \qquad \text{at } r=a. \tag{C.65}$$

Multiplication of Eq. (C.64) by $R_n\left(\beta_m,r\right)$ and Eq. (C.65) by $\bar{T}$ results

$$R_n\left(\beta_m,r\right)\left(-\frac{\partial \bar{T}}{\partial r}+H_i\left(\bar{T}-\bar{T}_i\right)=0\right), \tag{C.66}$$

$$\bar{T}\left(-\frac{\mathrm{d}R_n\left(\beta_m,r\right)}{\mathrm{d}r}+H_iR_n\left(\beta_m,r\right)=0\right). \tag{C.67}$$

Subtracting Eq. (C.66) from Eq. (C.67):

$$\begin{aligned}&\left(-R_n\left(\beta_m,r\right)\frac{\partial \bar{T}}{\partial r}+\bar{T}\frac{\mathrm{d}R_n\left(\beta_m,r\right)}{\mathrm{d}r}\right)\Bigg|_{r=a}\\&\quad+H_iR_n\left(\beta_m,a\right)\left(\bar{T}-\bar{T}_i\right)-H_iR_n\left(\beta_m,a\right)\bar{T}=0,\end{aligned} \tag{C.68}$$

or,

$$-\left(R_n\left(\beta_m,r\right)\frac{\partial \bar{T}}{\partial r}-\bar{T}\frac{\mathrm{d}R_n\left(\beta_m,r\right)}{\mathrm{d}r}\right)\Bigg|_{r=a}=H_i\bar{T}R_n\left(\beta_m,a\right). \tag{C.69}$$

Substituting Eqs. (C.63) and (C.69) into Eq. (C.57) provides

$$\begin{aligned}\frac{\mathrm{d}\tilde{\bar{T}}\left(\beta_m,n,t\right)}{\mathrm{d}t}+\alpha\beta_m^2\tilde{\bar{T}}\left(\beta_m,n,t\right)=\alpha_r&\left\{\left(H_e\bar{T}_eb\right)+\frac{\bar{\dot{q}}b}{k_r}\right\}R_n\left(\beta_m,b\right)\\&+\alpha_r\left(H_i\bar{T}_ia\right)R_n\left(\beta_m,a\right),\end{aligned} \tag{C.70}$$

which is an ordinary differential equation with respect to t.

Step 3: Solution for transform and inversion

The differential equation given in Eq. (C.70) along with the initial condition can be expressed in double transform, using inverse integral relations defined in Eqs. (C.39) and (C.40) as

$$\frac{\mathrm{d}\tilde{\bar{T}}\left(\beta_m,n,t\right)}{\mathrm{d}t}+\alpha_r\beta_m^2\tilde{\bar{T}}\left(\beta_m,n,t\right)=A_n\left(\beta_m,n,t\right), \tag{C.71}$$

where

$$A_n\left(\beta_m,n,t\right)=\alpha_r\left(H_e\overline{T}_e b+\frac{\overline{\dot{q}}b}{k}\right)R_n\left(\beta_m,b\right)+\alpha_r\left(H_i\overline{T}_i a\right)R_n\left(\beta_m,a\right). \tag{C.72}$$

In Eq. (C.72), the terms $\overline{\dot{q}}$, $\overline{T}_e$ and $\overline{T}_i$ are expressed as

$$\overline{\dot{q}}=\int_0^{2\pi} q\left(\theta\right)\cos n\left(\theta-\phi\right)\mathrm{d}\theta, \tag{C.73}$$

$$\overline{T}_e=\int_0^{2\pi} T_e\left(\theta\right)\cos n\left(\theta-\phi\right)\mathrm{d}\theta, \tag{C.74}$$

and

$$\overline{T}_i=\int_0^{2\pi} T_i\left(\theta\right)\cos n\left(\theta-\phi\right)\mathrm{d}\theta. \tag{C.75}$$

Initial condition:

$$\tilde{\overline{T}}\left(\beta_m,n,t\right)=\tilde{\overline{F}}\left(\beta_m,n\right) \quad \text{for} \quad t=0. \tag{C.76}$$

Let $p_1=\alpha_r\beta_m^2$, $p_2=A\left(\beta_m,n,t\right)$ and $p_3=\int p_1\left(t\right)\mathrm{d}t$. This enables the Eq. (C.71) to be written in the following form:

$$\frac{\mathrm{d}\tilde{\overline{T}}\left(\beta_m,n,t\right)}{\mathrm{d}t}+p_1\tilde{\overline{T}}\left(\beta_m,n,t\right)=p_2. \tag{C.77}$$

The solution of the Eq. (C.77) provides

$$\tilde{\overline{T}}\left(\beta_m,n,t\right)=\exp\left(-p_3\right)\left\{\int\exp\left(p_3\right)p_2\mathrm{d}t+C\right\}, \tag{C.78}$$

where C is an arbitrary constant, which can be evaluated using the initial condition. Substituting the value of p_1, p_2 and p_3 into Eq. (C.78):

$$\tilde{\overline{T}}\left(\beta_m,n,t\right)=\exp\left(-\alpha_r\beta_m^2t\right)\left\{\int\exp\left(\alpha_r\beta_m^2t\right)A_n\left(\beta_m,n,t\right)\mathrm{d}t+C\right\}, \tag{C.79}$$

Evaluating the integral term in Eq. (C.79), the following expression is obtained:

$$\tilde{\overline{T}}\left(\beta_m,n,t\right)=\frac{A_n\left(\beta_m,n,t\right)}{\alpha_r\beta_m^2}+\exp\left(-\alpha_r\beta_m^2t\right)C. \tag{C.80}$$

Using the initial condition given in Eq. (C.76) at $t = 0$, C can be obtained as follows:

$$C=\tilde{\overline{F}}\left(\beta_m,n\right)-\frac{A_n\left(\beta_m,n\right)}{\alpha_r\beta_m^2}. \tag{C.81}$$

Substitution of Eq. (C.81) into Eq. (C.80), provides

$$\bar{\bar{T}}\left(\beta_m,n,t\right)=\frac{A_n\left(\beta_m,n,t\right)}{\alpha_r\beta_m^2}+\bar{\bar{F}}\left(\beta_m,n\right)\exp\left(-\alpha_r\beta_m^2t\right)-\left(\frac{A_n\left(\beta_m,n,t\right)}{\alpha_r\beta_m^2}\right)\exp\left(-\alpha_r\beta_m^2t\right). \tag{C.82}$$

Substituting Eq. (C.82) into Eq. (C.39), the temperature distribution is obtained as

$$T\left(r,\theta,t\right)=\frac{\varepsilon}{\pi}\sum_{n=0}^{\infty}\sum_{m=1}^{\infty}\frac{R_n\left(\beta_m,r\right)}{N_n\left(\beta_m\right)}\left\{\begin{aligned}&\exp\left(-\alpha_r\beta_m^2t\right)\bar{\bar{F}}\left(\beta_m,n\right)\\&+\left(\frac{A_n\left(\beta_m,n,t\right)}{\alpha_r\beta_m^2}\right)\left(1-\exp\left(-\alpha_r\beta_m^2t\right)\right)\end{aligned}\right\} \tag{C.83}$$

where

$$\bar{\bar{F}}\left(\beta_m,n\right)=\int_a^b\int_0^{2\pi}rR_n\left(\beta_m,r\right)\cos n\left(\theta-\phi\right)F\left(r,\theta\right)\mathrm{d}\theta\mathrm{d}r. \tag{C.84}$$

The series solution of Eq. (C.83) can be expressed as

$$\begin{aligned}T\left(r,\theta,t\right)=&\frac{1}{2\pi}\sum_{m=1}^{\infty}\frac{R_0\left(\beta_m,r\right)}{N_0\left(\beta_m\right)}\left\{\exp\left(-\alpha_r\beta_m^2t\right)\bar{\bar{F}}\left(\beta_m,0\right)+\left(\frac{A_0\left(\beta_m,0,t\right)}{\alpha_r\beta_m^2}\right)\left(1-\exp\left(-\alpha_r\beta_m^2t\right)\right)\right\}\\&+\frac{1}{\pi}\sum_{n=1}^{\infty}\sum_{m=1}^{\infty}\frac{R_n\left(\beta_m,r\right)}{N_n\left(\beta_m\right)}\left\{\exp\left(-\alpha_r\beta_m^2t\right)\bar{\bar{F}}\left(\beta_m,n\right)+\left(\frac{A_n\left(\beta_m,n,t\right)}{\alpha_r\beta_m^2}\right)\left(1-\exp\left(-\alpha_r\beta_m^2t\right)\right)\right\},\end{aligned} \tag{C.85}$$

where

$$A_0\left(\beta_m,0,t\right)=\alpha_r\left(H_e\bar{T}_eb+\frac{\bar{\dot{q}}b}{k_r}\right)R_0\left(\beta_m,b\right)+\alpha_r\left(H_i\bar{T}_ia\right)R_0\left(\beta_m,a\right), \tag{C.86}$$

The expression of $R_0\left(\beta_m,b\right)$ and $R_0\left(\beta_m,a\right)$ is obtained from Eqs. (D.51) and (D.59) taking $n = 0$, respectively. Eq. (C.85) can be written as

$$\begin{aligned}T\left(r,\theta,t\right)=&\frac{1}{2\pi}\sum_{m=1}^{\infty}\frac{R_0\left(\beta_m,r\right)}{N_0\left(\beta_m\right)}\exp\left(-\alpha_r\beta_m^2t\right)\bar{\bar{F}}\left(\beta_m,0\right)\\&+\frac{1}{2\pi}\sum_{m=1}^{\infty}\frac{R_0\left(\beta_m,r\right)}{N_0\left(\beta_m\right)}\frac{A_0\left(\beta_m,0,t\right)}{\alpha_r\beta_m^2}\left\{1-\exp\left(-\alpha_r\beta_m^2t\right)\right\}\\&+\frac{1}{\pi}\sum_{n=1}^{\infty}\sum_{m=1}^{\infty}\frac{R_n\left(\beta_m,r\right)}{N_n\left(\beta_m\right)}\left\{\exp\left(-\alpha_r\beta_m^2t\right)\bar{\bar{F}}\left(\beta_m,n\right)+\left(\frac{A_n\left(\beta_m,n,t\right)}{\alpha_r\beta_m^2}\right)\left(1-\exp\left(-\alpha_r\beta_m^2t\right)\right)\right\},\end{aligned} \tag{C.87}$$

Substituting Eq. (C.86) into Eq. (C.87) one obtains

$$T(r,\theta,t)=\frac{1}{2\pi}\sum_{m=1}^{\infty}\frac{R_0(\beta_m,r)}{N_0(\beta_m)}\exp\left(-\alpha_r\beta_m^2t\right)\bar{\bar{F}}(\beta_m,0)$$
$$+\frac{1}{2\pi}\sum_{m=1}^{\infty}\frac{R_0(\beta_m,r)}{N_0(\beta_m)}\left\{\frac{\alpha_r\left(H_e\bar{T}_eb+\frac{\bar{\dot{q}}b}{k_r}\right)R_0(\beta_m,b)}{\alpha_r\beta_m^2}\right\}\left\{1-\exp\left(-\alpha_r\beta_m^2t\right)\right\}$$
$$+\frac{1}{2\pi}\sum_{m=1}^{\infty}\frac{R_0(\beta_m,r)}{N_0(\beta_m)}\left\{\frac{\alpha_r\left(H_i\bar{T}_ia\right)R_0(\beta_m,a)}{\alpha_r\beta_m^2}\right\}\left\{1-\exp\left(-\alpha_r\beta_m^2t\right)\right\}$$
$$+\frac{1}{\pi}\sum_{n=1}^{\infty}\sum_{m=1}^{\infty}\frac{R_n(\beta_m,r)}{N_n(\beta_m)}\left\{\exp\left(-\alpha_r\beta_m^2t\right)\bar{\bar{F}}(\beta_m,n)+\left(\frac{A_n(\beta_m,n,t)}{\alpha_r\beta_m^2}\right)\left(1-\exp\left(-\alpha_r\beta_m^2t\right)\right)\right\},\tag{C.88}$$

Simplification of Eq. (C.88) yields

$$T(r,\theta,t)=\frac{1}{2\pi}\sum_{m=1}^{\infty}\frac{R_0(\beta_m,r)}{N_0(\beta_m)}\exp\left(-\alpha_r\beta_m^2t\right)\bar{\bar{F}}(\beta_m,0)$$
$$+\frac{1}{2\pi}\sum_{m=1}^{\infty}\frac{R_0(\beta_m,r)}{N_0(\beta_m)}\frac{\left\{\left(H_e\bar{T}_eb+\frac{\bar{\dot{q}}b}{k_r}\right)R_0(\beta_m,b)\right\}}{\beta_m^2}\left\{1-\exp\left(-\alpha_r\beta_m^2t\right)\right\}$$
$$+\frac{1}{2\pi}\sum_{m=1}^{\infty}\frac{R_0(\beta_m,r)}{N_0(\beta_m)}\frac{\left(H_i\bar{T}_ia\right)R_0(\beta_m,a)}{\beta_m^2}\left\{1-\exp\left(-\alpha_r\beta_m^2t\right)\right\}$$
$$+\frac{1}{\pi}\sum_{n=1}^{\infty}\sum_{m=1}^{\infty}\frac{R_n(\beta_m,r)}{N_n(\beta_m)}\left\{\exp\left(-\alpha_r\beta_m^2t\right)\bar{\bar{F}}(\beta_m,n)+\left(\frac{A_n(\beta_m,n,t)}{\alpha_r\beta_m^2}\right)\left(1-\exp\left(-\alpha_r\beta_m^2t\right)\right)\right\}.\tag{C.89}$$

Taking,

$$T_A=\frac{1}{2\pi}\sum_{m=1}^{\infty}\frac{R_0(\beta_m,r)}{N_0(\beta_m)}\exp\left(-\alpha_r\beta_m^2t\right)\bar{\bar{F}}(\beta_m,0),\tag{C.90}$$

$$T_B=\frac{1}{2\pi}\sum_{m=1}^{\infty}\frac{R_0(\beta_m,r)}{N_0(\beta_m)}\frac{\left\{\left(H_e\bar{T}_eb+\frac{\bar{\dot{q}}b}{k_r}\right)R_n(\beta_m,b)\right\}}{\beta_m^2}\left\{1-\exp\left(-\alpha_r\beta_m^2t\right)\right\},\tag{C.91}$$

$$T_C=\frac{1}{2\pi}\sum_{m=1}^{\infty}\frac{R_0(\beta_m,r)}{N_0(\beta_m)}\frac{\left(H_i\bar{T}_ia\right)R_0(\beta_m,a)}{\beta_m^2}\left\{1-\exp\left(-\alpha_r\beta_m^2t\right)\right\},\tag{C.92}$$

$$T_D = \frac{1}{\pi}\sum_{n=1}^{\infty}\sum_{m=1}^{\infty}\frac{R_n(\beta_m r)}{N_n(\beta_m)}\left[\exp\left(-\alpha_r\beta_m^2 t\right)\tilde{\tilde{F}}(\beta_m,n)+\left(\frac{A_n(\beta_m,n,t)}{\alpha_r\beta_m^2}\right)\left\{1-\exp\left(-\alpha_r\beta_m^2 t\right)\right\}\right]. \tag{C.93}$$

Equation (C.89) can be expressed in the following form:

$$T(r,\theta,t) = T_A + T_B + T_C + T_D \tag{C.94}$$

Now, the terms T_A, T_B, T_C, and T_D are evaluated separately as in the following.

Evaluation of T_A:

Using the relation of $R_n(\beta_m,r)$ from Eq. (D.22) into Eq. (C.84), it can be written as

$$\tilde{\tilde{F}}(\beta_m,n) = \int_0^{2\pi}\int_a^b r\left\{L_n J_n(\beta_m r) - V_n Y_n(\beta_m r)\right\}\cos n(\theta-\phi)F(r,\theta)\,\mathrm{d}\theta\mathrm{d}r, \tag{C.95}$$

The expression of L_n and V_n are defined by Eqs. (D.23) and (D.24) in Appendix D. In Eq. (C.95), Yiannopoulos *et al*. (1997) employed the initial condition: $F(r,\theta) = T_0$. One obtains the following expressions by using assumption of Yiannopoulos *et al*. (1997):

$$\tilde{\tilde{F}}(\beta_m,n) = T_0\int_a^b\int_0^{2\pi} rR_n(\beta_m,r)\cos n(\theta-\phi)\,\mathrm{d}\theta\mathrm{d}r. \tag{C.96}$$

Taking n=0, Eq. (C.96) can be written as

$$\tilde{F}(\beta_m,0) = T_0\int_a^b\int_0^{2\pi} rR_0(\beta_m,r)\,\mathrm{d}\theta\mathrm{d}r = 2\pi T_0\int_a^b rR_0(\beta_m,r)\,\mathrm{d}r. \tag{C.97}$$

Substituting the expression of $R_0(\beta_m,r)$ from Eq. (D.37) into Eq. (C.97) provides

$$\tilde{F}(\beta_m,0) = 2\pi T_0\left[\int_a^b\left\{r\left(L_0 J_0(\beta_m r) - K_0 Y_0(\beta_m r)\right)\right\}\right]\mathrm{d}r\,. \tag{C.98}$$

The general form of integration of Bessel functions is given by (Özisik, 1993)

$$\int r^n W_{n-1}(\beta_m r)\,\mathrm{d}r = \frac{1}{\beta_m} r^n W_n(\beta_m r) \qquad \text{for } W \equiv J, Y, I \tag{C.99}$$

where J is the first kind Bessel function of order n, Y is the second kind Bessel function of order n and I is the modified Bessel function of the first kind of order n. Integrating Eq. (C.98) between $r = a$ to $r = b$ using Eq. (C.99) for $n = 0$:

$$F(\beta_m,0)=\frac{2\pi T_0}{\beta_m}\left[L_0\left\{bJ_1(\beta_m b)-aJ_1(\beta_m a)\right\}-V_0\left\{bY_1(\beta_m b)-aY_1(\beta_m a)\right\}\right]. \quad \text{(C.100)}$$

Substituting Eq. (C.100) in Eq. (C.90) yields

$$T_A=\frac{1}{2\pi}\sum_{m=1}^{\infty}\frac{R_0(\beta_m,r)}{N_0(\beta_m)}\exp\left(-\alpha_r\beta_m^2 t\right) \times\frac{2\pi T_0}{\beta_m}\left[L_0\left\{bJ_1(\beta_m b)-aJ_1(\beta_m a)\right\}-V_0\left\{bY_1(\beta_m b)-aY_1(\beta_m a)\right\}\right], \quad \text{(C.101)}$$

Substituting the expression of $N_0(\beta_m)$ taking n = 0 from Eq. (D.72) into Eq. (C.101):

$$T_A=\frac{1}{2\pi}\sum_{m=1}^{\infty}\frac{R_0(\beta_m,r)}{\left(\frac{2}{\pi^2}\times\frac{K_0^2B_e-V_0^2B_i}{\beta_m^2K_0^2}\right)}\exp\left(-\alpha_r\beta_m^2 t\right) \times\frac{2\pi T_0}{\beta_m}\left[L_0\left\{bJ_1(\beta_m b)-aJ_1(\beta_m a)\right\}-V_0\left\{bY_1(\beta_m b)-aY_1(\beta_m a)\right\}\right]. \quad \text{(C.102)}$$

The expression of T_A is obtained as

$$T_A=T_0\sum_{m=1}^{\infty}\frac{R_0(\beta_m,r)}{F_0}G_0\exp\left(-\alpha_r\beta_m^2 t\right), \quad \text{(C.103)}$$

where

$$F_0=\frac{B_eK_0^2-B_iV_0^2}{K_0^2} \quad \text{(C.104)}$$

and

$$G_0=\frac{1}{2}\pi^2\beta_m\left[L_0\left(bJ_1(\beta_m b)-aJ_1(\beta_m a)\right)-V_0\left(bY_1(\beta_m b)-aY_1(\beta_m a)\right)\right]. \quad \text{(C.105)}$$

Evaluation of T_B:

Substituting the expressions of $N_0(\beta_m)$ and $\bar{T}_e$ from Eqs. (D.72) and (C.74) taking n = 0 into Eq. (C.91):

$$T_B=\frac{1}{2\pi}\sum_{m=1}^{\infty}\frac{R_0(\beta_m,r)}{\frac{2}{\pi^2}\frac{F_0}{\beta_m^2}}\frac{\left(H_e 2\pi T_e b+\frac{b\bar{q}}{k_r}\right)R_0(\beta_m,b)}{\beta_m^2}\left\{1-\exp\left(-\alpha_r\beta_m^2 t\right)\right\}. \quad \text{(C.106)}$$

The expression of $\bar{q}$ taking n=0:

$$\bar{q}=\int_0^{2\pi}q(\theta)\mathrm{d}\theta, \quad \text{(C.107)}$$

Equation (C.4) provides the heat flux input into the roll $q(\theta)$, at the outer surface

$$\bar{\dot{q}} = \int_{\phi-\beta}^{\phi+\beta} q(\theta)\,\mathrm{d}\theta + \int_{\phi+\beta}^{2\pi+\phi-\beta} q(\theta)\,\mathrm{d}\theta = \int_{\phi-\beta}^{\phi+\beta} q(\theta)\,\mathrm{d}\theta + 0 = 2\beta\dot{q}. \tag{C.108}$$

Use of Eq. (C.108) into Eq. (C.106), provides

$$T_B = \frac{1}{2\pi}\sum_{m=1}^{\infty} \frac{R_0(\beta_m, r)}{\frac{2}{\pi^2}\frac{F_0}{\beta_m^2}} \frac{\left(H_e b 2\pi T_e + \frac{\dot{q} 2b\beta}{k_r}\right) R_0(\beta_m, b)}{\beta_m^2} \left\{1 - \exp\left(-\alpha_r \beta_m^2 t\right)\right\}, \tag{C.109}$$

The expression, $R_0(\beta_m, b)$ from Eq. (D.51) is substituted into Eq. (109) and the expression for T_B is obtained as

$$T_B = \left(\pi H_e T_e + \frac{\dot{q}}{k_r}\beta\right) \sum_{m=1}^{\infty} \frac{R_0(\beta_m, r)}{F_0} \left\{1 - \exp\left(-\alpha_r \beta_m^2 t\right)\right\}. \tag{C.110}$$

Evaluation of T_C:

Substituting the expression $N_0(\beta_m)$ and $\bar{T}_i$ from Eqs. (D.72) and (C.75), respectively and taking $n = 0$ into Eq. (C.92):

$$T_C = \frac{1}{2\pi}\sum_{m=1}^{\infty} \frac{R_0(\beta_m, r)}{\frac{2}{\pi^2}F_0} 2\pi T_i H_i a \left\{R_0(\beta_m, a)\right\} \left\{1 - \exp\left(-\alpha_r \beta_m^2 t\right)\right\}. \tag{C.111}$$

Rearranging Eq. (C.111) the expression for T_C is obtained as

$$T_C = \frac{\pi^2}{2} H_i a T_i \sum_{m=1}^{\infty} \frac{R_0(\beta_m, r)}{F_0} R_0(\beta_m, a) \left\{1 - \exp\left(-\alpha_r \beta_m^2 t\right)\right\}. \tag{C.112}$$

Evaluation of T_D:

Expanding the series of Eq. (C.93), one obtains

$$\begin{aligned} T_D = {} & \frac{1}{\pi}\sum_{n=1}^{\infty}\sum_{m=1}^{\infty} \frac{R_n(\beta_m, r)}{N_n(\beta_m)} \exp\left(-\alpha_r \beta_m^2 t\right) \tilde{\bar{F}}(\beta_m, n) \\ & + \frac{1}{\pi}\sum_{n=1}^{\infty}\sum_{m=1}^{\infty} \frac{R_n(\beta_m, r)}{N_n(\beta_m)} \left(\frac{A_n(\beta_m, n, t)}{\alpha_r \beta_m^2}\right) \left(1 - \exp\left(-\alpha_r \beta_m^2 t\right)\right), \end{aligned} \tag{C.113}$$

Taking,

$$T_{D1} = \frac{1}{\pi}\sum_{n=1}^{\infty}\sum_{m=1}^{\infty} \frac{R_n(\beta_m, r)}{N_n(\beta_m)} \tilde{\bar{F}}(\beta_m, n) \exp\left(-\alpha_r \beta_m^2 t\right), \tag{C.114}$$

$$T_{D2}=\frac{1}{\pi}\sum_{n=1}^{\infty}\sum_{m=1}^{\infty}\frac{R_n\left(\beta_m,r\right)}{N_n\left(\beta_m\right)}\frac{A_n\left(\beta_m,n,t\right)}{\alpha_r\beta_m^2}\cos n\left(\theta-\phi\right)\left\{1-\exp\left(-\alpha_r\beta_m^2t\right)\right\}. \tag{C.115}$$

The expression of Eq. (C.113) can be expressed as

$$T_D=T_{D1}+T_{D2}. \tag{C.116}$$

Substituting Eq. (C.84) into Eq. (C.114):

$$T_{D1}=\frac{1}{\pi}\sum_{n=1}^{\infty}\sum_{m=1}^{\infty}\frac{R_n\left(\beta_m,r\right)}{N_n\left(\beta_m\right)}\left(\int_a^b\int_0^{2\pi}rR_n\left(\beta_m,r\right)\cos n\left(\theta-\phi\right)F\left(r,\theta\right)\mathrm{d}r\mathrm{d}\theta\right)\exp\left(-\alpha_r\beta_m^2t\right), \tag{C.117}$$

or,

$$\begin{aligned}T_{D1}=&\frac{1}{\pi}\sum_{n=0}^{\infty}\sum_{m=1}^{\infty}\frac{R_n\left(\beta_m,r\right)}{N_n\left(\beta_m\right)}\left\{\left(\int_a^b rR_n\left(\beta_m,r\right)F\left(r,t\right)\mathrm{d}r\right)\exp\left(-\alpha_r\beta_m^2t\right)\right\}\\&\times\frac{1}{\pi}\sum_{n=0}^{\infty}\sum_{m=1}^{\infty}\frac{R_n\left(\beta_m,r\right)}{N_n\left(\beta_m\right)}\left(\int_0^{2\pi}\cos n\left(\theta-\phi\right)F\left(\theta\right)\mathrm{d}\theta\right)\exp\left(-\alpha_r\beta_m^2t\right).\end{aligned} \tag{C.118}$$

The integral expression in Eq. (C.118):

$$\int_0^{2\pi}F\left(\theta\right)\cos n\left(\theta-\phi\right)\mathrm{d}\theta=0. \tag{C.119}$$

Thus,

$$T_{D1}=0. \tag{C.120}$$

Now, substituting the expression $N_n\left(\beta_m\right)$ from Eq. (D.72) into Eq. (C.115):

$$T_{D2}=\frac{1}{\pi}\sum_{n=1}^{\infty}\sum_{m=1}^{\infty}\frac{R_n\left(\beta_m,r\right)}{\frac{2}{\pi^2}\frac{F_n}{\beta_m^2}}\frac{A_n\left(\beta_m,n,t\right)}{\alpha_r\beta_m^2}\cos n\left(\theta-\phi\right)\left\{1-\exp\left(-\alpha_r\beta_m^2t\right)\right\}, \tag{C.121}$$

Rearranging Eq. (C.121):

$$T_{D2}=\frac{\pi}{2}\sum_{n=1}^{\infty}\sum_{m=1}^{\infty}\frac{R_n\left(\beta_m,r\right)}{F_n}\frac{A_n\left(\beta_m,n,t\right)}{\alpha_r}\cos n\left(\theta-\phi\right)\left\{1-\exp\left(-\alpha_r\beta_m^2t\right)\right\}. \tag{C.122}$$

Substitution of Eq. (C.72) into Eq. (C.122) provides

$$\begin{aligned}T_{D2}=&\frac{\pi}{2}\sum_{n=1}^{\infty}\sum_{m=1}^{\infty}\frac{R_n\left(\beta_m,r\right)}{F_n}\left\{\left(H_e\bar{T}_eb+\frac{b\bar{q}\left(n\right)}{k}\right)R_n\left(\beta_m,b\right)+H_i\bar{T}_iaR_n\left(\beta_m,a\right)\right\}\\&\times\cos n\left(\theta-\phi\right)\left\{1-\exp\left(-\alpha_r\beta_m^2t\right)\right\}.\end{aligned} \tag{C.123}$$

The terms $\overline{T}_e$ and $\overline{T}_i$ are equal to zero in Eq. (C.123) due to cyclic definite integral of cosine function from 0 to 2π. Thus, Eq. (C.123) becomes

$$T_{D2} = \frac{\pi}{2}\sum_{n=1}^{\infty}\sum_{m=1}^{\infty}\frac{R_n(\beta_m, r)}{F_n}\left(\frac{b\overline{q}(n)}{k}\right)R_n(\beta_m, b)\cos n(\theta-\phi)\left\{1-\exp\left(-\alpha_r\beta_m^2 t\right)\right\} \quad \text{(C.124)}$$

From the boundary condition of Eq. (C.4), $\overline{q}(n)$ is evaluated as

$$\overline{q}(n) = \int_0^{2\pi} q(\theta)\cos n(\theta-\phi)\,\mathrm{d}\theta, \quad \text{(C.125)}$$

where

$$q(\theta) = \begin{cases} \dot{q} & \text{for } (\phi-\beta) \le \theta \le (\phi+\beta) \\ 0 & \text{for } (\phi+\beta) < \theta < (2\pi+\phi-\beta) \end{cases}. \quad \text{(C.126)}$$

Equation (C.126) provides

$$\overline{\dot{q}}(n) = \int_{\phi-\beta}^{\phi+\beta} q(\theta)\cos n(\theta-\phi)\,\mathrm{d}\theta + \int_{\phi+\beta}^{2\pi+\phi-\beta} q(\theta)\cos n(\theta-\phi)\,\mathrm{d}\theta, \quad \text{(C.127)}$$

Use of Eq. (C.126), Eq. (C.125) can be written as

$$\overline{\dot{q}}(n) = \int_{\phi-\beta}^{\phi+\beta} \dot{q}\cos n(\theta-\phi)\,\mathrm{d}\theta, \quad \text{(C.128)}$$

Integrating Eq. (C.128) between $\theta = (\phi-\beta)$ to $\theta = (\phi+\beta)$:

$$\overline{\dot{q}}(n) = \dot{q}\left\{\frac{\sin n\beta - (-\sin n\beta)}{n}\right\} = 2\dot{q}\frac{\sin n\beta}{n}. \quad \text{(C.129)}$$

Substituting the expression of $R_n(\beta_m, b)$ from Eq. (D.51) in Eq. (C.129):

$$T_{D2} = 2\frac{\dot{q}}{k}\sum_{n=1}^{\infty}\sum_{m=1}^{\infty}\frac{R_n(\beta_m, r)}{F_n}\frac{\sin n\beta}{n}\cos n(\theta-\phi)\left\{1-\exp\left(-\alpha_r\beta_m^2 t\right)\right\}. \quad \text{(C.130)}$$

Inserting Eqs. (C.120) and (C.130) into Eq. (C.116), the expression for T_D is obtained as

$$T_D = 2\frac{\dot{q}}{k}\sum_{n=1}^{\infty}\sum_{m=1}^{\infty}\frac{R_n(\beta_m, r)}{F_n}\frac{\sin n\beta}{n}\cos n(\theta-\phi)\left\{1-\exp\left(-\alpha_r\beta_m^2 t\right)\right\}. \quad \text{(C.131)}$$

Substituting the expression of T_A, T_B, T_C and T_D from Eqs. (C.103), (C.110), (C.112) and (C.131), respectively in Eq. (C.94); the final expression to find out the transient temperature distribution for stationary heat source is obtained as

$$\begin{aligned} T(r,\theta,t) = {} & T_0 \sum_{m=1}^{\infty} \frac{R_0(\beta_m, r)}{F_0} G_0 \exp\left(-\alpha_r \beta_m^2 t\right) \\ & + \left(\pi H_e T_e + \frac{\dot{q}}{k_r}\beta\right) \sum_{m=1}^{\infty} \frac{R_0(\beta_m, r)}{F_0} \left\{1 - \exp\left(-\alpha_r \beta_m^2 t\right)\right\} \\ & + \frac{\pi^2}{2} H_i a T_i \sum_{m=1}^{\infty} \frac{R_0(\beta_m, r)}{F_0} R_0(\beta_m, a) \left\{1 - \exp\left(-\alpha_r \beta_m^2 t\right)\right\} \\ & + 2\frac{\dot{q}}{k_r} \sum_{n=1}^{\infty} \sum_{m=1}^{\infty} \frac{R_n(\beta_m, r)}{F_n} \frac{\sin n\beta}{n} \cos n(\theta - \phi) \left\{1 - \exp\left(-\alpha_r \beta_m^2 t\right)\right\}, \\ & t > 0,\ a \le r \le b,\ 0 \le \theta \le 2\pi. \end{aligned} \tag{C.132}$$

Equation (C.136) provides the transient temperature distribution in the hollow cylinder for the stationary heat source. For steady-state temperature distribution for stationary heat source the following form can be obtained by setting t to infinity:

$$\begin{aligned} T(r,\theta) = {} & \left(\pi H_e T_e + \frac{\dot{q}}{k_r}\beta\right) \sum_{m=1}^{\infty} \frac{R_0(\beta_m, r)}{F_0} + \frac{\pi^2}{2} H_i a T_i \sum_{m=1}^{\infty} \frac{R_0(\beta_m, r)}{F_0} R_0(\beta_m, a) \\ & + 2\frac{\dot{q}}{k_r} \sum_{n=1}^{\infty} \sum_{m=1}^{\infty} \frac{R_n(\beta_m, r)}{F_n} \frac{\sin n\beta}{n} \cos n(\theta - \phi). \end{aligned} \tag{C.133}$$

C.2 Solution of Heat Conduction Equation with Moving Heat Source

In this section, the solution of the heat conduction problem with time dependent boundary conditions can be related to the solution of the same problem with time independent boundary conditions by means of Duhamel's theorem (Özisik,1993). Duhamel's theorem provides a convenient approach for obtaining solution to heat conduction problems with time dependent boundary conditions by utilizing the solution of time independent boundary conditions. Figure C.2 shows the schematic diagram of moving heat source with stationary roll.

Consider a two-dimensional heat conduction problem with time boundary condition in the form

$$\frac{\partial^2 T}{\partial r^2}+\frac{1}{r}\frac{\partial T}{\partial r}+\frac{1}{r^2}\frac{\partial^2 T}{\partial \theta^2}=\frac{1}{\alpha_r}\frac{\partial T}{\partial t}, \tag{C.134}$$

$$-k_r\frac{\partial T}{\partial r}+h_i\left(T-T_i\right)=0 \qquad \text{at } r=a, \tag{C.135}$$

$$k_r\frac{\partial T}{\partial r}+h_e\left(T-T_e\right)=q(\theta) \qquad \text{at } r=b, \tag{C.136}$$

where $q(\theta)$ is the heat flux at the outer surface, h_e is the convective heat transfer coefficient at the outer surface, h_i is the convective heat transfer coefficient at the inner surface and T_e is the ambient temperature. The heat flux at the outer surface at any time is expressed as

$$q\left(\theta\right)=\begin{cases}\dot{q} & \text{for } \left(\omega t-\beta\right)\le\theta\le\left(\omega t+\beta\right)\\ 0 & \text{for } \left(\omega t+\beta\right)\le\theta\le\left(2\pi+\omega t-\beta\right)\end{cases}, \tag{C.137}$$

The initial condition is expressed as

$$T\left(r,\theta,t\right)=T_0 \quad \text{for } t=0 \quad \text{in region } a<r<b, \tag{C.138}$$

where T_0 is the initial temperature of the roll.

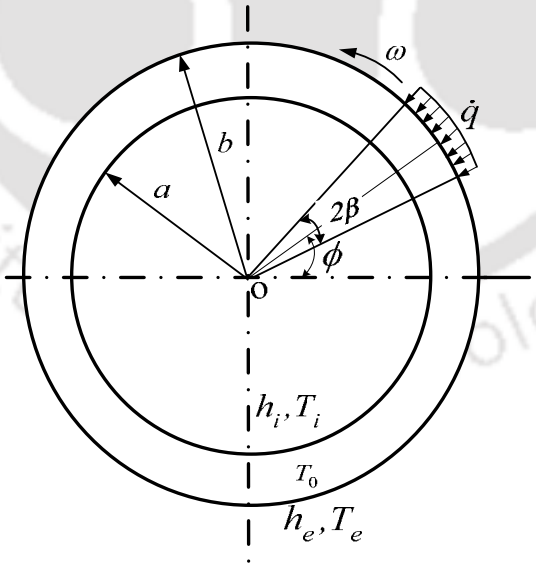

Fig. C.2. A moving heat source with stationary roll

The problem defined by Eqs. (C.134)–(C.138) cannot be solved by conventional methods because $\dot{q}$ is the function of time. Therefore, instead of solving the problem directly, the solution is expressed interms of the solution of the simpler auxiliary problem called fundamental solution (Özisik,1993). Let $\Omega(r,\theta,t,\tau)$ be the solution of Eq. (C.134) on the assumption that $\dot{q}$ is independent of time. Then $\Omega(r,\theta,t,\tau)$ is the fundamental solution of the auxiliary problem defined as

$$\frac{\partial^2\Omega}{\partial r^2}+\frac{1}{r}\frac{\partial\Omega}{\partial r}+\frac{1}{r^2}\frac{\partial\Omega^2}{\partial\theta^2}=\frac{1}{\alpha_r}\frac{\partial\Omega}{\partial t}, \tag{C.139}$$

boundary conditions:

$$k_r\frac{\partial\Omega}{\partial r}+h_e\left(T-T_e\right)=q(\theta) \qquad \text{at } r=b, \tag{C.140}$$

$$-k_r\frac{\partial\Omega}{\partial r}+h_i\left(T-T_i\right)=0 \qquad \text{at } r=a, \tag{C.141}$$

initial condition:

$$\Omega(r,\theta,t,\tau)=T_0 \quad \text{for } t=0. \tag{C.142}$$

The heat source position is expressed as

$$q(\theta)=\begin{cases}\dot{q} & \text{for } (\omega\tau-\beta)\le\theta\le(\omega\tau+\beta)\\ 0 & \text{for } (\omega\tau+\beta)<\theta<(2\pi+\omega\tau-\beta)\end{cases}, \tag{C.143}$$

where τ is a parameter.

The problem defined in Eqs. (C.139)–(C.143) can be solved with the techniques expressed in Section C.1 because $q(\theta)$ does not depend on time. Then, Duhamel's theorem relates the solution $T(r,\theta,t)$ of the problem given in Eqs. (C.134)–(C.138) to the solution $\Omega(r,\theta,t,\tau)$ of the auxiliary problem given in Eqs. (C.139)–(C.143) by the following integral expression (Özisik,1993):

$$T(r,\theta,t)=\frac{\partial}{\partial t}\int_{\tau=0}^{t}\Omega(r,\theta,t-\tau)\mathrm{d}\tau. \tag{C.144}$$

Assuming that the solution of problem given in Eqs. (C.139)–(C.143) is similar to the problem given in Eqs. (C.1) –(C.5) (expressed in Eq. (C.132)). Thus,

$$\begin{aligned}\Omega(r,\theta,t) = T_0 \sum_{m=1}^{\infty} \frac{R_0(\beta_m, r)}{F_0} G_0 \exp\left(-\alpha_r \beta_m^2 t\right) \\ + \left(\pi H_e T_e + \frac{\dot{q}}{k_r}\beta\right) \sum_{m=1}^{\infty} \frac{R_0(\beta_m, r)}{F_0} \left\{1 - \exp\left(-\alpha_r \beta_m^2 t\right)\right\} \\ + \frac{\pi^2}{2} H_i a T_i \sum_{m=1}^{\infty} \frac{R_0(\beta_m, r)}{F_0} R_0(\beta_m, a) \left\{1 - \exp\left(-\alpha_r \beta_m^2 t\right)\right\} \\ + 2\frac{\dot{q}}{k_r} \sum_{n=1}^{\infty}\sum_{m=1}^{\infty} \frac{R_n(\beta_m, r)}{F_n} \frac{\sin n\beta}{n} \cos n(\theta - \omega t) \left\{1 - \exp\left(-\alpha_r \beta_m^2 t\right)\right\},\end{aligned} \tag{C.145}$$

Substituting Eq. (C.145) into Eq. (C.144), one obtain

$$\begin{aligned}T(r,\theta,t) = T_0 \sum_{m=1}^{\infty} \frac{R_0(\beta_m, r)}{F_0} G_0 \exp\left(-\alpha_r \beta_m^2 t\right) \\ + \left(\beta \frac{\dot{q}}{k_r} + \pi H_e T_e\right) \sum_{m=1}^{\infty} \frac{R_0(\beta_m, r)}{F_0} \left\{1 - \exp\left(-\alpha_r \beta_m^2 t\right)\right\} \\ + \frac{\pi^2}{2} a H_i T_i \sum_{m=1}^{\infty} \frac{R_0(\beta_m, r)}{F_0} R_0(\beta_m, a) \left\{1 - \exp\left(-\alpha_r \beta_m^2 t\right)\right\} \\ + 2\frac{\dot{q}}{k_r} \sum_{n=1}^{\infty}\sum_{m=1}^{\infty} \frac{R_n(\beta_m, r)}{F_n} \times \frac{\sin n\beta}{n} \\ \times \frac{\cos n(\theta - \omega t) - \lambda_n \sin n(\theta - \omega t) + (\lambda_n \sin n\theta - \cos n\theta)\exp\left(-\alpha_r \beta_m^2 t\right)}{1 + \lambda_n^2},\end{aligned} \tag{C.146}$$

where λ_n is defined as

$$\lambda_n = \frac{\omega n}{\alpha_r \beta_m^2}. \tag{C.147}$$

Hence, Eq. (C.146) provides the transient temperature distribution in the hollow cylinder for a moving heat source with time dependent boundary conditions. The location of rotating heat source can be expressed as $\phi = \omega t$ and θ denotes the point of temperature measurement. For steady-state temperature distribution for moving heat source the following form can be obtained by setting t to infinity

$$\begin{aligned}T(r,\theta) = \left(\pi H_e T_e + \frac{\dot{q}}{k_r}\beta\right) \sum_{m=1}^{\infty} \frac{R_0(\beta_m, r)}{F_0} + \frac{\pi^2}{2} H_i a T_i \sum_{m=1}^{\infty} \frac{R_0(\beta_m, r)}{F_0} R_0(\beta_m, a) \\ + 2\frac{\dot{q}}{k_r} \sum_{n=1}^{\infty}\sum_{m=1}^{\infty} \frac{R_n(\beta_m, r)}{F_n} \frac{\sin n\beta}{n} \frac{\cos n(\theta - \phi) - \lambda_n \sin n(\theta - \phi)}{1 + \lambda_n^2}.\end{aligned} \tag{C.148}$$

Appendix D

Derivation of the Eigenfunctions $R_n(\beta_m, r)$ and Norm $N_n(\beta_m)$

D.1 Derivation of the Eigenfunctions $R_n(\beta_m, r)$ in Eq. (C.16)

The representation of an arbitrary function $T(r,t)$ defined in a finite interval $a \le r \le b$ in terms of the eigenfunctions of the eigenvalue problem is given in Eq. (C.16). For the sake of completeness the differential equation along with the boundary condition is rewritten as

$$\frac{\mathrm{d}^2 R_n(\beta_m, r)}{\mathrm{d}r^2} + \frac{1}{r}\frac{\mathrm{d}R_n(\beta_m, r)}{dr} + \left(\beta_m^2 - \frac{n^2}{r^2}\right) R_n(\beta_m, r) = 0 \qquad \text{in} \quad a \le r \le b, \tag{D.1}$$

boundary conditions:

$$-\frac{\mathrm{d}R_n(\beta_m, r)}{\mathrm{d}r} + H_i R_n(\beta_m, r) = 0 \qquad \text{at } r = a, \tag{D.2}$$

$$\frac{\mathrm{d}R_n(\beta_m, r)}{\mathrm{d}r} + H_e R_n(\beta_m, r) = 0 \qquad \text{at } r = b. \tag{D.3}$$

Assuming eigenfunctions $R_n(\beta_m, r)$ in the form:

$$R_n(\beta_m, r) = c_1 J_n(\beta_m r) + c_2 Y_n(\beta_m r). \tag{D.4}$$

Differentiating Eq. (D.4) with respect to r :

$$\frac{\mathrm{d}R_n(\beta_m, r)}{\mathrm{d}r} = c_1 \frac{\mathrm{d}J_n(\beta_m r)}{\mathrm{d}r} + c_2 \frac{\mathrm{d}Y_n(\beta_m r)}{\mathrm{d}r}, \tag{D.5}$$

or,

$$\frac{\mathrm{d}R_n(\beta_m, r)}{\mathrm{d}r} = c_1 \beta_m J_n'(\beta_m r) + c_2 \beta_m Y_n'(\beta_m r), \tag{D.6}$$

Two properties of the Bessel function of the first and second kind are (Kreyszig, 1999)

$$J_n'(x) = \frac{J_{n-1}(x) - J_{n+1}(x)}{2}, \tag{D.7}$$

and

$$Y_n'(x) = \frac{Y_{n-1}(x) - Y_{n+1}(x)}{2}. \tag{D.8}$$

Use of Eqs. (D.7) and (D.8) into Eq. (D.6), taking $x = \beta_m r$:

$$\frac{\mathrm{d}R_n(\beta_m, r)}{\mathrm{d}r} = c_1\left(\frac{\beta_m J_{n-1}(\beta_m r) - \beta_m J_{n+1}(\beta_m r)}{2}\right) + c_2\left(\frac{\beta_m Y_{n-1}(\beta_m r) - \beta_m Y_{n+1}(\beta_m r)}{2}\right) \tag{D.9}$$

The following are the other two relations of the Bessel function of the first and second kinds (Kreyszig, 1999):

$$J_{n-1}(x) = \frac{2n}{x} J_n(x) - J_{n+1}(x), \tag{D.10}$$

and

$$Y_{n-1}(x) = \frac{2n}{x} Y_n(x) - Y_{n+1}(x)\ . \tag{D.11}$$

Use of Eqs. (D.10) and (D.11) into Eq. (D.9), taking $x = \beta_m r$:

$$\begin{aligned}\frac{\mathrm{d}R_n(\beta_m, r)}{\mathrm{d}r} = {} & c_1\left(\frac{\beta_m}{2}\left\{\frac{2n}{\beta_m r} J_n(\beta_m r) - J_{n+1}(\beta_m r)\right\} - \beta_m J_{n+1}(\beta_m r)\right) \\ & + c_2\left(\frac{\beta_m}{2}\left\{\frac{2n}{\beta_m r} Y_n(\beta_m r) - Y_{n+1}(\beta_m r)\right\} - \beta_m Y_{n+1}(\beta_m r)\right),\end{aligned} \tag{D.12}$$

Simplification of Eq. (D.12) provides

$$\frac{\mathrm{d}R_n(\beta_m, r)}{\mathrm{d}r} = c_1\left(\frac{n}{r} J_n(\beta_m r) - \beta_m J_{n+1}(\beta_m r)\right) + c_2\left(\frac{n}{r} Y_n(\beta_m r) - \beta_m Y_{n+1}(\beta_m r)\right). \tag{D.13}$$

Putting $r = b$ in Eq. (D.13), one obtains

$$\left.\frac{\mathrm{d}R_n(\beta_m, r)}{\mathrm{d}r}\right|_{r=b} = c_1\left(\frac{n}{b} J_n(\beta_m b) - \beta_m J_{n+1}(\beta_m b)\right) + c_2\left(\frac{n}{b} Y_n(\beta_m b) - \beta_m Y_{n+1}(\beta_m b)\right). \tag{D.14}$$

Equation (D.4) gives at $r = b$:

$$R_n(\beta_m, r)\big|_{r=b} = c_1 J_n(\beta_m b) + c_2 Y_n(\beta_m b). \tag{D.15}$$

Substituting Eq. (D.14) and (D.15) into Eq. (D.3) results

$$c_1\left(\frac{n}{b}J_n(\beta_m b)-\beta_m J_{n+1}(\beta_m b)\right)+c_2\left(\frac{n}{b}Y_n(\beta_m b)-\beta_m Y_{n+1}(\beta_m b)\right) + H_e\left\{c_1 J_n(\beta_m b)+c_2 Y_n(\beta_m b)\right\}=0. \tag{D.16}$$

Separating the coefficient of c_1 and c_2 in Eq. (D.16) one obtains

$$c_1\left(\frac{n}{b}J_n(\beta_m b)+H_e J_n(\beta_m b)-\beta_m J_{n+1}(\beta_m b)\right) + c_2\left(\frac{n}{b}J_n(\beta_m b)+H_e Y_n(\beta_m b)-\beta_m Y_{n+1}(\beta_m b)\right)=0, \tag{D.17}$$

or,

$$c_1\left\{\left(\frac{n}{b}+H_e\right)J_n(\beta_m b)-\beta_m J_{n+1}(\beta_m b)\right\} +c_2\left\{\left(\frac{n}{b}+H_e\right)Y_n(\beta_m b)-\beta_m Y_{n+1}(\beta_m b)\right\}=0. \tag{D.18}$$

Equation (D.18) provides

$$c_2=\frac{-c_1\left\{\left(\frac{n}{b}+H_e\right)J_n(\beta_m b)-\beta_m J_{n+1}(\beta_m b)\right\}}{\left\{\left(\frac{n}{b}+H_e\right)Y_n(\beta_m b)-\beta_m Y_{n+1}(\beta_m b)\right\}}=-K\left\{\left(\frac{n}{b}+H_e\right)J_n(\beta_m b)-\beta_m J_{n+1}(\beta_m b)\right\}, \tag{D.19}$$

and

$$c_1=\frac{-c_2\left\{\left(\frac{n}{b}+H_e\right)Y_n(\beta_m b)-\beta_m Y_{n+1}(\beta_m b)\right\}}{\left\{\left(\frac{n}{b}+H_e\right)J_n(\beta_m b)-\beta_m J_{n+1}(\beta_m b)\right\}}=K\left\{\left(\frac{n}{b}+H_e\right)Y_n(\beta_m b)-\beta_m Y_{n+1}(\beta_m b)\right\}. \tag{D.20}$$

where K is the constant.

Substituting c_1 and c_2 into Eq. (D.4), yields

$$R_n(\beta_m,r)=K\left\{\left(\frac{n}{b}+H_e\right)Y_n(\beta_m b)-\beta_m Y_{n+1}(\beta_m b)\right\}J_n(\beta_m r) -K\left\{\left(\frac{n}{b}+H_e\right)J_n(\beta_m b)-\beta_m J_{n+1}(\beta_m b)\right\}Y_n(\beta_m r), \tag{D.21}$$

or,

$$R_n(\beta_m,r)=K\left\{L_n J_n(\beta_m r)-V_n Y_n(\beta_m r)\right\}. \tag{D.22}$$

Taking the expression of L_n and K_n as follows:

$$L_n = \left(\frac{n}{b} + H_e\right) Y_n(\beta_m b) - \beta_m Y_{n+1}(\beta_m b), \tag{D.23}$$

and

$$V_n = \left(\frac{n}{b} + H_e\right) J_n(\beta_m b) - \beta_m J_{n+1}(\beta_m b). \tag{D.24}$$

Differentiating Eq. (D.22) with respect to r:

$$\frac{\mathrm{d}R_n(\beta_m, r)}{\mathrm{d}r} = K\left\{L_n \frac{\mathrm{d}}{\mathrm{d}r} J_n(\beta_m r) - V_n \frac{\mathrm{d}}{\mathrm{d}r} Y_n(\beta_m r)\right\} \tag{D.25}$$

or,

$$\frac{\mathrm{d}R_n(\beta_m, r)}{\mathrm{d}r} = K\left\{L_n \beta_m J_n'(\beta_m r) - V_n \beta_m Y_n'(\beta_m r)\right\}. \tag{D.26}$$

Use of Eqs. (D.7) and (D.8) into Eq. (D.26), taking $x = \beta_m r$, provides

$$\frac{\mathrm{d}R_n(\beta_m, r)}{\mathrm{d}r} = K\left\{L_n \beta_m \left(\frac{J_{n-1}(\beta_m r) - J_{n+1}(\beta_m r)}{2}\right) - V_n \beta_m \left(\frac{Y_{n-1}(\beta_m r) - Y_{n+1}(\beta_m r)}{2}\right)\right\}. \tag{D.27}$$

Use of Eqs. (D.10) and (D.11) into Eq. (D.9) taking $x = \beta_m r$ provides

$$\begin{aligned}\frac{\mathrm{d}R_n(\beta_m, r)}{\mathrm{d}r} = {} & KL_n \beta_m \frac{n}{\beta_m r} J_n(\beta_m r) - \frac{J_{n+1}(\beta_m r)}{2} - \frac{J_{n+1}(\beta_m r)}{2} \\ & - KV_n \beta_m \left(\frac{n}{\beta_m r} Y_n(\beta_m r) - \frac{Y_{n+1}(\beta_m r)}{2} - \frac{Y_{n+1}(\beta_m r)}{2}\right).\end{aligned} \tag{D.28}$$

Simplifying,

$$\frac{\mathrm{d}R_n(\beta_m, r)}{\mathrm{d}r} = K\left\{L_n \left(\frac{n}{r} J_n(\beta_m r) - \beta_m J_{n+1}(\beta_m r)\right) - V_n \left(\frac{n}{r} Y_n(\beta_m r) - \beta_m Y_{n+1}(\beta_m r)\right)\right\}. \tag{D.29}$$

Substituting $r = a$ into Eq. (D.29) provides

$$\left.\frac{\mathrm{d}R_n(\beta_m, r)}{\mathrm{d}r}\right|_{r=a} = K\left\{L_n \left(\frac{n}{a} J_n(\beta_m a) - \beta_m J_{n+1}(\beta_m a)\right) - V_n \left(\frac{n}{a} Y_n(\beta_m a) - \beta_m Y_{n+1}(\beta_m a)\right)\right\}. \tag{D.30}$$

Equation (D.22) provides at $r = a$:

$$R_n(\beta_m, r)\big|_{r=a} = K\left\{L_n J_n(\beta_m a) - V_n Y_n(\beta_m a)\right\} \tag{D.31}$$

Using Eq. (D.30) and (D.31) in Eq. (D.2), yields

$$-\left[K\left\{L_n\left(\frac{n}{a}J_n(\beta_m a)-\beta_m J_{n+1}(\beta_m a)\right)-V_n\left(\frac{n}{a}Y_n(\beta_m a)-\beta_m Y_{n+1}(\beta_m a)\right)\right\}\right] + H_i K\left\{L_n J_n(\beta_m a)-V_n Y_n(\beta_m a)\right\}=0. \tag{D.32}$$

or,

$$\left\{L_n\left(\frac{n}{a}J_n(\beta_m a)-\beta_m J_{n+1}(\beta_m a)\right)-V_n\left(\frac{n}{a}Y_n(\beta_m a)-\beta_m Y_{n+1}(\beta_m a)\right)\right\} = H_i L_n J_n(\beta_m a)-H_i V_n Y_n(\beta_m a). \tag{D.33}$$

Simplifying Eq. (D.33):

$$L_n\left\{\left(\frac{n}{a}-H_i\right)J_n(\beta_m a)-\beta_m J_{n+1}(\beta_m a)\right\}=V_n\left\{\left(\frac{n}{a}-H_i\right)Y_n(\beta_m a)-\beta_m Y_{n+1}(\beta_m a)\right\}, \tag{D.34}$$

or,

$$K_n L_n - V_n W_n = 0, \tag{D.35}$$

where

$$K_n=\left(\frac{n}{a}-H_i\right)J_n(\beta_m a)-\beta_m J_{n+1}(\beta_m a), \tag{D.36}$$

$$W_n=\left(\frac{n}{a}-H_i\right)Y_n(\beta_m a)-\beta_m Y_{n+1}(\beta_m a). \tag{D.37}$$

Equation (C.35) is the transcendental characteristic equation for finding out the positive roots β_m. The eigenfunctions of Eq. (D.1) is given as

$$R_n(\beta_m, r)=L_n J_n(\beta_m r)-V_n Y_n(\beta_m r). \tag{D.38}$$

D.2 Derivation of the Norm $N_n(\beta_m)$ in Eq. (C.21)

The norm is defined as

$$N_n(\beta_m)=\int_a^b r R_n^2(\beta_m, r)\,\mathrm{d}r. \tag{D.39}$$

Integration of the Bessel function is given as (Özisik, 1993)

$$\int r G_n^2(\beta_m, r)\,\mathrm{d}r=\frac{1}{2}r^2\left[G_n'^2(\beta_m, r)+\left(1-\left(\frac{n}{\beta_m r}\right)^2\right)G_n^2(\beta_m, r)\right], \tag{D.40}$$

where $G_n(\beta_m, r)$ is the Bessel function of the first or second kind of order n.

Use of Eq. (D.40) into Eq. (D.39) provides

$$N_n(\beta_m) = \frac{r^2}{2}\left[R'^2(\beta_m, r) + \left(1 - \left(\frac{n}{\beta_m r}\right)^2\right) R_n^2(\beta_m, r) \right]\Bigg|_{r=a}^{r=b}, \tag{D.41}$$

or,

$$N_n(\beta_m) = \frac{b^2}{2}\left[R_n'^2(\beta_m, b) + \left(1 - \left(\frac{n}{\beta_m b}\right)^2\right) R_n^2(\beta_m, b) \right] - \frac{a^2}{2}\left[R_n'^2(\beta_m, a) + \left(1 - \left(\frac{n}{\beta_m a}\right)^2\right) R_n^2(\beta_m, a) \right]. \tag{D.42}$$

Equation (D.41) needs the terms $R_n'^2(\beta_m, b)$ $R_n'^2(\beta_m, a)$ $R_n^2(\beta_m, b)$ $R_n^2(\beta_m, a)$.

Equations (D.10) and (D.11) can be written as

$$J_{n+1}(x) = \frac{n}{x} J_n(x) - J_n'(x), \tag{D.43}$$

and

$$Y_{n+1}(x) = \frac{n}{x} Y_n(x) - Y_n'(x). \tag{D.44}$$

Use of Eqs. (D.43) and (D.44) into Eqs. (D.23) and (D.24), taking $x = \beta_m b$, yields

$$L_n = H_e Y_n(\beta_m b) + \beta_m Y_n'(\beta_m b), \tag{D.45}$$

and

$$V_n = H_e J_n(\beta_m b) + \beta_m J_n'(\beta_m b). \tag{D.46}$$

Use of Eqs. (D.43) and (D.44) into Eqs. (D.36) and (D.37), taking $x = \beta_m a$, yields

$$K_n = -H_i J_n(\beta_m a) + \beta_m J_n'(\beta_m a), \tag{D.47}$$

and

$$W_n = -H_i Y_n(\beta_m a) + \beta_m Y_n'(\beta_m a). \tag{D.48}$$

Substituting Eqs. (D.45) and (D.46) into Eq. (D.38),

$$R_n(\beta_m, r) = \{H_e Y_n(\beta_m b) + \beta_m Y_n'(\beta_m b)\} J_n(\beta_m r) - \{H_e J_n(\beta_m b) + \beta_m J_n'(\beta_m b)\} Y_n(\beta_m r). \quad (D.49)$$

Putting $r = b$ in Eq. (D.49) results

$$R_n(\beta_m, b) = \{H_e Y_n(\beta_m b) + \beta_m Y_n'(\beta_m b)\} J_n(\beta_m b) - \{H_e J_n(\beta_m b) + \beta_m J_n'(\beta_m b)\} Y_n(\beta_m b). \quad (D.50)$$

Simplification of Eq. (D.50) provides

$$R_n(\beta_m, b) = \beta_m \{J_n(\beta_m b) Y_n'(\beta_m b) - Y_n(\beta_m b) J_n'(\beta_m b)\}. \quad (D.51)$$

Using Wronskian relation for the Bessel function (Özisik, 1993),

$$R_n(\beta_m, b) = \beta_m \left(\frac{2}{\pi \beta_m b}\right). \quad (D.52)$$

Thus,

$$R_n(\beta_m, b) = \frac{2}{\pi b}, \quad (D.53)$$

or,

$$R_n^2(\beta_m, b) = \frac{4}{\pi^2 b^2}. \quad (D.54)$$

Substituting the expression of L_n from Eq. (D.35) into Eq. (D.38),

$$R_n(\beta_m, r) = \frac{V_n W_n}{K_n} J_n(\beta_m r) - V_n Y_n(\beta_m r), \quad (D.55)$$

or,

$$R_n(\beta_m, r) = \frac{V_n}{K_n} \{W_n J_n(\beta_m r) - K_n Y_n(\beta_m r)\}. \quad (D.56)$$

Substituting the expression for K_n and W_n from Eqs. (D.47) and (D.48) into Eq. (D.56)

$$R_n(\beta_m, r) = \frac{V_n}{K_n} \times \{-H_i Y_n(\beta_m a) + \beta_m Y_n'(\beta_m a)\} J_n(\beta_m r) - \frac{V_n}{K_n} \times \{-H_i J_n(\beta_m a) + \beta_m J_n'(\beta_m a)\} Y_n(\beta_m r). \quad (D.57)$$

Equation (D.57) provides at $x = a$:

$$R_n(\beta_m, a) = \frac{V_n}{K_n} \times \{-H_i Y_n(\beta_m a) + \beta_m Y_n'(\beta_m a)\} J_n(\beta_m a) - \frac{V_n}{K_n} \times \{-H_i J_n(\beta_m a) + \beta_m J_n'(\beta_m a)\} Y_n(\beta_m a). \quad (D.58)$$

Simplifying,

$$R_n(\beta_m, a) = \frac{V_n}{K_n}\beta_m \left\{ J_n(\beta_m a) Y_n'(\beta_m a) - J_n'(\beta_m a) Y_n(\beta_m a) \right\}. \tag{D.59}$$

Using Wronskian relation for the Bessel function (Özisik, 1993):

$$R_n(\beta_m, a) = \frac{V_n}{K_n}\beta_m \left(\frac{2}{\pi \beta_m a} \right). \tag{D.60}$$

Thus,

$$R_n(\beta_m, a) = \frac{2}{\pi a}\frac{V_n}{K_n}, \tag{D.61}$$

or,

$$R_n^2(\beta_m, a) = \frac{4}{\pi^2 a^2}\frac{V_n^2}{K_n^2}. \tag{D.62}$$

Now, the expression of $R_n'(\beta_m, b)$ can be evaluated using boundary conditions given in Eq. (D.3) for $r = b$:

$$\frac{\mathrm{d}R_n(\beta_m, b)}{\mathrm{d}r} = -H_e R_n(\beta_m, b), \tag{D.63}$$

or,

$$\beta_m R_n'(\beta_m, b) = -H_e R_n(\beta_m, b). \tag{D.64}$$

Thus,

$$R_n'(\beta_m, b) = -\frac{H_e}{\beta_m} R_n(\beta_m, b), \tag{D.65}$$

or,

$$R_n'^2(\beta_m, b) = \frac{H_e^2}{\beta_m^2} R_n^2(\beta_m, b). \tag{D.66}$$

Similarly, the expression of $R_n'(\beta_m, a)$ can be evaluated using boundary conditions given in Eq. (D.2) for $r = a$ (Özisik, 1968):

$$\frac{\mathrm{d}R_n(\beta_m, a)}{\mathrm{d}r} = H_i R_n(\beta_m, a), \tag{D.67}$$

or,

$$\beta_m R_n'(\beta_m, a) = H_i R_n(\beta_m, a). \tag{D.68}$$

Thus,

$$R_n'(\beta_m, a) = \frac{H_i}{\beta_m} R_n(\beta_m, a) \tag{D.69}$$

or,

$$R_n'^2(\beta_m,a)=\frac{H_i^2}{\beta_m^2}R_n^2(\beta_m,a). \tag{D.70}$$

Substituting Eqs. (D.66) and (D.70) into Eq. (D.44) yields

$$N_n(\beta_m)=\frac{b^2}{2}\left[\frac{H_e^2}{\beta_m^2}R_n^2(\beta_m,b)+\left\{1-\left(\frac{n}{\beta_m b}\right)^2\right\}R_n^2(\beta_m,b)\right]$$
$$-\frac{a^2}{2}\left[\frac{H_i^2}{\beta_m^2}R_n^2(\beta_m,a)+\left\{1-\left(\frac{n}{\beta_m a}\right)^2\right\}R_n^2(\beta_m,a)\right]. \tag{D.71}$$

Substituting Eqs. (D.54) and (D.62) into Eq. (D.71) provides

$$N_n(\beta_m)=\frac{b^2}{2}\left[\frac{H_e^2}{\beta_m^2}\times\frac{4}{\pi^2b^2}+\left\{1-\left(\frac{n}{\beta_m b}\right)^2\right\}\times\frac{4}{\pi^2b^2}\right]$$
$$-\frac{a^2}{2}\left[\frac{H_i^2}{\beta_m^2}\times\frac{4}{\pi^2a^2}\frac{V_n^2}{K_n^2}+\left\{1-\left(\frac{n}{\beta_m a}\right)^2\right\}\times\frac{4}{\pi^2a^2}\frac{V_n^2}{K_n^2}\right], \tag{D.72}$$

or,

$$N_n(\beta_m)=\frac{2}{\pi^2\beta_m^2}\left[H_e^2+\beta_m^2\left\{1-\left(\frac{n}{\beta_m b}\right)^2\right\}\right]-\frac{2}{\pi^2\beta_m^2}\frac{V_n^2}{K_n^2}\left[H_i^2+\left\{1-\left(\frac{n}{\beta_m a}\right)^2\right\}\right]. \tag{D.73}$$

or,

$$N_n(\beta_m)=\frac{2}{\pi^2\beta_m^2}B_e-\frac{2}{\pi^2\beta_m^2}\frac{V_n^2}{K_n^2}B_i \tag{D.74}$$

where

$$B_e=H_e^2+\beta_m^2\left\{1-\left(\frac{n}{\beta_m b}\right)^2\right\}, \tag{D.75}$$

and

$$B_i=H_i^2+\beta_m^2\left\{1-\left(\frac{n}{\beta_m a}\right)^2\right\}. \tag{D.76}$$

Equation (D.74) provides

$$N_n(\beta_m)=\frac{2}{\pi^2\beta_m^2}\left(B_e-B_i\frac{V_n^2}{K_n^2}\right), \tag{D.77}$$

or,

$$N_n(\beta_m)=\frac{2}{\pi^2\beta_m^2}\left(\frac{B_eK_n^2-B_iV_n^2}{K_n^2}\right), \tag{D.78}$$

$$F_n=\frac{B_eK_n^2-B_iV_n^2}{K_n^2}. \tag{D.79}$$

Hence, n is zero or positive integer.

Appendix E

Derivation of Eq. (3.39) by Method of Eigenfunctions (Kim *et al.* 2009)

The derivation of Eq. (3.39) is given in concise form in Appendix A of Kim *et al.* (2009). For sake of ready reference, an elaborate derivation of the expression is described as follows:

Let us consider homogeneous boundary value problem

$$\frac{\mathrm{d}^2\phi_n(y)}{\mathrm{d}y^2}+\lambda_n^2\phi_n(y)=0, \tag{E.1}$$

with boundary condition

$$\frac{\mathrm{d}\phi_n(y)}{\mathrm{d}y}=0 \quad \text{at } y=0, \tag{E.2}$$

and

$$\frac{\mathrm{d}\phi_n(y)}{\mathrm{d}y}=0 \quad \text{at } y=h. \tag{E.3}$$

The general solution of Eq. (E.1) can be written as

$$\phi_n(y)=A\cos(\lambda_n y)+B\sin(\lambda_n y). \tag{E.4}$$

Differentiating Eq. (E.4) with respect to y:

$$\frac{\mathrm{d}\phi_n(y)}{\mathrm{d}y}=-A\lambda_n\sin(\lambda_n y)+B\lambda_n\cos(\lambda_n y). \tag{E.5}$$

Using Eqs. (E.2) and (E.3) into Eq. (E.4) such that

at $y = 0$:

$$B=0, \tag{E.6}$$

at $y = h$:

$$\phi_n(y)\neq 0. \tag{E.7}$$

Hence, $A = 1$. Therefore, the eigenfunctions are given by

$$\phi_n(y)=\cos(\lambda_n y), \tag{E.8}$$

where

$$\lambda_n = \frac{n\pi}{h}. \tag{E.9}$$

Any piecewise smooth function can be expanded in terms of these eigenfunctions

$$T(y,t) = \sum_{n=0}^{\infty} a_n(t)\ \phi_n(y) = \sum_{n=0}^{\infty} a_n(t)\ \cos(\lambda_n \mathrm{y}), \tag{E.10}$$

Differentiating Eq. (E.10) with respect to *t*:

$$\frac{\partial T(y,t)}{\partial t} = \sum_{n=0}^{\infty} \frac{\partial a_n(t)}{\partial t}\ \cos(\lambda_n y), \tag{E.11}$$

Multiplying Eq. (E.11) by $\cos(\lambda_n \mathrm{y})$ and integrating 0 to *h*:

$$\frac{\partial a_n(t)}{\partial t}\left(\int_0^h \cos^2(\lambda_n y)\ \mathrm{d}y\right) = \int_0^h \frac{\partial T(y,t)}{\partial t}\cos(\lambda_n y)\ \mathrm{d}y, \tag{E.12}$$

From Eq. (3.34), the one-dimensional heat conduction equation can be written as

$$\frac{\partial T(y,t)}{\partial t} = \frac{k_s}{\rho_s c_{ps}}\frac{\partial^2 T(y,t)}{\partial y^2} + \frac{\dot{Q}(y)}{\rho_s c_{ps}}, \tag{E.13}$$

Inserting Eq. (E.13) into Eq. (E.12), the following equations is obtained as

$$\frac{\partial a_n(t)}{\partial t} = \frac{\int_0^h \left(\frac{k_s}{\rho_s c_{ps}}\frac{\partial^2 T(y,t)}{\partial y^2} + \frac{\dot{Q}(y)}{\rho_s c_{ps}}\right)\cos(\lambda_n y)\ \mathrm{d}y}{\int_0^h \cos^2(\lambda_n y)\ \mathrm{d}y}. \tag{E.14}$$

In order to derive the expression for $a_n(t)$, let us consider Green's formula

$$\int_0^h \left[u\frac{\partial^2 v}{\partial y^2} - v\frac{\partial^2 u}{\partial y^2}\right]\mathrm{d}y = \left(u\frac{\partial v}{\partial y} - v\frac{\partial u}{\partial y}\right)\Bigg|_0^h, \tag{E.15}$$

where

$$u = T(y,t), \tag{E.16}$$

and

$$v = \cos(\lambda_n y). \tag{E.17}$$

Substituting Eqs. (E.16) and (E.17) into Eq. (E.15) such that

$$\int_0^h \left\{ T(y,t)\frac{\partial^2 \cos(\lambda_n y)}{\partial y^2} - \cos(\lambda_n y)\frac{\partial^2 T(y,t)}{\partial y^2} \right\} \mathrm{d}y = \left(T(y,t)(-\lambda_n)\sin(\lambda_n y) - \cos(\lambda_n y)\frac{\partial T(y,t)}{\partial y} \right)\Bigg|_0^h, \tag{E.18}$$

Using the given boundary conditions in Eqs. (3.35) and (3.36) into Eq. (E.18) such that

$$\int_0^h \left\{ T(y,t)\left(-\lambda_n^2\right)\cos(\lambda_n y) - \cos(\lambda_n y)\frac{\partial^2 T(y,t)}{\partial y^2} \right\} \mathrm{d}y = \left(T(h,t)(-\lambda_n h)\sin(\lambda_n h) - \cos(\lambda_n h)\frac{\dot{q}_s}{k_s} - 0 \right). \tag{E.19}$$

Equation (E.19) can be written as

$$\int_0^h \left\{ \frac{\partial^2 T(y,t)}{\partial y^2}\cos(\lambda_n y) \right\} \mathrm{d}y = \left(-\lambda_n^2\right)\int_0^h T(y,t)\cos(\lambda_n y)\,\mathrm{d}y + (-1)^n \frac{\dot{q}_s}{k_s}. \tag{E.20}$$

Substituting Eq.(E.20) in Eq.(E.14):

$$\frac{\partial a_n(t)}{\partial t} = \frac{\frac{k_s}{\rho_s c_{ps}}\left(-\lambda_n^2\right)\int_0^h \left(T(y,t)\cos(\lambda_n y)\right)\mathrm{d}y + \frac{1}{\rho_s c_{ps}}(-1)^n \dot{q}_s + \frac{1}{\rho_s c_{ps}}\int_0^h \left(\dot{Q}\cos(\lambda_n y)\right)\mathrm{d}y}{\int_0^h \cos^2(\lambda_n y)\,\mathrm{d}y}. \tag{E.21}$$

Using Eqs. (E.14) and (E.21) the following equations is obtained as

$$\frac{\partial a_n(t)}{\partial t} = \frac{k_s\left(-\lambda_n^2\right)a_n(t)}{\rho_s c_{ps}} + \frac{2}{h\rho_s c_{ps}}\left\{ (-1)^n \dot{q}_s + \int_0^h \dot{Q}\cos(\lambda_n y)\mathrm{d}y \right\}. \tag{E.22}$$

Case 1: If $n = 0$:

$$\frac{\mathrm{d}a_0(t)}{\mathrm{d}t} = \frac{2}{h\rho_s c_{ps}}\left\{ \dot{q}_s + \int_0^h \dot{Q}\cos(\lambda_n y)\mathrm{d}y \right\}, \tag{E.23}$$

Case: 2: If $n \neq 0$:

$$\frac{\mathrm{d}a_n(t)}{\mathrm{d}t} = \frac{\left(-\lambda_n^2\right)k_s a_n(t)}{\rho_s c_{ps}} + \frac{2}{h\rho_s c_{ps}}\left\{ (-1)^n \dot{q}_s + \int_0^h \dot{Q}\cos(\lambda_n y)\mathrm{d}y \right\}, \tag{E.24}$$

Integrating Eq. (E.24) with respect to *t*:

$$a_0(t) = \frac{2}{h\rho_s c_{ps}}\left(\dot{q}_s + \int_0^h \dot{Q}\,dy\right)t + a_0(0), \tag{E.25}$$

Using the given initial condition in Eq. (3.37), the following relation is obtained as

$$a_0(0) = \frac{1}{h}\int_0^h T_0(y)dy, \tag{E.26}$$

If $t = 0$ and $n \neq 0$, then

$$a_n(0) = \frac{2}{h}\int_0^h (T_0(y)\cos(\lambda_n y)dy. \tag{E.27}$$

Rearranging Eq. (E.24)

$$\frac{da_n(t)}{dt} + \frac{\lambda_n^2}{\rho_s c_{ps}}a_n(t) = \frac{2}{h\rho_s c_{ps}}\left\{(-1)^n \dot{q}_s + \int_0^h \dot{Q}\cos(\lambda_n y)dy\right\}. \tag{E.28}$$

The general solution of Eq. (E.18) can be obtained by introducing integrating factor (I.F) such that

$$a_n(t)(\text{I.F.}) = \int_0^t \left\{(\text{I.F.})\frac{2}{h\rho_s c_{ps}}\left[(-1)^n \dot{q}_s + \int_0^h \dot{Q}\cos(\lambda_n y)dy\right]\right\}dt + C, \tag{E.29}$$

where

$$\text{I.F.} = \exp\left(\lambda_n^2 \frac{k_s}{\rho_s c_{ps}}t\right), \tag{E.30}$$

and C is a constant, which is equal to $a_n(0)$.

Using Eq. (E.30) into Eq. (E.29):

$$a_n(t)\exp\left(\lambda_n^2 \frac{k_s}{\rho_s c_{ps}}t\right) = \int_0^t \left\{\exp\left(\lambda_n^2 \frac{k_s}{\rho_s c_{ps}}t\right)\frac{2}{h\rho_s c_{ps}}\left((-1)^n \dot{q}_s + \int_0^h \dot{Q}\cos(\lambda_n y)dy\right)\right\}dt + a_n(0), \tag{E.31}$$

or,

$$a_n(t) = \exp\left(-\lambda_n^2 \frac{k_s}{\rho_s c_{ps}}t\right)\left\{a_n(0) + \frac{2}{h\rho_s c_{ps}}\int_0^t \left(\dot{q}_s \exp\left(\lambda_n^2 \frac{k_s}{\rho_s c_{ps}}t\right)\right)dt\right\} + \frac{2}{\lambda_n^2 k_s h}\left(1 - \exp\left(-\lambda_n^2 \frac{k_s}{\rho_s c_{ps}}t\right)\right)\int_0^h \dot{Q}\cos(\lambda_n y)dy. \tag{E.32}$$

Eq. (E.10) can be written as

$$T\left(y,t\right)=\sum_{n=0}^{\infty}a_n\left(t\right)\cos\left(\lambda_n \mathrm{y}\right)=a_0\left(t\right)+\sum_{n=1}^{\infty}a_n\left(t\right)\cos\left(\lambda_n y\right). \tag{E.33}$$

Using Eq. (E.32) into Eq. (E.33):

$$T\left(y,t\right)=a_0(0)+\frac{2}{h\rho_s c_p}\left(\dot{q}_s+\int_0^h \dot{Q}\mathrm{d}y\right)t+\sum_{n=1}^{\infty}a_n\left(t\right)\cos\left(\lambda_n y\right). \tag{E.34}$$

Inserting Eq. (E.32) into Eq. (34) and after manipulating the following equation for transient temperature distribution in the bite zone is obtained as

$$T(y,t)=\frac{1}{h}\int_0^h T_a(y)\mathrm{d}y+\frac{1}{h\rho_s c_{ps}}\left(\dot{q}_s+\int_0^h \dot{Q}\mathrm{d}y\right)t+\sum_{n=1}^{\infty}\left[\left\{\exp\left(-\lambda_n^2\frac{k_s}{\rho_s c_{ps}}t\right)\left\{a_n(0)+\frac{2(-1)^n}{h\rho_s c_p}\int_0^t\left(\dot{q}_s\exp\left(\lambda_n^2\frac{k}{\rho_s c_p}t\right)\right)\mathrm{d}t\right\}\right\}\right.$$
$$\left.+\frac{2}{\lambda_n^2 k_s h}\left(1-\exp\left(-\lambda_n^2\frac{k_s}{\rho_s c_{ps}}t\right)\right)\int_0^h \dot{Q}\cos\left(\lambda_n y\right)\mathrm{d}y\right]\cos\left(\lambda_n y\right), \tag{E.35}$$

where

$$\lambda_n=\frac{n\pi}{h}, \tag{E.36}$$

and

$$a_n\left(0\right)=\frac{2}{h}\int_0^h T_a\left(y\right)\cos\left(\lambda_n y\right)\mathrm{d}y\,. \tag{E.37}$$

Appendix F

Derivation of Eq. (3.48) using Method of Separation of Variables

The solution of one-dimensional heat conduction equation given by Eq. (3.48) can be obtained by employing a method of separation of variables (Kreyszig, 1999).

$$\text{Let } \theta(y,t) = T_e(y,t) - T_a, \tag{F.1}$$

where $T_e(y,t)$ is the temperature of strip at the exit of the roll bite and T_a is the ambient temperature. The following solution is derived into three steps as follows:

Step 1: Two ordinary differential equations

$$\theta(y,t) = T_e(y,t) - T_a = F(y)G(t), \tag{F.2}$$

which are product of functions, each depending only on one variable *y* and *t*. Differentiating Eq. (F.2) with respect to *t*:

$$\frac{\partial \theta(y,t)}{\partial t} = F(y)\dot{G}(t). \tag{F.3}$$

Differentiating Eq. (F.3) twice with respect to *y*:

$$\frac{\partial^2 \theta(y,t)}{\partial y^2} = F''(y)G(t). \tag{F.4}$$

Substituting Eqs. (F.3) and (F.4) into Eq. (3.35) taking $T(y,t) = \theta(y,t)$ as

$$F''(y)G(t) = \frac{1}{\alpha_s}F(y)\dot{G}(t), \tag{F.5}$$

or,

$$\alpha_s F''(y)G(t) = F(y)\dot{G}(t). \tag{F.6}$$

where α_s is the thermal diffusivity of the strip material. Dividing Eq. (F.6) by $\alpha_s F''(y)G(t)$:

$$\frac{1}{1} = \frac{F(y)\dot{G}(t)}{\alpha_s F''(y)G(t)}, \tag{F.7}$$

After rearranging Eq. (F.7), the following expression is obtained:

$$\frac{\dot{G}(t)}{\alpha_s G(t)} = \frac{F''(y)}{F(y)} = -\lambda_n^2, \tag{F.8}$$

where n = 1, 2, 3, …

Note that in Eq. (F.8) dot denote the derivative of function $G(t)$ with respect to t and primes denote the derivative of function $F(y)$ with respect to y. The equality in Eq. (F.8) is satisfied if each group of functions is equated to an arbitrary separation constant such that

$$\dot{G}(t) + \alpha_s \lambda_n^2 G(t) = 0, \tag{F.9}$$

and

$$F''(y) + \lambda_n^2 F(y) = 0. \tag{F.10}$$

The general solution of Eq. (F.9) provides

$$G(t) = B_n \exp\left(-\alpha_s \lambda_n^2 t\right), \tag{F.11}$$

where B_n is an arbitrary constant.

The solution of Eq. (F.10) can be written as

$$F(y) = A\cos(\lambda_n y) + B\sin(\lambda_n y). \tag{F.12}$$

where A and B are the constant. The complete solution for $\theta(y,t)$ is constructed by the product of theses elementary solutions is given as

$$\theta(y,t) = F(y)G(t). \tag{F.13}$$

Inserting Eqs. (F.11) and (F.12) into Eq. (F.13) provides

$$\theta(y,t) = \left\{A\cos(\lambda_n y) + B\sin(\lambda_n y)\right\}\left\{B_n \exp\left(-\alpha_s \lambda_n^2 t\right)\right\}, \tag{F.14}$$

or,

$$\theta(y,t) = \left\{A\cos(\lambda_n y) + B\sin(\lambda_n y)\right\}\exp\left(-\alpha_s \lambda_n^2 t\right). \tag{F.15}$$

Differentiating Eq. (F.15) with respect to y:

$$\frac{\partial \theta(y,t)}{\partial y} = \left(-A\lambda_n \sin\lambda_n y + B\lambda_n \cos\lambda_n y\right)\exp\left(-\alpha^2 \lambda_n^2 t\right), \tag{F.16}$$

Step 2: Satisfying the boundary conditions

At $y = 0$ the following boundary conditions is given as

$$\frac{\partial\theta(y,t)}{\partial y} = 0 \qquad \text{at} \quad y = 0. \tag{F.17}$$

Inserting Eq. (F.16) into Eq. (F.17) provides

$$B = 0. \tag{F.18}$$

At $y = h$ the following boundary conditions is given as

$$\frac{\partial\theta(y,t)}{\partial y} = -\frac{h_a}{k_s}\left(T(h,t) - T_a\right) = -\frac{h_a}{k_s}\theta(h,t) \qquad \text{at} \quad y = h, \tag{F.19}$$

where h_a is the convective heat transfer losses of strip surface, k_s is the thermal conductivity of the strip material. Substituting Eqs. (F.16) and (F.18) in Eq. (F.19):

$$-\frac{h_a}{k_s}\theta(h,t) = \left(-A\lambda_n \sin\lambda_n h\right) \times \exp\left(-\alpha_s \lambda_n^2 t\right). \tag{F.20}$$

After rearranging Eq. (F.20), the following form is obtained:

$$\theta(h,t) = \frac{Ak_s\lambda_n\left(\sin\lambda_n h\right)}{h_a}\exp\left(-\alpha_s\lambda_n^2 t\right). \tag{F.21}$$

Substituting Eq. (F.18) into Eq. (F.15) yields

$$\theta(h,t) = \left\{A\cos\left(\lambda_n h\right) + 0\right\} \times \exp\left(-\alpha_s\lambda_n^2 t\right). \tag{F.22}$$

Equations (F.21) and (F.22) yields

$$\frac{Ak_s\lambda_n\left(\sin\lambda_n h\right)}{h_a} = A\cos\left(\lambda_n h\right), \tag{F.23}$$

or,

$$k_s\lambda_n \sin\left(\lambda_n h\right) - h_a \cos\left(\lambda_n h\right) = 0. \tag{F.24}$$

Equation (F.24) is the transcendental characteristic equation for finding out the positive roots λ_n.

Step 3: Solution of the entire problem using Fourier series along with the given initial condition

The general solution of Eq. (3.41) can be written as assuming $\theta(y,t) = T(y,t) - T_a$ (Kreyszig, 1999)

$$\theta(y,t) = \sum_{n=1}^{\infty} C_n \cos(\lambda_n y) \exp(-\alpha_s \lambda_n^2 t). \tag{F.25}$$

The given initial condition can be written as

$$T(y,0) = T_e(y), \quad \text{at } t = 0, \tag{F.26}$$

or,

$$\theta(y,t) = \theta(y,0), \quad \text{at } t = 0. \tag{F.27}$$

Using Eq. (F.27) into Eq. (F.25) provides

$$\theta(y,0) = \sum_{n=1}^{\infty} C_n \cos(\lambda_n y). \tag{F.28}$$

Equation (F.28) is expanding with the index n:

$$\begin{aligned}\theta(y,0) = {} & C_1 \cos(\lambda_1 y) + C_2 \cos(\lambda_2 y) + C_3 \cos(\lambda_3 y) + ... \\ & + C_n \cos(\lambda_n y) + C_{(n+1)} \cos(\lambda_{(n+1)} y).\end{aligned} \tag{F.29}$$

Multiplying $C_n \cos(\lambda_n y)$ on both sides of Eq. (F.29) and integrate from 0 to h. This provides

$$\begin{aligned}\int_0^h \theta(y,0)\cos(\lambda_n y)\,dy = {} & \int_0^h C_1 \cos(\lambda_1 y)\cos(\lambda_n y)dy + \int_0^h C_2 \cos(\lambda_2 y)\cos(\lambda_n y)dy + ... \\ & + \int_0^h C_n \cos(\lambda_n y)\cos(\lambda_n y)dy + \int_0^h C_{(n+1)}\cos(\lambda_{(n+1)} y)\cos(\lambda_n y)dy.\end{aligned} \tag{F.30}$$

If two functions $f(y)$ and $g(y)$ are orthogonal over the interval $0 \le y \le h$ with weighting function C_n (Kreyszig, 1999) such that

$$f(y)g(y) = \int_0^h C_n f(y) g(y) dy = 0. \tag{F.31}$$

Using the cosine Fourier series to obtain the constant C_n such that

$$\int_0^h \theta(y,0)\cos(\lambda_n y)\mathrm{d}y = \int_0^h C_n \cos^2(\lambda_n y)\ \mathrm{d}y\,, \tag{F.32}$$

or,

$$C_n = \frac{\int_0^h \theta(y,0)\cos(\lambda_n y)\mathrm{d}y}{\int_0^h \cos^2(\lambda_n y)\,\mathrm{d}y}. \tag{F.33}$$

Substituting Eq. (F.1) into Eq. (F.33) provides

$$C_n = \frac{\int_0^h \left[\left\{T_e(y,0) - T_a\right\}\cos(\lambda_n y)\right]\mathrm{d}y}{\int_0^h \left\{1+\cos(2\lambda_n y)\right\}\mathrm{d}y}\,. \tag{F.34}$$

Integrating Eq. (F.34) between 0 to h:

$$C_n = \frac{\int_0^h T_e(y,0)\cos(\lambda_n y)\mathrm{d}y - \dfrac{T_a\sin(\lambda_n h)}{\lambda_n}}{\dfrac{h}{2}+\dfrac{\sin(2\lambda_n h)}{4\lambda_n}}, \tag{F.35}$$

or,

$$C_n = \frac{4\lambda_n\int_0^h T_e(y)\cos(\lambda_n y)\mathrm{d}y - 4T_a\sin(\lambda_n h)}{2\lambda_n h+\sin(\lambda_n h)}. \tag{F.36}$$

Inserting Eq. (F.36) into Eq. (F.25) yields

$$\theta(y,t) = \frac{4\lambda_n\int_0^h T_e(y)\cos(\lambda_n y)\mathrm{d}y - 4T_a\sin(\lambda_n h)}{2\lambda_n h+\sin(2\lambda_n h)}\cos(\lambda_n y)\exp\left(-\alpha_s\lambda_n^2 t\right). \tag{F.37}$$

Using Eq. (F.1) into Eq. (F.37) putting h=h_2/2:

$$T(y,t) = T_a + \sum_{n=1}^{\infty}\left(\frac{4\lambda_n\int_0^{\frac{h_2}{2}} T_e(y)\cos(\lambda_n y)\mathrm{d}y - 4T_a\sin\left(\lambda_n\dfrac{h_2}{2}\right)}{\lambda_n h_2+\sin(\lambda_n h_2)}\right)\cos(\lambda_n y)\exp\left(-\alpha_s\lambda_n^2 t\right). \tag{F.38}$$

Equation (F.38) provides the temperature distribution of exit strip at any location just after the roll bite.

Appendix G

A User Defined DFLUX Subroutine in FORTRAN Language

```
**********************************************************************
** DFLUX FOR ABAQUS/STANDARD INCORPORATING HEAT FLUX AT OUTER
** PERIPHERY OF THE ROLL.
**********************************************************************
      SUBROUTINE DFLUX(FLUX,SOL,KSTEP,KINC,TIME,NOEL,NPT,COORDS,
     1  JLTYP,TEMP,PRESS,SNAME)
C
      INCLUDE 'ABA_PARAM.INC'
C
      DIMENSION FLUX(1), TIME(1), COORDS(3)
      CHARACTER*80 SNAME
      real w, x, y, z, t, r, xr, yr, q, THETA, ARC

      parameter (PI = 3.141592654)

      parameter (RO = 0.250)   ! Outer radius of the roll

      w = 0.1                  !  Omega in rad/sec
      q = 5E6                  !  Heat flux in W/m2
      x = COORDS(1)            !  x axis coordinate
      y = COORDS(2)            !  y axis coordinate
      z = COORDS(3)            !  z axis coordinate
      t=Time(1)                !  time  in sec

      THETA=(8.0*PI)/180.0     ! THETA in radian (Here 8 degree is the angle)

      ARC = THETA*RO           ! Contact length of heat source

      xr=RO*cos(w*t)

      yr=RO*sin(w*t)

      r= sqrt((x-xr)**2+(y-yr)**2)   ! Instanteneous location of  the heat source

      if (r.LE.ARC) then

        FLUX(1)= q

      else

        FLUX(1)=0

      end if

      JLTYP = 0

      RETURN
END
```

Appendix H

Some Results of Parametric Study Using Fast Finite Element Analysis of Flat Rolling Process

The thermal analysis of the roll and the strip is carried out by using FEM based software package while the input is taken from the FEM deformation module (Appendix A). The main purpose is to develop a methodology to improve the computational efficiency for carrying out the thermo-mechanical analysis by FEM. In the present work, FEM deformation module developed in FORTRAN and FEM package software ABAQUS is used to find out the temperature in the roll and strip. It is assumed that the heat flux input into the roll over the roll-strip interface is constant. The steady-state temperature distribution of the roll and the strip is obtained by ABAQUS. For this heat generation due to plastic deformation and friction is calculated employed by FEM deformation module based on Eulerian flow formulation (Appendix A). The heat generated due to plastic deformation and frictional work at the roll bite is used as input in the thermal analysis of the roll and the strip. The heat partition factor between the roll and the strip is obtained by matching the average temperature of the roll and the strip at the roll-strip interface. The mesh sensitivity analysis is carried out to choose the optimum number of elements and is presented in Section 3.5.

The parametric study is carried out to see the influence of roll radius, effect of yield stresses of the material and convective heat transfer coefficients at the outer roll periphery. The thickness of hollow rolls is kept constant at 20 mm in the present study. The thermal properties of roll and strip are given in Table 3.15 and the constitutive relation of the strip material is given by Eq. (3.26). An iterative procedure involving thermal and mechanical analysis in sequence is employed.

Table H.1 shows the computed average temperature at the roll-strip interface for different rolling speeds. It is observed from Table H.1 that the minimum temperature at the roll-strip interface occurs for the smallest roll radius and the maximum temperature occurs at the highest roll radius. The heat generation due to

plastic deformation and friction energy is more at larger roll radius. On the other hand, at constant production rate, the angular velocity of roll decreases with increasing roll radius. Hence, the contact time of strip and roll at the interface increases. Table H.1 shows that increasing the exit speed of the strip from 1 to 2 m/s, the average temperature at roll-strip interface increases. The higher exit speed of the strip also implies higher angular velocity of the roll. Although, the power per unit volume may not change significantly, the time available for the cooling of roll reduces. Hence, temperature obtained at higher speed is more than that at lower speed.

Table H.1. Typical results for the effect of roll diameter on the interface temperature (h_1 = 1mm, r_d = 24%, h_i = 2.6 W/m^{2}K, μ = 0.14, $(\sigma_Y)_0$ = 400 MPa b = 0.052, n = 0.295, T_0 = 30 °C)

Roll radius R (mm)	Average temperature at the roll-strip interface (°C)			
	V_2 = 1 m/s		V_2 = 2 m/s	
	h_e = 10 W/m^2-°C	h_e = 260 W/m^2-°C	h_e = 10 W/m^2-°C	h_e = 260W/m^2-°C
35	77.25	75.21	95.56	94.82
65	123.42	94.5	145.1	111.25
130	214.21	178.72	231.62	197.85

The effect of convective heat transfer losses is one of the important process parameter controlling the thermal damage of work roll and thus increasing the roll life in rolling mill. The change in the convective heat transfer coefficient is studied for various values of the roll radius. The analysis is performed with two initial temperatures of strip, 30 and 200 °C, for h_e = 10 and 260 W/m^2°C. The thickness of the hollow roll is kept constant at 20 mm during the study. The material of strip is steel. The yield stress of strip $(\sigma_Y)_0$, material hardening parameter (b, n), exit speed of rolling (V_2), inlet thickness of the strip (h_1) and coefficient of friction (μ) is given in Figs. H.1 and H.2. Figures H.1 and H.2 show the average temperature at the roll-strip interface with respect to different roll radii. It is observed from Figs. H.1 and H.2 that the average temperature at the roll-strip interface decreases with increase in the convective heat transfer coefficient. The difference between average temperatures at roll-strip interface at two convective heat losses is more pronounced

at higher roll radius. Similarly, the rise in average temperature at the roll-strip interface is more for the case of lower initial temperature of strip.

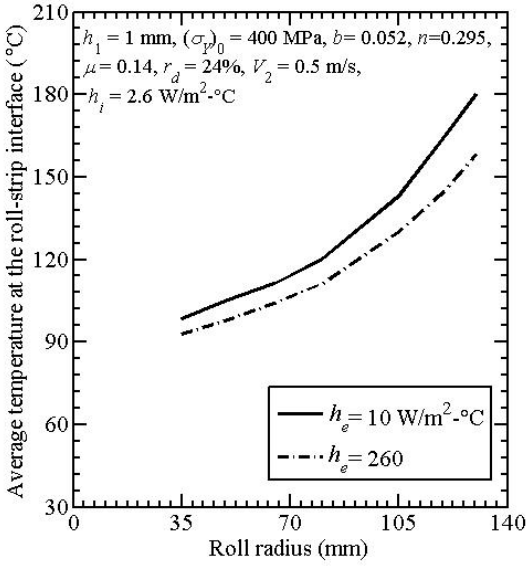

Fig. H.1. Effect of convective heat transfer coefficient on the average temperature at the roll-strip interface with initial temperature of strip 30 °C

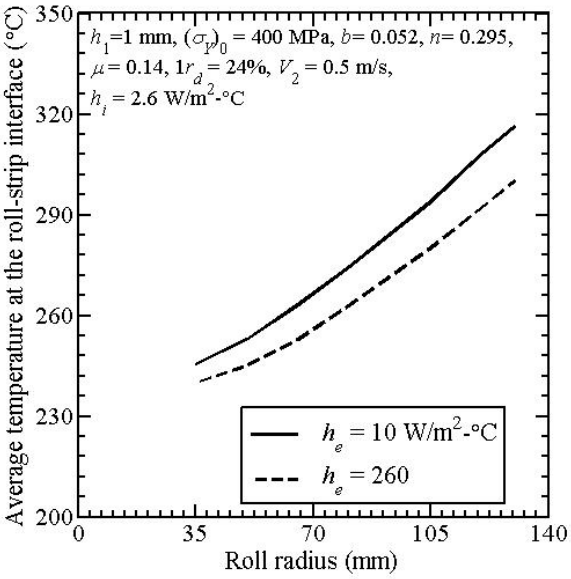

Fig. H.2. Effect of convective heat transfer coefficient on the average temperature at the roll-strip interface with initial temperature of strip 200 °C

Another investigation is made by comparing the average temperature at the roll-strip interface for different flow stresses of the material. It is observed from Fig.

H.3 that with the increase of yield stress by 10% and material hardening parameters by 20%, the average temperature at the interface increases more than 50 °C at roll radius R = 130 mm. However, with the decrease of roll radius the variation of temperature also decreases. For similar reduction and rolling speed, the strip with higher flow stress has a higher average temperature at the roll-strip interface. As material becomes harder, more rolling power is required which causes the temperature of the strip to increase.

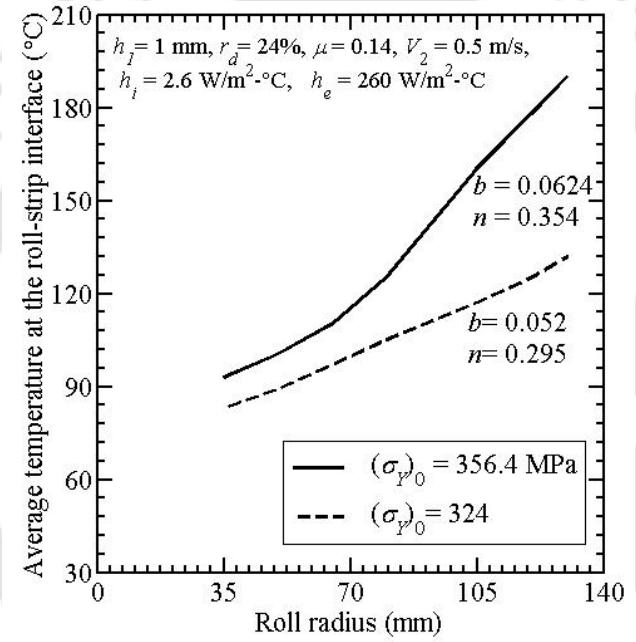

Fig. H.3. Effect of different yield stress of different material parameters on the average temperature at the roll-strip interface with initial temperature of strip 30 °C

In the present work, fast finite element analysis is carried out to develop a computationally efficient methodology for estimating the steady-state temperature distribution in rolling. The methodology is implemented on FEM based package ABAQUS. It has been observed that ABAQUS takes a lot of time for steady-state thermal analysis of roll. The fast FEM analysis takes less than 10 minutes screen time to find out the steady-state temperature distribution. Hence, the proposed methodology can be useful for analyzing the steady-state temperature distribution in rolling for composite and functionally graded materials.

Appendix I

Sequential Quadratic Programming (SQP) Methods

Sequential quadratic programming (SQP) method uses a quadratic model for the objective function and a linear model of the constraint in sequence. A nonlinear program in which the objective function is quadratic and the constraints are linear is called a quadratic program (QP). SQP actually solves a sequence of quadratic programming (QP) problems till the convergence is obtained (Rao, 2013).

Consider the following optimization problem with *l* equality and *m* inequality constraints:

$$\text{Minimize } f(\mathbf{x}),$$

$$\text{subject to} \quad h_i(\mathbf{x}) = 0, \quad i = 1 \text{ to } l,$$

$$\text{and} \quad g_j(\mathbf{x}) \le 0, \quad j = 1 \text{ to } m \tag{I.1}$$

where $\mathbf{x} = (x_1, x_2, ..., x_n)^T$ is a column vector of *n* real-valued design variables.

At a particular guess point, Eq. (H.1) is converted to the following quadratic form:

$$Q = \{\nabla f(\mathbf{x})\}^T \mathbf{d} + \frac{1}{2}\mathbf{d}^T \boldsymbol{H}\mathbf{d},$$

subject to

$$h_i(\mathbf{x}) + (\nabla h_i)^T \mathbf{d} = 0, \quad i = 1, 2, \ldots, l, \tag{I.2}$$

$$g_j(\mathbf{x}) + (\nabla g_j)^T \mathbf{d} \le 0, \quad j = 1, 2, \ldots, m,$$

where $\mathbf{d}^T = \lfloor d_1, d_2, \cdots, d_n \rfloor$ is the vector of decision variables of the problem and $\boldsymbol{H}$ is the Hessian matrix of the Lagrange function of Eq. (I.1) considering equality and active non-equality constraints.

The Lagrange function, $L(\mathbf{x}, \lambda)$, corresponding to the problem of Eq. (I.1) can be defined as

$$L(\mathbf{x}, \lambda) = f(\mathbf{x}) + \sum_{j=1}^{m} \lambda_j g_j(\mathbf{x}) + \sum_{i}^{l} \lambda_{m+i} h_i(\mathbf{x}), \tag{I.3}$$

where λ_j and λ_{m+i} are the Lagrange multipliers for j^{th} inequality constraints and i^{th} equality constraints respectively. The Karush-Kuhn-Tucker (KKT) necessary condition can be stated as

$$\sum_{j=1}^{m} \lambda_j \nabla g_j(\mathbf{x}) + \sum_{i}^{l} \lambda_{m+i} \nabla h_i(\mathbf{x}) = -\nabla f(\mathbf{x}). \tag{I.4}$$

For a particular guess points, the gradient of the objective function can be written as

$$\nabla f(\mathbf{x})^{\mathrm{T}} = \begin{bmatrix} \dfrac{\partial f}{\partial x_1} & \dfrac{\partial f}{\partial x_2} & \cdots & \dfrac{\partial f}{\partial x_n} \end{bmatrix} \tag{I.5}$$

and the Hessian matrix of the Lagrange function can be written as

$$H = \begin{bmatrix} \dfrac{\partial^2 L}{\partial x_1^2} & \dfrac{\partial^2 L}{\partial x_1 \partial x_2} & \cdots & \dfrac{\partial^2 L}{\partial x_1 \partial x_n} \\ \dfrac{\partial^2 L}{\partial x_2 \partial x_1} & \dfrac{\partial^2 L}{\partial x_2^2} & \cdots & \dfrac{\partial^2 L}{\partial x_2 \partial x_n} \\ \cdots & \cdots & \cdots & \cdots \\ \cdots & \cdots & \cdots & \cdots \\ \cdots & \cdots & \cdots & \cdots \\ \dfrac{\partial^2 L}{\partial x_n \partial x_1} & \dfrac{\partial^2 L}{\partial x_n \partial x_2} & \cdots & \dfrac{\partial^2 L}{\partial x_n^2} \end{bmatrix}. \tag{I.6}$$

For the solution, an appropriate starting value of non-zero Lagrange multiplier $\boldsymbol{\lambda}^0$ can be obtained by employing least square method. This provides

$$\boldsymbol{\lambda}^0 = \left(\mathbf{G}^{\mathrm{T}}\mathbf{G}\right)^{-1} \mathbf{G}^{\mathrm{T}} \left\{\nabla f(\mathbf{x})\right\}^{T}, \tag{I.7}$$

where **G** indicates the set of active constraints at the point **x**.

The variable **d** in Eq. (I.2) is the search direction for getting the optimum solution. Assume that the minimum point $\mathbf{x}_p$ is obtained by the expression:

$$\mathbf{x}_p = \mathbf{x} + \delta \mathbf{d}, \tag{I.8}$$

where δ is a step length chosen to reduce the value of a suitable merit function along the direction **d**. Once the value of $\mathbf{x}_p$ is substituted in the merit function, the merit

function becomes the function of scalar δ. The optimum value of δ can be found by a one-dimensional search technique *e.g.*, golden section search algorithm (Rao, 2013). The merit function can be the function of the following form:

$$M = R\left\{ f(\mathbf{x}) + \sum_{j=1}^{m} \left\{ \max\left(0, g_j(\mathbf{x})\right) \right\} + \sum_{i=1}^{l} \left| h_i(\mathbf{x}) \right| \right\}, \tag{I.9}$$

where R is a very large value called the penalty parameter.

At the obtained optimum point $\mathbf{x}_p$, the objective function is again converted to the form of Eq. (I.2), *i.e.*, a quadratic approximation for the function and a linear approximation for the constraints is used. After this, the procedure is repeated starting from solving a QP problem by a method similar to Simplex method (Taha, 2000). Thus, the optimization process is iterative and the iterations are continued till the convergence is obtained. In this thesis, inbuilt function FMINCON of MATLAB® is used to implement SQP algorithm.

Appendix J

Typical empirical models showing the dependency of flow stress

S.No.	Material models	Comments
1.	$\sigma_y = 100\left(1+0.9\varepsilon^{0.355}\right)$	Ludwik law used to validate the cold rolling results with the experimental data Jeswiet and Zhou (1975). The material of strip is made of aluminum alloy.
2.	$\sigma_y = \left(\sigma_Y\right)_0 \left\{1+\frac{\varepsilon}{b}\right\}^n$	Swift's generalized power law, suitable for a wider range of strains. It is used for simulating the cold rolling in the present thesis.
3.	$\sigma_y = B\dot{\varepsilon}^m \varepsilon^n$	The flow stress relation considering strain and strain-rate with temperature dependency. For validating the steady-state temperature distribution in warm rolling with the experimental results of Serajzadeh and Mohammadzadeh (2007). Serajzadeh and Mohammadzadeh (2007) found the constants *m*, *n* and *B* by experimentally (employed in Chapter 3).
4.	$\sigma_y = \sigma_1 + n_4\varepsilon$ for $\varepsilon \geq 0.1$, $\sigma_y = \sigma_2\left(\frac{\varepsilon}{0.1}\right)^{n_5}$ for $\varepsilon < 0.1$,	This relation is used to validate the transient temperature distribution in warm rolling. Lenard and Malinowski (1993) conducted a series of compression test using appropriate values of strain-rates at temperatures of 22, 100 200 and 300 °C for commercially pure aluminum alloy sample. The parameters of the flow stress are provided in Table 4.5.

5.	$\sigma_y = \left(A + B\varepsilon_{eq}^{n_1}\right)\left[1 + C\ln\frac{\dot{\varepsilon}_{eq}}{\dot{\varepsilon}_0}\right]\left[1 - \left(\frac{T - T_{amb}}{T_m - T_{amb}}\right)^{m_1}\right]$	Johnson and Cook material model is widely used in metal forming processes. It is used for carrying out the master simulations of warm rolling and these simulations are taken in lieu of real shop floor experiments in Chapter 6.
6.	$\sigma_y = \sigma_0 \varepsilon_{eq}^{n} \left(\frac{\dot{\varepsilon}}{\dot{\varepsilon}_r}\right)^{\beta_1} \left(\frac{T}{T_{\mathrm{m}}}\right)^{-\gamma}$	Inverse modelling is employed to estimate the flow stresses in Chapter 6. This model may not be valid over wide ranges of strain, strain-rate and temperature. However, it is always possible to select smaller domains for fitting this model.
7.	$\sigma_y = \sigma_0 \varepsilon_{eq}^{n} \left(\frac{T}{T_{\mathrm{m}}}\right)^{-\gamma}$	This power law neglecting the strain-rate dependency. In this thesis, it is used to validate the results of inverse modelling in Chapter 6.
8.	$\sigma_y = K\varepsilon_{eq}^{n}$	Holloman law deviates at low strain, for high strain-rate may be treated total as well as plastic strain-rate. The constants K and n are temperature dependent.

Publications from this Research Work

International Journals

1. V. Yadav, A.K. Singh and U.S. Dixit, (2016), Experimental validation of strategy for the inverse estimation of mechanical properties and coefficient of friction in flat rolling, Journal of Institutions of Engineers, India Series C, doi 10.1007/s40032-016-0293-2.
2. V. Yadav, A.K. Singh and U.S. Dixit, (2015), Inverse estimation of thermal parameters and friction coefficient during warm flat rolling process, International Journal of Mechanical Sciences, **96-97**, pp. 182–198.
3. V. Yadav, A.K. Singh and U.S. Dixit, (2014), An Approximate Method for Computing the Temperature Distributions in Roll and Strip during Rolling Process, Proceeding of Institution of Mechanical Engineers, Part B, Journal of Engineering Manufacture, **228**, pp. 1118–1130.
4. V. Yadav, J. Thakuria, A.K. Singh and U.S. Dixit, (2013), An Approximate Fast Finite Element Analysis of Temperature Distribution in Rolling, International Journal of Mechatronics and Manufacturing Systems, **6**, pp. 381–396.

Book Chapters

1. U.S. Dixit, V. Yadav and A.K. Singh (2016), Estimation of temperature distribution in flat rolling, in Rolling of Advanced High Strength Steels: Theory, Simulation and Practice, edited by Jingwei Zhao and Zhengyi Jiang, CRC Press, in press.
2. V. Yadav, A.K. Singh and U.S. Dixit, (2015), An efficient inverse method for determining the material parameters and coefficient of friction in warm rolling process, in Advances in Material Forming and Joining, edited by R. Ganesh Narayanan and U.S. Dixit, Springer (New Delhi).

International/ National Conferences

1. V. Yadav, A.K. Singh and U.S. Dixit, (2015), Determination of friction in cold and warm rolling processes, Proceedings of the Thirtieth National Convention of Production Engineers and National Seminar on Sustainable Manufacturing, July 18-19, 2015, The Institution of Engineers (India), Tripura State Center, Agartala [Enhanced version of this paper is submitted as Journal #1].

2. V. Yadav, A.K. Singh and U.S. Dixit, (2014), An efficient inverse method for determining the material parameters and coefficient of friction in warm rolling process, 5th International & 26th All India Manufacturing Technology, Design and Research Conference (AIMTDR 2014), December 12th-14th, 2014, IIT Guwahati, India, pp. 66-1–66-7 [Enhanced version of this paper is published as Book chapter # 2].
3. V. Yadav, A.K. Singh and U.S. Dixit, (2012), An Approximate method for computing the temperature distributions in roll and strip during rolling process, 4th International & 25th All India Manufacturing Technology, Design and Research Conference (AIMTDR 2012), December 14th-16th, 2012, Jadavpur University, Kolkata, India, pp. 80–85 [Enhanced version of this paper is published as Journal #3].